

UNCLASSIFIED

AD NUMBER

AD865512

LIMITATION CHANGES

TO:

Approved for public release; distribution is unlimited.

FROM:

Distribution authorized to U.S. Gov't. agencies and their contractors;
Administrative/Operational Use; 15 JAN 1970.
Other requests shall be referred to Air Force Technical Applications Center, Washington, DC.

AUTHORITY

AFTAC ltr 25 Jan 1972

THIS PAGE IS UNCLASSIFIED

AD 865512

A COMPARISON OF THE LAKE SUPERIOR AND NEVADA TEST SITE SOURCE REGIONS

15 January 1970

Prepared For

AIR FORCE TECHNICAL APPLICATIONS CENTER
Washington, D. C.

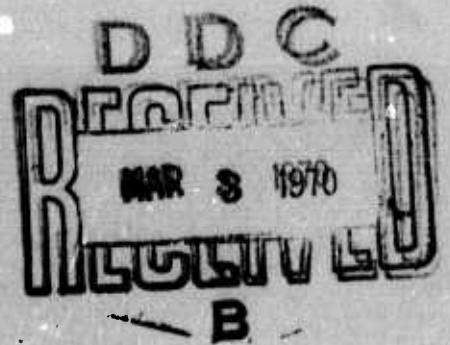
By

P. Glover

SEISMIC DATA LABORATORY

S. S. Alexander

CONSULTANT TO THE SEISMIC DATA LABORATORY



Under

Project VELA UNIFORM

Reproduced by the
CLEARINGHOUSE
for Federal Scientific & Technical
Information Springfield Va. 22151

Sponsored By

ADVANCED RESEARCH PROJECTS AGENCY
Nuclear Monitoring Research Office
ARPA Order No. 624

This document is subject to special export controls and each transmittal to foreign governments or foreign nationals may be made only with prior approval of Chief, AFTAC.

Alexander, Va. 22313

**BEST
AVAILABLE COPY**

A COMPARISON OF THE LAKE SUPERIOR AND NEVADA
TEST SITE SOURCE REGIONS

SEISMIC DATA LABORATORY REPORT NO. 243

AFTAC Project No.:	VELA T/9706
Project Title:	Seismic Data Laboratory
ARPA Order No.:	624
ARPA Program Code No.:	9F10
Name of Contractor:	TELEDYNE INDUSTRIES, INC.
Contract No.:	F33657-69-C-0913-PZ01
Date of Contract:	2 March 1969
Amount of Contract:	\$ 2,000,000
Contract Expiration Date:	1 March 1970
Project Manager:	Royal A. Hartenberger (703) 836-7647

P. O. Box 334, Alexandria, Virginia

AVAILABILITY

This document is subject to special export controls and each transmittal to foreign governments or foreign nationals may be made only with prior approval of Chief, AFTAC.

This research was supported by the Advanced Research Projects Agency, Nuclear Monitoring Research Office, under Project VELA-UNIFORM and accomplished under technical direction of the Air Force Technical Applications Center under Contract F33657-69-C-0913-PZ01.

Neither the Advanced Research Projects Agency nor the Air Force Technical Applications Center will be responsible for information contained herein which may have been supplied by other organizations or contractors, and this document is subject to later revision as may be necessary.

ABSTRACT

Two particular source regions, Lake Superior and the Nevada Test Site are documented in detail using available geological and geophysical observations. Each is discussed individually in relation to its setting in the prevailing regional crust and upper mantle structure of the mid-continent and the Basin and Range respectively. Comparison of the two source areas indicates that they are markedly different from one another not only at shallow depths but throughout the upper mantle as well. Location accuracies for events at both sites are quite comparable, however, a large bibliography documents the extensive literature relevant to Lake Superior and the Nevada Test Sites.

ACKNOWLEDGEMENTS

We were aided considerably in the preparation of this report by the cooperation afforded us by many of the participants in the Lake Superior Seismic Experiment and Project Early Rise. We particularly wish to thank L. C. Pakiser, W. H. Jackson and J. C. Roller of the National Center for Earthquake Research, USGS, Menlo Park, California; R. P. Meyer, R. Anzoleaga, and R. J. Wold of the University of Wisconsin; and D. E. Willis, of the University of Michigan for their valuable assistance. We also acknowledge useful discussions with C. B. Archambeau, R. F. Roy, J. S. Steinhart, W. H. Mansfield, and T. J. Cohen. Messers C. B. Archambeau, E. A. Flinn and D. G. Lambert, R. P. Meyer, and R. J. Wold kindly allowed us to use hitherto unpublished figures as illustrations in this report. It is with sincere appreciation that we acknowledge the diligence of R. O. Ahner, and Mrs. Honor Johnson of the Seismic Data Laboratory in analyzing the film data and preparing much of the material for inclusion in this report. J. R. Woolson also aided us considerably in particular aspects of this investigation.

TABLE OF CONTENTS

	Page No.
ABSTRACT	
INTRODUCTION	1
PHYSICAL SETTING OF LAKE SUPERIOR EXPERIMENTS	5
Geologic Environment	5
The Relationship of Lake Superior to the Canadian Shield	5
Geology of the Lake Superior Basin	9
Geophysical Evidence on Crustal Structure Under Lake Superior	12
Seismic Measurements	13
Refraction Studies	13
Surface Wave Dispersion Observations	18
Gravity Data	19
Aeromagnetic Data	24
Heat Flow Observations	27
Seismicity of the Lake Superior Region	29
A Geophysical Model for the Crust Beneath the Early Rise Shot Point	30
DISCUSSION	34
EPICENTER LOCATIONS, TRAVEL-TIMES, AND UPPER MANTLE STRUCTURE FOR LAKE SUPERIOR REGION	39
Location of the October 1964 Shots Using the LRSM and Observatory Networks	39
Travel-Times and Upper Mantle Structures from Events in Lake Superior	45
PHYSICAL SETTING OF THE NEVADA TESTS	51
Geological Environment	51
The Relationship of the Nevada Test Site to the Basin and Range	51

TABLE OF CONTENTS (Cont'd.)

	Page No.
Geology of the Nevada Test Site	56
Geophysical Evidence on Crustal Structure Under the Nevada Test Site	59
Seismic Measurements	
Refraction Studies	59
Surface Wave Dispersion Observations	64
Gravity Data	65
Aeromagnetic Data	68
Heat Flow Data	69
Seismicity	70
A Geophysical Model for the Crust Beneath Yucca Flat, Nevada Test Site	70
Discussion	74
LOCATION OF EVENTS AT NTS, TRAVEL-TIMES AND UPPER MANTLE STRUCTURE FOR THE BASIN AND RANGE PROVINCE	78
Location of NTS Using the LRSM and Observatory Network	78
Travel-Times and Upper Mantle Structure for the Basin and Range Province	80
COMPARISON OF THE LAKE SUPERIOR AND NEVADA TEST SITE SOURCE REGIONS	86
IMPLICATIONS	92
REFERENCES	

LIST OF FIGURES

Figure Title	Figure No.
Locations of shots fired during the 1963 Lake Superior Seismic Experiment. (After Smith et al, 1966b.)	1
Locations of recording profiles occupied during Project Early Rise. (After Iyer et al, 1969.)	2
Structural map of the Canadian Shield. (Adopted from Stockwell, 1962; 1964.)	3
The model CANSD for the crust and upper mantle beneath the Canadian shield derived from surface wave dispersion data. (Brune and Dorman, 1963.) Dashed line indicates the P-wave model obtained by Barr (1967) from body wave data.	4
Locations of shot points and recording stations for the 1965 Hudson Bay crustal experiment. (After Hobson, 1967.)	5
Generalized geologic map of the Lake Superior region. (After Halls, 1966.)	6
Bottom topography of Lake Superior. (After Hough, 1958.)	7
Geologic cross section through Isle Royale and Keweenaw Peninsula. A and A' are observed Bouguer gravity profiles, B and C residual Bouguer gravity profiles after effects of Keweenawan rocks are removed. Patterns represent geologic units, as follows: Jacobsville Sandstone, small dots; Freda Sandstone and Nonesuch Shale, large dots; Copper Harbor Conglomerate, circles; Portage Lake Series, solid black; pre Keweenawan rocks, no pattern. (After White, 1966b.)	8
Locations of the principal recording stations during the 1963 Lake Superior Seismic Experiment. (After Smith et al, 1966.)	9

LIST OF FIGURES (Cont'd.)

Figure Title	Figure No.
Models for the crust beneath Lake Superior obtained by Smith et al, (1966 a,b), Berry and West, (1966 a,b) and O'Brien (1968). Slanted velocity values are those obtained by O'Brien; upright ones and those given by Smith et al.	10
t^2-x^2 plot for data recorded at Otter Cove, Woodsman and Tom. Theoretical travel-times are for reflections from interfaces showing in model. (After O'Brien, 1968.)	11
Locations of stations and shot points for the University of Wisconsin shallow seismic profiling study. (Courtesy of R.P. Meyer, University of Wisconsin Geophysical and Polar Research Center.)	12
Model obtained by Anzoleaga et al, (1969) for shallow crustal structure in western Lake Superior along profile shown in Figure 12. (Courtesy of R.P. Meyer, University of Wisconsin Geophysical and Polar Research Center.)	13
Compilation of results from seismic refraction surveys in the vicinity of Lake Superior plotted as a fence diagram.	14
Contour map showing probable depth to the Moho in the Lake Superior region. Data for crust beneath Lake Superior are taken from O'Brien (1968).	15
Theoretical fundamental mode Rayleigh wave dispersion computed for CANSD and a series of crustal-models for Lake Superior discussed in the text.	16
Bouguer gravity map of the area 38°-57°N, 78°-104°W compiled from data published by Weber and Goodacre (1966), Woollard and Joesting (1964), Innes (1960), McConnell (1966), and a series of maps compiled by Dominion Observatory of Canada.	17

LIST OF FIGURES (Cont'd.)

Figure Title	Figure No.
Structural map of Lake Superior showing positions of known faults and of those inferred from geophysical data.	18
Total magnetic intensity map of Lake Superior. (After Hinze et al, 1966 and Wold and Ostenso, 1966.)	19
Shallow structure in Lake Superior from aeromagnetic data. (After Wold and Ostenso, 1966 and Hinze et al, 1966.)	20
Residual total magnetic intensity contour map of eastern Lake Superior showing labelled anomalies referred to in the text. (After Hinze et al, 1966.)	21
Heat flow observations in Lake Superior showing the 3 heat principal flow regimes. (After Steinhart et al, 1968.)	22
Earthquakes of the United States through 1963 exclusive of California and western Nevada. (After Eppley, 1965.)	23
Locations of the 38 shots detonated during Project Early Rise. Arrows indicate directions to the shot points beyond 1 km; values in parentheses indicate the distance.	24
Location of the continuous sub-bottom profiling survey through Early Rise shot point conducted by the University of Wisconsin in 1966. Times of particular locations are indicated along each line. (Courtesy of R.J. Wold, University of Wis.)	25
Continuous sub-bottom profile through Early Rise shot point recorded along track shown in Figure 25. (Courtesy of R.J. Wold, University of Wis.)	26

LIST OF FIGURES (Cont'd.)

Figure Title	Figure No.
First arrival data from reversed seismic refraction profiles through the Early Rise shot point. (Anzoleaga et al, 1969.) Reciprocity of apparent velocities suggests the refractors are very nearly horizontal. (Courtesy of R.P. Meyer, University of Wisconsin Geophysical and Polar Research Center.)	27
Locations of LRSM stations and Vela Observatories which recorded some or all of the October, 1964 series of shots in Lake Superior.	28
Actual and computed locations of the October, 1964 series of shots using the whole LRSM and observatory network.	29
Reduced travel-times and travel-times anomalies relative to WMO for shot 49A.	30
Actual and computed locations of October, 1964 series of shots using the eastern and western stations in the LRSM and observatory network separately.	31
Assumed geometry at source in Spence and Alexander's method for relative event location.	32
Plot of travel time difference between shot 46A and 49A as a function of azimuth to LRSM stations and Vela Observatories illustrating method of determining relative location of shot 46A.	33
Locations of October, 1964 series of shots computed using Spence and Alexander's method.	34
Reduced travel-times obtained during Project Early Rise. Solid curve represents theoretical travel-times calculated from model NCER 1. (After Iyer et al, 1969.)	35

LIST OF FIGURES (Cont'd.)

Figure Title	Figure No.
Model NCER 1 derived by Iyer et al, (1969) from the smoothed travel-time data collected during Project Early Rise. (After Iyer et al, 1969.)	36
Calculated travel-time curves for the P-wave model of Lewis and Meyer shown in Figure 39 (solid curve) superimposed on record section from the Early Rise profile 1. Dotted curve represents theoretical travel times for P-SV conversions at base of crust. (After Lewis and Meyer, 1968.)	37
Record sections showing shear wave portion of filtered horizontal and vertical traces, with theoretical travel-times for Lewis and Meyer's model superimposed. (After Lewis and Meyer, 1968.)	38
Model for the crust and upper mantle to the west of Lake Superior obtained by Lewis and Meyer (1968).	39
Reduced travel-times from Early Rise profiles 2, 3, and 4 and theoretical travel-time curves computed from Early Rise Model 1 (solid line) and Early Rise Model 2 (dashed line). Structures shown in insert. (After Green and Hales, 1968.)	40
Reduced travel-times from Early Rise profile 5 showing four branches of travel-time curve identified by Willis (1968). Figure courtesy of D. E. Willis, University of Michigan.	41
Reduced travel-times of first arrivals recorded along Early Rise profile 6. (After Roller and Jackson, 1966a, b.)	42
Reduced travel-times to Canadian stations for arrivals from Project Early Rise and the Hudson Bay seismic experiment. Solid curve represents theoretical travel-times calculated from model shown above curve. (After Barr, 1967.)	43

LIST OF FIGURES (Cont'd.)

Figure Title	Figure No.
Record section for Early Rise profile 8 showing three distinct branches of the travel-time curve. Note small amplitudes beyond 1100 km. (After Mereu and Hunter, 1969.)	44
Physiographic outline of the United States showing locations of profiles and stations used by Archambeau et al, (1969) to derive CIT 100 structure series. (After Archambeau et al, 1969.)	45
Model CIT 111-P for P-wave structure in the Basin and Range mantle province. (After Archambeau et al, 1969.)	46
Shear wave velocity models for the Basin and Range mantle province derived by Kovach and Robinson (1969) from $dT/d\Delta$ measurements of long-period S-waves recorded at the extended TFO array. (Courtesy of R.L. Kovach, Stanford University.)	47
Heat flow in the western United States. (After Archambeau and Davies, 1969.)	48
Profile across the Sierra Nevada and the Basin and Range showing correlation of increase in heat flow with decrease in Pn velocity across the physiographic boundary. (Courtesy of C.B. Archambeau, California Institute of Technology.)	49
Location of the Nevada Test Site (NTS).	50
Generalized geologic map of the Yucca Flat area, Nevada Test Site. (After Hinrichs, 1968.)	51
Structural map of the Yucca Flat area, Nevada Test Site showing major thrust plates. (Adopted from Barnes et al, 1963.)	52
Compilation of results from seismic refraction surveys in the western United States plotted as a fence diagram.	53

LIST OF FIGURES (Cont'd.)

Figure Title	Figure No.
Fundamental and higher mode Love wave group velocity dispersion data across the Basin and Range province obtained by Alexander, 1963. Dotted lines represent theoretical, group velocity dispersion curves computed from model 35 CM 2. (After Alexander, 1963.)	54
Fundamental and higher mode Rayleigh wave group velocity dispersion across the Basin and Range province from two events in Utah. Solid line represents theoretical group velocity curves computed from model 35 CM2. (After Alexander, 1963.)	55
Fundamental and higher mode Love and Rayleigh wave group velocity dispersion across the Basin and Range province from Montana earthquake aftershock sequence. Solid line represent theoretical curves computed from model 35 CM2. (After Alexander, 1963.)	56
Model 35 CM2 for the crustal and upper mantle structure beneath the Basin and Range province. (After Alexander, 1963.)	57
Regional Bouguer gravity fold in the vicinity of NTS. (Adapted from Miscellaneous Geologic Investigations Map 1-532-B, published by U.S. Geological Survey, 1968.)	58
Detailed Bouguer gravity anomaly map of Yucca Flat, Nevada Test Site. Note that all values are negative. (After Healey, 1968.)	59
Total magnetic intensity in the vicinity of the Nevada Test. (Adapted from Miscellaneous Geologic Investigations Map 1-532-A, published by U.S. Geological Survey, 1968.)	60

LIST OF FIGURES (Cont'd.)

Figure Title	Figure No.
Epiceenters of shallow events in the vicinity of the Nevada Test Site for the period January 1960 through January 1968 as determined by the U.S. Coast and Geodetic Survey. (No distinction as to number of events occurring at a given location.)	61
Locations of aftershocks following the detonation of underground nuclear explosions Benham on Dec. 19, 1968 at NTS.	62
Theoretical fundamental mode Rayleigh wave dispersion computed from models YF111 and 35 CM2.	63
Locations of events at NTS computed using only stations with epicentral distances greater than seventeen degrees, with and without travel-time anomaly corrections.	64
Locations of events at NTS computed using whole LRSM and Observatory network, with and without anomaly corrections.	65
Observed travel-times from the Shoal-Fallon southeast profile and theoretical travel-time curve (solid line) calculated from model CIT 111P. (After Archambeau et al, 1969.)	66
P-wave travel time anomalies. (After Cleary and Hales, 1966.)	67
Observed and theoretical amplitudes from Shoal-Fallon southeast profile. (After Archambeau et al, 1969.)	68
Q structure for CIT 100 series of models. (After Archambeau et al, 1969.)	69

LIST OF FIGURES (Cont'd.)

Figure Title	Figure No.
The CIT 100 series of models showing range of upper mantle structures in the western United States. (After Archambeau et al, 1969.)	70
Upper mantle P-wave velocity distributions for model CIT 204 (Johnson 1967) and NTS-NE19. (Julian and Anderson, 1968.) Figure from Julian and Anderson, 1968.	71
Fit of $dT/d\Delta$ calculated from two extremes CIT 100 series models with observed $dT/d\Delta$ at TFO. (After Archambeau et al, 1969.)	72
Comparison of a crustal column for Lake Superior based on model ERLS 112 with a similar column for NTS based on model YF111.	73
P-wave models from Early Rise compared with CIT 111P.	74.
S-wave models for the Canadian Shield compared with models for the western United States.	75
Summary of geophysical observations in a section from the Pacific Ocean to Lake Superior. (After Archambeau et al, 1969.)	76

LIST OF TABLES

Table Title	Table No.
Member of the North American Seismic Group participating in the 1963 Lake Superior Experiment.	1
Organizations participating in Project EARLY RISE.	2
Description of rocks outcropping in vicinity of Lake Superior.	3
Plausible crustal models for the EARLY RISE shot point.	4
Travel-time anomalies (in seconds) for the October 1964 series of shots in western Lake Superior calculated from shot 49A.	5
Locations of the October 1964 shots computed using Herrin 68 travel-time tables.	6
Locations of the October 1964 shots obtained from the LRSM and Observatory network without the LRSM stations in Arizona.	7
Location of the October 1964 shots obtained from the Eastern and Western networks of stations.	8
Locations of 9 shots at Lake Superior relative to shot 49A using Spence and Alexander (1968, 1969) method.	9
Description of rocks outcropping in vicinity of Yucca Flat, Nevada Test Site.	10
A plausible crustal model for Yucca Flat area, NTS.	11
Travel-time anomalies (in seconds) for NTS computed using Herrin 1968 travel-time tables.	12

LIST OF TABLES (Cont'd.)

Table Title	Table No.
Locations of events at NTS using only LRSM stations and observatories at epicentral distances greater than 17°.	13
Locations of events at NTS using whole LRSM and observatory network.	14
Locations of 3 large events at NTS relative to Dumont (after Spence and Alexander, 1969).	15
Origin times and locations of Early Rise shots.	A-1
Origin times and locations of October 1964 shots.	A-2
First arrival data for shot 49A.	A-3
First arrival data for shot 45E.	A-4
First arrival data for shot 46A.	A-5
First arrival data for shot 45D.	A-6
First arrival data for shot 47A.	A-7
First arrival data for shot 45C.	A-8
First arrival data for shot 73A.	A-9
First arrival data for shot 45B.	A-10
First arrival data for shot 48A.	A-11
First arrival data for shot 45A.	A-12

INTRODUCTION

Between July 8 and July 30, 1963 a series of 78 chemical explosions was detonated along three shot lines in Lake Superior (Figure 1) as part of a large cooperative undertaking designed to study intensively the crust and upper mantle beneath a limited geographical region by explosion seismology. Because crustal structure deduced from explosion seismology has long been confused by the subjective judgements of the individual interpreting the data, a number of groups from institutions in the United States and Canada, collectively referred to as the North American Seismic Group (for a list of participants, see Table 1) agreed to record these shots in order to secure a number of independent interpretations. In addition, the participants agreed that the first-arrival data be made available in one place (Steinhart, 1964) and to provide access to the seismograms obtained.

The Lake Superior region was chosen because previous investigators (Steinhart and Meyer, 1961) had suggested that the shield areas of the world are especially uniform and structurally simple; other results from several previous studies of crustal structure in the area of the southern Canadian Shield surrounding Lake Superior (Slichter, 1951; Tatel and Tuve, 1952; Hodgson, 1953 a,b) lent support to this contention. However, the expected simple structure was not found. Rather, the crust under Lake Superior is probably as structurally complex as anywhere in North America. To date, the pooled first arrival data obtained during the 1963 Lake Superior Experiment have been interpreted by three groups: Smith et al, (1966a,b) and Berry and West (1966a,b) used the time term approach (Scheidtger and Willmore, 1957) whereas O'Brien (1968) used the method of matching structure to reduce the data and deduce a velocity-depth model. As is to be expected, the three models differ

significantly, although all suggest that the seismic velocities in the crust are extraordinarily high (P-wave velocities greater than 6.6 km/sec at depths of only 10 km) and that in an overall sense the structure beneath the Lake is synclinal. In the discussions which follow, we examine the validity of the assumptions underlying these three interpretations and attempt to determine what effect, if any, they might have on the derived models.

The one ton charges detonated during the 1963 Lake Superior Seismic Experiment were recorded at surprisingly large distances by stations in the LRSM and VELA observatory network (Steinhart, 1964; Mansfield and Evernden, 1966a,b; Bancroft, 1966). In October of 1964 the U.S. Geological Survey detonated a series of ten shots ranging in size from 2 to 20 thousand lbs of TNT in an experiment designed to investigate the unusually low attenuation of P-waves in the Interior Plains of the United States that was observed during the 1963 experiment and to determine whether an upper-mantle "shadow zone" for P-waves exists beneath the plains (Roller and Jackson, 1966a,b). The U. S. Geological Survey recorded these ten shots at 35 stations along a profile extending from the Bayfield Peninsula to Denver, Colorado. Roller and Jackson (1966 a,b) analyzed the travel-time and amplitude data recorded along this profile and found that the P-wave velocity increased with depth to 100 km at which depth they found a high-velocity (8.5 km/sec) layer. They also noted that the amplitude of Pn attenuated as $1/\Delta$, in contrast with the attenuation of $1/\Delta^3$ commonly observed in the western United States.

The successful observation of the 1963 and 1964 shots at large distances, plus the unusually low attenuation and high Pn velocities compared with the western United States that were

observed during the Lake Superior and other seismic experiments in the eastern United States led to a third seismic experiment at Lake Superior in 1966. Named Project Early Rise, this experiment consisted of 38 shots each of 10,680 lbs. of Dupont Nitramon WW(EL) which were detonated at a common shot point off the Keweenaw Peninsula during a twenty-one day period in July 1966 and recorded along extensive profiles which radiated outwards from the shores of the Lake (Figure 2). The recording profiles were located so that the data would yield information on the structure of the crust and upper mantle beneath the central portion of the North American continent. Ten members of the North American Seismic Group (Table 2) occupied the stations on these profiles. Warren et al, (1967) have published a compendium of first arrival data obtained during Project Early Rise.

Lewis and Meyer (1968), Green and Hales (1968), and Mereu and Hunter (1969) have interpreted some of the data collected during Project Early Rise and their results indicate that the structure of the upper mantle beneath the Canadian Shield is quite different from that beneath the western United States as found by Niazi and Anderson (1965), Johnson (1967) and Archambeau et al, (1969). Thus in comparing Lake Superior as a seismic source region with the Nevada Test Site we must examine the regional setting of the two areas. To accomplish this, we have attempted to summarize what is currently known about the physical properties of the crust and upper mantle beneath the two areas and derived geophysical models for the crust beneath the Early Rise shot point and Yucca Flat, Nevada Test Site.

In constructing possible crustal models for the Early Rise shot point and the Yucca Flat area of the Nevada Test Site we show the range of uncertainty in the various parameters where

they are known. We should point out, however, that we have been unable to apply any tests for uniqueness to these models. Nevertheless, in view of the constraints placed on the possible choices by the varied data which we consider, we believe that the models are sufficiently representative of the crust and upper mantle in the two areas to serve as a basis for comparison of the two source regions.

PHYSICAL SETTING OF LAKE SUPERIOR EXPERIMENTS

Geologic Environment

The Relationship of Lake Superior to the Canadian Shield

The Canadian Shield forms a large stable area of more than two million square miles in the northeastern part of North America (Figure 3). A shield is typically an area of Precambrian igneous and metamorphic rocks which have been eroded to a convex surface with little relief and overlain at its margins by much younger gently dipping sedimentary rocks which increase in thickness away from the shield. Where these sediments attain considerable thickness, the rocks of the shield form the basement. These latter areas which have remained relatively unaffected by later orogenies are generally referred to as stable continental interiors, or in the case of the United States, the Interior Lowlands (King, 1959, p. 23).

The Canadian shield departs from the ideal case in several important ways as a result of Phanerozoic deformations (King 1959, p. 11). Beginning in Cretaceous time (King, *ibid.*) the northeastern part of the shield underwent severe deformation which, continuing through the Tertiary, resulted in the dissection and uplift of the present day northeastern margin of the shield to form the Torngat Mountains of Labrador and the mountainous peaks of Baffin Land. The relationship of Greenland to the Canadian Shield is problematical. However if Greenland once constituted part of the shield, it is likely that it was separated from the major part of the shield at the same time that the "mountains" formed. During the Pleistocene and Recent, the Canadian Shield was subjected to glacial loading which resulted in its being depressed beneath the center of the ice caps. Of the three ice caps which originally covered the shield, only the ice cap on Greenland remains.

Glacial erosion considerably altered the topography of the shield, denuding it of much of its sedimentary cover and forming the many small lakes of the shield's interior and the much larger lakes (the Great Lakes) along its margins. The Canadian Shield conforms more closely to the definition of a shield area along its southern, south-east and south-west borders (King, 1959, p. 10). Here the shield passes beneath the sedimentary rocks of the Interior Lowlands whose scarps face the interior of the shield.

Seismological studies of the crust and upper mantle beneath the Canadian Shield reflect this long period of relative stability. Brune and Dorman (1963) studied phase velocities for fundamental mode Love and Rayleigh waves along extended paths across the Canadian Shield supplemented by group velocity data and travel times for body waves. Figure 4 shows the model CANSND which best fits their data. Brune and Dorman found that the crust was relatively uniform over the shield and could be approximated by a three-layer crust some 35 km thick. Shear wave velocities in the upper mantle indicate a low-velocity zone about 200 km thick beginning at a depth of 115 km where the shear wave velocity decreases by 0.2 km/sec. CANSND shows the P-wave velocity slowly increasing with depth from 8.1 km/sec at the Moho to 8.3 km/sec at 315 km where there is a sharp increase to 8.7 km/sec.

Recently Barr (1967) has published the results of a study of P-wave data from chemical explosions in Hudson Bay and Lake Superior. Figure 4 also shows his proposed model for P-wave velocities in the upper mantle beneath the Canadian Shield. The discontinuities in P-wave velocity are determined from the positions of cusps in the observed travel-time data. The depths of the discontinuities in P-wave velocity are in close agreement with the depths of the discontinuities in S-wave velocity found by Brune and Dorman (1963). Barr (1967)

finds no evidence for a P-wave low velocity zone and concludes that the P-wave velocity structure in the upper mantle is comparatively uniform across the Canadian Shield.

Heat flow measurements in continental shield areas, including the Canadian Shield, reflect their geologic stability. In a review of heat flow data Lee and Uyeda (1965) concluded that the global mean heat flow is $1.5 \pm 10\%$ $\mu\text{cal}/\text{cm}^2\text{-sec}$ at 95% confidence level. They found no significant difference between the mean oceanic and mean continental heat flow but concluded that in general, regional heat flow variations greater than $0.2 \mu\text{cal}/\text{cm}^2\text{-sec}$ are significant. For the Canadian Shield, Lee and Uyeda found a mean heat flow of $0.9 \pm 0.1 \mu\text{cal}/\text{cm}^2\text{-sec}$ for 145 measurements made in Lake Superior as reported by Steinhart et al, (1968). The low heat flow in the Canadian Shield is not due solely to the effects of Pleistocene glaciation since the mean for seven determinations of heat flow in the Australian Shield, which was not glaciated, is $1.0 \pm 0.1 (5) \mu\text{cal}/\text{cm}^2\text{-sec}$ (Lee and Uyeda, 1965). Rather, low heat flow values, $0.9 \pm 0.2 \mu\text{cal}/\text{cm}^2\text{-sec}$, are characteristic of shield areas throughout the world. Considering that shield areas have an abundance of radiogenic rocks in the crust (granites, gneisses, etc.) which contribute to the measured heat flow, the mantle heat flow under the shields must be very low indeed compared to oceanic and tectonically active areas.

Although the Canadian Shield has behaved as a single entity since Cambrian times it is composed of a series of provinces with different ages, structural histories and lithologies. The shield is presently divided into seven geologic provinces (Figure 3). Radiometric dating (Stockwell 1962, 1964) has shown that the rocks of the Superior Province were

involved in the Kenoran orogeny 2.5 ± 0.1 b.y. ago, those of the Churchill Province in the Hudsonian orogeny 1.7 ± 0.1 b.y. ago, and those of the Grenville Province in the Grenville orogeny 0.9 ± 0.06 b.y. ago.

Data obtained in recent seismic refraction surveys suggests that the gross crustal structure and thickness also varies among the three major provinces. Mereu and Hunter (1969) in an analysis of data obtained during Project Early Rise (Warren et al, 1967) conclude that the crust is 30 - 35 km thick under the Superior Province to the west of Hudson Bay whereas under the Churchill Province to the north it is greater than 40 km thick. The indicated increase in crustal thickness takes place across a region about 200 km wide to the north of the Nelson River and correlates with a large linear gravity anomaly (Innes, 1960). Mereu and Hunter (1967) suggest that a model consisting of a single 6.3 km/sec layer for the crust, a P_n velocity of 8.05 km/sec and a 8.43 km/sec layer at a depth of 84 ± 3 km is required to fit their data.

The crustal thickness of 40 km found by Mereu and Hunter (1969) to the west of Churchill agrees with the earlier results of Hunter and Mereu (1967), Ruffman and Keen (1967), and Hobson et al, (1967). These authors interpreted the travel-times recorded during the 1966 Hudson Bay Experiment (Figure 5) and though specific details in interpretation differ among the three papers, all conclude that the crust is approximately 40 km thick at Churchill (Figure 5), decreases to 25 - 30 km 150 km west of the Ottawa Islands and then increases rapidly to 40 km again under Povungnituk. The data from the N-S profile suggest that the crust is 25 - 30 km thick under Chesterfield Inlet and increases in thickness to 35 - 40 km in the center of the bay. The rapid 12 km increase in crustal thickness to the west and north of Ottawa Island corresponds

to the projection of the Superior-Churchill province boundary eastwards beneath the Hudson Bay. The data also indicate a single layered crust with a velocity of 6.3 km/sec covered by a thin veneer of Phanerozoic sediments which occupy the sedimentary basin which forms the Hudson Bay. This sedimentary basin is not reflected in the Moho topography which consists of a N-S trending trough superimposed upon an E-W oriented saddle. All three papers report a P_n velocity of 8.2 to 8.3 km/sec beneath the Hudson Bay.

Thus, geophysical studies to date indicate that the upper mantle beneath the Canadian Shield is laterally relatively uniform. The crustal structure however is not laterally uniform. The various provinces recognized by geologists appear to have differences in gross crustal structure which extend to the base of the crust. The greater part of Lake Superior is situated in one of these provinces, the Southern Province, along the southern margin of the shield. There is every indication that crustal structure beneath the Lake is as complicated as anywhere else in the Canadian Shield.

Geology of the Lake Superior Basin

The geology of the Lake Superior region has been under investigation for more than a century. Excellent accounts of the earlier work can be found in Lane (1911), Van Hise and Leith (1911), and Butler and Burbank (1929). More up-to-date accounts which take into consideration recent geophysical data can be found in White (1966a, 1966b) and Halls (1966). These geologic data and their interpretation provide the background necessary to interpret the results obtained during the 1963-4 Lake Superior Experiments and Project Early Rise of 1966.

Rocks outcropping in the immediate vicinity of Lake Superior can be divided into four groups in order of increasing age:

1. Recent glacial deposits
2. Paleozoic sediments
3. Keweenawan rocks
4. pre-Keweenawan rocks

Figure 6 shows the areal distribution of pre-glacial rocks in the region. Table 3 summarizes the pertinent stratigraphic data. Cores taken in the Lake itself (Zumberge and Gast, 1961; Zumberge, 1962) suggest that the Cambrian rocks which outcrop along the southeast shore of Lake Superior extend beneath parts of the lake.

The oldest rocks outcropping in the Lake Superior region are the Archean rocks of the Ontarian and Timinskamian (Halls, 1966) or Timiskaming (Stockwell, 1964) and thus are older than 2.4 b.y. These rocks then formed the basement of an E-W trending geosyncline which occupied much of the western part of the present day lake and probably extended eastwards along the northern shores of Lake Huron. The lack of Animikean or Huronian rocks, the structural trend, and the Kenoran dates of the rocks exposed along the eastern shore of Lake Superior suggest that the Penokean orogeny did not extend into western Ontario. Deposition of Animikean rocks and their equivalents in this trough terminated with the Penokean orogeny 1.8 - 1.6 b.y. ago which is equated by Stockwell to the Hudsonian orogeny in the Churchill province to the north. The Animikean rocks along the northern shore of Lake Superior were only slightly deformed by the Penokean orogeny, the deformation being more intensive in central Minnesota, northern Michigan, and Wisconsin.

After a short period of erosion a large structural basin

developed in which lower Keweenawan sediments accumulated. These are overlain by a very thick series of basic lava flows, the Middle Keweenawan lavas. The sources for the lavas have not been recognized. Subsidence of the Lake Superior basin kept pace with the eruption of the lavas (White, 1966b), and continued after the volcanism had stopped and the deposition of the Upper Keweenawan sediments began. The Keweenawan lavas are intruded by the Duluth Gabbro which has a radiometric age of 1.0 b.y. The lavas are thus younger than 1.6 b.y. and older than 1.0 b.y. The age of the Upper Keweenawan sediments is uncertain. They are younger than the lavas, but sedimentation in the Lake Superior basin continued into the Cambrian (Hamblin, 1961) with only minor interruptions, which suggests that they were deposited between 1.0 b.y. and 0.6 b.y. ago.

Lake Superior itself is a large (83,000 km²) temperate fresh-water lake with a mean depth of 150 m and a maximum depth of 400 m. (Hart and Tilton, 1966), which occupies the greater part of the Keweenawan basin. Figure 7 shows the configuration of the bottom topography. In the west the lake bottom is strongly asymmetric being deepest along the Minnesota shore, whereas in the eastern sector the lake bottom is made up of a series of ridges and troughs orientated approximately N-S. These latter features are probably the result of glacial scouring (Wold and Ostenso, 1966).

At the present day the Keweenawan rocks form a large syncline first recognized by Irving (1883), most of which is covered by the lake (Figure 6). In the western half of the lake the inferred synclinal axis trends NE. Off the Keweenaw Peninsula it trends E-W, and in the eastern half of the lake it trends NW-SE. There is strong evidence from gravity, aeromagnetic, borehole and seismic data (Lyons, 1959;

Theil, 1956; Craddock et al, 1963; Zietz, 1965; Cohen, 1966; Cohen and Meyer, 1966), that the Keweenaw rocks continue southwards from the southwest end of Lake Superior in a narrow trough as far as Kansas and that they are closely associated with the mid-continent gravity high (Woollard and Joesting, 1964). Gravity data obtained by Bacon (1957) tentatively suggest that the Keweenaw rocks persist southward from the eastern end of the Lake also.

Although the gross structure of the Lake Superior region has been known for some time, the details of the structure are still poorly known. White (1966b) has interpreted the structure between Isle Royale and the Keweenaw Peninsula from geologic data. His interpretation is shown in Figure 8. White gives the permissible range of thickness for the sedimentary rocks as 3 to 7 km. The inferred thickness of the sedimentary section is dependent upon how the dip of the upper surface of the Keweenaw lavas is extrapolated; the most probable thickness is 5km. The total thickness of the lavas is unknown, but White (1966b) estimates them to be 6.5 km thick on Keweenaw Point and 4.5 km thick on Isle Royale based on Lane's (1911) stratigraphic correlation between the two outcrops, although White points out that they may be as thick as 9.5km.

Geophysical Evidence on Crustal Structure Under Lake Superior

Seismic refraction, gravity and aeromagnetic surveys have been conducted in the vicinity of Lake Superior in recent years. Since 1963 extensive seismic refraction, underwater gravity, magnetic and heat flow surveys have been made in the lake itself. The results of much of this work are published in Monograph 10 of the American Geophysical Union (Steinhart and Smith, 1966) and the Carnegie Institution of

Washington Year Books for 1963 through 1967. Because the seismic data are of primary concern in this report, we shall examine them first and attempt to discriminate among those crustal models which fit the seismic data by using the remaining geophysical and geological data.

Seismic Measurements

Refraction Studies. - The 1963 Lake Superior Seismic Experiment consisted primarily of a series of one ton shots fired along a line from Duluth to Otter Cove (Figure 1), which were recorded by a number of stations (Figure 9) situated at either end of the profile. In addition, data were obtained from two secondary profiles, the Bayfield Peninsula-Sibley Peninsula profile also referred to as the Gambler Line in some publications, and the Keweenaw Peninsula-Michipicoten profile or South Line. Steinhart (1964) has published shot locations and origin times, station locations, and first arrival data from this experiment.

When the first arrival data for stations at either end of the profile are plotted as reversed travel-time distance plots (for example, see Smith et al., 1966a; Berry and West, 1966a) it is clear that a simple dipping-layer model is inadequate to explain the observations. In an attempt to overcome these difficulties, Berry and West (1966a,b) and Smith et al., (1966a,b) have interpreted the first arrival data using the time-term method, originally described by Scheidegger and Willmore (1957).

The velocity-depth crustal models obtained by Berry and West and Smith et al., are shown in Figure 10. Both models are for the main profile orientated approximately E-W (Figure 1). Each model has a two layer crust, although the thickness and velocity of the two layers varies between the two models. The

models are in agreement to the extent that they show a considerable thickening (some 15 - 20 km) of the crust to the east of the Apostle Islands. The Berry and West model (Berry and West, 1966a,b), has an upper layer about 3 - 5 km thick under the shores of the lake with an assumed velocity of 5.5 km/sec which attains a maximum thickness of 12 km west of the Apostle Islands. The lower crustal layer has an assumed velocity of 6.6 km/sec. The depth to the Moho is 30 km at the western extremity of the profile decreasing to 26 km off the western shore of the lake and increasing to a maximum of 57 km approximately 70 km west of Otter Cove; to the east of this point the crustal thickness decreases abruptly to 48 km. Smith et al, (1966a) interpret this sharp change as a fault.

The upper layer of Smith et al,'s model (Figure 10) shows considerable lateral variation in both velocity and thickness. The thickness is roughly constant at 5 km under the lake, but increases rapidly to more than 10 km to the east of Otter Cove. The velocity in this layer (assumed) varies laterally from 4.8 km/sec to 6.2 km/sec. The lower crustal layer everywhere has a velocity of 6.8 km/sec. Depths to the Moho are similar to Berry and West's model. They range from 35 km under station Zipgun, to 28 km under the western shore of the lake, increasing rapidly to 63 km some 70 km west of Otter Cove. Again there is a sharp decrease in depth at this point of around 10 km, and the depth to the Moho continues to decrease eastwards to 30 km under Foylet. The P_n velocity of 8.07 km/sec closely agrees with the 8.1 km/sec found by Berry and West.

The Lake Superior Seismic Experiment, as conducted, does not meet the theoretical requirements of the time-term method rigorously. In particular, the P_n time-terms for shots close to either end of the lake were obtained mainly from stations located on only one side of the shot. The structure of the

crust-mantle interface from the P_n time-term analysis is thus considerably exaggerated and displaced westward by approximately 70 km (O'Brien, 1968) since there was a preponderance of recording stations along the western shore of the lake. O'Brien (1968) has reinterpreted the data from the 1963 Lake Superior Experiment using the method of matched profiles. (O'Brien's model, again for the main E-W profile, is also shown in Figure 10).

The upper layer in O'Brien's model is 6 - 8 km thick and represents the near surface rocks. The velocity in this layer varies laterally from 4.7 km/sec to 4.9 km/sec, and was determined rather than assumed. This surface layer is underlain by a single layer, the upper-surface velocity of which varies laterally from 6.6 km/sec to 6.7 km/sec and in which the velocity increases slightly with depth to 6.75 km/sec at the base of the crust. The depth to the Moho ranges from 45 km under the western shore of the lake to 35 km off the Bayfield Peninsula, increases to a maximum of 54 km approximately 130 km west of Otter Cove and then decreases to 42 km under the eastern shore of the lake. The weighted mean crustal velocity for this model is 6.75 km/sec which agrees well with the 6.85 km/sec which O'Brien obtained from t^2-x^2 analyses of wide-angle reflections from the Moho, the 6.8 km/sec used by Smith et al, to convert the P_n time-terms to depths, and the 6.9 km/sec layer at a depth of 8 km under the western half of Lake Superior reported by Anzoleaga et al, (1969).

O'Brien also discusses a three layered crustal model, the third layer of which has a velocity of around 7.0 km/sec. This model (Figure 11) is based on intra-crustal reflections recorded at Otter Cove, Tom, and Woodsman. The depth to the reflector is 15 km near the eastern shore and 25 km in the east-central sector of the lake. In addition, O'Brien attributes

late arrivals recorded at stations X-ray and Tyro in the western sector of the lake to reflections. However, these arrivals are more scattered and could not be correlated over any distance. The records at the stations Yankee and Victor did not show distinct reflections, but the amplitudes of the first arrival were 10 times those recorded at stations Tyro, Woody, and X-ray. Similar large amplitudes were also found by Roller and Jackson (1966a) to the southwest of the lake. O'Brien suggests that these are due to reinforcement of the first arrival by the reflection on account of the small travel-time difference between these two phases at this distance.

The small amplitude of the reflections in the eastern section of the lake suggests that they may be due to a second-order discontinuity in velocity. Until additional evidence is forthcoming, we prefer the two layer model. The wide angle reflection data does indicate, according to O'Brien (1968), that the P-wave velocity increases with depth beneath the lake and suggests that there are no low velocity layers present within the crust.

Over the period 1964 to 1967 the University of Wisconsin continued shallow seismic refraction profiling in the western half of Lake Superior. Anzoleaga et al, (1969) have interpreted the shallow structure from 4 profiles along the line of the 1963 Knife River, Minnesota to Otter Cove, Ontario (Figure 12) profile using the gravity data of Wold (1968) as a constraint. Figure 13 shows the model derived by Anzoleaga et al, (1969). The shallow structure above the upper refractor of Smith et al, (1966a, 1966b) is divided into three layers with P-wave velocities of 3.3 - 3.5 km/sec, 4.5 - 4.7 km/sec and 5.4 - 5.6 km/sec respectively which pinch out under the Minnesota shore of the lake against a 6.5 km/sec dipping layer. The

structure shows a thickening of all three layers centered some 150 km from the Knife River station to form a basin, the position of which is coincident with the gravity low mid-way between the Bayfield Peninsula and Isle Royale (Figure 17). Anzoleago et al, (1969) find a velocity of 6.9 km/sec for the upper refractor, which is in agreement with the velocity of 6.8 km/sec found by Smith et al, (1966a, 1966b) and the 6.75 - 6.85 km/sec reported by O'Brien (1968). From its spatial configuration, the 6.5 km/sec layer probably represents the Duluth Gabbro. The remaining three layers above the 6.8 - 6.9 km/sec refractor are probably the Upper Keweenawan sediments and the Keweenawan lavas.

O'Brien's model gives a two-dimensional view of crustal structure along an E-W line through Lake Superior. In an attempt to define the structure of the Lake Superior basin in three dimensions, we have plotted fence-diagrams, Figure 14, showing crustal structure in the vicinity of Lake Superior based on the results of earlier workers in this area and the data obtained during Project Early Rise. To the south of the lake the work of Steinhart et al, (1961) indicates total crustal thicknesses ranging from 36 - 42 km and P_n velocities of 8.1 km/sec. The crustal models obtained by Steinhart et al, (1961) suggest that the arrivals can be explained by a two-layer crust consisting of a thin layer with a P-wave velocity of 4.6 - 5.5 km/sec overlying a thicker layer with a velocity of 6.3 - 6.4 km/sec. However, there were indications in North Central Wisconsin that the deeper layer should be considered as two layers with velocities of 6.1 and 6.5 km/sec, and for the Keweenaw Profile, Steinhart et al, (1961) suggest that two layers with velocities of 6.4 and 6.7 km/sec are indicated. To the southwest of Duluth, Cohen (1966) and Cohen and Meyer (1966) found crustal thicknesses of 46 km along the axis of the Midcontinental Gravity High, with a 6.5 - 6.6/sec layer

occurring at a depth of 1.8 km and an apparent P_n velocity of 8.1 km/sec. R. P. Meyer (personal communication, 1969) has re-examined this data and believes that velocities as high as 6.9 km/sec may be appropriate for the major crustal layer. Along the gravity low flanking the eastern margin of the high, Cohen (1966) and Cohen and Meyer (1966) found velocities similar to those found along the axis of the high, however the 6.5 - 6.6 km/sec layer occurs at a depth of 4.6 km and the crustal thickness is only 42 km. In an analysis of travel-time data from Early Rise, Mereu and Hunter (1969) found that to the north and east of Lake Superior the crust is 30 - 35 km thick under the Superior Province of the Canadian Shield, thickening to greater than 40 km under the Churchill Province. They found mean velocities along a profile north of Lake Superior for $P_g = 6.30$ km/sec and $P_n = 8.05$ km/sec.

Thus, the Lake Superior crustal syncline, on the basis of the refraction data presented above, is clearly delineated. Figure 15 is a contour map of the Moho depth in the vicinity of Lake Superior based solely on the refraction data discussed above. The high mean crustal velocities, 6.7 - 6.9 km/sec, found under Lake Superior have not been reported from areas outside the lake with one exception. Recent examination of refraction data recorded along a path entirely within the Midcontinental Gravity High to the southwest of the lake suggests that the high velocities of 6.9 km/sec at depths of 8 km beneath the lake reported by Anzoleaga et al, (1969) may be present along axis of the Midcontinental Gravity High (R.P. Meyer, personal communication, 1969).

Surface Wave Dispersion Observations. - We have been unable to find any published observations of surface wave dispersion across Lake Superior. Brune and Dorman (1963) have published curves showing Love and Rayleigh dispersion across

the Canadian Shield and derived a model (Figure 4) based on their observations. However, none of the paths studied by Brune and Dorman cross the lake. Additional data are provided by Pilant (1967) who studied Rayleigh wave dispersion in North America. Pilant measured phase and group velocities using the WWSSS network and prepared a series of contour maps showing observed fundamental mode phase velocities over North America as a function of period. We have taken the values at Lake Superior and plotted them together with the theoretical dispersion curve predicted by Brune and Dorman's model CANSD. Figure 16 shows the results.

Pilant's observed values fall systematically below the theoretical curve at periods shorter than 50 seconds. However, we can attach no great significance to this since the deviation from the theoretical curve is less than the contour interval of Pilant's data.

Because the mean crustal thickness, the mean crustal P-wave velocity and hence by inference the mean shear wave velocity and density are different beneath Lake Superior from those incorporated in the model CANSD, we do not anticipate that the CANSD phase velocity dispersion curve shown in Figure 16 will be representative of the Lake Superior region. This can be seen from the theoretical dispersion curve also shown in Figure 16 which was computed for a composite Lake Superior model (Table 4) derived from seismic refraction and gravity observations.

Gravity Data

During September 1964 the Dominion Observatory of Canada conducted a reconnaissance underwater gravity survey in Lake Superior (Weber and Goodacre, 1966). Additional data along

the south shore of the lake and in Keweenaw Bay were collected in August 1964 by the University of Wisconsin (Wold and Ostenso, 1966). Weber and Goodacre have computed Bouguer anomaly values from these data and presented a contour map showing Bouguer anomalies in the Lake Superior region at 10 mgal intervals. The anomalies over the lake were joined to existing gravity maps of the areas surrounding the lake, (Innes, 1960; Woollard and Joesting, 1964; McConnell, 1966). The resulting map (Weber and Goodacre, 1966, Figure 2) covers the area 45 - 50°N, 83 - 93°W.

Since 1964 the University of Wisconsin has completed a gravity survey of Lake Superior on a 5-mile grid, occupying some 1600 stations (Wold, 1968). Although there are some minor differences in detail between Wold's map and the earlier results of Weber and Goodacre (1966), the overall features are similar (R. J. Wold, personal communication, 1969).

In order to examine the relationship between the gravity field at Lake Superior and the surrounding area on a regional basis, we have compiled a Bouguer anomaly map of the area 38 - 57°N, 79 - 104°W (Figure 17). The base map scale was $1:2.5 \times 10^6$ to correspond to scales of geological, tectonic, and gravity maps of the United States published by the U. S. Geological Survey. The contour interval is 10 mgal. The majority of the data are from the sources quoted by Weber and Goodacre (1966) with additional data from a series of maps compiled by the Dominion Observatories Branch, Department of Mines and Technical Surveys, Ottawa, Canada.

The most conspicuous feature on the gravity map is the Midcontinental Gravity High which runs northeast from Kansas through Iowa and appears to terminate south of the Bayfield Peninsula in Wisconsin. It is composed of four elongate areas

of strong positive Bouguer anomalies flanked by regions of pronounced negative anomalies. Black (1955) has interpreted these anomalies as indicating "an echelon rift pattern developed in the crust during late Precambrian time and genetically related to the development of the Lake Superior geosyncline during the Proterozoic". However, the relative lows which separate the highs could equally be due to thinning of the perturbing body since the magnetic anomalies associated with the high do not show signs of appreciable offset.

Seismic refraction studies (Cohen, 1966; Cohen and Meyer, 1966) on the Midcontinental Gravity High indicate that the crust is somewhat thicker (46 km) than in the surrounding areas (42 km). They also indicate high velocity rocks at shallow depths under the high and somewhat deeper under the lows. Cohen and Meyer (1966) found rocks with P-wave velocity of 6.5 km/sec under the high. However, recent data suggest that the 6.9 km/sec rocks found beneath Lake Superior (Anzoleaga et al, 1969) may be present at shallow depths under the high (R. P. Meyer, personal communication, 1969). The gravity lows correlate well with the thick accumulations (up to 5.0 km) of low velocity sediments found by Cohen and Meyer (1966).

The seismic studies support the hypothesis postulated by Thiel (1956) and Craddock et al, (1963) that the positive anomalies are due to thick accumulations of Keweenaw volcanic rocks in a synclinal trough which has been uplifted to form a horst and that the negative anomalies flanking the highs are due to thick accumulations of low density sediments.

To the southwest of the Bayfield Peninsula the Bouguer anomalies change from +60 mgal to -80 mgal over a distance of 100 km. In this region the synclinal axis of the Lake Superior syncline swings E-W before turning NE-SW and passing under the lake between the Bayfield and Keweenaw peninsulas. The reversed

faults which bound the horst, the Douglas Fault to the north and the Lake Owen fault to the south, also swing E-W in this area (Figure 18).

The large negative gravity anomaly over the Bayfield Peninsula correlates with a large accumulation of Upper Keweenaw sediments whose thickness has been estimated by White (1966) as 7 - 9 km. To the east of the Bayfield Peninsula there is a region of broad positive anomalies which extends from the Porcupine Mountains and the Keweenaw Peninsula to Isle Royale. To the west of the Bayfield Peninsula there is a large positive anomaly centered over the Minnesota shore.

Apart from three small closed highs centered over Michipicoten Island, over Marathon, and to the south of Isle St. Ignace, the remainder of the anomalies over Lake Superior are negative. The mean Bouguer anomaly over the lake is -25 mgal as compared to the average value of -45 mgal over the surrounding highlands (Weber and Goodacre, 1966).

The gravity high over the Minnesota shore of Lake Superior correlates with the outcrop of the North Shore Volcanics which are intruded by the Duluth Gabbro, a lopolithic body which from geologic evidence thins lakewards from the shore. If the 6.5 km/sec layer in Figure 13 represents the Duluth Gabbro, then the seismic refraction data of Anzoleaga et al, (1969) are consistent with this interpretation. According to White (1966a) the Keweenaw rocks to the east of Beaver Bay complex are separated from those under the rest of Lake Superior by a narrow ridge in the pre-Keweenaw surface over which the lavas thin. However, the gravity data suggest that the structure is more complicated than this.

The closed circular low NW of the Bayfield corresponds to

a relatively thick sedimentary basin filled by low velocity sediments (Anzoleaga et al., 1969) occupying a 50 km wide depression in the upper surface of the Keweenawan lavas which themselves appear to occupy a trough in the pre-Keweenawan surface.

The origin of the positive anomaly between the Keweenaw Peninsula and Isle Royale is more uncertain. There are steep gradients in the Bouguer anomalies over the Keweenaw fault and the Isle Royale fault. These faults (Figure 18), are reversed or thrust faults which, by analogy with the structure southeast of Ashland, suggest that the lavas occupy a synclinal trough which has been uplifted to form a horst. However, O'Brien's (1968) interpretation of the structure along the 1963 main line profile shows a decrease in thickness of the upper layer of his model through this region. This is somewhat surprising since the profile is coincident with the inferred synclinal axis at this point, although uplift and erosion of the syncline as suggested above could account for such a result.

The gravity data from the eastern sector of the lake indicate a quite different structure from that in the western sector. The broad negative anomalies suggest thick accumulations of sediments. However, the mean anomaly over the lake is positive with respect to the surrounding areas of the shield (-25 mgals vs. -45 mgals) which together with the known outcrops of Keweenawan lavas on Michipicoten Island and the eastern shore, suggest that lavas are present at depth beneath eastern Lake Superior. This interpretation is consistent with the seismic data discussed earlier and the aeromagnetic data discussed below.

Aeromagnetic Data

Wold and Ostenso (1966) and Hinze et al, (1966) have compiled a total magnetic intensity map of the Lake Superior region from some 22,000 km of flight lines spaced at 9.6 km intervals. Their map is reproduced as Figure 19. From this data Wold and Ostenso (1966) have interpreted the geologic structure under the western half of the lake and Hinze et al. (1966) have interpreted the structure under the eastern section. Together their interpretations supplement the evidence from seismic and gravity data above.

In the western section of the lake the magnetic anomalies indicate a broad closed low which extends from the Bayfield Peninsula to the north of the Keweenaw Peninsula. Flanking the magnetic low to the north and south there are a series of magnetic highs. Along the south shore of the lake these highs correlate with the Keweenawan lavas in the upthrust block between the Douglas and Lake Owen faults and the Keweenawan lavas exposed to the north of the Keweenaw fault on the Keweenaw Peninsula. North of the low, the positive anomalies correlate with exposures of the Duluth Gabbro and the North Shore Volcanics. The positive anomaly over Isle Royale correlates with the exposures of lakeward dipping Keweenawan lavas.

The magnetic low is evident in the N-S aeromagnetic profiles across the western half of the lake (Figure 20) which are remarkably smooth. The broad low correlates with the inferred synclinal axis and the smoothness of the negative anomalies suggest that the trough is occupied by a thick section of sediments. The trend of the anomalies in the vicinity of the Bayfield Peninsula is consistent with the interpretation of White (1966a) who suggested that the horizon which gives rise to these particular anomalies is high within the sequence of Keweenawan lavas and outlines the nose of a NE

plunging syncline. The results of this detailed survey support White's (1966a) postulate that the lavas thin over a N-S ridge in the pre-Keweenawan surface between the Bayfield Peninsula and Beaver Bay which White had suggested on the basis of data collected from eleven reconnaissance profiles across the lake.

To the east of the Keweenaw Peninsula, the character of the anomalies changes markedly. The anomalies in this area form a series of closed highs and lows (Figure 21). However, the magnetic low in the western part of the lake can be traced east of the Keweenaw Peninsula where it swings approximately N-S and extends into the Northern Peninsula of Michigan suggesting that the sedimentary basin does also. The magnetic anomaly minimum, B, of Figure 21 also correlates with a Bouguer gravity anomaly minimum (Bacon, 1957), further supporting this interpretation of the magnetic anomaly (Hinze et al, 1966.)

The positive anomaly, C, in Figure 21 correlates with the exposures of Keweenawan volcanics along the Keweenaw Peninsula and its axis also swings through E-W to join with the N-S trending axis of anomaly D which is a continuation of anomaly C (Hinze et al, 1966) extending south at least as far as the northern shore of Lake Michigan. The configuration of anomaly D indicates that the volcanics dip eastwards and are more deeply buried to the south.

Along the northern and eastern shores of Lake Superior there are a series of six positive anomalies. Anomaly E is a continuation of the anomaly associated with the Keweenawan lavas outcropping on Isle Royale. The configuration of the Anomaly E indicates that the lavas dip SW (Hinze et al, 1966) into the Keweenawan syncline. This anomaly is separated from anomaly G by the Isle Royale thrust fault. The configuration of anomaly G indicates that the lavas dip toward the axis of

the basin (Hinze et al, 1966). Anomaly F correlates with the outcrop of Keweenaw lavas on Michipicoten Island, which suggests that the source of the anomaly is a sequence of basic volcanics dipping westward into the basin (Hinze et al., 1966). To the north anomaly F merges into another magnetic high, anomaly F passes into the E-W trending anomaly H, which Hinze et al, 1966 interpret as being due to an uplifted block of volcanics overlain by a thin veneer of clastic sediments. The southernmost anomaly I correlates with the Keweenaw volcanics of Maimainse Point, which dip at 30° towards the lake (Thompson, 1953). From the magnetic data, the volcanics appear to extend beneath Whitefish Point. Anomaly J is similar in shape to I but has no expression in the surface geology.

The aeromagnetic profiles also indicate the extent of faulting within Lake Superior. We have combined Wold and Ostenso's interpretation of the structure of the western half of Lake Superior with Hinze et al.'s interpretation of the structure of the Lake Superior Basin. Firstly, in the western half of the lake the magnetic data clearly delineate the thrust faults which bound the upthrust central block of the syncline. Secondly, although the aeromagnetic data indicate that the syncline is continuous under the eastern part of the lake, they suggest that the structure is somewhat different. The thrust faults which parallel the synclinal axis in the western part of the lake give way to a series of faults which cut across the structure east of the Keweenaw Peninsula. And thirdly, the magnetic data suggest that either the Douglas Fault dies out beyond central Bayfield County or that it continues at great depth and has small displacements (Patenaude, 1966). There is no evidence from the aeromagnetic data to suggest that the Isle Royale Fault is an extension of the Douglas Fault.

Heat Flow Observations

The Carnegie Institution of Washington began a regional heat flow survey of Lake Superior in 1966 which they completed in 1967. The results of this survey are shown in Figure 22 which is taken from Steinhart et al., (1968). Although the mean value of the measurements ($1.0 \pm 0.2 \mu\text{cal}/\text{cm}^2\text{-sec}$) is in good agreement with the mean heat flow over the Canadian Shield, the range of the observations (0.5 to $1.5 \mu\text{cal}/\text{cm}^2\text{-sec}$) is quite large; rapid variations in heat flow taking place over a few tens of kilometers. Steinhart et al., (1968) conclude that these variations are not due to measurement errors which only account for deviations of 10% nor are they due to errors related to topography, etc., which contribute less than 10% to the observed variations. If these conclusions are correct, then the variations in heat flow must reflect variations in structure beneath the lake.

Steinhart et al., (1968) divided the heat flow patterns in Lake Superior into three anomalies (see Figure 22). The first of these, the "north shore low" with heat flow values of $0.5 - 0.9 \mu\text{cal}/\text{cm}^2\text{-sec}$ correlates with known exposures of Keweenaw lavas and with near surface occurrences of the lavas as inferred from gravity and magnetic data. In the eastern and central part of the lake the "central high" with heat flow values of $1.0 - 1.5 \mu\text{cal}/\text{cm}^2\text{-sec}$ correlates with the gravity and magnetic anomalies associated with the Upper Keweenaw sediments. In the western part of the lake the heat flow high correlates only with the magnetics (Steinhart et al, 1968). The third anomaly, the "central low" is characterized by heat flow values between 0.8 and $1.0 \mu\text{cal}/\text{cm}^2\text{-sec}$. Although there are lavas exposed along the Keweenaw Peninsula where the heat flow is low there are no gravity or magnetic

highs which correlate with the closed heat flow low to the northeast of the peninsula.

The broad correlation of heat flow anomalies in Lake Superior with the near surface geology suggests that the lateral variations in lithology of the upper 10 km of the crust may be sufficient to explain the observed differences in heat flow. Steinhart et al, (1968) state that although such a model could qualitatively explain the observations, quantitatively it would require that the Oronto group of sediments have the equivalent radioactivity of a granite. Despite this objection, Steinhart et al. (1968) ascribe the heat flow anomalies to variations in composition of the upper 10 km of the crust, claiming that variations in total crustal thickness alone are insufficient to account for the wide range of the observations.

The fact that the broad heat flow anomalies seem to correlate with the synclinal structure of Lake Superior, with high values occurring along the axis of the syncline and low values on the flanks can be explained simply by the geometry of the synclinal structure in the crust. One can show that the synclinal axis should exhibit the highest heat flow values assuming a laterally uniform temperature at depth (the Moho, say) below the syncline. The maximum lateral variation in heat flow depends on the "wave-length" of the syncline in cross-section and the "amplitude" of its undulation. The same effect would explain the correlation of smaller anomaly highs with topographic lows in the lake bottom and vice versa but not the observed magnitude of the anomalies.

Seismicity of the Lake Superior Region

To determine the seismicity of the Lake Superior region, we searched the Preliminary Determination of Epicenters cards published by the U. S. Coast and Geodetic Survey for events occurring in the area $45 - 52^{\circ}\text{N}$, $80 - 100^{\circ}\text{W}$ for the period January 1960 through January 1968. We found only one small event located at 48.1°N 90.0°W . However, in the literature we found reports of two other significant earthquakes (July 26, 1905 and May 26, 1906) which occurred before the installation of a sensitive seismic recording network in the United States (Eppley, 1965). Both events were located near Lake Superior on the Keweenaw Peninsula. The July 26, 1905 event was felt over the entire Keweenaw Peninsula and caused damage at several places. The May 26, 1906 event caused damage and significant elevation changes at the Atlantic Mine on Keweenaw Peninsula; it affected an area about 160 km in diameter. In addition there are two earthquakes located somewhere in central Minnesota (Figure 23) which may also be associated with Lake Superior tectonics. The best documented event occurred on 3 September 1917 and caused damage at Brainard and Staples, Minnesota. The other in the same general region, occurred during 1867 but little is known about it. Both events are located in the vicinity of the Midcontinental Gravity High where it passes under the southwest tip of Lake Superior.

Thus in recent years the Lake Superior region has been relatively aseismic. However, the observed faulting discussed above suggests that the area must have been tectonically active in the geologic past.

A Geophysical Model for the Crust Beneath the Early Rise Shot Point

During Project Early Rise, 38 shots each consisting of 4,844 kg (0.005 KT) of DuPont Nitramon WW(EL) (Borcherdt et al, 1967) were detonated on the bottom of Lake Superior during July, 1966. Borcherdt et al., (1967) located the actual shot points from the travel-times of hydro-acoustic waves recorded by six hydrophone stations around Lake Superior. Figure 24 shows the computed shot points. The shots fall within a radius of 0.7 km from the mean shot point (47.55°N , 88.94°W) with the exception of four shots. Of these four, three are within approximately 1 km of 47.55°N , 88.94°W ; the fourth, shot #1 is located some 3.3 km to the east of the mean shot point. The coordinates of the 38 shot points and the origin times are included in Appendix I.

The University of Wisconsin conducted continuous sub-bottom profiling surveys in western Lake Superior (Figure 25) during 1966. Figure 26 is a profile through the Early Rise shot point (Personal communication, R. J. Wold, 1968) obtained using a salt water bag sparker system which excites 80 - 150 Hz acoustic waves. The profile shows that the lake bottom in the immediate vicinity of the Early Rise shot point is nearly horizontal with little or no relief. The two way travel-times of the acoustic waves reflected from the bottom at the Early Rise shot point is 0.275 sec.

To convert the two-way travel-times to a water depth, we need to know the velocity of sound in the lake. Browning et al, (1968) have published velocity-depth profiles obtained at three locations in eastern Lake Superior during September 1967. These profiles show that the velocity is almost constant at 1422 m/sec for depths greater than 50 m. Between 50 m and the surface the velocity increases approximately linearly to 1445 m/sec.

Therefore, considering the lake as a two layered model, a 50 m thick layer with velocity of 1434 m/sec overlying a lower layer with a velocity of 1422 m/sec, we calculated the depth of the lake beneath the Early Rise shot point to be 196 m. This result agrees closely with the depth of approximately 190 m reported by Borchardt et al , (1967).

The University of Wisconsin (Anzoleaga et al, 1969) has also conducted shallow seismic refraction profiling through the Early Rise shot point (Figure 12). Figure 27 shows the first arrivals from the reversed profile. The close agreement between the apparent velocities of the four sets of arrivals recorded from the eastern shot point with those from the western shot point suggests that the shallow layers are very nearly horizontal. Figure 13 shows Anzoleaga et al interpretation of the shallow structure beneath the western half of Lake Superior.

The velocity of 6.9 km/sec for the first major crustal layer is somewhat higher than the velocity reported by Smith et al, (1966a,b), Berry and West (1966ab) and O'Brien (1968). Since it is unlikely that the P-wave velocity is constant in the major crustal layer, but rather increases with depth, we will adopt 6.8km/sec for the velocity of this layer, a value which represents a mean of the reported measurements. The choice of a thickness for the major crustal layer also presents some difficulties. O'Brien's (1968) model (Figure 10) indicates that the crust is approximately 40 km thick, 100 km to the west of the Early Rise shot point and 50km thick, 100 km east of the shot point. To the west of the shot point, the Moho dips 7°E. However, to the east of the shot point the dip is highly irregular. Since we are attempting to construct a plane-parallel layered model, we will adopt a total crustal thickness of 48 km, implying that the major

crustal layer is 40km thick beneath the Early Rise shot point. The P_n velocity in the Lake Superior region is well defined at 8.1 km/sec.

The shear wave velocities for the crust beneath Lake Superior are less well known. Lewis and Meyer (1968) report shear wave arrivals with apparent velocities of 3.65 km/sec and 3.80 km/sec recorded on the Keweenaw Peninsula during the 1963 Lake Superior Seismic Experiment from shots fired in the western half of the lake. In their model, Lewis and Meyer (1968) assign a shear wave velocity of 3.65 km/sec to the upper 10 km of the crust. However, this is almost certainly too high for the uppermost layers of the model proposed by Anzoleaga et al (1969). Therefore, in constructing our models (Table 4) we have calculated the shear wave velocities in layers 1, 2, and 3 from the compressional wave velocities assuming a value of Poisson's ratio $\sigma = 0.25$. Since Poisson's ratio may be somewhat greater than this in the shallow layers, their true shear velocities may be lower than computed. The velocity of S_n is 4.72 km/sec, taken from Lewis and Meyer's model. This velocity for S_n is in agreement with Brune and Dorman's (1963) observations in the Canadian Shield.

To complete the model we need to know the density distribution. Anzoleaga et al, (1969) constructed their model (Figure 13) from the P-wave arrival data, and constrained their results to fit the gravity data of Wold (1968). The densities of layers 1, 2, 3 are similar to the densities of Jacobsville Sandstone, 2.37 gm/cm³; Oronto Group, 2.62 gm/cm³; and mafic rocks, 2.92 gm/cm³; obtained empirically by White (1966) which are in general agreement with the results of earlier workers (e.g. Thiel, 1956). The density of the 6.9 km/sec layer is 3.10 gm/cm³ (Anzoleaga et al, 1969). When the gravity anomaly of the crustal model ERLS111 is calculated with respect

to CANSD, a density of 3.10 gm/cm^3 for the 40 km thick layer gives an anomaly of +221 mgals which does not agree with the observed anomaly of approximately +60 mgals with respect to the Canadian Shield near Lake Superior. That is, from the Bouguer gravity map (Figure 17), the Bouguer anomaly at the Early Rise Shot Point is ≈ 0 mgals while the mean value in the area surrounding Lake Superior is ≈ -60 mgal. If the density of the 40 km thick layer is reduced to 3.0 gm/cm^3 (or alternately if the density in some 40 km of the shield model is increased by 0.1 gm/cm^3) then the anomaly relative to CANSD is +57 mgals in close agreement with the observed anomaly. Thus, the relative anomaly between the observed Bouguer gravity at the Early Rise shot point and the area surrounding Lake Superior is in good agreement with the Bouguer anomaly between the new model ERLS112 and CANSD assuming that the mean density of the 40 km thick layer is 3.0 gm/cm^3 . Throughout we have adopted Lewis and Meyer's (1968) value of ρ for the upper mantle, 3.342 gm/cm^3 .

In addition to models ERLS111 and ERLS112, we have constructed a third model, ERLS121 assuming a Poisson's ratio of 0.25 throughout the crust and a density of 3.10 gm/cm^3 for the 6.8 km/sec layer. Of the three models, ERLS112 is probably the most representative. Figure 16 shows the theoretical fundamental mode Rayleigh wave dispersion waves computed from these models.

DISCUSSION

The geophysical investigations of the properties of the earth's crust beneath Lake Superior over the past decade have shown that Irving's (1883) hypothesis that the crust beneath Lake Superior has been downwarped to form a broad syncline is correct. However, the same investigations have also shown that the crustal structure is considerably more complex than was originally supposed. Nevertheless there is a strong correlation between the inferred geology, structure and geophysical properties of the shallow part of the earth's crust in the Lake Superior region. For the deeper part, the results from the 1963 Lake Superior Seismic Experiment suggest that the structure of the lower crust is considerably more complex than was originally supposed. In view of the high seismic velocities for the lower crust observed by all investigators, the deeper structure of the Lake Superior region probably is not representative of the Canadian Shield as a whole.

In the western half of Lake Superior, the central part of the syncline has been upthrust to form a horst. This portion of the structure appears to be genetically related to the Midcontinental Gravity High. There is an excellent correlation between the surface geology, gravity, magnetics, heat flow and the shallow seismic refraction results. All suggest that the Keweenaw lavas and sediments are contained in a synclinal trough approximately 10 km deep, the axis of which is orientated in a NE - SW direction. The results of Anzoleaga et al , (1969) suggest that many of the gravity and magnetic anomalies in the region particularly those where large gradients are involved, can be explained by lateral variations in structure of the upper 10 km of the crust.

To the east of the Keweenaw Peninsula the shallow crustal structure and the pattern of the anomalies change. The axis of the syncline swings from NE-SW west of the peninsula to NW-SE east of it. The positive gravity anomalies with steep flanking gradients which form the Midcontinental Gravity High die out in the vicinity of the Keweenaw Peninsula. This, together with the apparent disappearance of the high angle thrust faults which uplift the crustal block of the syncline in the western half of the lake suggests that there may be a radical discontinuity in crustal structure beneath the eastern section of the lake.

In the eastern section of the lake, there is less shallow seismic refraction data and the patterns of the anomalies change. However, the refraction data are sufficient to indicate that the near surface layers vary laterally in thickness and velocity. These variations together with the heat flow, magnetic and gravity data suggest that the structure of the shallow part of the crust is probably synclinal, although the magnetic data are indicative of block faulting rather than thrust faulting. If the magnetic highs in the southeastern part of Lake Superior are caused by Keweenaw lavas at shallow depths and the magnetic lows by Upper Keweenaw sediments, then the shallow synclinal structure probably persists to the south-east shore of Lake Superior. This continuance is reasonable on geologic grounds and is tentatively supported by the gravity work of Bacon (1957).

The variation of the deeper structure beneath Lake Superior is less well known. In Figure 15 we show a contour map of the depth to the Moho in the Lake Superior region based solely on a compilation of the available seismic refraction data. This interpretation of the Moho structure depends heavily on the results of O'Brien (1968) for the crustal structure

beneath the main line of the 1963 Lake Superior Seismic Experiment. We chose to incorporate O'Brien's structure rather than either Berry and West's (1966a,b) model or Smith et al,'s (1966a,b) model because the latter data do not fulfill the requirements of the time-term method which was used to derive them. Interpretation of the Lake Superior travel-time data by this method results in a significant exaggeration of the Moho structure. Additional support of the choice of the O'Brien (1968) structure is that it satisfactorily explains the observations of Bednarek and Meyer (1966). Bednarek and Meyer (1966) plotted reduced travel-times to the WWSSN station MDS ($t - \Delta/8.1$) seconds minus the shot point time-term reported by Berry and West (1966a) as a function of distance from the Zipgun station and found that the difference remained constant at about 3.4 seconds for stations less than 375 km from Zipgun. For the more distant stations, i.e., the stations in the western half of the lake where the most rapid variations in crustal thickness occur, the differences increase with range attaining a maximum value of 5.0 seconds at the western end of the lake. If instead of the time-term for the shot point, the delay time for the ray offset to west of the shot point is subtracted from the reduced travel time, the difference remains constant and is independent of range from Zipgun (O'Brien, 1968).

Figure 15 shows that the crust beneath Lake Superior attains a thickness greater than 50 km. However, the figure also shows that these unusually large crustal thicknesses are probably confined to the eastern section of Lake Superior. The crust thins rapidly northwest of Lake Superior, and has a normal thickness for the Canadian Shield (≈ 35 km) to the northeast of the lake in Ontario. Earlier refraction work (Steinhart et al, 1961) indicate that the crust thins to the south of Lake Superior also.

The unusually high velocity of the major crustal layer reported by several investigators (Smith et al, 1966a,b; O'Brien, 1968; Anzoleaga et al, 1969) appears to be largely confined to the crust beneath Lake Superior. Seismic refraction profiles in the area around the Lake indicate that the corresponding layer has a velocity of 6.3 to 6.4 km/sec, which is similar to values found further north in the shield. The only evidence for the existence elsewhere in this region of velocities as high as 6.9 km/sec at depths as shallow as 8 km deep in the crust is data obtained during a recent re-examination of the travel-times from shots in Lake Superior recorded along a profile entirely within the Midcontinental Gravity High (R.P. Meyer, personal communication 1969). Thus the occurrence of the unusually high velocities appears to correlate with the occurrence of the Keweenaw lavas. However, Halls (1969) has examined compressional wave velocities in the Portage Lake lavas and demonstrated that sample velocities in the slightly metamorphosed members at 2 Kb pressure are insufficient to explain the high velocity (6.6 - 6.9 km/sec) of the upper refractor. But, Halls found that amphibole-bearing volcanics, which represent a higher metamorphic grade, taken from near the base of the Keweenaw extrusive sequence, had sample velocities of 6.7 km/sec at 2Kb and thus possibly represent the top surface of the upper refractor. This suggests that possible sources for these lavas are magmas which pervaded the deeper layers of the crust. However, more conclusive data will be required to validate this hypothesis.

Based on all the geophysical and geologic data discussed above, we have constructed a composite plane-layered model ERLS112 (Table 4) which we believe is representative of the crustal structure beneath the Early Rise shot point as it is presently known. Clearly this model, as any plane-layered

crustal model must, represents a major simplification of the true crustal structure in what is clearly a structurally complex area. Furthermore, the shear velocities and densities in this model are indirectly inferred estimates rather than established quantities. Nevertheless, Model ERLS112 will serve as a useful basis for comparison of the structure beneath the Early Rise shot point and that at Yucca Flat, NTS.

EPICENTER LOCATIONS, TRAVEL-TIMES, AND UPPER MANTLE STRUCTURE FOR LAKE SUPERIOR REGION

In this section of the report we deal with the observed travel-times from shots in Lake Superior which were recorded by stations at regional and teleseismic ($\Delta > 1000$ km) distances. Because the 1963 Lake Superior Seismic Experiment was primarily intended to establish the crustal structure beneath the lake itself, there was no extensive station coverage at large distances; consequently, we will limit our discussion of travel-times to data obtained from the October 1964 series of shots and project Early Rise in 1966 for which many recording stations were available. The October 1964 series of shots affords an excellent opportunity to assess our ability to detect and locate events in Lake Superior since five of the ten shots were fired in essentially the same location, whereas the remaining five were detonated at neighboring points. During project Early Rise, 38 shots were detonated at essentially a common location, the recordings being made over long profiles which for the most part radiated from the shot point (Figure 2). Inversion of the travel-times and amplitude data recorded along these profiles yields a series of velocity-depth structures for the upper mantle for eastern North America.

Location of the October 1964 Shots Using the LRSM and Observatory Networks

In October 1964, the U. S. Geological Survey fired a series of ten shots in western Lake Superior. The shots ranged in five sizes from 907kg (0.001 KT) to 9070 kg (0.01 KT), one shot of each size being detonated at a common location. The locations, origin times, and shot sizes were originally reported by Roller and Jackson (1966). As reported, the loca-

tions for shots 46A and 47A are in error. The correct locations determined from hydrophone data (W. H. Jackson, personal communication, 1969) are given in Table A-2 of Appendix I, together with the water depth at each shot point (J. C. Roller, personal communication, 1969) as determined by the firing ship's depth finder.

We determined the arrival-times and amplitudes at those LRSM stations and observatories which recorded these shots; these observations are tabulated in Tables A-3 through A-12 of Appendix I (Basic Observational Data). The arrival-times were obtained by visually cross-correlating the trace from each shot with the trace from shot 49A at each station. For the smaller shots, we were not able to discern any arrival at many of the more distant stations. However, for completeness, these stations are included in Tables A-3 through A-12 of Appendix I. Figure 28 shows the distribution of LRSM stations which recorded the October 1964 shots.

From the travel-times in Tables A-3 through A-12 of Appendix I, we located the 10 shots with the computer program SHIFT (Chiburis, 1968). These locations are given in Table 6. This program minimizes the relative travel-time anomaly errors for a set of stations rather than travel-time residual errors which are used in the program LOCATE (Flinn, 1963;1965). The travel-time anomaly at a station i relative to station j may be defined as (Chiburis, 1968):

$$A_{i/j} = T_i - T_j - H_i + H_j + e_i - e_j \quad (1)$$

where T is the observed travel-time, H is the expected travel-time computed from the Herrin 68 travel-time tables, and e is an ellipticity and elevation correction. The anomaly error is then

$$dA_{i/j} = A_{i/j} - \bar{A}_{i/j} \quad (2)$$

where $\bar{A}_{i/j}$ is the previously determined relative anomaly for the region in which the event occurs, and the quantity to be minimized becomes

$$E_{i/j} = dA'_{i/j} - dA_{i/j} \quad (3)$$

where $dA'_{i/j}$ is the theoretical relative anomaly given by

$$dA'_{i/j} = \frac{\partial A_{i/j}}{\partial \lambda} d\lambda + \frac{\partial A_{i/j}}{\partial \phi} d\phi + c_j \quad (4)$$

c_j is the mean error at the reference station and λ and ϕ are the longitude and latitude of the trial epicenter respectively.

Figure 29 shows the epicenters of the 10 shots as computed from the whole LRSM and observatory network without the anomaly corrections $\bar{A}_{i/j}$. The computed epicenters for all 10 shots lie to the east of the respective shot points. The distance between the epicenter and shot point is outside the 95% confidence ellipse for the computed epicenter.

Since there are no values of $\bar{A}_{i/j}$ currently available for the Lake Superior region, we re-computed the epicenters for nine of the shots using travel-time anomalies from shot 49A relative to station WMO (Table 5) as estimates of $\bar{A}_{i/j}$ (Table 6). The recomputed epicenters (Figure 29) with the exception of 46A, still lie to the east of the respective shot points. However, the mean location error is now only 2.1 km, and the shot point falls within the 95% confidence ellipse in all cases. The mean area of the 95% confidence ellipses is now 31.2 km² compared to 465.0 km² without anomalies for the same network of stations (Table 6). It is of interest to note that Figure 29 suggests that, knowing the location of shot 49A and hence the displacement vector

of the epicenter computed without anomaly corrections, we could have improved the location of the remaining nine shots by simply graphically subtracting the displacement vector for shot 49A from their computed locations. This is a consequence of having basically the same set of receiving stations, hence the same bias, in each case.

The travel-times to the ten Arizona stations (see insert, Figure 28) are systematically late with respect to the Herrin 68 travel-times. Since these stations are located over a small distance and azimuth range, they may be expected to bias the locations. We recomputed the epicenters for all ten shots again using the LRSM and observatory network, but with only two of the stations shown in the insert to Figure 28, TFO and KN-UT. The results are shown in Table 7. Without anomalies, the mean location error is reduced to 12.6 km and the azimuth of the computed epicenter from the actual shot point increased by around 5° . The mean area of the 95% confidence ellipse decreases slightly despite the smaller number of stations used in the location. However, the actual shot point still falls outside the 95% confidence ellipse for the computed epicenter. With anomaly corrections, these locations are essentially the same as those obtained using the whole network.

Figure 30 shows that there are considerable differences in travel-times between stations in the eastern and western United States with respect to the Herrin 68 travel-time tables. The eastern stations beyond 1000 km recorded early arrivals, whereas the western stations beyond 2000 km are systematically late by about two seconds. Similar variations in travel-times were reported by Mansfield and Evernden (1966) for the 1963 Lake Superior Seismic Experiment. To investigate the effect of these regional differences in travel-times on the computed

epicenters, we divided the LRSM and observatory network into two groups of stations. One group contained all stations east of the Rocky Mountains (Figure 28); the other contained all stations within and to the west of the Rocky Mountains. The locations computed using these two networks with no anomaly corrections are shown in Figure 31 and Table 8.

The results for the eastern network alone show considerable improvement over those obtained from the whole network. The mean displacement of the computed epicenters is only 8.5 km. The mean area of confidence ellipses is somewhat larger, probably because of the smaller number of stations used in computing the locations. In all cases, the actual shot point lies within the 95% confidence ellipse for the computed epicenter. The results for the western stations show the computed epicenters considerably displaced to the southwest. This is not what one would expect from a consideration of the observed travel-times, which are late with respect to Herrin 68 times. However, since all stations are located in one quadrant, the program adjusted the origin time until the slope of the travel-time curve fitted the slope of the theoretical travel-time curve, with the result that the estimated origin times are late by some 9 seconds; thus allowing the computed epicenters to move southwest. The 95% confidence ellipses have a mean area of approximately $12,000 \text{ km}^2$ and are elongated in a NE-SW direction with axial ratios of around 4:1. This reflects the narrow distance and azimuth aperture of the network (Flinn, 1965).

Spence and Alexander (1968, 1969) have developed an alternative method for relative event location based on a scheme used by Gutenberg (Richter, 1958; Appendix X) to improve the location of shallow teleseisms. We define the travel-time difference to a given station from two seismic events as:

$$t' = T_1 - T_2$$

when T_1 is the observed travel-time from the reference and T_2 is the travel-time from the event whose location we wish to determine. Then for two surface events (Figure 32) we may express t' at a distant station as,

$$t' = \frac{\sin i_o}{v_o} \bar{\delta} \cdot \bar{r} = \frac{\sin i_o}{v_o} \delta \cos (\alpha - \phi)$$

where i_o is the take-off angle at the source, v_o the P-wave velocity at the source, $\bar{\delta}$ is the distance vector between reference event and the unknown event, whose length δ and azimuth α we wish to determine, and \bar{r} is the unit vector along the azimuth ϕ from the reference event to the station. But $\frac{\sin i_o}{v_o}$ is simply $p(\Delta)$, the seismic ray parameter. Thus by plotting $d = \frac{t'}{p(\Delta)}$ vs ϕ we can estimate δ and α from the amplitude and intercepts of the resulting waves (Figure 33).

Selecting shot 49A as the reference event, we formed the quantity t' by an approximation to $p(\Delta)$ given by the first difference of the Herrin 68 travel-time tables about Δ for each station, to form $d(\phi)$. The values of d for each shot-pair were then fitted by least-squares to a smooth curve from which we calculated δ and α . Figure 34 shows the relative locations of the 1964 series of shots computed by this method. The mean location error (see Table 9) is 2.0 km. Both the locations and the location errors are similar to those computed from the travel-time anomalies.

The results of locating the ten shots using program SHIFT, show that utilizing the whole LRSM and observatory network, we are able to locate events in Lake Superior to within 15.6 km of the actual locations. The results also show that

for the whole network there is an apparent "location bias," since the computed epicenters lie on almost a common azimuth from the actual shot points. This may be due to the geometry of the array since there are only two stations between 325° and 100° in azimuth from the shot points. Removing the western stations from the LRSM and observatory network improves the location in that it reduces the distance of the computed epicenter from the shot point. However, the area of the confidence ellipse for the computed epicenter increases. This is due primarily to the smaller number of stations in the eastern network since the azimuthal aperture of the network remains fixed. The accuracy and precision of the locations from the western network of stations is poor. This is largely due to the narrow azimuthal aperture (29°).

Using travel-time anomalies obtained from one of the shots, we were able to locate (with Program SHIFT) the remainder to within 2.1 km with a high degree of confidence. The relative locations obtained using the Spence and /lexander approach were quite comparable in accuracy (average 2.0 km) which is expected because both methods account for variations in propagation velocity to individual stations. The 2 km accuracy, therefore, probably represents the practical limit on location of events at Lake Superior using this network. Moreover, in view of the known structural complexity of Lake Superior the travel-time anomalies derived using shot 49A as the master event probably cannot be used to locate events to this accuracy if they are more than about 25 km from shot 49A.

Travel-times and Upper Mantle Structures from Events in Lake Superior

Figure 2 shows the configuration of the seismic refraction profiles which were used to record the Early Rise shots.

Warren et al, (1967) and Iyer et al, (1969) have published preliminary travel-times and amplitudes of the first arrivals recorded during Project Early Rise. In addition, Warren et al, (1967) show record sections for many of the profiles. Some detailed analyses of this data have been published by Lewis and Meyer (1968), Green and Hales (1967a,b; 1968), Barr (1967), Mereu and Hunter (1969) and Willis (1968). Roller and Jackson (1966a,b) have reported on travel-times for the October 1964 series of shots in Lake Superior. Iyer et al. (1969) published an analysis of all the first-arrival data from Project Early Rise and derived a P-wave velocity model from the combined data. After extensive smoothing, they inverted the resulting travel-time data by the usual Wiechert-Herglotz method (Bullen, 1963). By treating the data in this manner they effectively averaged out any regional differences in travel-times. Since it is these regional differences in travel-times and their implications which we wish to examine, we will simply show the reduced travel-times from Project Early Rise (Figure 35) together with their theoretical travel-times calculated from the model NCER 1 shown in Figure 36.

Lewis and Meyer (1968) investigated the upper mantle to the west of Lake Superior using P and S wave arrivals recorded along a profile extending from 400 km to 2500 km due west of the Lake (Profile 1 in Figure 2). Figure 37 shows a record section for Profile 1 showing the P-wave arrivals compared with the arrivals computed from the model obtained by Lewis and Meyer (Figure 39). Figure 38 is a similar figure showing the S-wave arrivals compared with the theoretical travel-times computed from their model. An interesting feature of Lewis and Meyer's model (Figure 39) is the rapid increase in P-wave velocity at a depth of 126 km which is accompanied by a sharp decrease in shear wave velocity. At 150 km depth there

is a zone 40 km thick in which the P-wave velocity decreases by 0.04 km/sec. This is the region in which the shear waves show a pronounced low velocity zone. Both the P-wave and S-wave velocities increase abruptly at 450km depth. Lewis and Meyer (1968) also calculated two distributions of density with depth from the two relationship between P-wave velocity and density given by Birch (1964).

To the southwest of Lake Superior, Green and Hales (1967a,b; 1968) investigated travel-times along two radial profiles (Profiles 2 and 3 in Figure 2) and an arcuate profile (Profile 4). Figure 40 shows the travel-times of the first arrivals and the theoretical travel-time curves computed from the two models shown in the insert. The travel-times from Early Rise Model 1 fit the observed data to within 0.8 sec. Early Rise Model 2 is an alternative model with a low velocity zone between 130 and 160 km depth. The theoretical travel-times from this model, shown by a dashed line in Figure 38, also fit the observations well, accounting for the offset in the observed times at 1500 km. However, Green and Hales (1968) emphasize that this offset could be accounted for by reading error or lateral variations (in crustal thickness or mean crustal velocity), and prefer Early Rise Model 1, concluding that the low velocity zone for P-waves is either very thin or occurs at a depth greater than 150 km beneath the central United States. The travel-times along a profile northeast from the GNOME explosion near Carlsbad, New Mexico (Romney et al, 1962; Lehmann, 1964), which essentially reverses Profile 2, agree well with the travel-times calculated from Early Rise Model 1.

Profile 5 in Figure 2 very nearly reverses an earlier profile occupied by the University of Michigan to record shots fired in the Atlantic during the 1962 North Carolina Experiment

(Meyer et al, 1965), the CHASE series of underwater explosions in the Atlantic, and the East Coast On-Shore Off-Shore Experiment (Hales et al, 1967). Figure 41 is a plot of the travel times of the first arrivals from the Early Rise shots recorded along Profile 5. Willis (1968) has inverted this data to obtain the following P-wave velocity model for the Lake Superior end of the profile.

<u>Velocity km/sec</u>	<u>Depth km</u>	<u>Thickness km</u>
4.8	0	2.9
6.2	2.9	22.5
7.7	25.4	25.0
8.3	50.4	21.6
8.4	72.0	∞

For the southern end of the profile, Willis (1968) found a 28 km thick crust at the continental margin and the higher velocity layer (8.4 km/sec) at a depth of 99 km.

Also to the southwest of Lake Superior, Roller and Jackson (1967 a, b) analyzed the travel-times from the October 1964 series of shots along a profile extending from the Bayfield Peninsula to Denver, Colorado, which was extended to central Arizona by incorporating several of the LRSM stations. Figure 42 shows Roller and Jackson's results. Roller and Jackson (1967a,b) fit two linear segments to the mantle first-arrival data representing waves with apparent velocities of 8.2 km/sec and 8.5 km/sec, the crossover occurring at a distance of 1100 km from the shot point.

Barr (1967) studied the travel-times for the Early Rise shots and the Hudson Bay seismic experiments in 1965 recorded at the standard seismograph stations maintained across Canada by the Dominion Observatory. The P-wave travel-times were

referenced to a standard crust by subtracting the difference between the time-term for the Early Rise shot point (4.15 sec obtained from Berry and West's (1966) data) and the mean time-term from the Hudson Bay shots (3.56 sec. derived from the data obtained by Hobson et al, (1967)) from the Early Rise travel-times. This reduced the Early Rise times by 0.59 sec. The corrected travel-times from the Lake Superior shots together with those from the Hudson Bay experiment are shown in Figure 43. Figure 43 also shows the theoretical travel-times calculated from Barr's model. In constructing this model, Barr (1967), determined the positions of the cusps in the observed travel-times to ensure that no low velocity layers were omitted from his model. Barr (1967) concludes that no low velocity zones for P-waves in the upper (350 km of the) mantle are indicated by his data.

The 8.42 km/sec layer in Barr's model occurs at 126 km depth. However, the first arrivals at three of his stations are:

$$\text{BLC } T = 8.27 + \frac{\Delta}{8.41} \text{ at } 310\text{-}960 \text{ km}$$

$$\text{FFC } T = 7.27 + \frac{\Delta}{8.21} \text{ at } 720\text{-}1390 \text{ km}$$

$$\text{FBC } T = 10.41 + \frac{\Delta}{8.49} \text{ at } 790\text{-}1340 \text{ km}$$

When combined, these arrivals yield

$$T = 6.74 + \frac{\Delta}{8.22} \text{ at } 310\text{-}1390 \text{ km distance range}$$

One can readily see that two of the three independent station velocities, BLC and FBC, are significantly higher than the velocity from the combined data. Barr (1967) attributes these higher velocities to local structure in the upper mantle beneath

the Moho under the Hudson Bay, since the immediate sub-crustal velocity is known from earlier work (Hobson et al, 1967; Hall and Brisbin, 1961; Hodgson, 1953) to be very nearly 8.2 km/sec.

Mereu and Hunter (1969) have examined the travel-times to stations along a profile north from Lake Superior to Churchill, Manitoba (Profile 8 in Figure 2). The record section obtained by Mereu and Hunter (Figure 44) shows three distinct branches of the travel-time curve with apparent velocities of (a) 6.3 km/sec up to 2.4° , (b) 8.10 km/sec from 2.4° to 5.8° , (c) 8.54 km/sec from 5.8° to 13.4° . The branch of the curve with apparent velocity of 8.54 km/sec corresponds to arrivals refracted from a layer with velocity of 8.43 km/sec which, when corrected for earth curvature, occurs at a depth of 84 ± 3 km (Mereu and Hunter, 1969). The possibility of a low velocity zone in the upper mantle for P-waves cannot be ruled out on the basis of Mereu and Hunter's data since first arrivals in the distance range 1140 to 1350 km have very small amplitudes. There is also some suggestion of an offset in the travel-time curve occurring in this distance range.

Brune and Dorman (1963) in their study of surface wave dispersion across the Canadian Shield used the travel-times reported by Hodgson (1953a,b), Lehmann (1955), and Hall and Brisbain (1961) to supplement their surface-wave dispersion data in determining the model CANSD (Figure 2). Brune and Dorman (1963) report a P_n velocity of 8.18 km/sec at about 400 km distance increasing to 8.33 km/sec at about 2000 km, and a S_n velocity of 4.72 km/sec over this range. The compressional wave velocities in the lower layers of CANSD were assigned rather than observed.

PHYSICAL SETTING OF THE NEVADA TESTS

Geological Environment

The Relationship of the Nevada Test Site to the Basin and Range

The Basin and Range province covers a large area of the south-western United States (Figure 45). It has a characteristic landscape consisting of short, sub-parallel mountain ranges and intermontane desert basins (King, 1959, p.152). Much of the area (the Great Basin of King) is a region of interior drainage. The topography of the Basin and Range province is structurally controlled, consisting of a series of horst, grabens and tilted blocks which are bounded by Cenozoic normal faults (Eardley, 1962; Gilluly, 1963; Thompson, 1966; Thompson et al, 1967) and has been evolving since the time of the Cordilleran orogeny.

According to King (1957), during early Tertiary time, in the eastern section of the Great Basin deposition of lacustrine and fluvial sediments took place over a broad flood plain bounded to the east by the low lying hills of the Rocky Mountain region and the denuded Sierra Nevada Batholith to the west. During the middle Tertiary time, the western part of the Great Basin was covered by volcanic rocks, and in some areas was faulted and tilted during the middle Miocene. In the late Miocene and early Pliocene deposition of terrestrial sediments took place and fossil plants occurring in these rocks suggest that the whole area had only moderate relief and was relatively low-lying. Uplift of the Sierra Nevada block began in late Pliocene and continued into the Pleistocene. During this time the Great Basin area was disrupted by extensive block faulting, which resulted in the uplift of not only the present day mountains

but the basins also. Geophysical evidence suggests that this uplift is still taking place today.

The Basin and Range province is a tectonically active region. Seismological studies have shown that the structure of the crust and particularly the upper mantle is quite different from that found in non-tectonic regions. Hill and Pakiser (1966) in a study of a series of reversed seismic refraction profiles between Eureka, Nevada and Boise, Idaho concluded that the crust in the northern Basin and Range province consists of a 6.0 km/sec layer 19 to 24 km thick overlying a 6.7 km/sec layer some 10 to 12 km thick and that both the crust as a whole and the 6.7 km/sec layer increase in thickness at the boundary between the Basin and Range province and the western Snake River Plain. They also found a P_n velocity of 7.9 km/sec obtained by Pakiser (1963), Stuart et al, (1964), Pakiser and Steinhart (1964), and Healy and Ploger (1965). In addition to the northwards thickening, Hill and Pakiser find that the Moho shows local variations in depth of as much as 5 km under the Basin and Range province, which are probably due to faulting.

Hill and Pakiser's (1966) interpretation of crustal structure in the Northern Basin and Range has recently been verified by the work of Prodehl (1969). Prodehl reinterpreted the data accumulated by the U. S. Geological Survey during the years 1961-1964. He found that the mean crustal thickness in the northern Basin and Range province is 30 km, and the average P-wave velocity is 6.1 to 6.2 km/sec at depths of 15 or 20 km, there being good evidence for an intermediate layer in the northern but not in the southern part of the Great Basin. Alexander (1963) also found evidence for an intermediate layer from observations of surface wave dispersion across the Basin and Range province, although the intermediate layer in his model is somewhat deeper and has a higher velocity.

The physiographic delimitation of the Basin and Range is reflected in the spatial distribution of upper mantle provinces in the western United States. Archambeau et al. (1969) have demonstrated that a correspondence exists between patterns of compressional wave velocity at the top of the mantle (P_n velocity) P-wave travel-time delays and the various physiographic provinces; the Basin and Range province being characterized by anomalously low P_n velocities and positive P-wave delays with respect to the Jeffreys-Bullen travel-time tables. Its boundaries are defined by rapid changes in P_n velocity. Their results also show that variations in P_n velocities are manifestations of profound differences in the structure of the upper mantle. Figure 46 shows Archambeau et al.'s model CIT 111P for P-wave velocity structure beneath the Basin and Range province. The model shows no velocity reversals with depth but rather the low velocity zone (7.7 km/sec) for P-waves extends from a depth of 150 km to the base of the crust. This latter zone, on the basis of the results of Archambeau et al. (1968) is where major differences in mantle structure beneath the various physiographic provinces of the western United States probably occur.

Shear wave velocity models also indicate the presence of a low velocity zone in the mantle. Kovach (1968), and Kovach and Robinson (1969) have studied $dt/d\Delta$ for long period S-waves recorded at the extended TFO array in Arizona. The important features of their model which is shown in Figure 47 are (1) a thin lid zone, 9 km thick with a shear wave velocity of 4.5 km/sec overlying a low velocity zone; (2) a change in velocity gradient at a depth of 160 km followed by a gradual increase in velocity to a depth of 360 km; (3) a rapid increase in velocity beginning at a depth of 620 km. The main features of Kovach and Robinson's model are consistent with the

previous results of Toksoz and Anderson (1965) from studies of Love wave dispersion in tectonic regions.

Heat flow measurements in the Basin and Range province reported by Roy et al. (1968a) indicate a mean heat flow of $2.0 \mu\text{cal}/\text{cm}^2 \text{ sec}$ (Blackwell, 1969). More recent results reported by Warren et al. (1969) suggest that the mean heat flow may be as high as $2.21 \pm 0.43 \mu\text{cal}/\text{cm}^2\text{-sec}$ in the Basin and Range province south of 36°N . Both of these values are significantly higher than the world-wide mean heat flow of $1.5 \mu\text{cal}/\text{cm}^2\text{-sec}$ (Lee and Uyeda, 1965). Figure 48 summarizes the heat flow measurements made in the western United States to date. The high heat flow over the Basin and Range is clearly delimited. To the west, the mean heat flow in the Sierra Nevada is somewhat low ($\approx 0.9 \mu\text{cal}/\text{cm}^2 \text{ sec}$, mean of 7 values published by Roy et al, 1968c), and to the east in the Colorado Plateau and Texas Foreland, the heat flow is also somewhat low ($\approx 1.1 - 1.2 \mu\text{cal}/\text{cm}^2 \text{ sec}$, Warren et al, 1969). Roy and Blackwell (1966) investigated the heat flow transition between the Basin and Range province and the Sierra Nevada and found that the heat flow and seismic boundaries are coincident and about 50 km east of the structural and physiographic boundary (see Figure 49). When the contribution to the surface heat flow from sources within the upper 10 km of the crust is removed using the method of Roy et al, (1968b,c), the contrast is even sharper. This suggests that the broad heat flow anomaly over the Basin and Range province is not related to excess heat production in the upper crust, but rather that it is due to anomalously high heat flow in the upper mantle. Warren et al, (1969) examined the heat flow in the southeastern part of the Basin and Range and the Texas Foreland. Again, they found a sharp transition between the high ($> 2.0 \mu\text{cal}/\text{cm}^2 \text{ sec}$) heat flow in the Basin and Range and the normal or somewhat low ($\approx 1.0 \mu\text{cal}/\text{cm}^2 \text{ sec}$) heat flow in the Texas Foreland.

which takes place at 150 km. Warren et al, (1969) interpret the high heat flow in terms of high subcrustal temperatures. This interpretation is consistent with the geomagnetic data of Schmucker (1964) and the magnetotelluric data of Swift (1967) which indicate a zone of anomalously high electrical conductivity under southern Arizona and New Mexico. Both Schmucker (1964) and Swift (1967) have interpreted this zone to mean that the higher temperature isotherms are shallower in the Basin and Range than in the Texas Foreland.

The coexistence of high heat flow, low seismic velocities and the low values of Q in the upper mantle (Archambeau et al, 1969) suggests that the low velocity zone may be due to partial melting of the mantle material. The absence of a high velocity lid to the low velocity zone for P-waves in the Basin and Range province implies that the zone of partial melting extends to the base of the crust. Archambeau and Davies (1969) have examined the geophysical data and concluded that they are consistent with the hypothesis that the Basin and Range province overlies the extension of the East Pacific Rise (Heezen, 1960; Menard, 1960; Cook, 1966; Thompson, 1966) where the North American crustal plate has overridden the spreading zone. If this hypothesis is substantially correct, then we should expect observations of travel-times, amplitudes, and the associated models of crustal and mantle structure to appear anomalous when compared to the tectonically inactive or stable regions of North America.

In the following sections we summarize some of the observations which demonstrate the anomalous nature of the crust and mantle beneath Basin and Range province in much the same manner as we did above for Lake Superior. In particular, we shall be concerned with the derivation of a geophysical model for NTS which will serve as a basis for comparison between the

two regions.

The Nevada Test Site (NTS) is situated in the Great Basin section of the Basin and Range province (Figure 50) approximately 110 km to the northwest of Las Vegas. Some recent tests, for example FAULTLESS, have been conducted somewhat to the north of the main site, as were certain earlier events such as SHOAL. However, we will discuss, principally, the main test area shown in Figure 50, and will attempt to derive a geophysical model for the Yucca Flat area.

Geology of the Nevada Test Site

The geology of the Yucca Flat and Frenchman Flat area of the Nevada Test Site (Figure 51) is fairly well known from surface observations and borehole data. In 1952 Johnson and Hibbard conducted a reconnaissance survey of the area the results of which were published in 1957 (Johnson and Hibbard, 1957). Over the period 1960-63 the U. S. Geological Survey remapped the Yucca Flat area and conducted numerous subsurface investigations. The results are published in a series of Technical Letters and it is from these, together with Memoir 110 of the Geological Society of America (Eckel, 1968), that much of the information presented below is drawn.

Physiographically, Yucca Flat is a broad, relatively flat intermontane basin bordered to the north, east and west by mountains of moderate relief, and separated from Frenchman Flat to the south by a somewhat lower ridge of pre-Quaternary rocks. The basin is an area of inland drainage, a small playa (Yucca Lake) forming during the wet season at the southern margin of the flat.

In general, the mountains are composed of late Precambrian and Paleozoic sedimentary rocks and Cenozoic volcanics

whereas the valleys are filled with detritus derived from the surrounding mountains. The rocks exposed at the surface in the Yucca Flat area range in age from late-Precambrian to Recent. They may be conveniently divided into three main groups, the late-Precambrian-Permian, the Cenozoic volcanics, and the Quaternary and Recent valley fill. The stratigraphy of the area is summarized in Table 10. The first group consists of some 10.6 km of argillites, quartzites, limestones and dolomites which are divided into eight sequences on the basis of gross lithology and age (Barnes et al, 1963). The second group consists of volcanic rocks of Miocene or younger age (radiometric ages obtained from the ash flow tuffs range from 26 my to 7 my (Ekren, 1968)) locally more than 1.06 km thick (Barnes et al, 1963). (The above thicknesses refer to the stratigraphic section not the present vertical extent of these units.) These rocks are composed of tuffs, welded tuffs, tuffaceous sedimentary rocks and lava flows which were deposited on the deeply eroded surface of the Paleozoic rocks. Seven principal ash-flow tuffs have been recognized (Ekren, 1968) which range in lateral extent from 100 to 200 km, and are thought to have originated to the west of Yucca Flat. In the valleys both the volcanics and the pre-Cenozoic rocks are overlain by rocks of the third group, the Quaternary and Recent valley fill. These rocks are typical fluvial deposits composed of detritus from the local mountains, ranging from coarse agglomerates to fine silts and clays with locally occurring evaporites. Together these deposits are referred to as alluvium. The alluvium attains a maximum thickness of 0.61 km (Barnes et al, 1963) beneath the south-central portion of Yucca Flat.

Although the predominant structural pattern of the Yucca Flat area is the result of block faulting, detailed mapping has shown that the area is structurally very complex. Barnes

et al. (1963) divided the area into an eastern and western block, on the basis of the age of the outcropping rocks and the orientation of the major folds and faults along the line A-A' in Figure 52. The rocks in the eastern block are chiefly of late Precambrian and early Paleozoic age. Major folds trend northwest, and the high-angle faults strike north-northeast. The Paleozoic rocks in this block are often repeated by thrust faulting (Figure 52), which in some areas places late Precambrian and lower Paleozoic rocks over middle and upper Paleozoic strata. The Yucca Fault, which runs north-south through Yucca Flat is mostly within the eastern block. Quaternary movement along this fault has caused the eastern side to be down-thrown by as much as 0.3 km (Barnes et al, 1963).

In the western block, most of the outcropping pre-Cenozoic rocks are of late Paleozoic age. Here the rocks are folded along northeast trending axes, the younger Devonian to Permian rocks being overthrust by Cambrian and Ordovician rocks. The high-angle faults in this block are less regular in trend as can be seen from Figure 52. They are predominantly oriented north and north-northeast, with apparent vertical displacements of up to 0.45 km. Ekren (1968) attributes the change in strike from north to northeast in the northern part of NTS to bending of the faulted ranges caused by drag along the Las Vegas Valley shear zone (Longwell, 1960) as several of the northeast trending faults show left-lateral displacements of up to 4 km.

Yucca Flat itself lies between the two blocks. There are no outcrops of the basement. However, the structure and configuration of the Paleozoic and Tertiary rocks are fairly well-known from seismic, gravity, magnetic, and bore-hole data.

Geophysical Evidence on Crustal Structure under the Nevada Test Site

Many detailed geophysical investigations (summarized in Hazlewood et al, 1963) have been made of the Yucca Flat area in order to elucidate the shallow structure of the area. In addition, seismic surveys have been carried out over much of Nevada and the surrounding states. Many of these seismic profiles use events at NTS as sources of seismic energy and so it is not possible to obtain directly the deep crustal structure immediately beneath the test site itself from these profiles, and so we shall have to study the seismic data on a regional basis. In addition to the seismic data, local gravity data (Healey and Miller, 1963; Healey, 1968) and regional Bouguer gravity data (Joesting and Woollard, 1964) aeromagnetic data and regional heat flow data (Blackwell, 1969) are available. Furthermore, NTS lies in the area covered by the Transcontinental Geophysical Survey (USGS, 1968).

Seismic Measurements

Refraction Studies

Shallow seismic refraction studies (Hazelwood et al, 1963) were made in the Yucca Flat area to determine the thickness of the alluvium beneath the flat and the configuration of the Paleozoic and Tertiary rocks which form the basement. Table 10 summarizes the seismic velocities for the various rock types outcropping in the Yucca Flat region as reported by Hazelwood et al, (1963). The large variation in velocity for alluvium is due to the rapid increase in velocity with depth. The results of a seismic refraction survey in Yucca Flat aided in

the delineation of a buried Paleozoic ridge, which from gravity data (discussed below) and bore holes is known to extend north-south through the center of the flat.

The gross crustal structure in the vicinity of the Nevada Test Site is known from the U. S. Geological Survey's crustal refraction work reported in Hill and Pakiser (1966); Pakiser (1963); Eaton (1963); Diment et al, (1961); Gibbs and Roller, (1964, 1966); Johnson (1965), and Prodehl (1969). In addition, Pakiser and Hill (1963), and Ryall and Stuart (1963) used the travel-times of seismic phases generated by events at NTS to study crustal structure in the western United States. We have plotted the results of these surveys as a fence diagram (Figure 53).

To the north of NTS, Hill and Pakiser (1966) studied travel-times along a reversed profile to Boise, Idaho. Their results indicate that the crust is 30 km thick, 100 km north of NTS, increasing to 48 km under the western Snake River Plain 680 km to the north of the test site. In the vicinity of NTS, Hill and Pakiser (1966) (Figure 17, p. 412), show the crust composed of approximately 1 km of low-velocity "sediments" overlying a 19 km thick layer with velocity of 6.0 km/sec, a 10 km thick intermediate layer with a velocity of 6.7 km/sec, and a P_n velocity of 7.9 km/sec. Their model indicates considerable local variations in crustal thickness which Hill and Pakiser (1966) attribute to faulting at the base of the crust. The model also shows that both the crust as a whole and the 6.7 km/sec layer rapidly increase in thickness at the physiographic boundary between the northern Basin and Range Province and the western Snake River Plain. The P_n velocity found by Hill and Pakiser (1966) agrees with earlier

studies of similar data along the same profile by Pakiser and Hill (1963) and Knopoff and Teng (1965). The crustal thickness of 30 km at a point 100 km to the north of NTS agrees with the results obtained by Diment et al, (1961) from analyses of travel-times from events at NTS recorded along a 300 km line southeast from NTS to Kingman, Arizona.

To the east of NTS, Ryall and Stuart (1963), have interpreted travel-time data recorded along a profile from NTS to Ordway, Colorado. Their results indicate a two layered crust with velocities of 6.0 km/sec and 6.5 km/sec, which increases in thickness from 26 km at a point approximately 60 km east of NTS to 42 km thick beneath the western part of the Colorado Plateau 400 km distant from NTS. Ryall and Stuart (1965) found an apparent P_n velocity of 7.6 km/sec. The $2^\circ 35'$ E dip in the Moho is calculated on the assumption that the true P_n velocity at NTS is 7.9 km/sec. The thickness of the intermediate layer in this model is only 3.8 km. Therefore it could not possibly be recorded as a first arrival; the main evidence for its existence comes from the large amplitude second arrivals recorded in the distance range 123 - 319 km.

To the south of NTS, Gibbs and Roller (1964, 1966) have determined the crustal structure between NTS and Ludlow, California from seismograms recorded along a reversed profile between the two points. For events at NTS, they found that the first arrivals out to 155 km had a velocity of 6.10 km/sec which they correlate with P_g . In the distance range 155 km to 265 km south of NTS, the first arrivals had a velocity of 8.04 km/sec (P_n). South of Ludlow, in the distance range 315 km to 490 km, the first arrivals had a velocity of 7.75 km/sec (P_n). For events at Ludlow recorded northwards from Ludlow toward NTS, they found first arrivals with velocities of 6.10 km/sec (P_g), 6.80 km/sec (P^*), and 7.76 km/sec (P_n).

Gibbs and Roller (1964, 1966) interpret the high apparent velocity of P_n recorded south from NTS as evidence that the crust thins southwards and that the P_n velocity of 7.75 km/sec recorded south of Ludlow indicates that the Moho flattens out beyond 315 km from NTS. Their preferred crustal model (Model II) shows a total crustal thickness of 24 km at Ludlow and 34 km at NTS made up of the following layers:

<u>LUDLOW</u>		<u>NTS</u>	
$h_0 = 1.4$ km	$V_0 = 2.50$ km/sec	$h_0 = 1.0$	$V_0 = 2.50$ km/sec
$h_1 = 13.0$ km	$V_1 = 6.10$ km/sec	$h_1 = 13.0$	$V_1 = 6.10$ km/sec
$h_2 = 13.0$ km	$V_2 = 6.80$ km/sec	$h_2 = 20.0$	$V_2 = 6.80$ km/sec
$h_3 \dots$	$V_3 = 7.76$ km/sec	$h_3 = \dots$	$V_3 = 8.04$ km/sec

the thickness of the 6.10 km/sec layer being assumed. The dip of the Moho is 1.7° S (Gibbs and Roller 1964;1966).

Johnson (1965) has interpreted the crustal structure between Mono Lake, California and Lake Mead, Nevada. His profile crosses the NTS - Ludlow profile (Gibbs and Roller, 1964; 1966) approximately 80 km south of NTS. Figure 53 shows the structure obtained by Johnson (1965), and the structure obtained by Gibbs and Roller at the point where the two profiles intersect. The total crustal thickness of 33 km found by Johnson agrees well with the 32.5 km obtained by projecting the crustal thickness of 34 km at NTS found by Gibbs and Roller. However, the agreement could well be fortuitous since Johnson's model consists of a 1.9 km thick layer with velocity 3.0 km/sec (assumed), a 23 km thick layer with velocity 6.15 km/sec, an intermediate layer 8 km thick with a velocity of 7.10 km/sec and a P_n velocity of 7.80 km/sec, whereas the Gibbs and Roller model has an intermediate layer 20 km thick (see above).

Johnson's model is also interesting in that it shows sharp flexures of 6 km in the Moho 25 km south of Mono Lake and flexures of 2.5 km in the Moho 30 km north of Lake Mead, which correlate with large surface faults (Johnson, 1965). Between 100 km and 215 km SW of Mono Lake the crust thins from 40 km to 30 km in thickness. This latter feature (a monocline) has no surface expression; however Johnson (1965) found that the Bouguer gravity anomalies calculated from the refraction model using the empirical compressional wave velocity vs. density relations of J. E. Nafe and C. L. Drake (Talwani et al, 1959) fitted the observed Bouguer gravity anomalies along the profile.

Northwest of NTS Eaton (1963) interpreted the structure between Fallon, Nevada and Eureka, Nevada. Eaton found no wave refracted from the top of the intermediate layer as a first arrival on this profile; the main evidence for the existence of the intermediate layer comes from the tentative identification of the reflected phase $P_I P$. Assuming that an intermediate layer is present, Eaton (1963) found that the crust at Fallon is 22.3 km thick and consists of a 17.2 km thick layer with an adopted velocity of 6.0 km/sec, and a 6.9 km thick layer with velocity 6.6 km/sec. Beneath Eureka, Eaton calculated that the crust is 33.9 km thick, consisting of a 22.3 km thick 6.0 km/sec layer and a 11.6 km thick intermediate layer with velocity 6.6 km/sec. The P_n velocity, when corrected for the $2^\circ E$ dip in the Moho, is 7.82 km/sec. Assuming that the intermediate layer is absent, Eaton calculated that the crust (6.0 km/sec) is 22.2 km thick at Fallon and 31.5 km thick at Eureka, the true P_n velocity being 7.82 km/sec when corrected for the 1.7° dip of the Moho. The 32 - 34 km of crustal thickness at Eureka found by Eaton (1963) agrees well with 33 - 36 km crustal thickness in the vicinity of Eureka reported by Hill and Pakiser (1966, p. 401).

Recently Prodehl (1969) has reinterpreted the data from 46 seismic-refraction profiles recorded by the U. S. Geological Survey in the western United States during the years 1961 to 1966. He concludes that the average crustal thickness under the Basin and Range province is 30 km and the mean P-wave velocity of the upper 15 to 20 km of the crust is 6.1 to 6.2 km. Prodehl finds good evidence for an intermediate layer in the northern part of the Great Basin but not in the southern part. However he states that the curvature of the branch of the travel-time curves corresponding to the phase P_M^P , which is a dominant phase on all profiles, is explained by a relatively large velocity gradient at the base of the crust. Thus, Prodehl (1969) concludes that it is possible, but somewhat unlikely, that this zone of steep velocity gradients is 10 - 15 km thick beneath the southern part of the Great Basin.

Surface Wave Dispersion Observations

Alexander (1963) studied Love and Rayleigh wave group velocity dispersion across the Basin and Range province from recordings of two events along the Utah-Idaho border and the aftershock sequence of the Montana earthquake of August 1959. His data together with his model 35CM2 derived for the crustal and upper mantle structure of the Basin and Range province are shown in Figures 54, 55, 56, 57. An unusual feature of model 35CM2 is the 25 km thick layer with a S-wave velocity of 4.1 km/sec and a P-wave velocity of 7.7 km/sec at 25 km depth which Alexander (1963) designates section X. A thin high shear velocity layer at a depth of about 50 km is necessary to bring the theoretical group velocities of the fundamental mode Love and Rayleigh waves at the longer periods into agreement with the observations. Alexander (1963, p. 23) considers that the overall agreement of the model for the fundamental

mode Love and Rayleigh waves, the higher Love modes, and the second higher Rayleigh mode is good, and that the shape of the theoretical dispersion curve for the first higher Rayleigh mode agrees satisfactorily with the observations. The level of the computed higher-mode curves at the longer periods could be brought into better agreement with the observations if a correction for earth curvature were made to the model.

Parts of Model 35CM2 do not agree well with the recent P-wave data of Prodehl (1969) or with some of the work of the U. S. Geological Survey. These later results indicate a mean crustal thickness of 30 km in the Basin and Range province. Furthermore, the results of Hill and Pakiser (1966) suggest the existence of an intermediate layer in the crust of the Basin and Range province with a P-wave velocity of 6.7 km/sec. However, the shear velocity distribution of Model 35CM2 which is well constrained by the surface wave dispersion data could be put together with this P-velocity structure since surface wave dispersion is relatively insensitive to perturbations in P-wave velocity. We defer further examination of the correspondence between models obtained from refraction studies and the model obtained from the observation of surface wave dispersion across the Basin and Range province until a later section of this report.

Gravity Data

The results of gravity investigations at Yucca Flat and contiguous areas are reported in Hazelwood et al, (1963) and in Healey (1968). These studies were conducted in order to determine the structure of the pre-Cenozoic rocks which lie beneath Yucca Flat. Consequently, it is possible to determine the thickness and configuration of the Cenozoic volcanic rocks

and alluvium which constitute the valley fill in this area. On a regional basis, the Bouguer gravity map of the United States (Woollard and Joesting, 1964) and the Bouguer gravity map from the Transcontinental Geophysical Survey (U. S. Geological Survey, 1968) give data for the Basin and Range. Figure 58 shows the regional Bouguer gravity in the vicinity of NTS, whereas Figure 59 is a detailed map of the Yucca Flats area.

Although the rocks outcropping at NTS have a wide range of lithologies, they can be classified into three groups on the basis of bulk densities. The first group consists of the Precambrian and Paleozoic rocks which have an overall density range from 2.49 gm/cm^3 for quartzite to 2.85 gm/cm^3 for dolomite, with a mean density of approximately 2.67 gm/cm^3 (Hazelwood et al, 1963). The Mesozoic granitic rocks can conveniently be included in this group also. The second group consists of the Cenozoic lavas and welded tuffs. These rocks range in density from 1.8 to 2.8 gm/cm^3 , with a mean bulk density of 2.40 gm/cm^3 (Hazelwood et al, 1963). The third group consists of the non-welded and partially welded tuffs and the alluvium which taken together have a mean density of 1.95 gm/cm^3 . We have incorporated the densities of the individual rock types as listed by Healey and Miller (Hazelwood et al, 1963) in Table 10.

Figure 59 shows in detail the Bouguer gravity anomalies in the Yucca Flat area. The map taken from Healey (1963) incorporates the data compiled by Healey and Miller (1963) from 1400 gravity stations with approximately one observation per square km. The Bouguer gravity has a maximum value of -137 mgals at Mine Mountain and a minimum of -185 mgals over Emigrant Valley. There is a regional gradient of -0.6 mgal/km northwards across Yucca Flat (Healey and Miller, 1963) which

correlates with the trend of the mean elevation above sea-level across the Yucca Flat area. In general, the gravity highs correlate with the outcrops of the pre-Cenozoic rocks which form the mountains which surround Yucca Flat, whereas the gravity lows correlate with the thick deposits of alluvium beneath the flats.

A conspicuous feature on the Bouguer gravity map is the northward trending high which occurs over the western half of Yucca Flat. A major gravity low parallels this feature under the eastern half of the flat, a smaller low occurring along the western side of the flat. The gravity high is due to a buried ridge or horst approximately 2.4 km wide and about 18 km long which is bounded by high-angle faults (Healey and Miller, 1963) in the pre-Cenozoic surface. Geologic profiles across the ridge (Barnes et al., 1963) show the pre-Cenozoic erosion surface is 0.18 - 0.24 km below the present surface of the flat. The gravity low to the east of the high defines a trough approximately 32 km long and 4.8 km wide containing up to 1.4 km of Tertiary tuff and Quaternary alluvium. This value was determined from the gravity data (Healey and Miller, 1963; Healey, 1968) substantiated by the seismic work of Diment et al., (1959) and verified by drilling. Table 1 of Healey (1968) shows that the estimates based on gravity of the thickness of the valley fill at the 19 drill holes whose locations are shown in Figure 59 are accurate to within 17 percent indicating that the density contrasts between the various rocks in the area are fairly well known. To the east of Yucca Flat, the steep gradients away from the trough towards the Painted Ridge and Banded Mountain are indicative of faulting. Healey and Miller (1963) postulate that two high-angle faults may be present along the eastern margin of the trough. The gravity low to the west of the ridge, according to Healey and Miller (1963), represents a graben-like structure

let down between the Eleena Range and the buried ridge, in which up to 1 km of Cenozoic rocks have accumulated. The Yucca Fault (Barnes et al, 1963) runs along the eastern flank of the buried ridge for much of its length.

Aeromagnetic Data

Figure 60 shows the total magnetic intensity in the region of NTS. The figure covers the same area as the Bouguer gravity map (Figure 58) and is taken from the magnetic map compiled by Zietz and Kirby as part of the Transcontinental Geographical Survey (U. S. Geological Survey, 1968). The area of intense anomalies both positive and negative in the northwest part of NTS corresponds to the outcrop of Tertiary lavas. Some of these lavas have sufficient remanent intensity (both normal polarity and reversed polarity) to account for the aeromagnetic anomalies (Bath, 1968).

The large scale aeromagnetic map of the Yucca Flat area has been compiled by the U. S. Geological Survey from data collected in 1960 along profiles flown at 2400 meters with .8 km spacing (Hazelwood et al, 1963). The range in values of the total magnetic intensity over the Yucca Flat area is 750 gammas. There are two prominent positive magnetic anomalies which correlate with the Climax stock and the Gold Meadows intrusive. (These anomalies can be seen on Figure 60). Both are granitic bodies of Mesozoic age. The two positive anomalies are separated by a negative anomaly which Hazelwood et al, (1963) suggest is at least partially due to remanent magnetization in the volcanic rocks of the Rainer Mesa. Allingham (written communication, 1967, in Hinrichs, 1968) confirms that this negative anomaly is caused by a reversely polarized ash-flow tuff.

Over Yucca Flat itself, the magnetic intensity is relatively uniform with a gentle southward gradient of about 10 gammas/km (Hazelwood et al, 1963). This suggests that the area beneath the flat is uncomplicated by major intrusives. There is no expression in the aeromagnetic data shown in Figure 60, of the north-south trending ridge which was found from the interpretation of the gravity data (Healey and Miller, 1963). However a detailed aeromagnetic map of the north-central part of Yucca Flat published by Hinricks (Figure 6, 1968) shows a steep negative gradient along the eastern or downthrown side of the Yucca Fault.

Heat Flow Data

We were unable to find any published reports of heat flow determinations with the Nevada Test Site in the geophysical literature. However, Blackwell (1969) has prepared a map showing the distribution of heat flow determinations in the western United States (Figure 48). The mean heat flow for the Basin and Range province from Blackwell's data is approximately $2.0 \mu\text{cal}/\text{cm}^2\text{-sec}$. To the west of the Basin and Range province in the Sierra Nevada heat flow is low ($0.9 \mu\text{cal}/\text{cm}^2\text{sec}$ Roy and Blackwell, 1966) the transition taking place across a narrow zone 50 km east of the structural and physiographic boundary. To the east of the Basin and Range, in the Colorado Plateaus heat flow values are normal.

The heat flow in the western United States correlates very well with the P_n velocity and the Bouguer gravity measurements as shown in Figure 49.

Seismicity

We searched the Preliminary Determination of Epicenter cards published by the U. S. Coast and Geodetic Survey for the period January 1960 through January 1968 for events occurring within the $34 - 38^{\circ}\text{N}$, $114 - 119^{\circ}\text{W}$ with focal depths less than 35 km. We found 448 events, but only five small ($m_b < 4.5$) events actually occurred within NTS over this period that could not be attributed to a man-made event. However, Figure 61 shows that there were several events to the northeast and northwest of the test site. In addition, movement along the Yucca Fault has been observed after nuclear tests (Williams and Hoover, 1962; Dickey, 1968) as well as extensive fracturing along preferred directions parallel to joint sets in the bedrock unrelated to the Yucca Fault (Barosh, 1968). Furthermore, following a recent large explosion at the Nevada Test Site, Benham, significant microearthquake activity was observed, (Engdahl et al, 1969), (Healey and Hamilton, 1969) in the vicinity of the shot point. Aki et al, (1969) from an analysis of Love waves generated by Benham suggest that an earthquake was triggered about 0.5 seconds after the explosion. Figure 62 shows the aftershock pattern produced by the Benham event. This pattern clearly defines the prevailing north-south structural trend in the NTS area.

A Geophysical Model for the Crust Beneath Yucca Flat, Nevada Test Site

Nuclear explosions at the Nevada Test Site have been detonated at several locations within the test area and in various geologic media. Since the rocks exposed at NTS have a wide range of physical properties we will attempt to construct a plausible model for the crust beneath Yucca Flat and

because the shallow structure beneath the flat is itself complicated, the surface layers of the model must necessarily be somewhat idealized. However, because of the uncertainties as to the gross structure of the deeper part of the crust, differences in the near surface layers may be considered as second order effects for our purposes even though they may have a profound influence on calculations of yields from explosions.

The near surface structure beneath Yucca Flat is fairly well known, from well-logs, seismic, and gravity data. Therefore we have chosen to base the upper layers of our model on the structure and lithology logged by Williams and Cole (Williams et al, 1963) at drill hole UE4a, the location of which is shown in Figure 59. The strata encountered in drill hole UE4a consisted of approximately 0.17 km of alluvium overlying 0.82 km of tuff which rests on the Paleozoic rocks. Therefore, in constructing model YF111 we have adopted 0.2 km for the thickness of layer 1 and 0.8 km for the thickness of layer two.

Compressional wave velocities in alluvium at NTS range from a low of 0.65 km/sec at the surface to 1.65 km/sec for water saturated alluvium at a depth of 0.2 km (Hazelwood et al, 1963). Therefore for our model we have assumed a compressional wave velocity of 1.3 km/sec for layer one. For tuff, Hazlewood et al, (1963) found velocities ranging from 2.3 km/sec to 4.0 km/sec depending upon lithology. We have adopted 3.0 km/sec as the velocity in layer two of our model YF111. Sonic velocities in the Paleozoic limestones and dolomites which underlie the tuff in drill hole UE4a are typically 3.9 to 6.5 km/sec (Hazlewood et al, 1963). Data from a traverse across the buried Paleozoic ridge which was down the center of Yucca Flat (Hazlewood et al, 1963) suggest that the range of the seismic velocities may be somewhat lower than this.

The vertical thickness of the Paleozoic section beneath Yucca Flat is not known.

The bulk densities of the various rock types which occur at the Nevada Test Site are shown in Table 10. The mean density of the alluvium at Yucca Flat is 1.94 gm/cm^3 (Healey and Miller, 1963). Densities given by Healey and Miller (1963) for the various tuff units range from 1.94 gm/cm^3 in the non-welded tuffs to 2.50 gm/cm^3 for the welded tuffs. We have adopted a density of 2.2 gm/cm^3 for layer two of our model YF111. Densities in the Pre-cambrian and Paleozoic rocks range from 2.49 for quartzite to 2.85 for dolomite and average 2.67 gm/cm^3 (Healey and Miller, 1963).

Although the structure of the surficial layers at NTS is well documented, the structure of the deeper parts of the crust is only poorly known. We have been unable to find any reports of a deep seismic refraction study through the Yucca Flat area. However, four of the seismic refraction profiles shown in Figure 53 have used locations within NTS as shot points. Hence, we can estimate the deep crustal structure beneath NTS by extrapolation if we assume no rapid variations in crustal structure within a radius of approximately 50 km from the mean shot point ($37^\circ 10' \text{ N}$, $116^\circ 05' \text{ W}$). Extrapolating the depth to the Moho beneath NTS from the data obtained by Hill and Pakiser (1966), gives a total crustal thickness of 30 km. Diment et al, (1961) also report that the crust is about 30 km thick at NTS. Data from the unreversed profile east from NTS give a crustal thickness of about 25 km at NTS (Ryall and Stuart, 1963). The thickness of the crust beneath NTS is 34 km calculated from Model II of Gibbs and Roller (1966). The range of their determinations, 25 - 34 km suggests that the total crustal thickness may change within 50 km of the mean shot point. Therefore, we have adopted 30 km as the depth of the Moho in model YF111.

The attitude and thickness of the intermediate layer beneath NTS is even more uncertain. Based on the data of Hill and Pakiser (1966) an intermediate crustal layer with a velocity of 6.7 km/sec occurs at a depth of 20 km beneath NTS which is consistent with the conclusions of Prodehl (1969). Clearly, the 6.7 km/sec layer in the profile east of NTS is too thin (3.8 km thickness), to appear as a first arrival, and Ryall and Stuart (1963) only identify it from questionable secondary arrivals. For the NTS-Ludlow reversed profile, Gibbs and Roller (1966) found first arrivals with apparent velocities of 6.8 km/sec from shots fired at Ludlow but not from events at NTS. Nevertheless, Model II of Gibbs and Roller (1966) has a 20 km thick intermediate with a velocity 6.8 km/sec at the NTS end of the profile. However, some sort of intermediate layer probably exists to the south of NTS because Johnson (1965) found a 8 km thick layer with a velocity of 7.1 km/sec at 25 km depth at the point where his profile intersects that of Gibbs and Roller (1966). In constructing model YF111 we have adopted one km for the thickness of layer three, the near surface (4.5 km/sec) layer. We have divided the remainder of the crust into a 18 km thick "granitic" layer with a P-wave velocity of 6.7 km/sec. We have assigned a P_n velocity of 7.8 km/sec, in agreement with the results of Healey and Ploger (1965).

The shear wave velocity distribution in the Basin and Range Province is also poorly known. Model 35CM2 (Figure 57) gives the distribution of shear-wave velocity with depth which best fits the surface wave dispersion data from the Basin and Range Province (Alexander, 1963). The shear-wave velocity in the near surface layer is 2.2 km/sec, which gives a Poisson's ratio of 0.22 which we have used to calculate the shear-wave velocity in layers one, two and three of our model YF111. For

6.1 km/sec or "granitic" layer, Alexander (1963) obtained a shear wave velocity of 3.6 km/sec which corresponds to a Poisson's ratio of 0.23. We have adopted 3.6 km/sec as the S-wave velocity for layer three in our model.

Model 35MC2 has an intermediate section 25 km thick which occurs at a depth of 25 km. In this section the shear velocity is 4.1 km/sec whereas the P-wave velocity is 7.7 km/sec which gives a Poisson's ratio of 0.3. To make the S-wave portion of model YF111 compatible with the P-wave portion and the seismic refraction data, we have assigned a shear velocity of 4.0 km/sec to layer 5. This corresponds to a Poisson's ratio of 0.23 which is equivalent to Poisson's ratio in the "granitic" layer. We have adopted 4.5 km/sec for S_n which is in agreement with the model STAN-3 (Kovach and Robinson, 1969) and close to the S_n velocity given by Anderson and Julian (1969).

To complete our model we need to know the density for layers four and five of our model and in the upper mantle. For the "granitic" layer, Alexander (1963) found that a density of 2.78 gm/cm^3 was required in this layer to fit his dispersion data. This is close to the value of 2.80 gm/cm^3 for the density of crust below 5 km depth adopted by Thompson and Talwani (1964). Archambeau and Davis (1969) give the density of the 6.7 km/sec layer as 2.95 gm/cm^3 . We have adopted this value for our layer five. The density of the upper mantle given by several authors is very close to 3.30 gm/cm^3 and so we have incorporated this value in model YF111.

Discussion

Geological and geophysical investigations at the Nevada Test Site over the past decade show that Yucca Flat is an intermontane basin typical of the Basin and Range physiographic

province. The flat itself consists of an alluvium filled trough formed by a block of Paleozoic rocks which have been let down by north to northeast trending faults between the eastwards tilted blocks of Paleozoic strata which form the mountains to the east and west. Gravity, seismic refraction, and bore hole surveys showed that the alluvium at Yucca Flat attains a maximum thickness of 0.61 km. These surveys also revealed the presence of a north to northeast trending ridge of Paleozoic rock in the floor of the valley which protrudes through the Cenozoic volcanics. This ridge together with the known fault (Yucca Fault) which extends down the center of Yucca Flat indicate that the structure is considerably more complex than a simple graben and suggest that subsurface trough is probably a vested graben or "graben-in-graben" structure similar to that found beneath Dixie Valley (Thompson et al, 1967).

In addition to the seismic and gravity surveys, aeromagnetic surveys have also been conducted at NTS. The latter revealed that the two positive anomalies to the north of Yucca Flat correlate with two granitic intrusive bodies of Mesozoic age. The negative anomalies found in the vicinity of Yucca Flat correlate with outcrops of the Anozoic volcanics and probably result from reversely polarized flows within this sequence.

Although the near-surface structure at Yucca Flat is known in great detail, we have been unable to find any references pertaining to the deeper structure. Hence, we do not know the actual thickness of the Paleozoic rocks beneath Yucca Flat, for example. Therefore, in constructing the crustal models shown in Table 11, we have assigned them a thickness of 1 km. This choice is not quite as arbitrary as it may seem, since Hill and Pakiser (1966) indicate 1 km of low-velocity "sediments" to the north of NTS and Alexander (1963)

gives 2 - 3 km as the thickness for the "sedimentary" layer in the Basin and Range. At depths greater than 3 km the Paleozoic rocks, should they persist, are probably indistinguishable from the "granitic" layer in terms of velocity.

The structure of the remainder of the crust at NTS itself has not been determined directly. None of the seismic refraction profiles discussed above actually traverses the test site and hence the thickness of the crust, the number of layers and their velocities have to be inferred from structures determined at points 50 km away or more. Projecting the structures back to the mean shot point at NTS may not be valid if faults of the type proposed by Hill and Pakiser (1966) are present. However, because of the lack of data we were forced to make such a projection to construct our models. Projecting the structures back to the mean shot point at NTS, we obtained estimates of crustal thickness of NTS ranging from 25 km to 34 km. The most probable thickness is 30 km, the two extreme values representing thicknesses estimated from an unreversed profile (Ryall and Stuart, 1963) and a model in which a 20 km thick intermediate layer was assumed (Gibbs and Roller, 1966), respectively.

The existence of an intermediate crustal layer in the Basin and Range has still not been conclusively established. This is because identification of the intermediate layer relies for the most part on later arrivals on the seismograms, either refractions or, in many instances, reflections. In the case of a plane layered crust, composed of two layers with thicknesses h_1 and h_2 , and velocities V_1 and V_2 , over a half-space with velocity V_3 , the condition for a refraction from the intermediate layer (V_2) to appear as a first-arrival is

$$h_2 \frac{(V_3^2 - V_2^2)^{1/2}}{V_2(V_3 - V_2)} > h_1 \frac{(V_2^2 - V_1^2)^{1/2}}{V_1(V_2 - V_1)} - \frac{(V_3^2 - V_1^2)^{1/2}}{V_1(V_3 - V_1)}$$

If we consider the case where $V_1 = 6.1$ km/sec, $V_2 = 6.7$ km/sec, and $V_3 = 7.8$ km/sec, which are velocities commonly reported for the "granitic" layer, the intermediate layer, and P_n , we see that for a refraction from the intermediate layer to appear as a first arrival

$$h_2 > 0.53 h_1$$

Thus, for the profiles considered above, refractions from the intermediate layer theoretically should not appear as first arrivals, with the exception of the profile studied by Gibbs and Roller (1964).

From the crustal model for NTS obtained by Gibbs and Roller (1964), and extending the formula given above to the three-layer case, it is clear that refractions from the intermediate layer should occur on the seismograms from the NTS - Ludlow profile. The fact that Gibbs and Roller (1964) do not report first arrivals from the intermediate layer suggests that the 20 km thickness assigned to this layer is excessive. However, Hill and Pakiser (1966) observe that the upper boundary of the intermediate layer is much more clearly defined from recordings of chemical explosions than nuclear explosions, which may explain why Gibbs and Roller (1964) do not find 6.8 km/sec arrivals from events at NTS.

Although presence of the intermediate layer with the velocity and thickness indicated in our model YF111 cannot be established from first arrival data, there is an increasing body of evidence from secondary arrivals which justifies its inclusion in this model. In addition, the surface-wave data of Alexander (1963) suggest an intermediate layer is present although it is difficult to reconcile Alexander's model 35CM2 with the body-wave models.

LOCATION OF EVENTS AT NTS, TRAVEL-TIMES AND UPPER MANTLE STRUCTURE FOR THE BASIN AND RANGE PROVINCE

In this section of the report we deal with the location of events at NTS using the methods outlined in Section III of the report. We have extended the work of Chiburis (1968) so as to incorporate all available LRSM stations and Vela Seismological Observatories to facilitate a more direct comparison between the network's performance locating events at Lake Superior and locating events at NTS. We shall discuss the results of previous investigations of the travel times from events at NTS and combine these with results from other studies of the properties of the mantle beneath the western United States, in an attempt to derive a model for the structure beneath the Basin and Range province which is consistent with the surface wave dispersion data.

Location of NTS Using the LRSM and Observatory Network

Chiburis (1968) has located 19 events at NTS, with and without travel-time anomaly corrections, using the program SHIFT and only LRSM stations at distances greater than 17 degrees. However, the Herrin-68 travel-times were not available at the time this work was completed. We have recomputed the epicenters of the 19 events studied by Chiburis, using his travel-time data and the Herrin-68 travel-time tables. Figure 64 shows the results. The travel-time anomalies which we used as anomaly corrections are shown in Table 12. The results (Table 13) show that the mean location error for all 19 events is 21.2 km without anomaly corrections and 2.0 km for 17 of the events located using anomaly corrections.

Figure 64 shows the computed locations. There is considerable reduction in the area of the 95% confidence ellipses and the standard deviation of the residuals after travel-time anomaly corrections are made.

In locating the shots at Lake Superior, we found that using the whole LRSM and Observatory network of stations we were able to obtain satisfactory results. Therefore, in order to afford a more direct comparison, we relocated the same 17 of the 19 events at NTS discussed above using the whole network. We took the observed travel-times from the shot reports covering these events and rejected those readings designated questionable by the original analyst. Figure 65 shows the recomputed epicenters with and without anomaly corrections. The mean location error without anomaly corrections is 10.9 km (see Table 14) or approximately half of that when only stations for which $\Delta > 17^\circ$ were used. The mean location error with anomaly corrections (given in Table 12) is 3.2 km or 0.9 km greater than for the more distant group of stations. This increase probably results from possible instability of the anomalies at the shorter distances due to the influence of the complex velocity structure (Archambeau et al, 1969) of the crust and upper mantle under the western United States. The mean area of the 95% confidence ellipse is significantly less than that computed using the more distant stations both with and without anomaly corrections. However, both with and without anomaly corrections, the standard deviation of the residuals is larger for the whole network than when only stations where $\Delta > 17^\circ$ were used. This is probably due to reading error; Chiburis read his own data, whereas we used the shot report travel-times.

The azimuthal coverage of the LRSM network (about 130°) is insufficient to allow us to apply Spence and Alexander's method to the 19 events at NTS discussed above. Instead we simply

show (Table 15) Spence and Alexander's results (Spence and Alexander, 1969) for the locations of three large events at NTS relative to DUMONT which they computed using data from the WSSS network. For comparison, we have located the same three events using the method of Chiburis (1968) with the same travel-time data. The results are interesting in that although the mean location errors are about the same, Spence and Alexander's method yields poor results in terms of the azimuth for the computed location of BOXCAR, whereas Chiburis's method gives a poor location for FAULTLESS. We do not know the reason for this discrepancy.

Travel-Times and Upper Mantle Structure for the Basin and Range Province

P-wave, travel-times, amplitudes, phase velocities, and $dT/d\Delta$ in the western United States have been intensively studied by Niazi and Anderson (1965), Johnson (1967), Julian and Anderson (1968), and Archambeau et al, (1966,1967,1969). Velocity models of the upper mantle derived by these authors show rapid increases in velocity in the depth ranges 375 - 650 km and 650 to 700 km. Anderson (1967) and Fujisawa (1968) have discussed some of the implications of these rapid increases in velocity in terms of composition of the upper mantle. However, despite their similarities at depth, the models show some variations, particularly in the region of the low velocity zone. In a comprehensive study of travel-times, amplitudes, and phase velocities of P-waves from the Bilby and Shoal explosions and the Fallon, Nevada, earthquake, Archambeau et al, (1969) show that the various physiographic provinces correlate with differences in structure within the upper mantle. Archambeau et al, (1969) distinguish two basic types of upper mantle structures in the tectonic

region of western North America. These are a Basin and Range or depth zone mantle structure and a plateau-mountain mantle structure. As more data becomes available, further subdivisions of the latter structure may be necessary. Since the Nevada Test Site is located in the Basin and Range province, we are concerned chiefly with Archambeau, et al's model CIT 111P (Figure 46), although we will briefly discuss the other models. Figure 45 shows the location of the profiles which Archambeau, et al used to study the travel-times, amplitudes, and phase velocities from these events.

The Basin and Range model CIT 111P (Figure 46) was derived from data recorded along the Shoal-Fallon southeast profile (Figure 45); Shoal was a nuclear explosion detonated at the site of the Fallon, Nevada, earthquake of 20 July 1962, approximately 500 km northwest of NTS. Figure 66 shows the travel-time data for this profile together with the theoretical travel-time curve computed from model CIT 111P. As Archambeau, et al, (1969) point out, the fit of the first arrival branches of the travel-time curve is good. In addition, the later arrivals correlate with the appropriate extensions of the first arrival branches of the theoretical curves. This is important, particularly in the neighborhood of cusps where more than one phase is arriving, because the correlation of phases between records was achieved independently of any travel-time curve. (For details of the digital processes used see Archambeau et al, 1969).

The P_n velocity in model CIT 111P (Figure 46) is 7.7 km/sec which is consistent with the P_n velocity of 7.7 - 7.8 km/sec in the Basin and Range obtained from the refraction surveys discussed above. Furthermore, the P-wave delays through the upper mantle calculated from model CIT 111P are consistent with the observed P-wave delays for the Basin and

Range Province of 0.6 - 0.7 seconds with respect to the Jeffreys-Bullen travel-times (Figure 67) found by Cleary and Hales (1966).

In addition to satisfying the travel-time data, model CIT 111P also quantitatively explains the amplitude observations. Figure 68 shows the observed spectral amplitudes at 1.5 Hz obtained by Archambeau, et al, (1969) from the Shoal northeast profile together with the theoretical amplitudes calculated from the model CIT 111P. (The spectral amplitudes from the Fallon earthquake were not considered because of uncertainty as to the nature of the source spectrum and radiation pattern). The upper part of Figure 68 shows the "inferred" curves of amplitude versus distance, so called because they represent the mean variation of amplitude with distance for each branch. The large deviations in the observed amplitudes from these mean curves are attributed to differences in the crustal transfer function at the various recording stations by Archambeau, et al, (1969), and to interference effects where two phases arrive nearly simultaneously. However, the mean trend of the inferred curves agrees well with the theoretical amplitude-distance curves computed from model CIY 111P, as shown in the lower part of Figure 68. Because of this fit, Archambeau, et al, (1969) conclude that the velocity gradients in model CIT 111P are indicative of those which exist in the upper mantle and that rapid velocity variations near 150, 375 and 650 km depths are required to explain the observations.

Archambeau et al, (1969) have also derived a Q-structure for the Basin and Range province. They determined the observed spectral amplitudes from Shoal and Bilby at three frequencies, 0.5, 1.0 and 1.5 Hz and observed that the high-frequency amplitudes decreased most rapidly with increasing distance. To explain this observation, Archambeau et al,

(1969) constructed the Q-model for a frequency of 1.5 Hz shown in Figure 69, for the lower frequencies, they inferred a Q-model from the long-period surface wave data published by Anderson et al, (1965). In view of the uncertainties involved in determining Q either from body wave or surface wave data, we must consider the two Q-structures shown in Figure 69 as placing rough bounds on the possible range of variation of Q with depth and only suggest that Q at high frequencies is greater than at low frequencies. Nevertheless, the combined amplitude data from Bilby and Shoal are satisfactorily explained by $Q_{\text{crust}} = 1000$, $Q_{\text{mantle}} = 400$ at $f = 1.25$ Hz and $Q_{\text{crust}} = 1000$, $Q_{\text{mantle}} = 300$ at $f = 0.875$ Hz.

In addition to the Fallon-Shoal southeast profile, Archambeau et al, (1969) also analyzed travel-time and amplitude data from P-waves recorded along three additional profiles (Figure 45). From the Shoal-Fallon northeast profile, they derived a model for the upper mantle beneath the Snake River Plains - Northern Rockies province, model CIT 112P; from the Bilby southeast profile, model CIT 110P for the Colorado Plateau - Rocky Mountains; from the Bilby northeast profile, model CIT 109P for the eastern Basin and Range - Northern Rockies. Figure 70 shows all three of these models, together with CIT 111P. Below 200 km depth all four models are quite similar, the major difference being in the upper 200 km of the mantle. For the three plateau-mountain models, there is a high velocity (8.0 km/sec) lid to the upper mantle 30 to 60 km thick below which the P-wave velocity decreases rapidly reaching a minimum at a depth of 90 km. The velocity then increases with depth to the bottom of the low velocity zone at about 45 km depth where there is a region of large velocity gradients after which the velocity again increases with depth. The Basin and Range model (CIT 111P) on the other hand has no high velocity lid,

but rather the velocity remains nearly constant at 7.7 km/sec from the base of the crust to a depth of 135 km where again there is a region of large velocity gradients.

The results obtained by Archambeau et al, (1969) are in good agreement with the earlier results of Johnson (1967) who studied $dT/d\Delta$ from short-period P-waves in the distance range $3^\circ \leq \Delta \leq 30^\circ$ recorded at the extended TFO array in Arizona. The upper mantle model obtained by Johnson (1967), model CIT 204 in Figure 71, is essentially an average of the models obtained by Archambeau et al, (1969). This can be seen by considering Figure 72 which illustrates the excellent fit of the theoretical $dT/d\Delta$ curves calculated from Archambeau et al's two extreme models CIT 111P and CIT 109P with Johnson's (1967) data. Model CIT 109P is also similar to the model NTS-NE19 (Figure 71) obtained by Julian and Anderson (1968) from travel-times recorded along a profile northeast from NTS.

Kovach and Robinson (1969) studied $dT/d\Delta$ measurements for long-period S-waves from earthquakes in the distance range $14^\circ < \Delta < 40^\circ$ recorded at the extended TFO array in Arizona. Since these results were obtained in a manner analogous to that used by Johnson (1967) to study the P-wave velocity structure of the upper mantle under the western United States, Kovach and Robinson's model should be consistent with model CIT 204. Figure 47 shows the preferred STAN3 model obtained by Kovach and Robinson (1969) together with a simpler model STAN2 which, although it fits the observed data fairly well, results in poorer agreement with the observed travel-time residuals with respect to the Jeffreys-Bullen travel-time tables reported by Doyle and Hales (1967) for the distance range $28^\circ < \Delta < 82^\circ$. The main features of model STAN3 are a thin

high velocity 6.5 km/sec lid capping a broad low velocity zone centered at 100 km depth, and regions of rapid increases in velocity at depths of 360 km and 620 km. An important difference between STAN3 and CIT 100 series of models (Archambeau, et al, 1969) is the absence of the zone of rapid increase in shear velocity at a depth of 165 km the depth at which there is an increase in P-wave velocity in the latter models and the model CIT 204 (Johnson, 1967). However, the velocity gradient in model STAN3 does change at this depth (Kovach and Robinson, 1969).

Julian and Anderson (1968) also present a model CIT 19B for both P- and S-wave velocity structure in the western United States based on Love wave dispersion data. The P-wave velocities were derived from the S-wave data using the Poisson's ratio distribution appropriate to Gutenberg's model. Figure 75 shows model CIT 19B. Whereas the overall S-wave velocity distribution of model CIT 19B is similar to that of STAN3, the velocity gradients below the low velocity zone in CIT 19B are small except in the regions 350 - 450 km and 650 - 750 km. Also, the regions of high velocity gradients are higher for the surface wave model, and in the case of linear region of high velocity gradients, deeper than those for the body wave model STAN3.

COMPARISON OF THE LAKE SUPERIOR AND NEVADA TEST SITE SOURCE REGIONS

In preceding sections of this report we have discussed the diverse data pertaining to Lake Superior and the Nevada Test Site as seismic source regions separately. In this section of the report we compare and contrast the structure of the crust and upper mantle at Lake Superior as it is known, with the structure at NTS. This section will also serve as an overall summary to the preceding sections.

At Lake Superior we are dealing with a geologically old and stable regime, whereas at NTS we are concerned with a young, tectonically active region. The structure of the crust at Lake Superior has not changed radically over the last 500 million years. On the other hand, the crust at NTS is still being subjected to tectonic deformation. This continuing release of stress at NTS is manifest in the high level of seismic activity in the Basin and Range province and at NTS itself (Figures 61 and 62). The Lake Superior region is essentially aseismic.

The crustal structure at Lake Superior is complex despite its antiquity. All interpretations based on data collected during 1963 Lake Superior Seismic Experiment indicate considerable variation (50% to 100%) in crustal thickness in the region. Crustal thicknesses exceeding 50 km were reported indicating that Lake Superior is not a typical portion of the Canadian Shield. Unusually high velocities, 6.6 km/sec to 6.9 km/sec at depths of only 10 km, were found, further emphasising the abnormal nature of the crust beneath the Lake. These high velocities are thought to be due to metamorphism of the Keweenawan lavas through the amphibolite facies in the higher parts of the crust. The cause of the high velocities at depth

is not known, but is probably related to the emplacement of the lavas.

The shallow structure of the Lake Superior syncline supports this hypothesis, at least in part. In the western half of the Lake, the Keweenaw lavas are upthrust to form a horst which appears to be genetically related to the Mid-Continental Gravity High; Keweenaw lavas having been reported from boreholes along the axis of this feature together with velocities similar to those found at Lake Superior. The shallow layers of the crust at Lake Superior form a broad syncline, the axis of which swings around the Keweenaw Peninsula. Whether or not the syncline dies out at the southeast shore of Lake Superior is uncertain.

The shallow structure at NTS is much more complex than at Lake Superior. Whereas the wavelength of the near surface features at Lake Superior are of the order of 150 km, the wavelength at NTS is approximately 20 km. The near surface layers at NTS are repeated by thrust faulting and pervaded by Cenozoic and recent normal faults. Tilting of the faulted blocks has resulted in a series of northerly trending mountain ranges separated by deep intermontane valleys filled with sediments. Movement along the faults is still taking place.

The crust at NTS is thin compared to that at Lake Superior. The crustal thickness at NTS is approximately 30 km. In contrast to the Lake Superior region, the crustal thickness is relatively uniform throughout the Basin and Range province. Seismic refraction surveys in the Basin and Range province reveal a thick "granitic" layer with a P-wave velocity of about 6.1 km/sec. The layer occurs at depths of 2 to 5 km and has a mean thickness of approximately 20 km. The exact thickness of this layer is somewhat uncertain because of the indications of an "intermediate" layer with a velocity of 6.7 km/sec occurring

at the base of this crustal layer. However, this intermediate layer is quite variable in thickness and character over the Basin and Range province and its exact nature is somewhat uncertain. Nevertheless, it is clear that the mean crustal velocity at NTS is considerably less than at Lake Superior. Figure 73 illustrates this point.

There are considerable differences between the properties of the upper mantle at Lake Superior and those at NTS. Bouguer anomalies over the Basin and Range average about -120 mgal. At Lake Superior they are ≈ 0 , and values in the range -40 to -60 mgals are typical of the Canadian Shield as a whole. In the Basin and Range province heat flow is high ($> 2.0 \mu\text{cal}/\text{cm}^2\text{-sec}$) whereas at Lake Superior it is low ($0.9 \mu\text{cal}/\text{cm}^2\text{ sec}$). The high heat flow in the Basin and Range is not due to excessive heat generation in the crust. Rather, the work of Roy et al (1968) has demonstrated that it is due to anomalously high heat flow in the upper mantle. This high mantle heat flow correlates with high electrical conductivities at shallow depths in the upper mantle. Together these observations suggest partial melting in the upper mantle beneath NTS and the Basin and Range, but not at Lake Superior. This is consistent with the seismic data from both areas.

Regional differences in P-delays and P_n -velocities in North America have been known for some time. Figure 67 [Figure 3 of Archambeau et al (1969)] shows the P-wave travel-time anomalies with respect to the Jeffreys-Bullen tables (Jeffreys and Bullen, 1940) at North American stations obtained by Cleary and Hales (1966). The P travel-time anomalies observed at NTS range from +0.2 to +0.6 sec indicating the arrivals are consistently late. At Lake Superior, arrivals are early, the travel-time anomalies ranging from -0.6 sec to -1.0 sec. The differences in P-wave delays are reflected in the P_n velocities (Figure 49). In the

Lake Superior region P_n velocities are high (8.1 - 8.2 km/sec) whereas in the vicinity of NTS they are low (7.7 - 7.8 km/sec).

Archambeau et al, (1969) have lucidly demonstrated the relationships between P-wave velocity structure in the upper mantle and the physiographic provinces of the western United States. The travel-time data from Project Early Rise, when inverted to yield velocity structures for the upper mantle suggests that similar relationships exist for the eastern United States and the Canadian Shield. Figure 74 shows the model CIT IIIP for the Basin and Range province (Archambeau et al, 1969) together with the Canadian Shield model of Barr (1967), the model for the mantle province west of Lake Superior (Lewis and Meyer, 1968) and the model for the central United States (Green and Hales, 1968).

The most important difference between the P-wave models shown in Figure 74 is the structure of the upper mantle between 50 km and 150 km. The Basin and Range model (CIT IIIP) has a zone of low-velocities in this range with a region of rapid increase in velocity from 145 to 150 km. None of the Early Rise models show this. Instead all three models indicate sharp but relatively small increases in velocity at depths of less than 100 km. This Lewis and Meyer model is the only model in which the velocity decreases with depth in the range 140 to 160 km. Below 300 km, the Lewis and Meyer model differs significantly from the other models. This model has a thin region of high velocity gradients centered at 340 km, with a second region with much higher gradients at 445 km. The Barr model has a region of high velocity gradients starting at 370 km, as do the two models for the Basin and Range. (Note that only the upper 260 km of the Green and Hales model is based on Early Rise data; the deeper part of this model was based on travel-times from events at NTS).

Thus the main difference in the P-wave models for the two regions is the apparent absence of a low velocity zone in the upper 150 km of the mantle beneath the Canadian Shield. It is not clear at precisely what depth the "400 km" discontinuity occurs for the Canadian Shield. On the basis of the Lewis and Meyer model, which is for a path across the shield and the northern Rockies, this discontinuity is 50 km deeper than in the Basin and Range mantle province.

We can also compare the shear-wave models for the Canadian Shield and the western United States although the S-wave structures are less well known. Figure 75 shows the S-wave structure obtained by Lewis and Meyer (1968) from body-waves and the S-wave portion of CANSO together with STAN-3 (Kovach and Robinson, 1969) and the S-wave portion of Alexander's model 32 CM2. The most important difference between the structures is the presence of the deep low velocity zone for S-waves which occurs between 125 and 180 km depth in the Canadian Shield. Such a feature is not present in the Kovach and Robinson model, which indicates that the S-wave velocity increases smoothly through the region. The only other S-wave model with a low-velocity zone similar to this, is that obtained by Ibrahim and Nuttli (1967) from travel-times to stations distributed over the entire United States. However, there is not a low-velocity zone at this depth in the model US-26 derived by Anderson and Julian (1969) from a re-examination of this same data. Another difference between the Lewis and Meyer model and STAN-3 is the velocity structure around 600 km. STAN-3 which was made to be compatible with the P-wave model of Johnson (1967), has a region of large velocity gradients centered at 400 km (as does US 26), whereas the Lewis and Meyer S-model has a region of large velocity gradients at 450 km, also chosen to be compatible with the corresponding P-wave model.

The S-models from the Canadian Shield (CANSD) and the Basin and Range (35 CM2) derived from surface-wave dispersion studies offer only a very limited basis for comparison. CANSD models suggest that the S-wave velocity in the mantle beneath the Canadian Shield stays constant nearly to a depth of 135 km below which there is a broad low velocity zone extending to a depth of 315 km. Model 35 CM2 suggests that the S-wave velocity decreases beneath the Basin and Range between the depths of 70 and 125 km.

The differences in the properties of the upper mantle between Lake Superior are conveniently summarized in Figure 76. This figure, based primarily on the CIT 100 series of models traces the low-velocity zone from the Basin and Range, where it is thick and extends to the base of the crust, north-eastwards across the United States to the Superior Highlands, where it is either very thin or does not exist. A similar section to that shown in Figure 76 was derived independently by Green and Hales (1968).

IMPLICATIONS

The seismological differences, defined by the study, between the Lake Superior Region and the Nevada Test Site, underline the need to calibrate individually all of the earth's geological provinces where test sites may be located. Every major geophysical parameter affecting seismic wave propagation appears to differ between the two regions; these parameters include seismic velocities, attenuation, and regional stress patterns. The differences between the two regions extend from the near surface layers to at least 200 km depth in the upper mantle (and possibly even deeper) so that seismic observations at all distances can be expected to differ substantially for identical sources. Consequently it is extremely unlikely that the results, for NTS events, that depend on structure parameters can be generalized to apply to similar sources occurring in regions as dissimilar as Lake Superior.

These differences could have been predicted on an a priori basis from the models derived from surface geological studies which place Lake Superior on an ancient shield and NTS in a relatively modern mountain building region. However, in view of the work of Archambeau et al (1969) in the Western United States, it is important that the "fine structure" of the upper mantle as well as the crust be determined precisely because of their influence on such important identification criteria as source depth and location, M_s vs. m_b , and complexity. This detail is still largely lacking for the shield area containing Lake Superior. We can infer however that the seemingly low intrinsic absorption in the shield area would tend to sharpen the contrast between earthquakes and explosions relative to the NTS area, because spectral differences at the higher frequencies could be observed at greater teleseismic

distances. Moreover, the signal levels at any given distance should be uniformly higher for shield events of a given size. In addition, the lack of any strong regional stress in the shield would preclude significant low frequency contributions to the explosion signal due to stress release, such as seem to occur at the Nevada Test Site.

We believe that the promising new computational techniques now under development for wave propagation in media with complicated lateral and vertical variations in physical properties can be used to predict qualitatively the seismic signals for earthquakes and explosions in dissimilar source regions, provided significant detailed knowledge of the crust and upper mantle structure is available. However, the present study demonstrates how difficult it is to obtain reliable determinations of the "fine" structure in a region. Studies at least as comprehensive as those conducted around Lake Superior and NTS are required to document a region of interest.

Despite the gross differences in crustal and mantle structure we found that using the LRSM and observatory network the accuracy of absolute event locations in the regions is similar, namely 10 to 20 km. The areas of the 95% confidence ellipses for both regions are large, those for NTS being larger by a factor of two. Similarly, the accuracy of the relative event locations are of the same order for both regions. However, using the master event technique the error in location is only 2 to 3 km and the areas of the 95% confidence ellipses are correspondingly smaller. Judging by these results and other experiments such as LONG SHOT, these location accuracies appear to be rather typical of what to expect for different source regions.

This study clearly demonstrated the necessity of a "regionalized" approach to classifying seismic events. Each

source region of interest must be documented individually to provide the best chance of identifying a particular event from that region. There are at least two practical ways of doing this: (1, conduct detailed and comprehensive geophysical studies of the region similar to those for Lake Superior and NTS discussed in this report, and (2) use an empirical reference event approach whereby all events from the region are referred to a "standard" event for that region which can be located and identified with certainty. The latter is considerably less costly, but depends on having enough large events to cover the changes in the structure throughout the region of interest. We believe that present technology and computation capability make it feasible to document each source region of interest individually along these lines such that rapid and complete evaluation of any event can be routinely accomplished. The data brought together in this report can be used as the point of departure to develop such regionalized event evaluation procedures.

REFERENCES

- Aki, Keiiti, Paul Reasenberg, Tom De Fazio, and Yi-ben Tsai, Near-field and far-field seismic evidences for triggering of an earthquake, *Trans. Am. Geophys. Union*, 50(4), p 253, 1969.
- Alexander, S.S., Surface wave propagation in the Western United States, Ph.D. thesis, California Institute of Technology, Pasadena, 1963.
- Anderson, D.L., and B.R. Julian, Shear velocities and elastic parameters of the mantle, *J. Geophys. Res.*, 74(12), pp 3281-3286, 1969.
- Anderson, D.L., Latest information from seismic observations, in The Earth's Mantle, edited by T.F. Gaskell, pp 355-420, Academic Press, London, 1967.
- Anderson, D.L., Ari Ben-Menahem, and C.B. Archambeau, Attenuation of seismic energy in the upper mantle, *J. Geophys. Res.*, 70(8), pp 1441-1448, 1965.
- Anderson, D.L., and M.N. Toksoz, Surface waves on a spherical earth. 1. Upper mantle structure from Love waves, *J. Geophys. Res.*, 68(13), pp 3483-3500, 1963.
- Anzoleaga, Rodolfo, L.C. Ocola, and R.P. Meyer, Shallow structure western Lake Superior(Abstract), *Trans. Am. Geophys. Union*, 50(4), 1969.
- Archambeau, C.B., E.A. Flinn, and D.G. Lambert, Fine structure of the upper mantle, in press, 1969.
- Archambeau, C.B., and John Davies, A theoretical model of the geophysical evolution of the Basin and Range province (Abstract), *Trans. Am. Geophys. Union*, 50(4), p 317, 1969.

- Archambeau, C.B., R. Roy, D. Blackwell, Don L. Anderson, L. Johnson, and Bruce Julian, A geophysical study of continental structure, (Abstract), Trans. Am. Geophys. Union, 49(1), p. 328, 1968.
- Archambeau, C.B., E.A. Flinn, and D.G. Lambert, Detection, analysis, and interpretation of teleseismic signals, 2, (Abstract), Geophys. J. 13, 1967.
- Archambeau, C.B., E.A. Flinn, and D.G. Lambert, Detection, analysis, and interpretation of teleseismic signals, 1, J. Geophys. Res., 71(14), pp 3483-3501, 1966.
- Bacon, L.O., Relation of gravity to geological structure in Michigan's upper peninsula, in Geological Exploration, edited by A.K. Snelgrove, pp 54-58, Michigan College of Mining and Technology, Houghton, 1957.
- Bancroft, A.M., Seismic spectra and detection probabilities from explosions in Lake Superior, in The Earth Beneath the Continents, Geophys. Monograph 10, edited by J.S. Steinhart and T.J. Smith, pp 234-240, American Geophysical Union, Washington, D.C., 1966.
- Barnes, Harley, E.N. Hinrichs, F.A. McKeown, and P.P. Orkild, U.S. Geological Survey investigations of Yucca Flat, Nevada Test Site, Part A - Geology of the Yucca Flat area, U.S. Geol. Surv. Tech. Letter NTS-45A, pp 196, 1963.
- Barosh, P.J., Relationship of explosion-produced fracture patterns to geologic structure in Yucca Flat, Nevada Test Site, in Nevada Test Site, edited by E.B. Eckel, Geol. Soc. Am. Memoir. 110, pp 199-217, 1968.
- Barr, K.G., Upper mantle structure in Canada from seismic observations using chemical explosions, Can. J. Earth Sci., 4(5), pp 961-975, 1967.

- Bath, G.D., Aeromagnetic anomalies related to remanent magnetism in volcanic rock, Nevada Test Site, in Nevada Test Site, edited by E.B. Eckel, Geol. Soc. Am. Memoir 110, pp 135-146, 1968.
- Bednarek, A.R., and R.P. Meyers, Comparison of time term and P_n residual methods of interpreting first arrivals from the Lake Superior experiments, in The Earth Beneath the Continents, Geophys. Monograph 10, edited by J.S. Steinhart and T.J. Smith, pp 276-289, American Geophysical Union, Washington, D.C., 1966.
- Berry, M.J., and G.F. West, An interpretation of the first-arrival data of the Lake Superior experiment by the time-term method, Bull. Seismol. Soc. Am., 56(1), pp 141-171, 1966a.
- Berry, M.J., and G.F. West, A time-term interpretation of the first-arrival data of the 1963 Lake Superior experiment in The Earth Beneath the Continents, Geophys. Monograph 10, edited by J.S. Steinhart and T.J. Smith, pp 166-180, American Geophysical Union, Washington, D.C., 1966b.
- Birch, Francis, Density and composition of the earth's mantle and core, J. Geophys. Res., 69(20), 1964.
- Black, W.A., Study of the marked positive gravity anomaly in the northern midcontinent region of the United States (Abstract), Bull. Geol. Soc. Am., 66, p 1531, 1955.
- Blackwell, D.D., Heat-flow determinations in the northwestern United States, J. Geophys. Res., 74(4), pp 992-1007, 1969.
- Borchardt, C.A., R.P. Meyer, and J.R. Van Schaack, Project Early Rise: Shot times and locations, J. Geophys. Res., 74(17), pp 4442-4452, 1969.
- Borchardt, C.A., R.P. Meyer, and J.R. Van Schaack, Project EARLY RISE: Shot Times and Location, U.S. Geol. Survey Tech. Letter NCER-3, p 37., 1967.

- Browning, D.G., W.H. Thorp, and J.D. McElroy, Velocity and temperature profiles in Lake Superior, *J. Geophys. Res.*, 73(18), pp 6122-6124, 1968.
- Brune, James, and James Dorman, Seismic waves and earth structure in the Canadian Shield, *Bull. Seismol. Soc. Am.*, 53(1), pp 167-210, 1963.
- Bullen, K.E., An introduction to the theory of seismology, 3rd ed., pp 381, Cambridge University Press, New York, 1963.
- Chiburis, E.F., Precision location of underground nuclear explosions using teleseismic networks and predetermined travel-time anomalies, *Seismic Data Lab. Rept. 214*, p 50, Earth Sciences, A Teledyne Company, Alexandria, Virginia, 1968.
- Cleary, J.R., and A.L. Hales, An analysis of travel times of P waves to North American stations, in the distance range 32° to 100° , *Bull. Seismol. Soc. Am.*, 56(2), pp 462-489, 1966.
- Cohen, T.J., Explosion seismic studies of the mid-continent gravity high, Ph.D. thesis, University of Wisconsin, Madison, 1966.
- Cohen, T.J., and R.P. Meyer, The midcontinent gravity high: gross crustal structure, in The Earth Beneath the Continents, *Geophys. Monograph 10*, edited by J.S. Steinhart and T.J. Smith, pp 141-165, American Geophysical Union, Washington, D.C., 1966.
- Cook, K.L., Rift system in the Basin and Range province, in The World Rift System, *Geol. Surv. of Canada*, paper 66-14, pp 246-279, 1966.
- Dickey, D.D., Fault displacement as a result of underground nuclear explosions, in Nevada Test Site, edited by E.B. Eckel, *Geol. Soc. Am. Memoir 110*, pp 219-232, 1968.

- Diment, W.H., S.W. Stewart, and J.C. Roller, Crustal structure from the Nevada Test Site to Kingman, Arizona, from seismic and gravity observations, J. Geophys. Res., 66, pp 201-214, 1961.
- Diment, W.H., D.L. Healey, and J.C. Roller, Gravity and Seismic exploration in Yucca Valley, Nevada Test Site-- January - April, 1959, U.S. Geol. Surv., cy. TEI-545, open-file rept. p 41, 1959.
- Doyle, H.A., and A.L. Hales, An analysis of the travel times of S waves to North American stations in the distance range 28° to 82°, Bull. Seismol. Soc. Am., 57(4), pp 761-772, 1967.
- Eardley, A.J., Structural geology of North America, second edition Harper and Row, New York, 1962.
- Eaton, J.P., Crustal structure from San Francisco, California, to Eureka, Nevada, from seismic-refraction measurements, J. Geophys. Res., 68(20), pp 5789-5806, 1963.
- Eckel, E.B., ed., Nevada Test Site, Memoir 110, Geol. Soc. Am., 290 pp., 1968.
- Ekren, E.B., Geologic setting of Nevada Test Site and Nellis Air Force Range, in Nevada Test Site, edited by E.B. Eckel, Geol. Soc. Am. Memoir 110, pp 11-19, 1968.
- Engdahl, E.R., W.V. Mickey, S.R. Blockman, and K.W. King, The seismic regime following a large scale nuclear explosion (Abstract), Trans. Am. Geophys. Union, 50(4), p 248, 1969.
- Eppley, R.A., Earthquake history of the United States, Part 1 Stronger earthquakes of the United States, U.S. Coast and Geodetic Survey Publ. 41-1, U.S. Govt. Printing Office, p 120, 1965.

- Flinn, E.A., Confidence regions and error determinations for seismic event location, *Rev. Geophys.*, 3(1), pp 157-185, 1965.
- Flinn, E.A., Program descriptions: Z34 UES LOCATE, Digital Computing Section, Seismic Data Laboratory, United Electrodynamics, Alexandria, Virginia, 1963.
- Gibbs, J.F., and J.C. Roller, Crustal structure determined by seismic refraction measurements between the Nevada Test Site and Ludlow, California, *U.S. Geol. Surv. Prof. Paper* 550-D, pp 125-131, 1966.
- Gibbs, J.F. and J.C. Roller, Seismic-refraction measurements of crustal structure between Nevada Test Site and Ludlow, California, *U.S. Geol. Surv. Tech. Letter* 26, p 30, 1964.
- Gilluly, John, The tectonic evolution of the western United States, *Quart. J. Geol. Soc. London*, 119, pp 133-174, 1963.
- Green, R.W.E., and A.L. Hales, The travel times of P waves to 30° in the central United States and upper mantle structure, *Bull. Seismol. Soc. Am.*, 58(1), pp 267-289, 1968.
- Green, R.W.E. and A.L. Hales, Travel times from Lake Superior shots, 1966-Interim Report No. 1, Technical Report, Contract AF 49(638)-1746, Southwest Center for Advanced Studies, 1967a.
- Green, R.W.E. and A.L. Hales, Travel time from Lake Superior shots, 1966-Interim Report No. 2, Technical Report, Contract AF49(638)-1746, Southwest Center for Advanced Studies, 1967b.
- Green, R.W.E. and A.L. Hales, The travel times of P waves to 30° in the central United States and upper mantle structure, *Bull. Seismol. Soc. Am.*, 58(1), pp 267-289, 1968.

- Hales, A.L., C.E. Helsley, J.J. Dowling, and J.B. Nation, The eastcoast onshore offshore experiment: The first arrival phases, Southwest Center for Advanced Studies Technical Report No. AFOSR 67-9852, March, 1967.
- Hall, D.H. and W.C. Brisbin, A study of the Mohorovicic discontinuity near Flin Flon, Manitoba. Final report for Geophys. Res. Div., Air Force Cambridge Res. Labs., Office Aerospace Res., USAF, Bedford, Massachusetts, 1961.
- Hall, P.H. and Zoltan Majnal, Crustal structure of northwestern Ontario; refraction seismology, Can. J. Earth Sci., 6(1), pp 81-99, 1969.
- Halls, H.C., Compressional wave velocities of Keweenawan rock specimens from Lake Superior region, Can. J. Earth Sci., 6(4), pp 555-568, 1969.
- Halls, H.C., A review of the Keweenawan geology of the Lake Superior region, in The Earth Beneath the Continents, Geophys. Monograph 10, edited by J.S. Steinhart and T.J. Smith, pp 3-27, American Geophysical Union, Washington, D.C., 1966.
- Hamblin, W.K., Paleogeographic evolution of the Lake Superior region from Late Keweenawan to Late Cambrian time, Bull. Geol. Soc. Am., 72(1), pp 1-18, 1961.
- Hart, S.R., and G.R. Tilton, The isotope geochemistry of strontium and lead in Lake Superior sediments and water, in The Earth Beneath the Continents, Geophys. Monograph 10, edited by J.S. Steinhart and T.J. Smith, pp 127-137, American Geophysical Union, Washington, D.C., 1966.
- Hazelwood, R.M., D.L. Healey, and C.H. Miller, U.S. Geological Survey investigations of Yucca Flat, Nevada Test Site, Part B. Geophysical Investigation, U.S. Geol. Surv. Tech. Letter NTS-45, Part B, p 53, 1963.

- Healey, D.L., Application of gravity data to geologic problems at Nevada Test Site, in Nevada Test Site, edited by E.B. Eckel, Geol. Soc. Am. Memoir 110, pp 147-156, 1968.
- Healey, J.M., and S.L. Ploger, P_n arrivals recorded from nuclear explosions (Abstract), Trans. Am. Geophys. Union, 46(1), p 156, 1965.
- Healey, D.L., and C.H. Miller, Gravity investigations, in U.S. Geological Survey investigations of Yucca Flat, Nevada Test Site; Part B. Geophysical investigations, U.S. Geol. Surv. Tech. Letter: NTS-45, p 53, 1963.
- Healy, J.H., and R.M. Hamilton, Seismic activity following the "Benham" nuclear explosion (Abstract), Trans. Am. Geophys. Union, 50(4), p 268, 1969.
- Heezen, B.C., The rift in the ocean floor, Sci. American, 203, pp 98-110, 1960.
- Herrin, Eugene, and James Taggart, Regional variations in P_n velocity and their effect on the location of epicenters, Bull. Seismol. Soc. Am., 52(5), pp 1037-1046, 1962.
- Hill, D.P., and L.C. Pakiser, Crustal structure between the Nevada Test Site and Boise, Idaho, from seismic-refraction measurements, in The Earth Beneath the Continents, Geophys. Monograph 10, edited by J.S. Steinhart and T.J. Smith, pp 391-419, American Geophysical Union, Washington, D.C., 1966.
- Hinrichs, E.N., Geologic structure of Yucca Flat area, Nevada, in Nevada Test Site, edited by E.B. Eckel, Geol. Soc. Am. Memoir 110, pp 239-246, 1968.
- Hinze, W.J., N.W. O'Hara, J.W. Trow, and G.B. Secor, Aeromagnetic studies of eastern Lake Superior, in The Earth Beneath the Continents, Geophys. Monograph 10, edited by J.S. Steinhart and T.J. Smith, pp 95-110, American Geophysical Union, Washington, D.C., 1966.

- Hobson, G.D., Hudson Bay crustal seismic experiment: time and distance data, *Can. J. Earth Sci.*, 4(5) pp 879-900, 1967.
- Hobson, G.D., A. Overton, D.N. Clay, and W. Thatcher, Crustal structure under Hudson Bay, *Can. J. Earth Sci.*, 4(5), pp 929-947, 1967.
- Hodgson, J.H., A seismic survey in the Canadian Shield I; Refraction studies based on rockbursts at Kirtland Lake, Ontario, *Publ. Dominion Observatory, Ottawa*, 16(6), pp 113-163, 1963(a).
- Hodgson, J.H., A seismic survey in the Canadian Shield II: Refraction studies based on timed blasts, *Publ. Dominion Observatory, Ottawa*, 16(6), pp 167-181, 1963(b).
- Hough, J.L., *Geology of the Great Lakes*, pp 313, University of Illinois Press, Urbana, 1958.
- Hunter, J.A., and R.F. Mereu, The crust of the Earth under Hudson Bay, *Can. J. Earth Sci.*, 4(5), pp 949-975, 1967.
- Ibrahim, A.K., and O.W. Nuttli, Travel-time curves and upper-mantle structure from long-period S-waves, *Bull. Seismol. Soc. Am.*, 57(5), pp 1063-1092, 1967.
- Innes, M.J.S., Gravity and isostasy in northern Ontario and Manitoba, *Publ. Dominion Obs.*, Ottawa, 21, pp 263-338, 1960.
- Irving, R.D., The copper-bearing rocks of Lake Superior, U.S. Geol. Surv. Monograph 5, 1883.
- Iyer, H.M., L.C. Pakiser, and D.H. Warren, Project Early Rise: seismic probing of the upper mantle, *J. Geophys. Res.*, 74(17), 1969.
- Jeffreys, Harold, and K.E. Bullen, *Seismological tables*, Brit. Assn. Gray-Milne Trust, 1940.

- Johnson, L.R., Array measurements of P velocities in the upper mantle, J. Geophys. Res., 72(24), pp 6309-6325, 1967.
- Johnson, M.K., and D.E. Hibbard, Geology of the Atomic Energy Commission Nevada Proving Grounds area, Nevada, U.S. Geol. Surv. Bull. 1021-K, pp 333-384, 1957.
- Julian, B.R., and D.L. Anderson, Traveltimes, apparent velocities and amplitudes of body waves, Bull. Seismol. Soc. Am., 58(1), pp 339-366, 1968.
- King, P.B., The evolution of North America, Princeton University Press, p 190, 1959.
- Knopoff, Leon, and T.L. Teng, Analytical calculation of the seismic travel-time problem, Rev. Geophys., 3(1), pp 11-26, 1965.
- Kovach, R.L., Upper mantle structure in western North America from apparent velocities of S waves, paper presented at the Fall Meeting, American Geophysical Union, San Francisco, Dec. 2-5, 1968.
- Kovach, R.L., and Russell Robinson, A velocity model for the Basin and Range province (Abstract), Trans. Am. Geophys. Union, 50(4), 1969.
- Lane, A.C., The Keweenaw series of Michigan, Michigan Geol. Biol. Surv., Publ. 6, Geological Series No. 4, 1911.
- Lee, W.H.K., and Seiya Uyeda, Review of heat flow data, in Terrestrial heat flow, Geophys. Monograph 8, edited by W.H.K. Lee, pp 87-210, The American Geophysical Union, Washington, D.C., 1965.
- Lehmann, I., On the travel times of P as determined from nuclear explosions, Bull. Seismol. Soc. Am., 54(1), pp 123-139, 1964.

Lehmann, I., The times of P and S in northeastern America, *Ann. di Geofis.*, 8, pp 351-370, 1955.

Lewis, B.T.R., and R.P. Meyer, A seismic investigation of the upper mantle to the west of Lake Superior, *Bull. Seismol. Soc. Am.*, 58(2), pp 565-596, 1968.

Longwell, C.R., Possible explanation of diverse structural patterns in southern Nevada, *Am. Jour. Sci.*, 258-A, pp 192-203, 1960.

Lyons, P.L., The Greenleaf anomaly, a significant gravity feature, in Symposium on Geophysics in Kansas, Kansas Geol. Surv. Bull. 137, pp 105-120, 1959.

Mansfield, R.H., and J.F. Evernden, Long range seismic data from the Lake Superior Seismic Experiment 1963-1964, Tech. Rep. VU-66-1, Air Force Technical Applications Center, Headquarters United States Air Force, Washington, D.C., p 31, 1966.

Mansfield, R.H., and J.F. Evernden, Long-range seismic dates from the Lake Superior Seismic Experiment, in *The Earth Beneath the Continents*, Geophys. Monograph 10, edited by J.S. Steinhart and T.J. Smith, pp 249-269, American Geophysical Union, Washington, D.C. 1966b.

McConnell, R.K., The gravity field of northern central Ontario, Gravity Map series of Dominion Observatory, Nos. 21-25, in preparation, 1966.

McConnell, R.K., Jr., R.N. Gupta, and T.J. Wilson, Compilation of deep crustal seismic refraction profiles, *Rev. of Geophys.*, 4(1), pp 41-100, 1966.

Menard, H.W., The East Pacific Rise, *Science*, 132, pp 1737-1746, 1960.

- Mereu, R.F., and J.A. Hunter, Crustal and upper mantle structure under the Canadian shield from Project EARLY RISL data, Bull. Seismol. Soc. Am., 59(1), pp 147-165, 1969.
- Meyer, R.P., J.S. Steinhart, B.F. Howell, W.E. Bonini, D.E. Willis, and B.T.R. Lewis, 1962 North Carolina Cooperative experiment; shot positions, shot times, and travel times, University of Wisconsin (in publication), 1965.
- Niazi, Mansour, and D.L. Anderson, Upper mantle structure of western North America from apparent velocities of P waves, J. Geophys. Res., 70(18), pp 4633-4640, 1965.
- O'Brien, P.N.S., Lake Superior crustal structure - a reinterpretation of the 1963 seismic experiment, J. Geophys. Res., 73(8), pp 2669-2689, 1968.
- Pakiser, L.C., Structure of the crust and upper mantle in the western United States, J. Geophys. Res., 68(20), pp 5747-5756, 1963.
- Pakiser, L.C., and D.P. Hill, Crustal structure in Nevada and southern Idaho from nuclear explosions, J. Geophys. Res., 68(20), pp 5757-5766, 1963.
- Pakiser, L.C., and J.S. Steinhart, Explosion seismology in the western hemisphere, Chapter 5 in Research in Geophysics, vol. 2, Solid Earth and Interface Phenomena, edited by Hugh Odishaw, pp 123-147, Massachusetts Institute of Technology Press, Cambridge, 1964.
- Patenaude, R.W., A regional aeromagnetic survey of Wisconsin, in The Earth Beneath the Continents, Geophys. Monograph 10, edited by J.S. Steinhart and T.J. Smith, pp 111-126, American Geophysical Union, Washington, D.C., 1966.
- Pilant, W.L., Rayleigh wave phase and group velocities on the North American Continent (Abstract), Trans. Am. Geophys. Union, 48(1), p 207, 1967.

- Prodehl, Claus, Crustal structure of the central part of the western United States from seismic-refraction measurements (Abstract), Trans. Am. Geophys. Union, 50(4), p 239, 1969.
- Richter, C.F., Elementary seismology, W.H. Freeman and Co., San Francisco, p 768, 1958.
- Roller, J.C., and W.H. Jackson, Seismic wave propagation in the upper mantle: Lake Superior, Wisconsin, to central Arizona, J. Geophys. Res., 71(24), pp 5933-5941, 1966b.
- Roller, J.C., and W.H. Jackson, Seismic-wave propagation in the upper mantle: Lake Superior, Wisconsin to Denver, Colorado in The Earth Beneath the Continents, Geophys. Monograph 10, edited by J.S. Steinhart and T.J. Smith, pp 270-275, American Geophysical Union, Washington, D.C., 1966a.
- Romney, Carl, B.G. Brooks, R.H. Mansfield, D.S. Carder, J.N. Jordan and D.W. Gordon, Travel times and amplitudes of principal body phases recorded from Gnome, Bull. Seismol. Soc. Am., 52(5), pp 1057-1074, 1962.
- Roy, R.F., E.R. Decker, D.D. Blackwell, and Francis Birch, Heat flow in the United States, J. Geophys. Res., 73(16), pp 5207-5221, 1968a.
- Roy, R.F. Blackwell, D.D., Decker, E.R., and F. Birch, Heat generation of surface rocks and heat flow provinces (Abstract), Trans. Am. Geophys. Union, 49(1), p 319, 1968b.
- Roy, R.F., Blackwell, D.D., and F. Birch, Heat generation of plutonic rocks and continental heat flow provinces, Earth Planetary Sci. Letters, 5(1), pp 1-12, 1968c.
- Roy, R.F., and D.D. Blackwell, Heat flow in the Sierra Nevada and western Great Basin (Abstract), Trans. Am. Geophys. Union, 47, pp 179-180, 1966.

- Ruffman, Alan, and M.J. Keen, A time-term analysis of the first arrival data from the seismic experiment in Hudson Bay, 1965, Can. J. Earth Sci., 4(5), pp 901-928, 1967.
- Ryall, Alan, and D.J. Stuart, Traveltimes and amplitudes from underground nuclear explosions, J. Geophys. Res., 68(20), pp 5821-5835, 1963.
- Scheidegger, A.E., and P.L. Willmore, The use of a least squares method for the interpretation of data from seismic surveys, Geophysics, 22, pp 9-22, 1957.
- Schmucker, U., Anomalies of geomagnetic variations in the southwestern United States, J. Geomagn. and Geoelectr. 15, pp 193-221, 1964.
- Slichter, L.B., Crustal structure in the Wisconsin area, ONE Rept. N9 onr. 86200, 1951.
- Smith, T.J., J.S. Steinhart, and L.T. Aldrich, Lake Superior crustal structure, J. Geophys. Res., 71(4), pp 1141-1172, 1966a.
- Smith, T.J., J.S. Steinhart, and L.T. Aldrich, Crustal structure under Lake Superior, in The Earth Beneath the Continents, Geophys. Monograph 10, edited by J.S. Steinhart and T.J. Smith, pp 181-197, American Geophysical Union, Washington, D.C. 1966b.
- Spence, W.J., and S.S. Alexander, A method of determining the relative location of seismic events, Paper presented at the Fortieth Annual Meeting of the Eastern Section, Seismological Society of America, 17-19, October 1968.
- Spence, W.J., and S.S. Alexander, Relative event location, submitted Bull. Seismol. Soc. Am., 1969.

- Steinhart, J.S., S.R. Hart, and T.J. Smith, Heat flow, in the Report of the Director, Department of Terrestrial Magnetism, pp 360-367, Carnegie Institution of Washington Year Book 67, 1968.
- Steinhart, J.S., and T.J. Smith ed., The Earth Beneath the Continents, American Geophysical Union, Washington, D.C., p 663, 1966.
- Steinhart, J.S., Lake Superior seismic experiment: shots and travel times, J. Geophys. Res., 69(24), pp 5335-5352, 1964.
- Steinhart, J.S., and R.P. Meyer ed., Explosion studies of continental structure, Carnegie Institution of Washington Publ. 622, p 409, 1961.
- Steinhart, J.S., R.P. Meyer, and G.P. Woollard, Wisconsin-Upper Michigan, 1958-1959, in Explosion Studies of Continental Structure, edited by J.S. Steinhart and R.P. Meyer, pp 248-304, The Carnegie Institution of Washington, 1961.
- Stockwell, C.H., Geological Studies, in Age Determinations and Geological Studies, Geol. Survey Can. Paper 64-17, Part II, pp 1-21, 1964.
- Stockwell, C.H., A tectonic map of the Canadian Shield, in The Tectonics of the Canadian Shield, Roy. Soc. Can. Special Pub. No. 4, pp 6-15, 1962.
- Stuart, P.J., J.C. Roller, W.H. Jackson, and G.B. Mangan, Seismic propagation paths, regional travel times, and crustal structure in the western United States, Geophysics, 29, pp 178-187, 1964.
- Swift, C.M., A magnetotelluric investigation of an electrical conductivity anomaly in the southwestern United States, Ph.D. thesis, Massachusetts Institute of Technology, 1967.

- Talwani, Manik, G.H. Sutton, and J.L. Worzel, A crustal section across the Puerto Rico trench, *J. Geophys. Res.*, 64, pp 1545-1555, 1959.
- Tatel, H.E., and M.A. Tuve, Seismic waves from explosions, *Carnegie Inst. Washington Year Book* 51, p 67, 1952.
- Thiel, E.C., Correlation of gravity anomalies with the Keweenawan geology of Wisconsin and Minnesota, *Bull. Geol. Soc. Am.*, 67, 1079-1100, 1956.
- Thompson, G.A., L.J. Meister, A.T. Herring, T.E. Smith, D.B. Burke, R.L. Kovach, R.O. Burford, I.A. Salehi, and M.D. Wood, Geophysical study of basin-range structure Dixie Valley region, Nevada, Final Scientific Report Parts I-VIII, to U.S. Air Force Cambridge Research Laboratories, Stanford University, California, p 286, 1967.
- Thompson, G.A., The rift system of the western United States, in the World Rift System, *Geol. Surv. of Canada paper* 66-14, pp 280-290, 1966.
- Thompson, J.E., Geology of Mamainse Point copper area, *Ann. Rept. Ontario Dept. Mines*, 62(4), p 25, 1953.
- Van Hise, C.R., and C.K. Leith, The geology of the Lake Superior region, *U.S. Geol. Surv. Monograph* 52, 1911.
- Warren, R.E., J.G. Sclater, Victor Vacquier, and R.F. Roy, A comparison of terrestrial heat flow and transient geomagnetic fluctuations in the southwestern United States, *Geophysics*, 34(3), pp 463-478, 1969.
- Warren, S.H., J.H. Healy, J.C. Hoffman, Reinis Kempe, Srinivasreddy Rauula, and D.J. Stuart, Project Early Rise: traveltimes and amplitudes, *U.S.G.S. Tech. Letter NCER-6*, 1967.

- Weeber, J.R., and A.K. Goodacre, A reconnaissance underwater gravity survey of Lake Superior, in The Earth Beneath the Continents, Geophys. Monograph 10, edited by J.S. Steinhart and T.J. Smith, pp 56-65, American Geophysical Union, Washington, D.C. 1966.
- White, W.S., Tectonics of the Keweenaw Basin, western Lake Superior Region, U.S.G.S. Prof. Paper 524-E, Government Printing Office, Washington, D.C. p 23, 1966a.
- White, W.S., Geologic evidence for crustal structure in the western Lake Superior Basin, in The Earth Beneath the Continents, Geophys. Monograph 10, edited by J.S. Steinhart and T.J. Smith, pp 28-41, American Geophysical Union, Washington, D. C., 1966b.
- Williams, W.P., W.L. Emerick, R.E. Davis, and R.P. Snyder, U.S. Geological survey investigations in Yucca Flat Nevada test site Part C. - The underground test media of Yucca Flat, U.S. Geol. Surv. Tech. Letter NTS-45, Part C, p 251, 1963.
- Williams, W.P., and D.L. Hoover, Movement on the Yucca fault as a result of underground nuclear tests, Yucca Flat, Nevada Test Site, Nye County, Nevada: in U.S. Geol. Survey Tech. Letter, Yucca-29, 1962.
- Willis, D.E., An investigation of seismic wave propagation in the eastern United States, Ph.D. thesis, The University of Michigan, Ann Arbor, 1968.
- Willmore, P.L., and A.M. Bancroft, The time-term approach to refraction seismology, Geophys. J., 3 pp 419-432, 1960.
- Wold, R.J., Gravity survey of Lake Superior (Abstract), Trans. Am. Geophys. Union, 49(1), 1968.

- Wold, R.J., and N.A. Ostenso, Aeromagnetic, gravity, and sub-bottom profiling studies in western Lake Superior, in The Earth Beneath the Continents, Geophys. Monograph 10, edited by J.S. Steinhart and T.J. Smith, pp 66-94, American Geophysical Union, Washington, D.C., 1966.
- Woollard, G.P., and H.R. Joesting, Bouguer gravity anomaly map of the United States, U.S. Geological Survey, 1964.
- Zietz, I., Aeromagnetic study of the midcontinent gravity anomaly (Abstract), U.S. Progr. Rept. Intern. Upper Mantle Project, 1965.
- Zumberge, J.H., A new shipboard coring technique, J. Geophys. Res., 67(6), 2529-2536, 1962.
- Zumberge, J.H., and Paul Gast, Geological Investigations in Lake Superior, Geotimes, 6(4), pp 10-13, 1961.

TABLE I

Members of the North American Seismic Group participating in the 1963 Lake Superior Seismic Experiment.

INSTITUTION	PRINCIPAL CONTRIBUTORS
Carnegie Institution of Washington	L.T. Aldrich, I.S. Sacks, T.J. Smith, J.S. Steinhart, Z. Suzuki
Dominion Observatory, Canada	A.M. Bancroft, G.W. Sander
Graduate Research Center of the Southwest	K. Graham, A.L. Hales
Pennsylvania State University	B.F. Howell, Jr.
Princeton University	M. Dunne
University of Alberta	G. Cummings
University of Manitoba	D. Hall
University of Michigan	D.E. Willis, C.G. Bufe, G.E. Frantti
University of Minnesota	P. Farnham, T. Fitch, H. Mooney
University of Western Ontario	R.F. Mereu
University of Wisconsin	R.P. Meyer, T.J. Cohen
U.S. Geological Survey	J.M. Healy, W.H. Jackson, L.C. Pakiser, J.C. Roller, B.L. Tibbetts
Vela Seismological Center, AFTAC	R.H. Mansfield

TABLE 2

ORGANIZATION	PROFILES OCCUPIED
AFTAC	East Liverpool, Ohio, to South Mills, North Carolina.
	Chapleau, Ontario, to Glace Bay, Nova Scotia.
Southwest Center for Advanced Studies	Lake Superior, Michigan, to El Dorado, Arkansas.
	Lake Superior, Michigan, to Charleston, West Virginia.
	Colorado Springs, Colorado, to Charleston, West Virginia.
Stanford Research Institute	Chapleau, Ontario, to Schefferville, Quebec.
University of Alberta	Yorkton, Saskatchewan to Whitecourt, Alberta.
	Bow Island, Alberta, to Cold Lake, Alberta.
University of Manitoba	Lake of the Woods, Ontario, to Lake Manitoba, Manitoba.
University of Michigan	Bear Lake, Michigan, to Potters Hill, North Carolina.
University of Toronto	Southeastern Ontario.
University of Western Toronto	Lake Nipigon, to Smooth Rock Falls, Ontario.
	Port Arthur, Ontario, to Barlzon Lake, Manitoba.
University of Wisconsin	Bemidji, Minnesota, to Vancouver, Washington
U. S. Geological Survey	Saint Cloud, Minnesota, to Cedar City, Utah.
	Bemidji, Minnesota, to Miles City, Montana
	Ledve, Alberta, to Mile Post 750, B.C.
	Flin Flon, Manitoba, to Yellowknife, Northwest Territories.

TABLE 3.

Description of rocks outcropping in vicinity of Lake Superior

GEOLOGIC AGE	UNIT	LITHOLOGY	EST. THICKNESS m	BULK DENSITY		INTERRED - JAVE VELOCITIES (km/sec)
				gm/cm ³ (Rhie, 1956)	(Steinhart and Smith, 1966)	
Recent & Pleistocene	Post-till Lacustrine Sediments	Homogeneous gray clay	1-5			
		Varved gray clay	3-10			
		Varved red clay	1-2			
	Till	Generally clayey or sandy	20-30			
Paleozoic	On Shore: Glacial drift of Variable thickness					
	UNCONFORMITY					
	Silurian and Upper Cambrian	Franconian				
		Oresbachian				
	Bay of Groups	Red S/S & Sh.				3.40*
		Chequamegon Sandstone	300			
		Devils Island Sandstone	100	2.30	2.30 - 2.37	
		Orienta Sandstone	1000			
	UNCONFORMITY					
	Upper Keweenaw	Fieda Sandstone	up to 4000			
		Arkosol. feldspathic s/s. micaceous sh., coarse at base becoming finer at top				
		Wanetuch Shale	40-230	2.44	2.44-2.54	4.70*
	Middle Keweenaw	Copper Harbour Conglomerate	110-2000			
		Basaltic- andesitic lava flows with rare rhyolite lavas. Interbedded congl. and s/s. Increasing meta grade downwards. Lavas thickest at center of syncline; anygdules show lavas flowed outwards from center of basin. Source unknown. Thickness unknown.				
		Portage Lake Lavas	3000 to possibly 10,000	2.90	2.90-3.30 Diabase at 0.5-1.0 kb	5.60*
	Lower Keweenaw	Thunder Bay District: s/s. marl. sh. with locally thin congl., marl., car- bonate	<200			
	1.9 to 1.6 b.y.	Barron Quartzite				
		Puchung Formation	<60			
		In Northeastern Minnesota: Qtz. congl., Qtz. s/s				
	Animikiean	Consists of quartzites and dolomites at base, a lithologically variable sequence, and a thick sequence of graywacke. More quartzite, mudstone, shale at top. More strongly meta s. of Lake Superior.		2.67	2.70 2.80	
Precambrian	Kenoran Orogeny					
	2.4 b.y.					
	Timiskamian	Undifferentiated rocks of the Canadian Shield				
	Ontarian	Granites, gneisses, migmatites, green- stones, schists, etc.				

*Velocities inferred from refraction data of Anzolega et al. (1969).

TABLE 4

Plausible crustal models for the EARLY RISE shot point

LAYER No.	THICKNESS km	α km/sec	β km/sec	gm/cm ³
Model ERLS111				
1	1.0	3.40	1.96	2.30
2	1.5	4.70	2.72	2.65
3	5.5	5.60	3.24	2.90
4	20.0	6.80	3.65	3.10
5	20.0	6.80	3.80	3.10
6		8.10	4.72	3.42
Model ERLS112				
1	1.0	3.40	1.96	2.30
2	1.5	4.70	2.72	2.65
3	5.5	5.60	3.24	2.90
4	20.0	6.80	3.65	3.00
5	20.0	6.80	3.80	3.00
6		8.10	4.72	3.42
Model ERLS121				
1	1.0	3.40	1.96	2.30
2	1.5	4.70	2.72	2.65
3	5.5	5.60	3.24	2.90
4	40.0	6.80	3.93	3.10
5		8.10	4.68	3.42

TABLE 5

Travel-time anomalies for the October 1964 series of shots in western Lake Superior calculated from shot 49A.

<u>Station</u>	<u>Anomaly</u>	<u>Station</u>	<u>Anomaly</u>
GP-MN	+3.02	NL-AZ	+5.50
WF-MN	+4.02	WO-AZ	+6.07
RK-ON	+3.42	HR-AZ	+5.09
VO-IO	+4.09	GE-AZ	+5.00
RY-ND	+3.46	JR-AZ	+6.62
BR-PA	+2.63	LG-AZ	+6.13
BL-WV	+1.04	SG-AZ	+5.91
DH-NY	+1.81	SN-AZ	+5.75
CPO08	+2.10	RT-NM	+3.15
LS-NY	+2.21	UB010	+3.15
NP-NT	+4.66	HL2ID	+4.21
EU-AL	+2.02	BM003	+3.54
HN-ME	+0.05	LC-NM	+5.38
JE-LA	+4.41	KN-UT	+5.50
SV2QB	+0.47	EK-NV	+6.09
DR-CO	+2.60	TF060,1	+5.54
WM006	Reference Station	MN-NV	+5.58

(Residual -3.62 seconds)

TABLE 6
Locations of the October 1964 Shots Computed Using Herrin 68 Travel Time Tables

SHOT NO.	NO. OF STATIONS	Without Anomaly Correstions			With Anomaly Corrections				
		DISTANCE KM	AZIMUTH DEGREE	AREA KM ² *	SEC**	DISTANCE KM	AZIMUTH DEGREE	AREA KM ² *	SEC**
45A	27	16.9	81.7	450.1	1.40	2.5	74.6	40.1	0.42
48A	25	14.9	88.1	507.2	1.45	1.1	151.0	26.6	0.34
45B	20	14.1	81.4	560.6	1.45	1.9	106.7	27.3	0.32
73A	21	13.7	78.9	539.5	1.43	1.2	80.5	34.9	0.37
45C	29	16.8	86.7	440.5	1.42	1.7	59.3	28.6	0.36
47A	25	15.9	95.5	557.3	1.49	2.0	136.1	29.9	0.35
45D	28	16.9	80.8	433.0	1.42	3.3	54.2	38.4	0.43
46A	29	12.7	84.7	467.1	1.48	1.8	273.9	32.5	0.39
45E	32	18.6	72.2	360.9	1.45	3.0	45.5	26.5	0.39
49A	34	15.7	85.1	327.6	1.44	-	-	-	-
Mean	-	15.6	-	465.0	1.44	2.1	-	31.2	0.37

* Area of joint confidence regions for the epicentral coordinates at 95% level.
 **Standard deviation of travel-time residuals with zero mean.

TABLE 7
Locations of the October 1964 Shots Obtained from the LRSM & Observatory Network
Without the LRSM Stations in Arizona

SHOT NO.	NO. OF STATIONS	Without Anomalies			With Anomalies				
		DISTANCE KM	AZIMUTH DEGREE	AREA KM ² *	DISTANCE KM	AZIMUTH DEGREE	AREA KM ² *		
45A	21	14.1	86.9	484.9	1.38	2.6	75.6	44.9	0.42
48A	20	12.2	98.8	498.2	1.36	1.3	166.3	19.2	0.27
45B	17	11.2	86.9	496.4	1.29	1.7	115.5	18.1	0.25
73A	18	11.0	84.8	476.5	1.29	1.0	89.7	28.9	0.32
45C	22	13.4	92.5	435.2	1.33	1.4	61.1	30.6	0.35
47A	20	13.4	100.2	574.5	1.44	1.9	141.3	38.3	0.37
45D	23	13.9	86.1	379.7	1.28	2.6	54.6	29.0	0.35
46A	23	9.4	95.5	426.9	1.35	2.4	262.6	27.7	0.35
45E	25	15.0	73.3	330.6	1.32	2.5	43.3	16.9	0.30
49A	26	12.5	90.3	333.5	1.37	-	-	-	-
Mean		12.6		443.6	1.34	1.9		28.2	0.33

* Area of joint confidence regions for the epicentral coordinates at 95% level.
 ** Standard deviation of travel-time residuals with zero mean.

SHOT NO.	Eastern Stations				Western Stations					
	NO. OF STATIONS	Km	DISTANCE	DEGREE	SEC**	No. of STATIONS	Km	DISTANCE	DEGREE	SEC**
			AZIMUTH AREA					AZIMUTH AREA		
			Km ² *					Km ² *		
	</									

TABLE 9

Location of 9 Shots at Lake Superior Relative to Shot 49A Using Spence and
Alexander (1969) Method

SHOT NO.	Actual Location		Computed Location	
	Distance Km	Azimuth Degree	Distance Km	Azimuth Degree
73A	9.6	266.7	8.7	260.2
48A	11.9	241.7	13.0	232.0
47A	19.3	239.6	19.7	232.0
46A	26.2	250.8	28.3	248.9
45A	34.5	249.4	33.2	246.1
45B	33.1	249.1	32.2	246.1
45C	34.4	248.7	33.3	248.9
45D	32.8	253.0	30.4	254.5
45E	32.1	258.0	29.8	257.3
Mean				2.0

TABLE 10.
Description of rocks outcropping in vicinity of Yucca Flat,
Nevada Test Site

GEOLOGIC AGE		UNIT	LITHOLOGY	EST. THICKNESS m	RANGE OF DENSITIES gm/cm ³	P-WAVE VELOCITY km/sec
	Recent & Pleistocene	Alluvium, Colluvium	Gravel, sand, talus	610	1.65 - 1.94	0.65 - 1.65
Genozoac	Pliocene & Miocene	UNCONFORMITY "Tuff"	Plapi Canyon Weld, non-welded, zeolitized tuff, Older Volcanics Tuffaceous s/s, and lava flows	1129	1.94 - 2.50	2.3 - 4.0
	Permian (?) and Pennsylvanian	UNCONFORMITY Tippipah Limestone	Limestone	1068	Dolomite 2.78 - 2.85 Limestone 2.62 - 2.70 Quartzite 2.49 - 2.71 Argillite 2.65	3.9 6.5
Paleozoic	Mississippian	Eleena Formation	Argillite, l/s, qrtz, congl	2410		
	Upper & Middle Devonian	Devels Gate L/S & Nevada Formation	Dolomite, Limestone	1220		
	Devonian & Silurian & Ordovician		Limestone & Dolomite	458(?)		
	Middle & Lower Ordovician	Eureka Quartzite	Quartzite with minor l/s	400		
		Antelope Valley Limestone	Limestone	2806		
		Ninemile Formation	Claystone and Limestone			
		Goodwin Limestone	Limestone			
	Cambrian	Windfall Formation	Limestone, Dolomite		610	
		Punderberg Shale	Shale, with minor Limestone			
		Bonanza King F/M	Dolomite, Limestone, Shale			
		Carrara Formation	Siltstone, Limestone			
		Zabriskie Qtz	Quartzite	2532		
		Wood Canyon F/M	Quartzite, Siltstone, Dolomite			
	Precambrian	Stirling Quartzite	Quartzite, Siltstone		107	
		Johnnie F/M	Qtz, Sl/s, L/s, Dol			
Noonday Dolomite		Dolomite				

TABLE 11

A plausible Crustal Model for Yucca Flat Area, NTS

Layer	Thickness	α	β	
1	0.2	1.3	0.78	1.96
2	0.8	3.0	1.80	2.20
3	1.0	4.5	2.68	2.67
4	18.0	6.1	3.60	2.80
5	10.0	6.7	4.00	2.95
6		7.8	4.50	3.30

TABLE 12

Travel-Time Anomalies (in seconds) for NTS Computed Using
Herrin 1968 Travel-Time Tables

<u>Station</u>	<u>Anomaly</u>	<u>Source*</u>	<u>Station</u>	<u>Anomaly</u>	<u>Source*</u>
WI-NV	-0.12	A	AD-IS	+0.10	B
MV-CL	-0.41	A	AX2AL	+1.68	A
HL-ID	+0.42	A	BE-FL	+1.16	A
HL2ID	+0.42	E	BL-WV	=0.56	A
AZ-TX	+4.80	A	BR-PA	+0.71	A
TK-WA	+3.03	A	CPO08	+9.82	A
SK-TX	+4.62	A	DH-NY	-9.02	A
GI-MA	-0.01	A	EB-MT	+0.09	A
TD-NM	+0.32	A	EN-MO	+0.60	B
FR-MA	+0.36	A	EU-AL	+1.98	A
BX-UT	-9.67	A	GG-GR	+0.96	A
CP-CL	-0.79	A	HN-ME	+0.56	A
LAO10	+0.05	A	KC-MO	+1.70	D
WN-SD	+1.46	A	LZ-BV	+0.33	A
SE-MA	+3.95	B	NP-NT	+1.00	A
RG-SD	+0.69	C	OO-NW	-0.04	A
UBO10	+3.12	A	PG-BC	+2.69	F
DR-CO	-0.42	A	SI-BC	+2.78	A
BMO03	+2.63	A	WH2YK	+0.94	F
LC-NM	+2.56	A	SV2QB	-0.41	A
RT-NM	+0.41	A	SV3QB	-0.41	E
KN-UT	-0.98	A	PZ-PR	+1.22	A
WMO06	+2.97	A	LV-LA	+1.95	A
TFO06	+0.55	A	RK-ON	0.0	Reference Sta.
MN-NV	-0.95	A		(Residual = +0.70 Seconds)	

*Anomalies were determined from events as indicated below

A - Tan, Bilby

E - Same as previous station

B - Corduroy, Buff, Bronze

F - Commodore, Agile, Nash

C - Piledriver, Chartreuse, Dumont

D - Greeley

TABLE 13

Locations of Events at NTS Using Only LRSM Stations and Observatories at Epicentral Distances Greater Than 17°.

EVENT	No. of Stations	Without Anomaly Corrections			With Anomaly Corrections		
		Distance	Azimuth	Area	Distance	Azimuth	Area
		Km	Degree	Km ²	Km	Degree	Km ²
BUFF	8	10.9	164.5	3927.8	0.86	143.5	46.0
TURF	10	7.6	73.5	1153.7	0.43	94.6	502.1
CORDUROY	9	5.2	112.5	3092.6	0.92	52.4	167.4
NASH	7	13.4	96.9	8733.3	0.85	184.8	130.4
BOURBON	4	17.6	52.5	21691.0	0.39	264.4	5489.5
PILED RIVER	7	37.8	50.2	2182.9	0.48	31.9	99.4
BRONZE	9	8.4	0.7	1293.4	0.48	344.3	23.7
AUK	6	3.8	93.9	2975.5	0.51	252.9	152.1
PIRANHA	9	45.5	52.5	2441.1 ⁺	0.69	36.8	58.7
FORE	12	20.0	7.8	834.2 ⁺	0.47	321.4	331.7
GREELEY	13	11.3	38.3	2647.4	1.00	40.3	107.3
DUMONT	8	44.9	46.7	2655.8	0.61	4.9	54.6
CHARTREUSE	7	48.9	46.1	4087.5	0.60	21.4	97.7
COMMODORE	5	23.1	160.8	34498.3	0.69	282.2	237.9
AGILE	7	14.9	82.9	5364.0	0.66	37.1	190.9
SCOTCH	5	26.5	146.8	45678.3	0.80	84.3	2421.3
KLICKITAT	9	12.7	39.2	712.2	0.29	246.1	188.8
BILBY	14	8.3	349.5	897.5	0.60	---	---
TAN	8	42.0	48.4	2723.9	0.61	---	---
Mean		21.2		2857.7°	0.63		153.6
					2.3		0.13

* Area of joint confidence regions for the epicentral co-ordinates at 95% level.

** Standard deviation of travel-time residuals with zero mean.

+ Confidence ellipse does not contain shot point.

° Excluding BOURBON, COMMODORE, and SCOTCH.

TABLE 14

Locations of Events at NTS Using Whole LRSM and Observatory Network

EVENT	No. of Stations	Without Anomaly Corrections			With Anomaly Corrections		
		Distance Km	Azimuth Degree	Area KM ² *	Distance Km	Azimuth Degree	Area KM ² *
BUFF	17	21.2	210.6	1450.5	1.50	221.1	73.0
TURF	19	7.4	291.8	1632.6	1.63	319.3	285.8
CORDUROY	17	18.8	211.4	1038.3	1.27	15.7	43.3
NASH	12	6.7	222.9	1923.8	1.28	216.0	23.3+
BOURBON	9	14.4	227.7	2017.5	1.05	219.7	52.8
PILED RIVER	16	7.6	211.6	1059.9	1.26	348.0	58.2
BRONZE	16	10.4	285.1	1160.4	1.26	343.1	45.9
AUK	15	16.5	250.0	1846.0	1.60	264.0	327.1
PIRANHA ^o	--	--	--	--	--	--	--
FORE	30	12.0	266.3	761.8	1.81	305.5	94.1
GREELEY	19	8.2	240.2	878.7	1.12	53.9	65.4
DUMONT	17	9.4	212.9	1119.7	1.29	16.5	55.3
CHARTREUSE	15	11.9	220.0	1318.1	1.30	144.2	130.2
COMMODORE	12	12.3	218.9	1635.3	1.26	331.0	69.2
AGILE	--	--	--	--	--	--	--
SCOTCH	11	7.3	204.2	2148.0	1.34	129.8	198.4
KLICKITAT	22	4.7	216.7	777.1	1.47	316.9	90.3
BILBY	33	8.2	255.8	475.5	1.46	---	---
TAN	15	8.9	203.4	1134.5	1.18	---	---
MEAN		10.9		1316.3	1.36		107.5
							0.38

* Area of joint confidence regions for the epicentral co-ordinates at 95% level.

** Standard deviation of travel-times with zero mean.

+ Confidence ellipse does not contain shot point.

o Travel-times for additional stations not available.

TABLE 15

Location of 3 Large Events at NTS Relative
to DUMONT (After Spence and Alexander, 1969)

EVENT	Actual Location		Computed Location		Location Error
	Distance Km	Azimuth Degree	Distance Km	Azimuth Degree	Distance Km
Boxcar	40.8	300.2	40.7	291.5	6.0
Halfbeak	31.2	316.8	29.4	317.5	1.8
Faultless	169.6	355.4	170.4	355.3	0.7
Mean					2.8

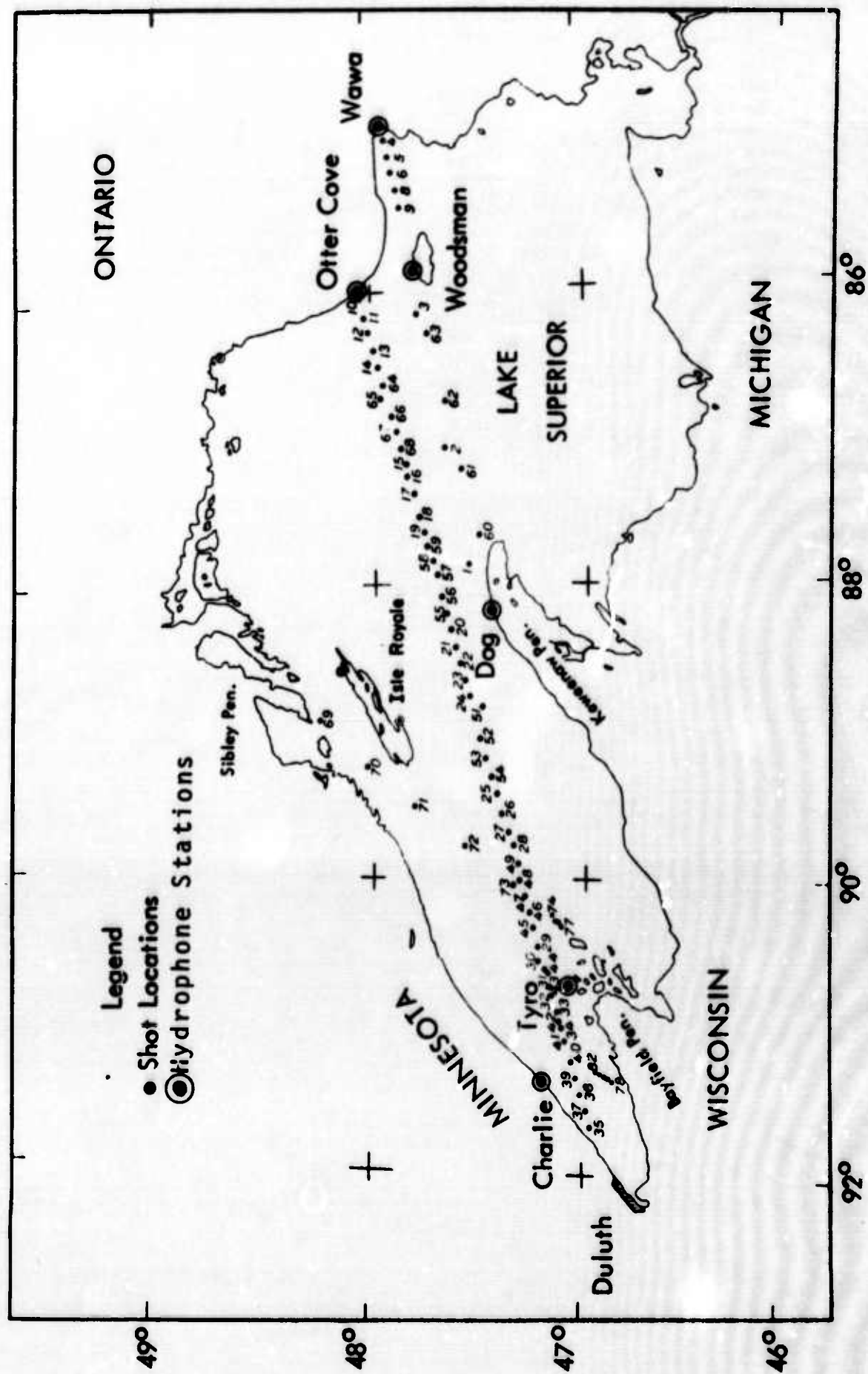


Figure 1. Locations of shots fired during the 1963 Lake Superior Seismic Experiment. (After Smith et al, 1966b.)

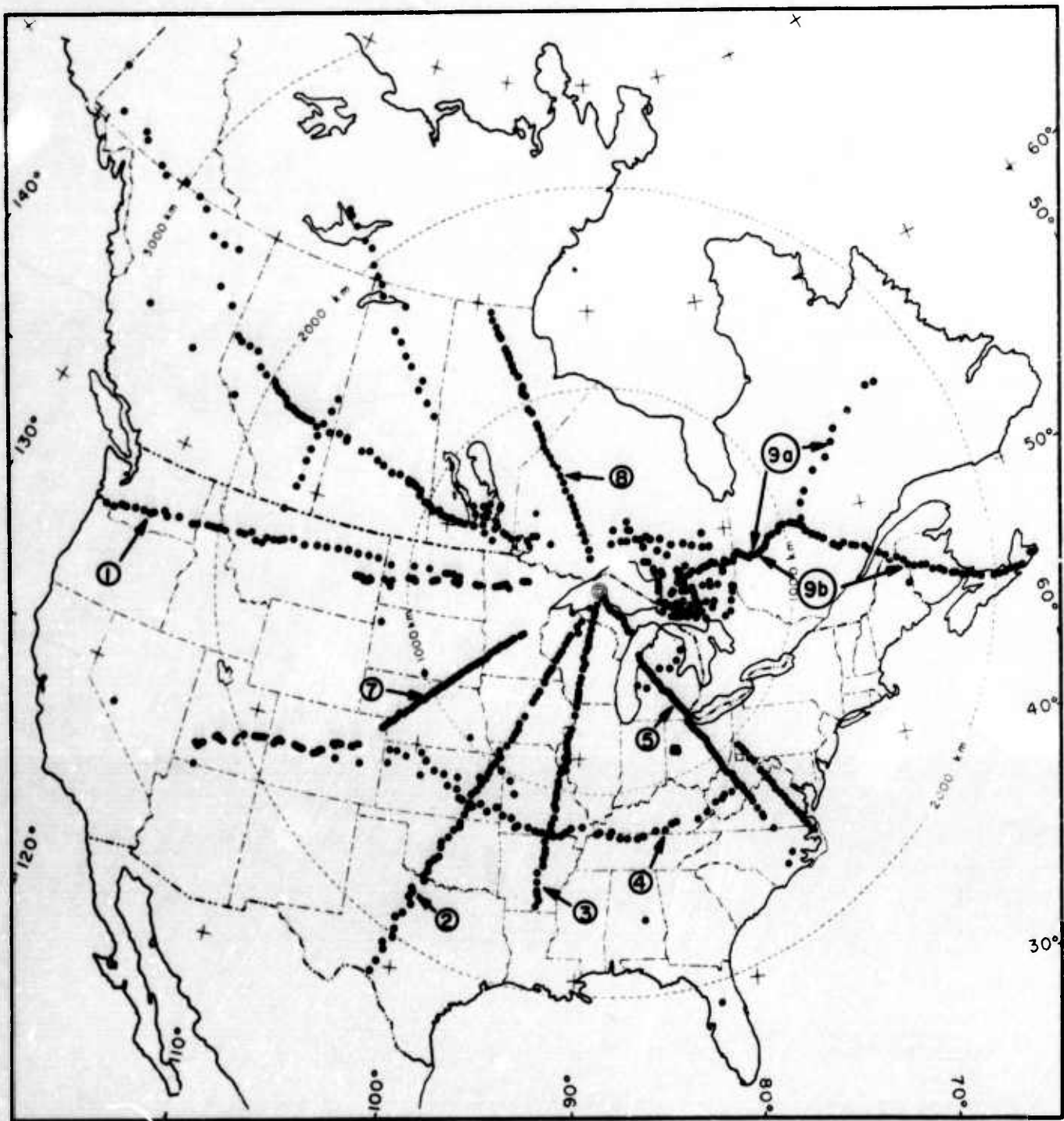


Figure 2. Locations of recording profiles occupied during Project Early Rise. (After Iyer et al , 1969.)

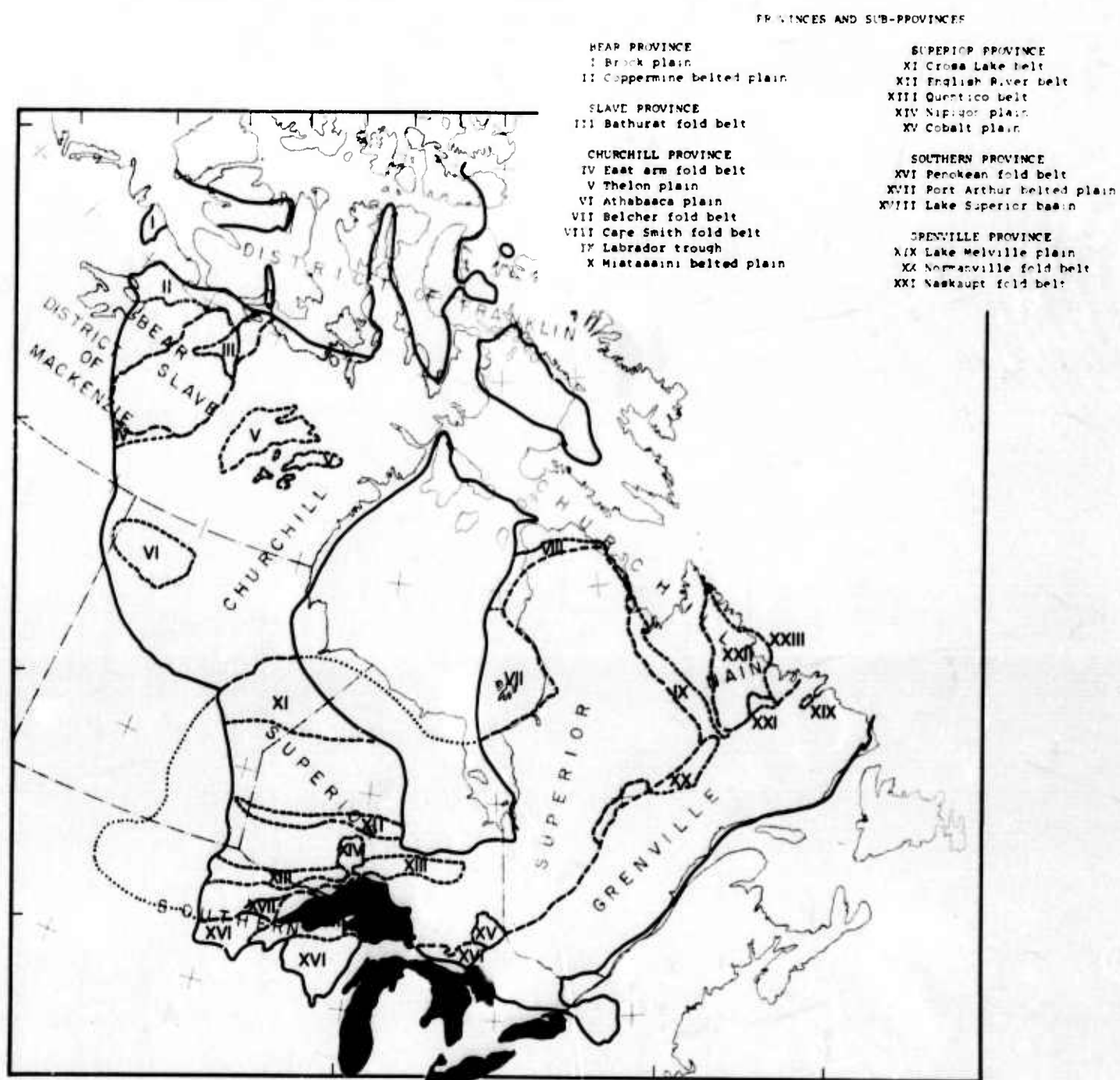


Figure 3. Structural map of the Canadian Shield. (Adopted from Stockwell 1962; 1964.)

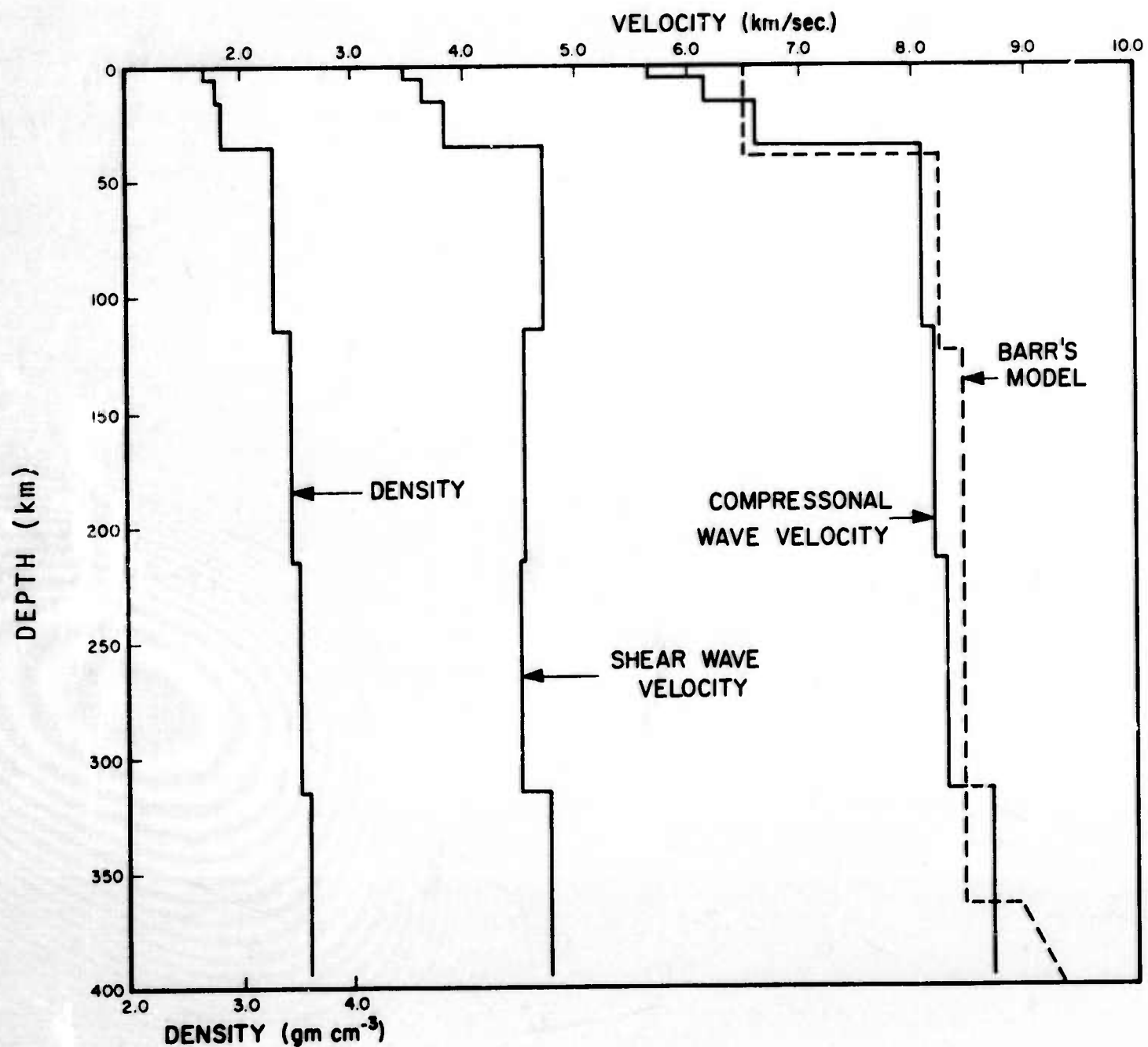


Figure 4. The model CANSD for the crust and upper mantle beneath the Canadian shield derived from surface wave dispersion data. (Brune and Dorman, 1963.) Dashed line indicates the P-wave model obtained by Barr (1967) from body wave data.



Figure 5. Locations of shot points and recording stations for the 1965 Hudson Bay crustal experiment. (After Hobson, 1967.)

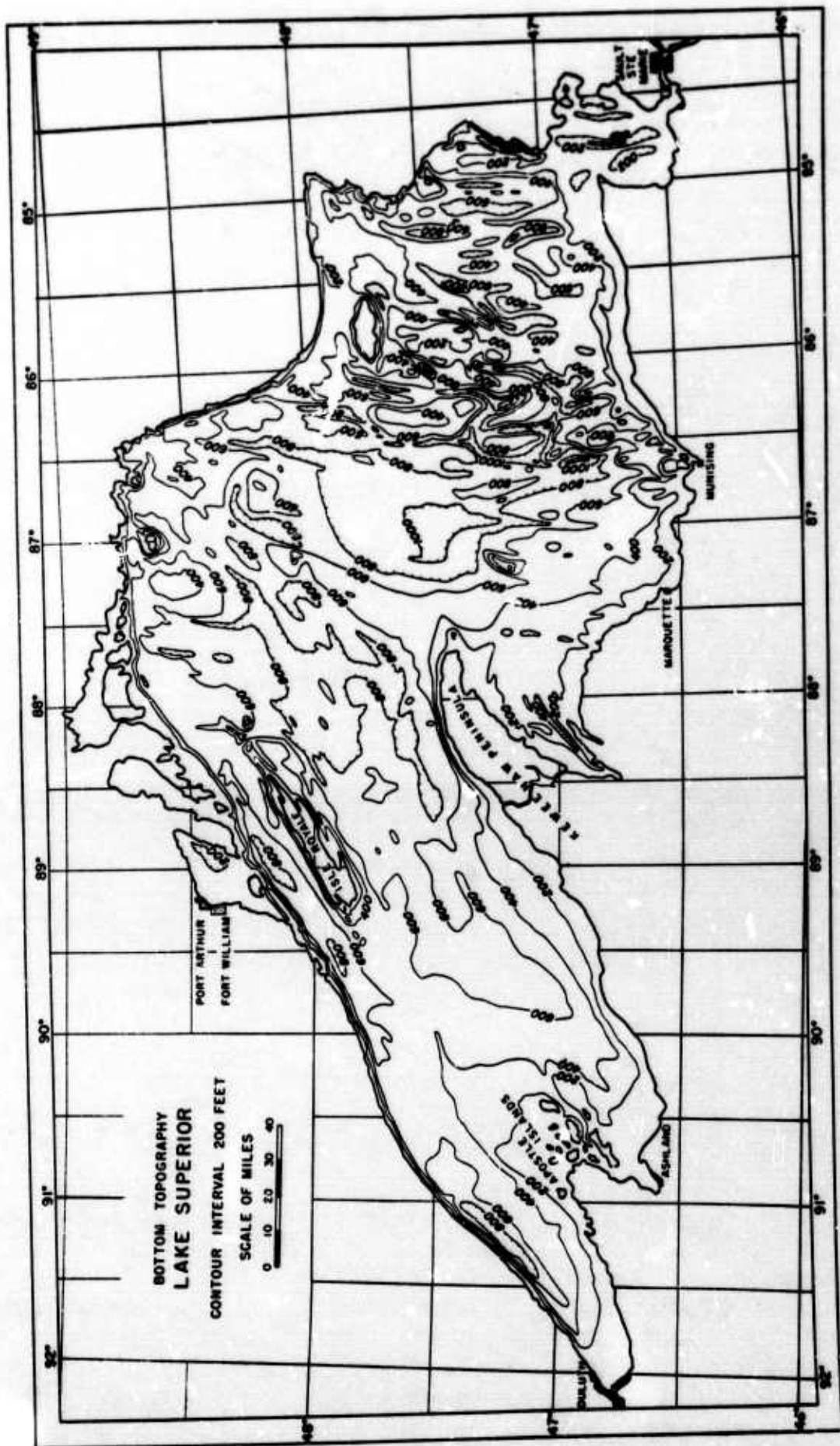


Figure 7. Bottom topography of Lake Superior. (After Hough, 1958.)

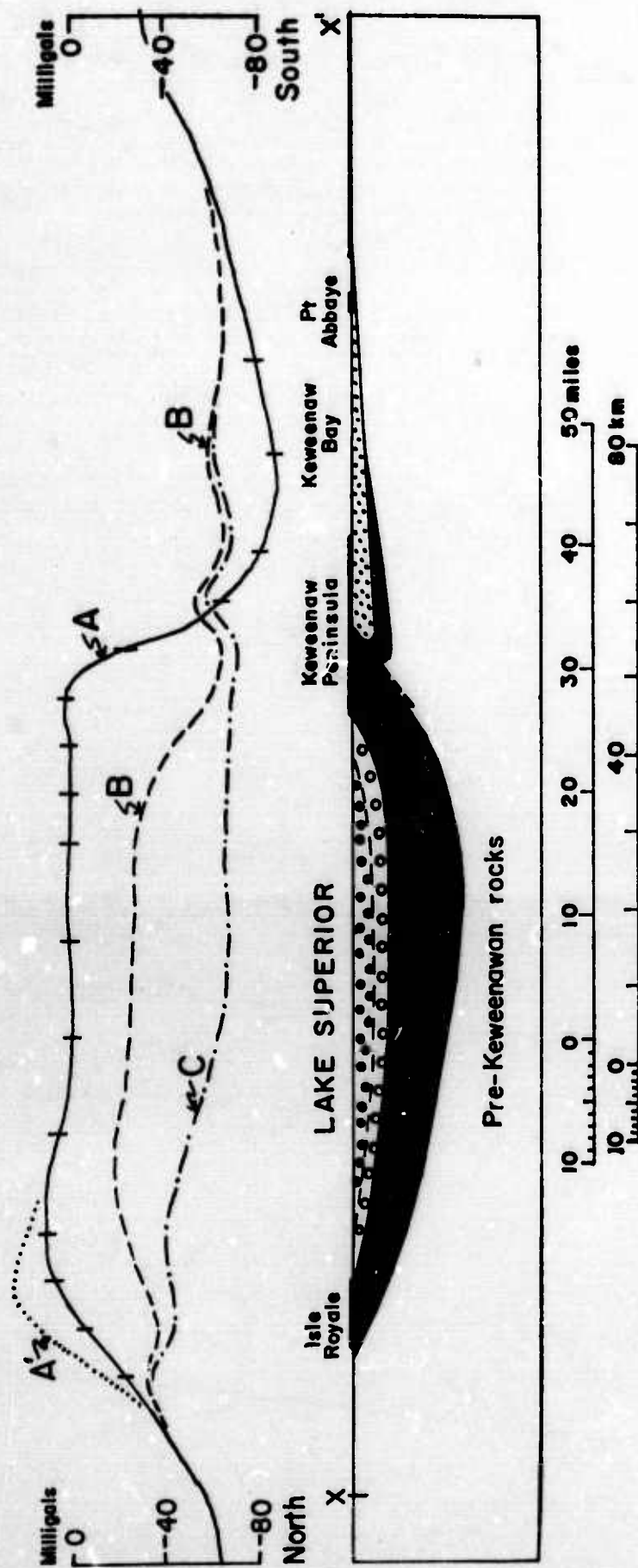


Figure 8. Geologic cross section 'through Isle Royale and Keweenaw Peninsula. A and A' are observed Bouguer gravity profiles, B and C residual Bouguer gravity profiles after effects of Keweenaw rocks are removed. Patterns represent geologic units, as follows: Jacobsville Sandstone, small dots; Freda Sandstone and Nonesuch Shale, large dots; Copper Harbor Conglomerate, circles; Portage Lake Series, solid black; pre-Keweenaw rocks, no pattern. (After White, 1966b.)

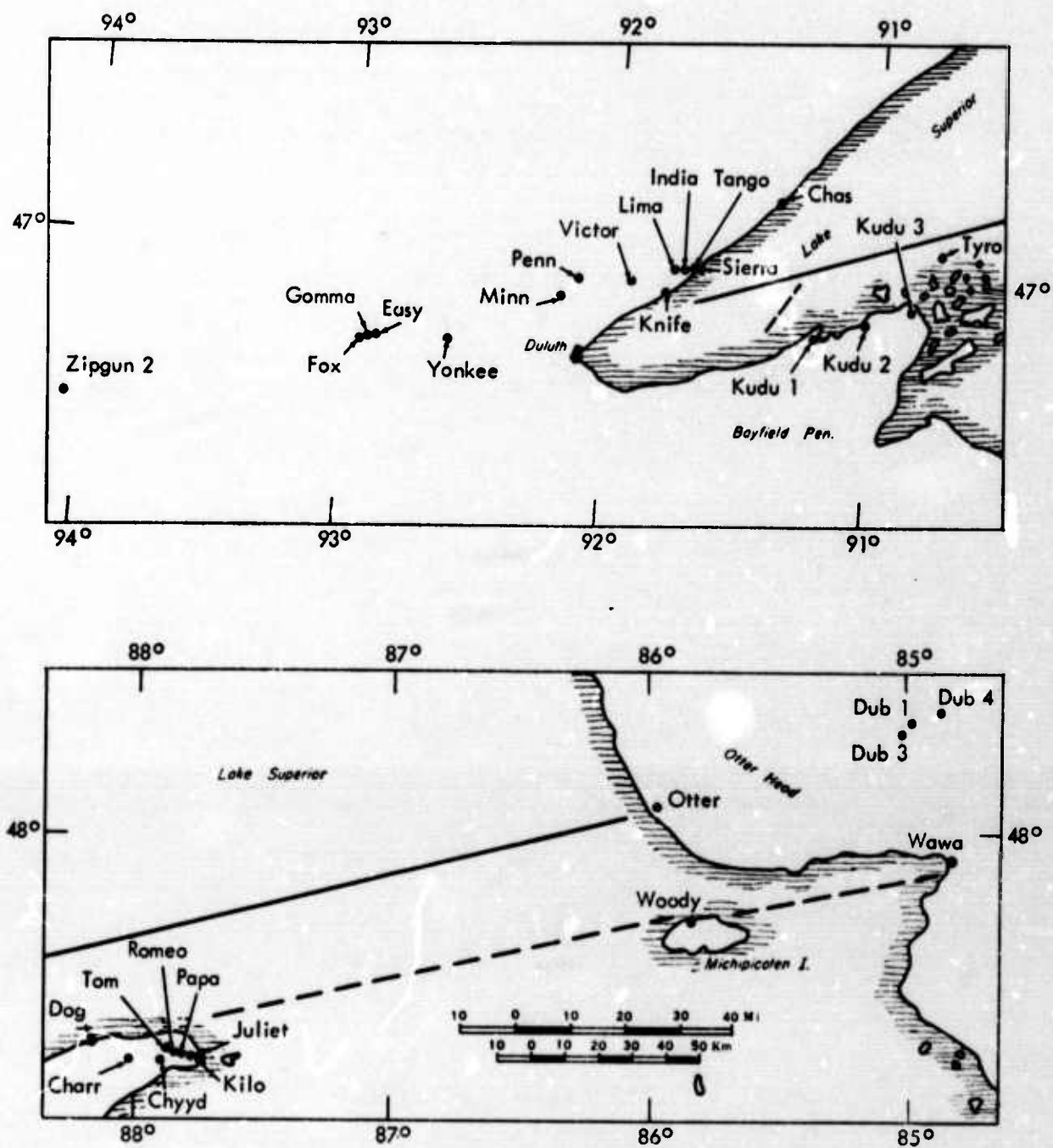


Figure 9. Locations of the principal recording stations during the 1963 Lake Superior Seismic Experiment. (After Smith et al, 1966.)

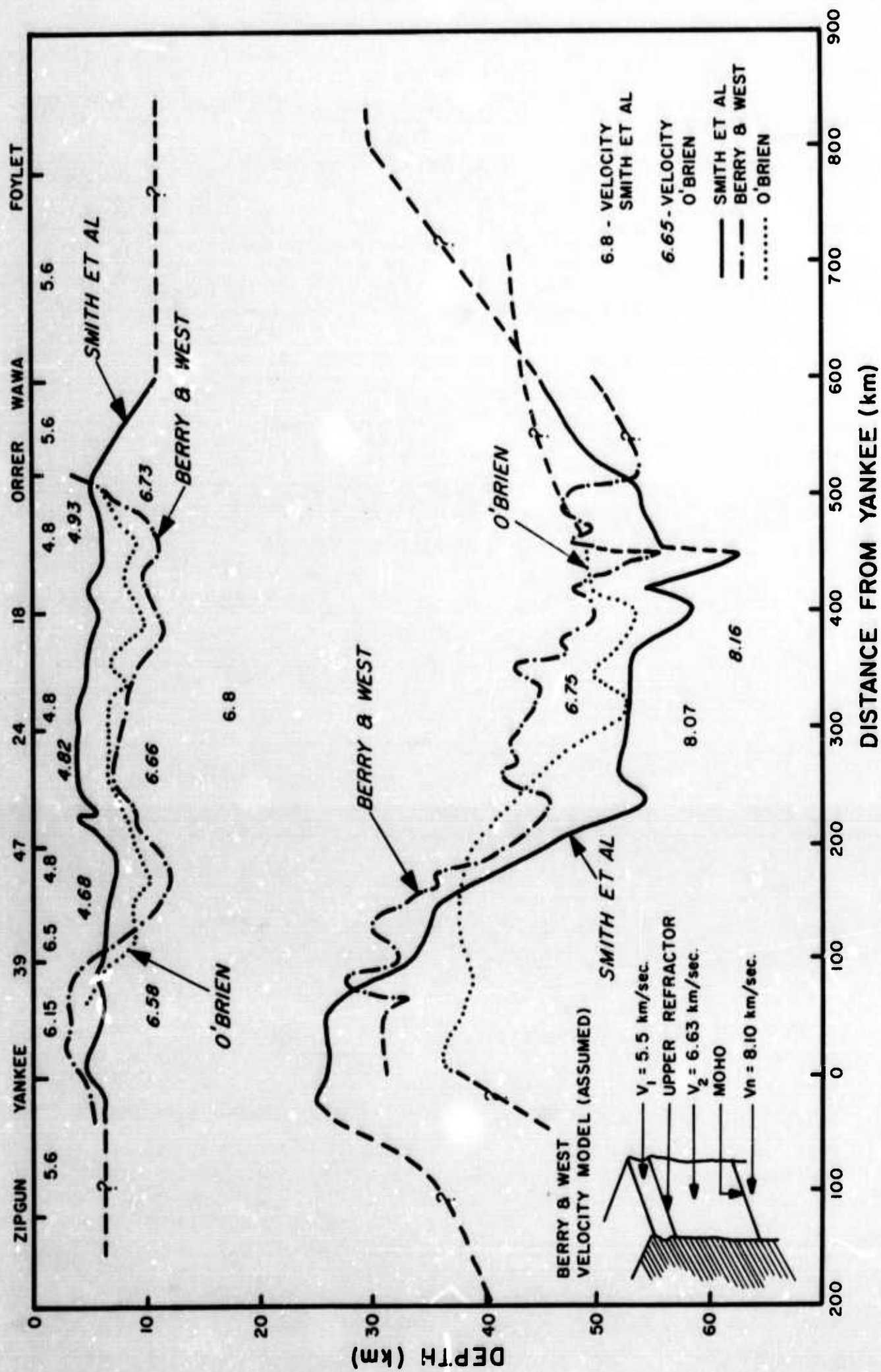


Figure 10. Models for the crust beneath Lake Superior obtained by Smith et al, (1966 a, b), Berry and West, (1966 a, b) and O'Brien (1968). Slanted velocity values are those obtained by O'Brien; upright ones and those given by Smith et al.

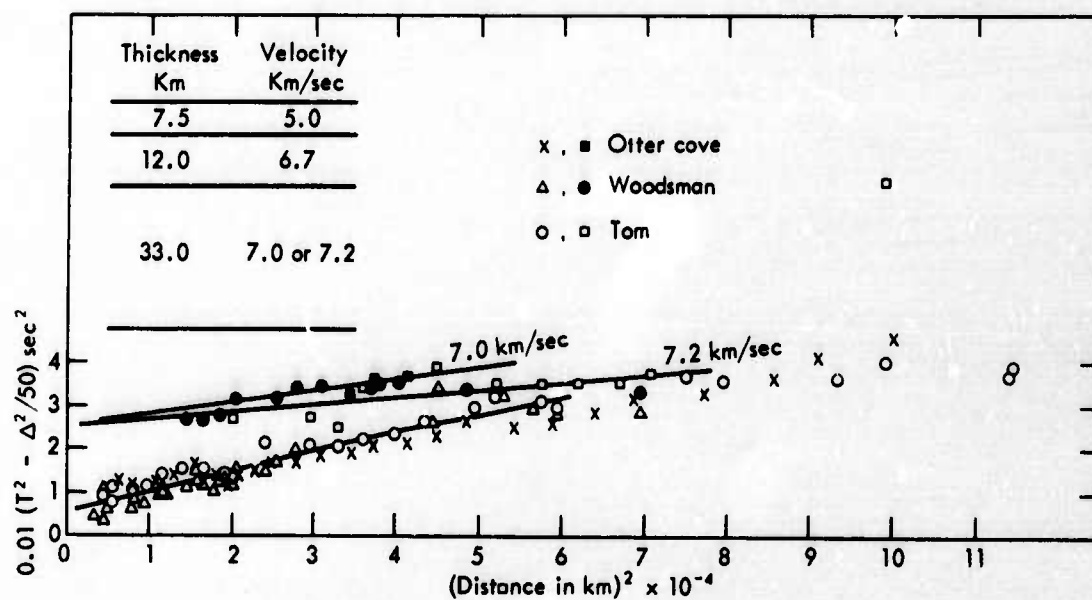


Figure 11. t^2-x^2 plot for data recorded at Otter Cove, Woodsman and Tom. Theoretical travel-times are for reflections from interfaces showing in model. (After O'Brien, 1968.)

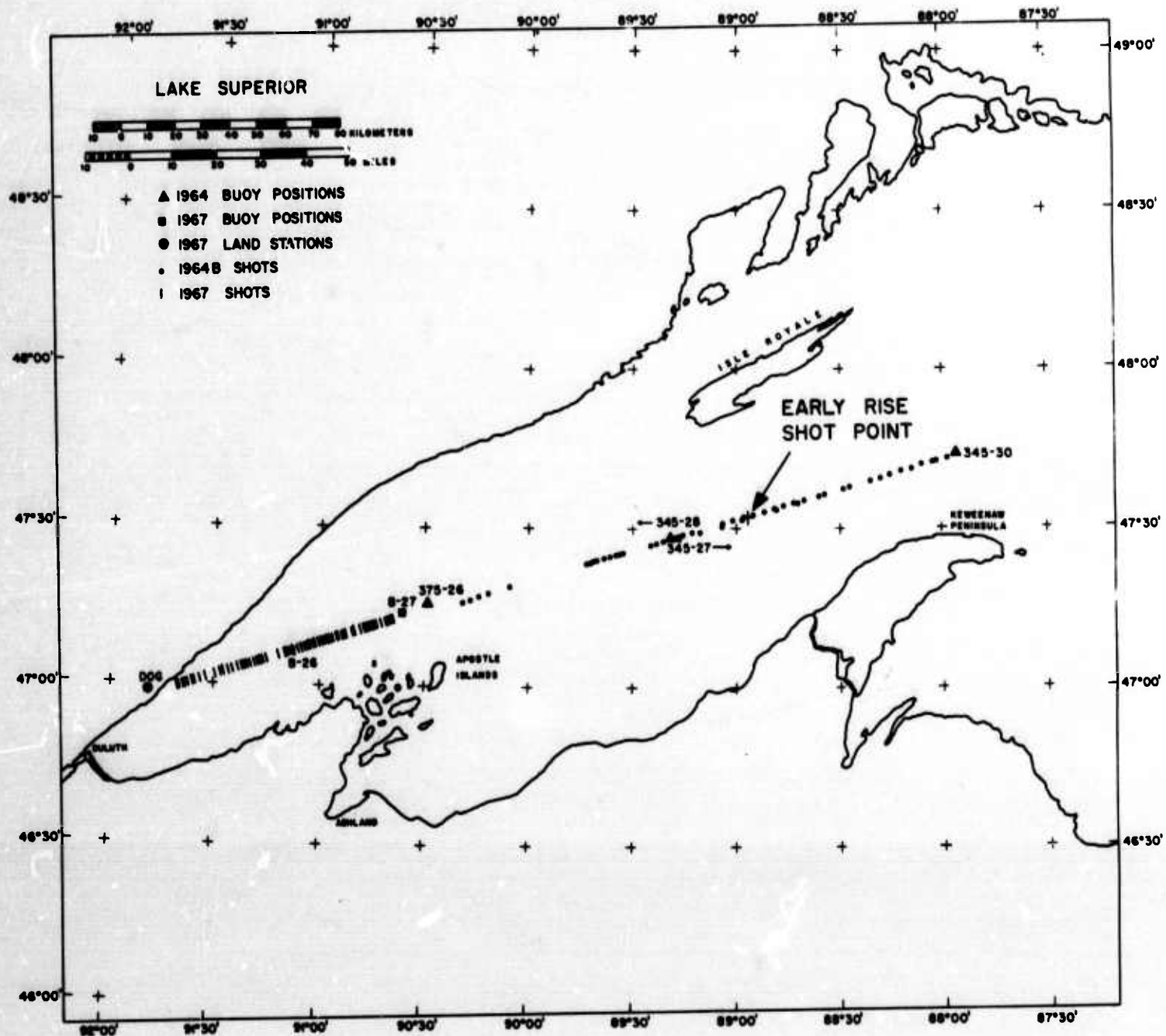


Figure 12. Locations of stations and shot points for the University of Wisconsin shallow seismic profiling study. (Courtesy of R.P. Meyer, University of Wisconsin Geophysical and Polar Research Center.)

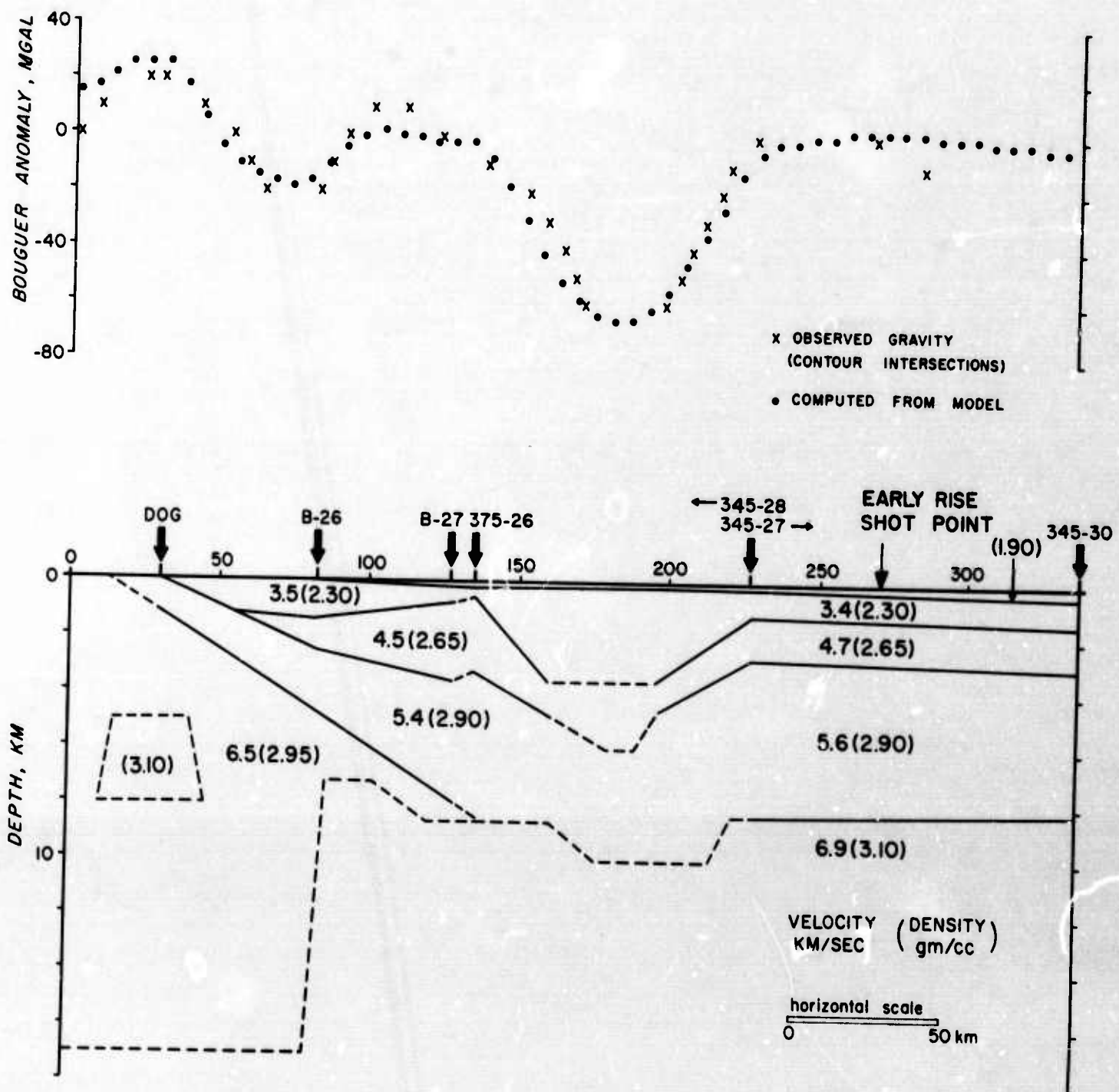


Figure 13. Model obtained by Anzoleaga et al (1969) for shallow crustal structure in western Lake Superior along profile shown in Figure 12. (Courtesy of R.P. Meyer, University of Wisconsin Geophysical and Polar Research Center.)

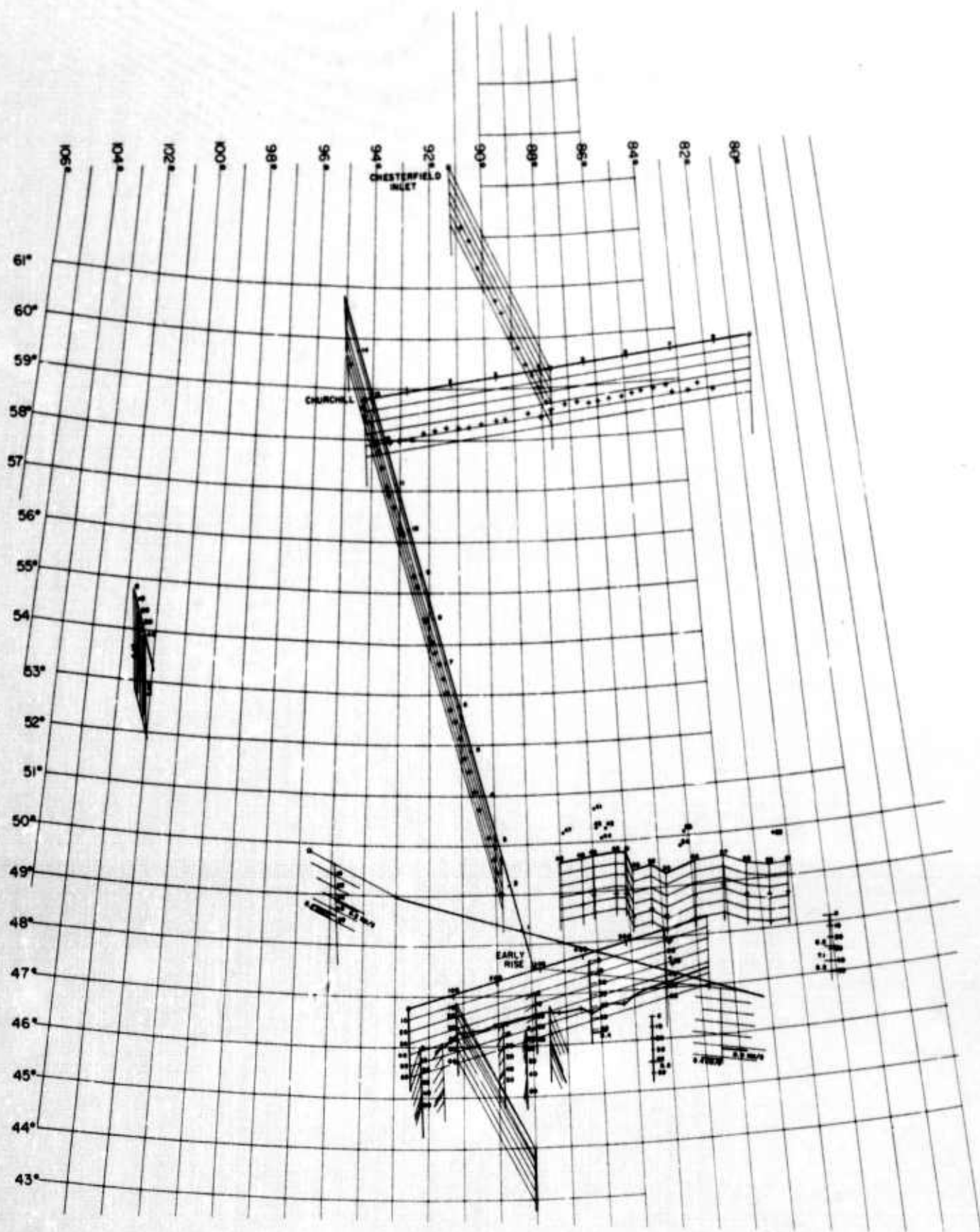


Figure 14. Compilation of results from seismic refraction surveys in the vicinity of Lake Superior plotted as a fence diagram.

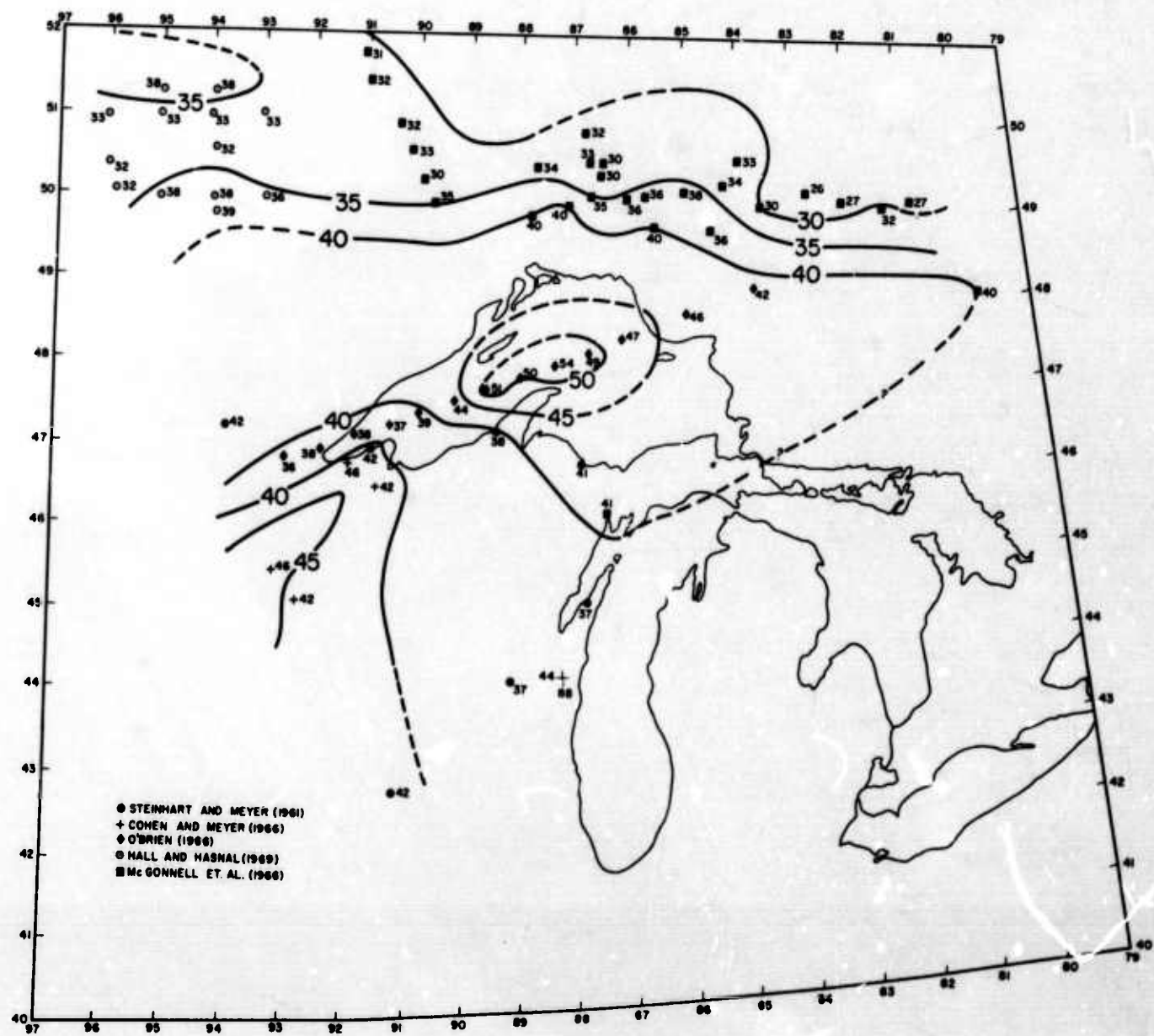
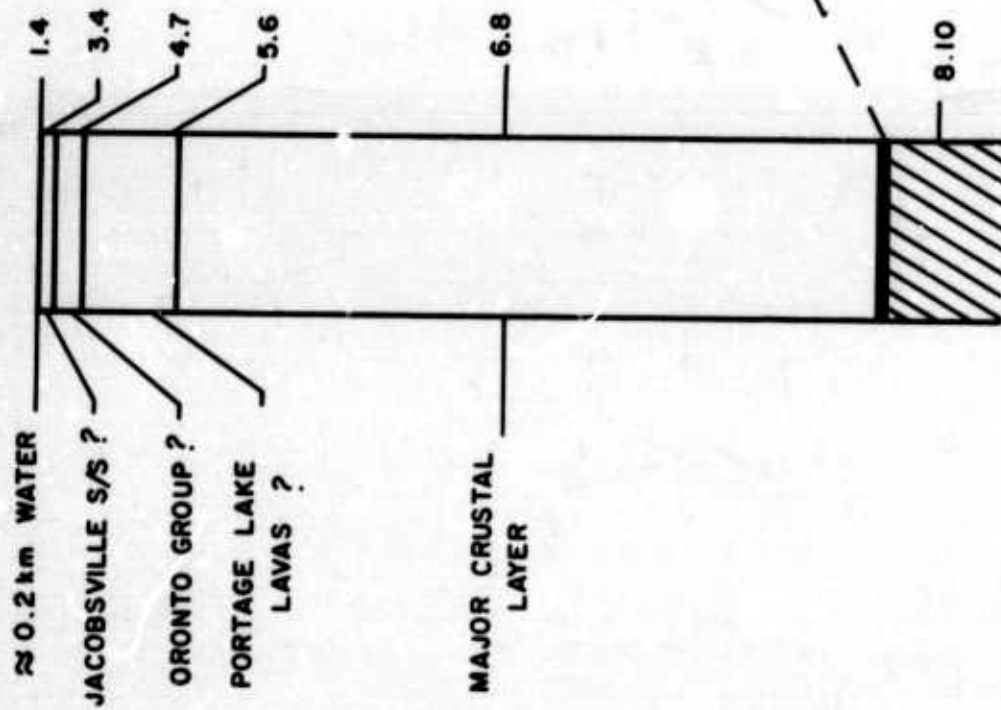


Figure 15. Contour map showing probable depth to the Moho in the Lake Superior region. Data for crust beneath Lake Superior are taken from O'Brien (1968).

EARLY RISE



YUCCA FLAT

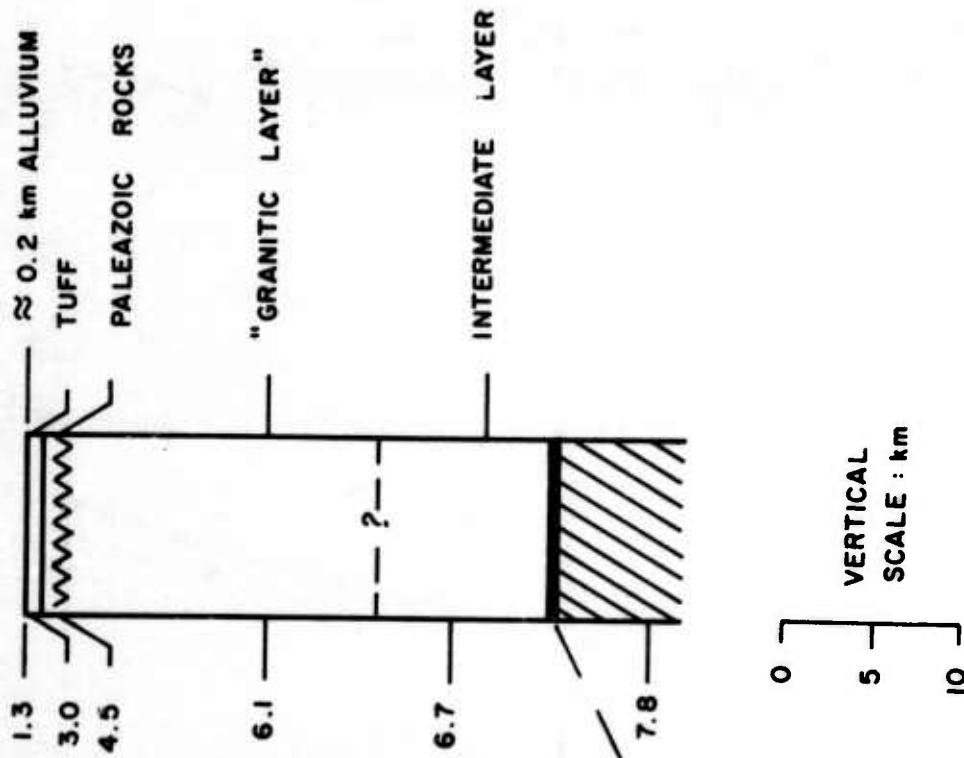


Figure 16. Theoretical fundamental mode Rayleigh wave dispersion computed for CANSD and a series of crustal models for Lake Superior discussed in the text.

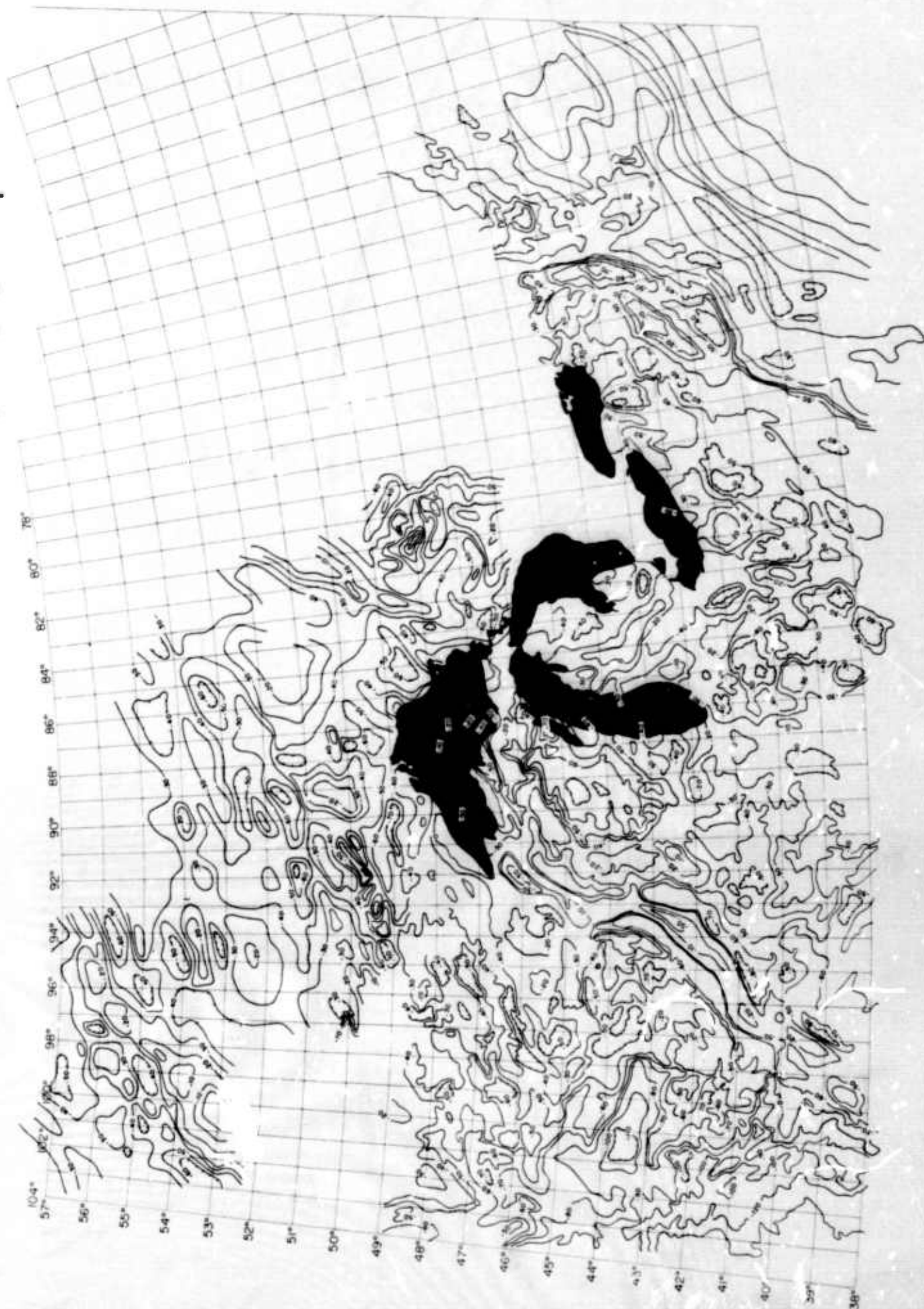


Figure 17. Bouguer gravity map of the area 38° - 51° N, 78° - 104° W compiled from data published by Weber and Goodacre (1966), Woollard and Joesting (1964), Innes (1960), McConnell (1966), and a series of maps compiled by Dominion Observatory of Canada.

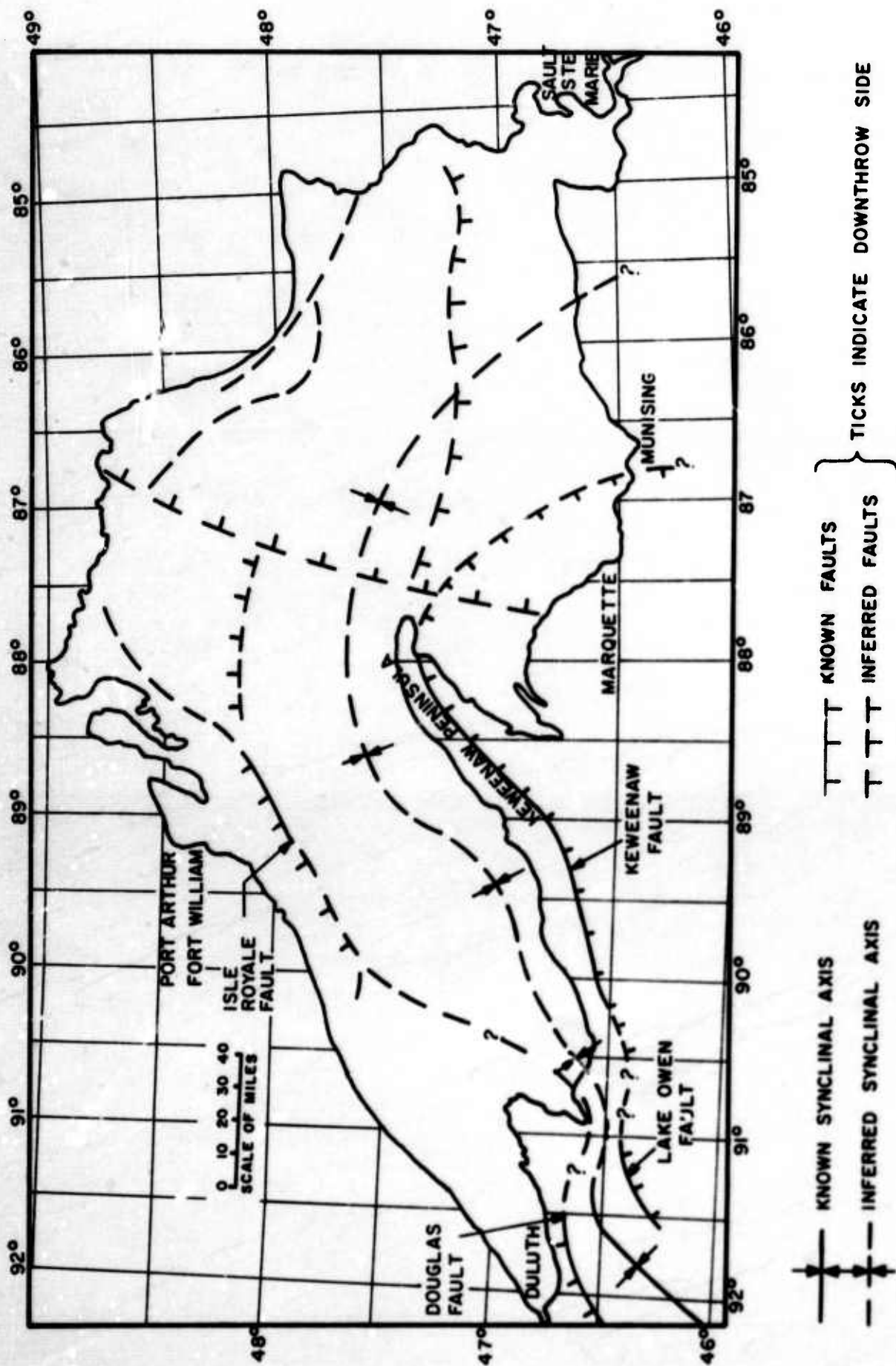


Figure 18. Structural map of Lake Superior showing positions of known faults and of those inferred from geophysical data.

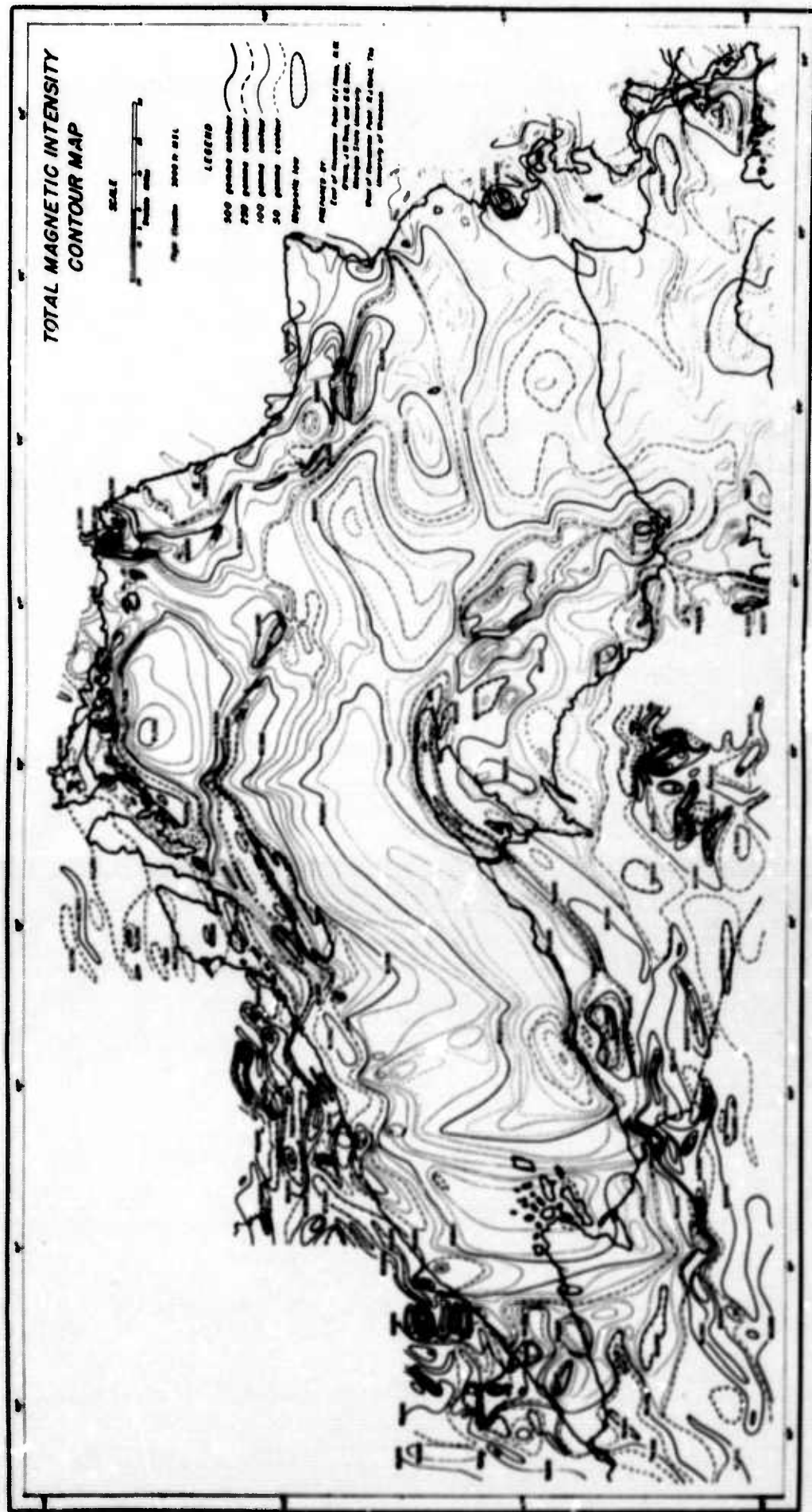


Figure 19. Total magnetic intensity map of Lake Superior (after Nino et al., 1966 and Wild and Ostensio, 1966).

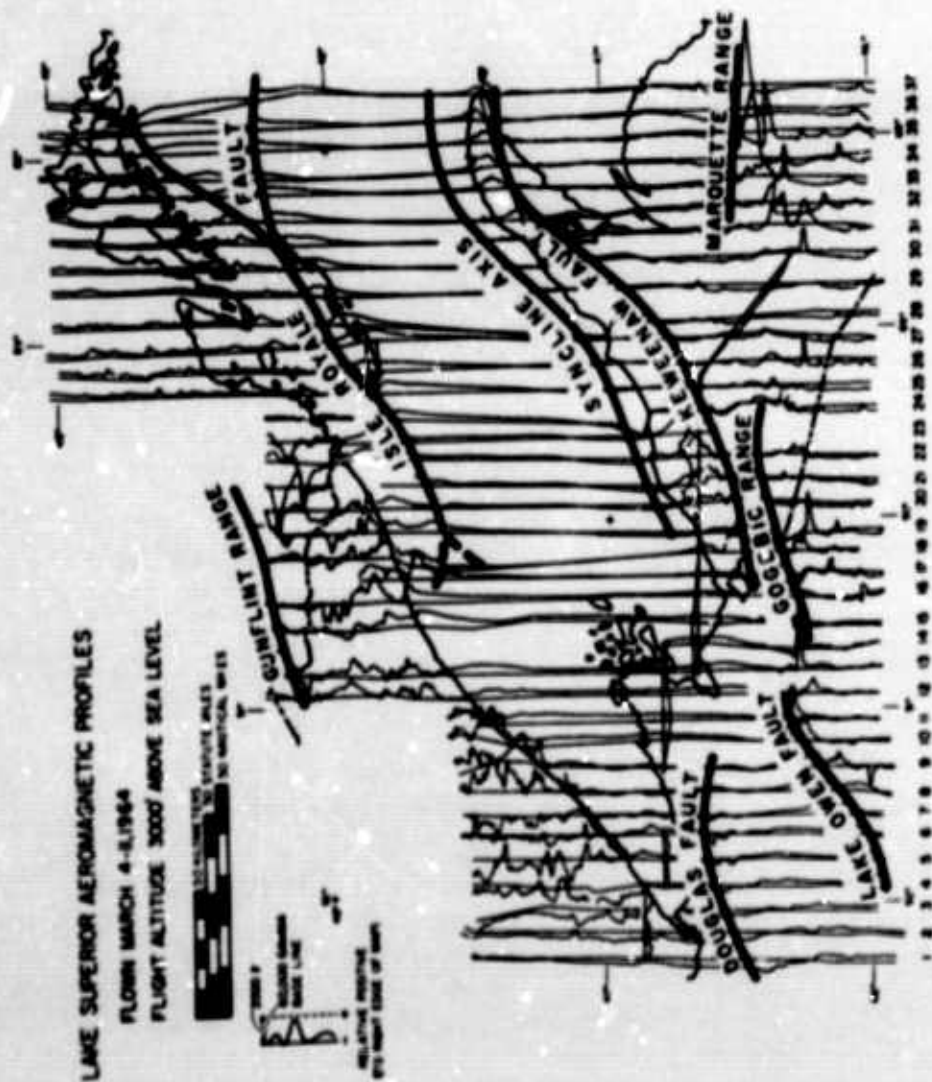
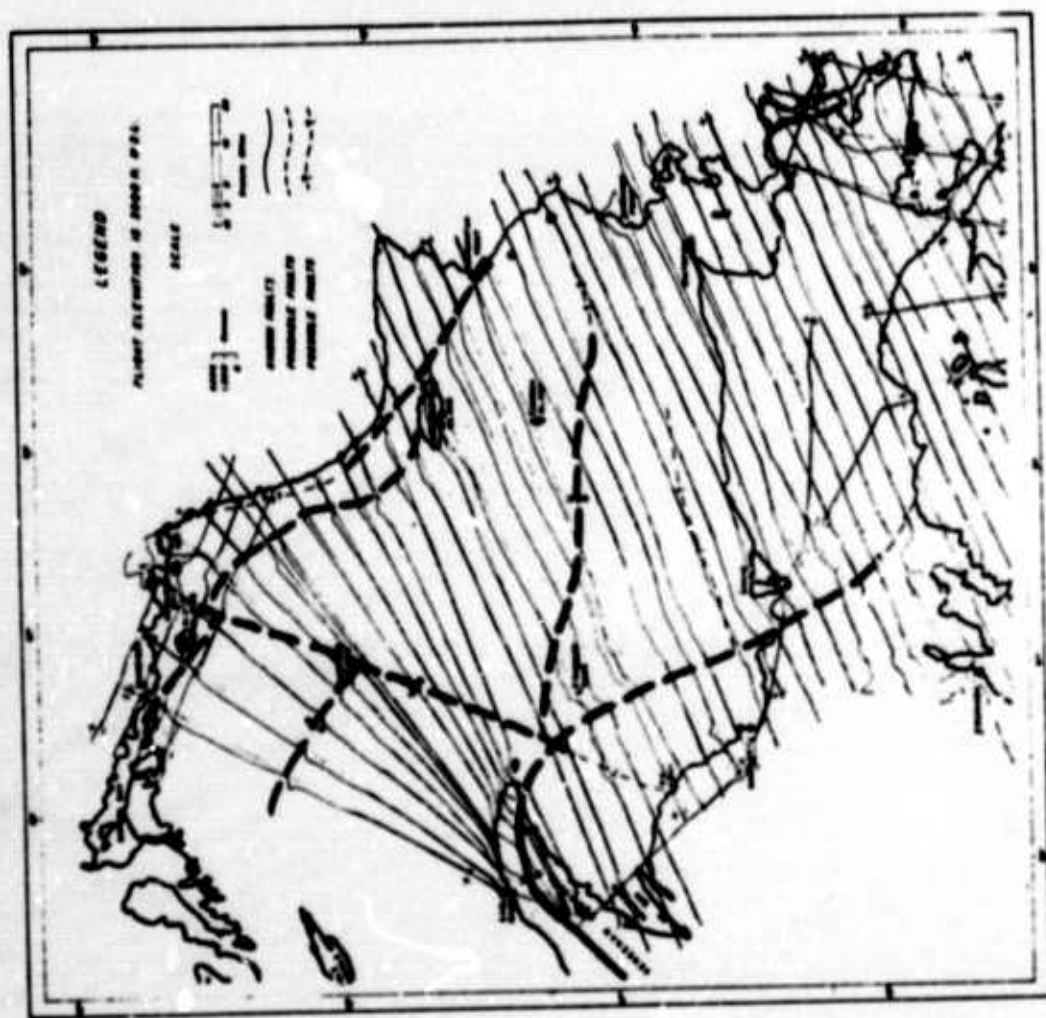


Figure 20. Shallow structure in Lake Superior from aeromagnetic data. (After Wold and Ostenso, 1966 and Hinze et al., 1966.)



Figure 21. Residual total magnetic intensity contour map of eastern Lake Superior showing labelled anomalies referred to in the text. (After Hinze et al., 1966.)

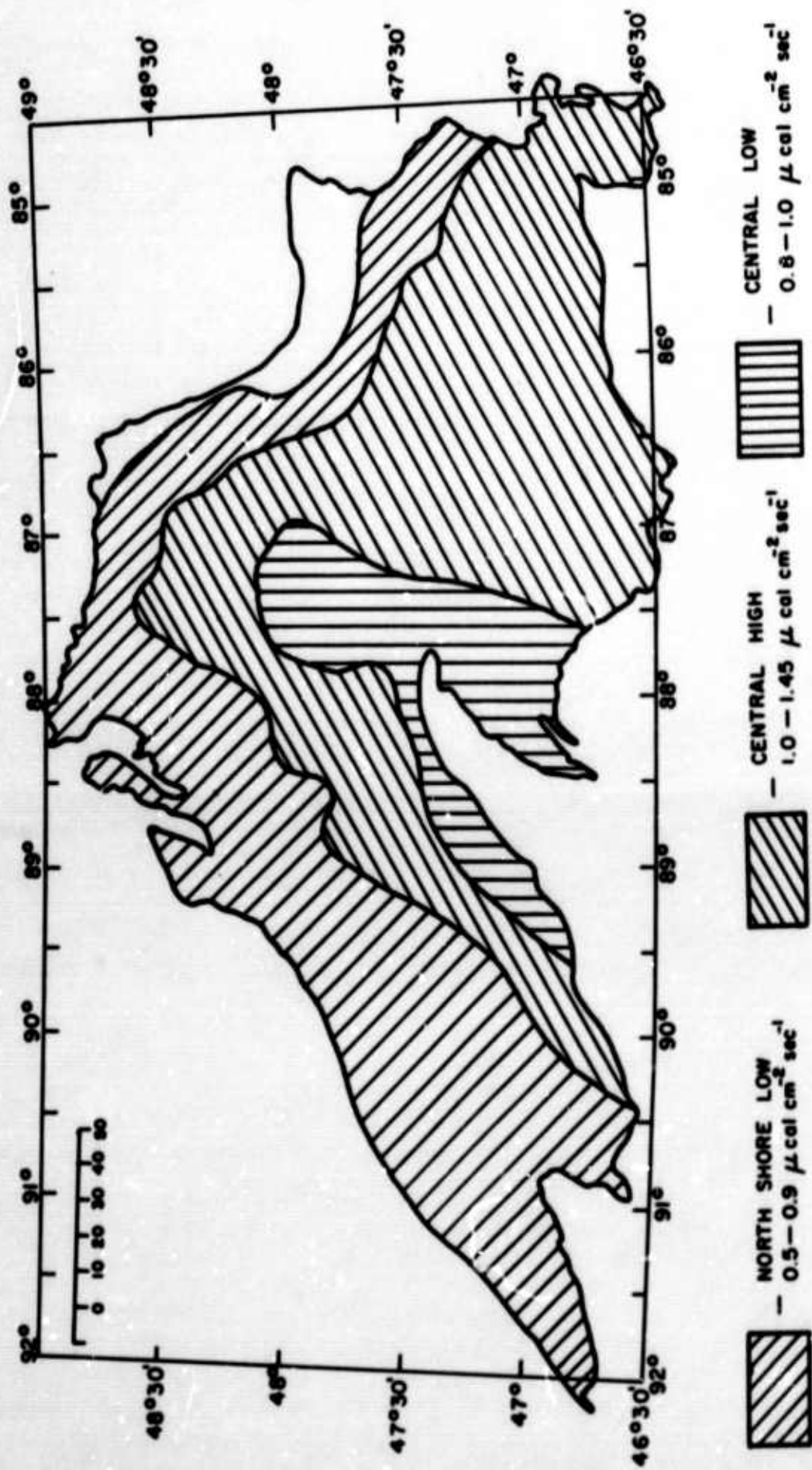


Figure 22. Heat flow observations in Lake Superior showing the 3 heat principal flow regimes. (After Steinhart et al., 1968.)

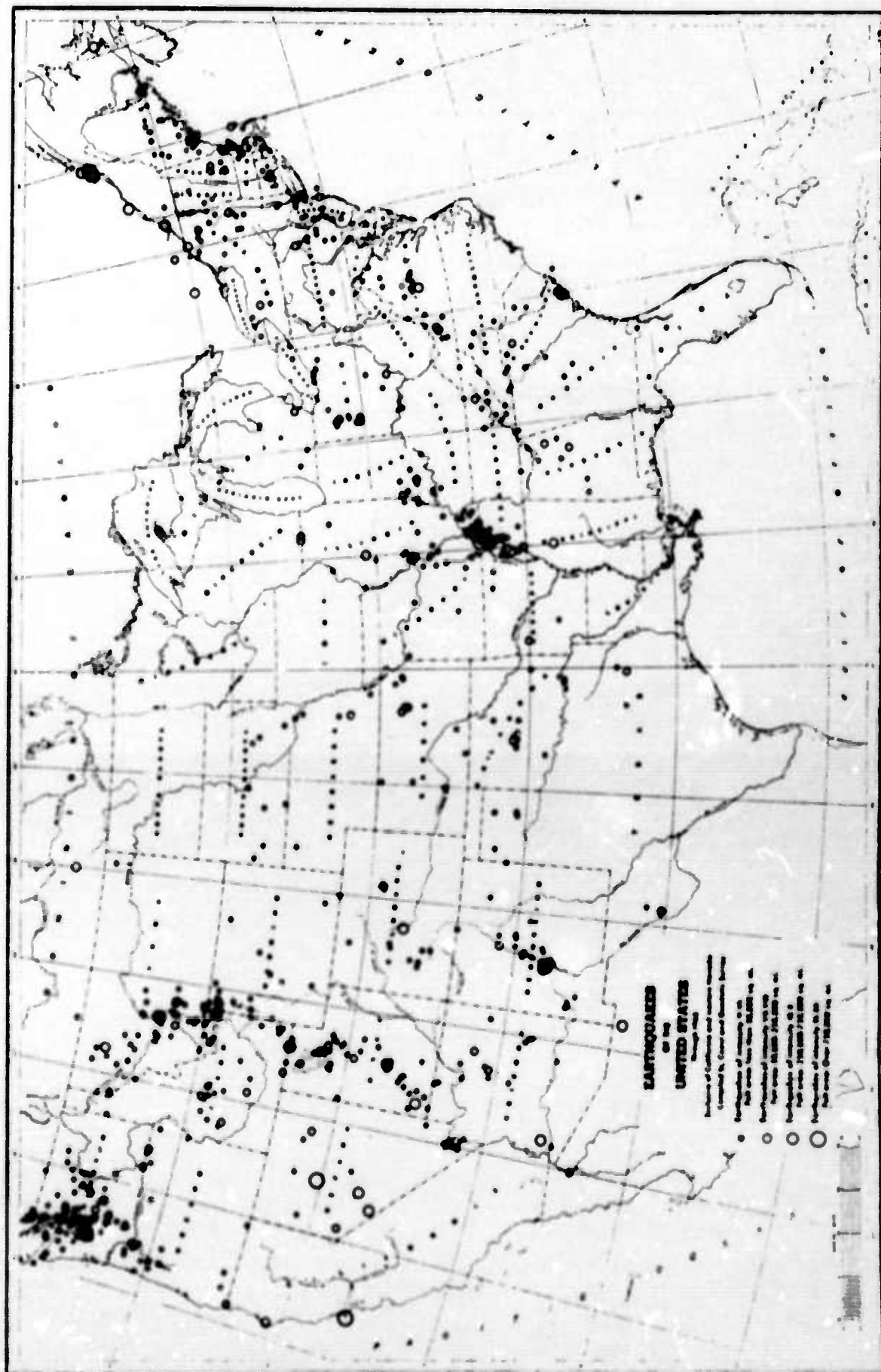


Figure 23. Earthquakes of the United States through 1963 exclusive of California and western Nevada. (After Eppley, 1965.)

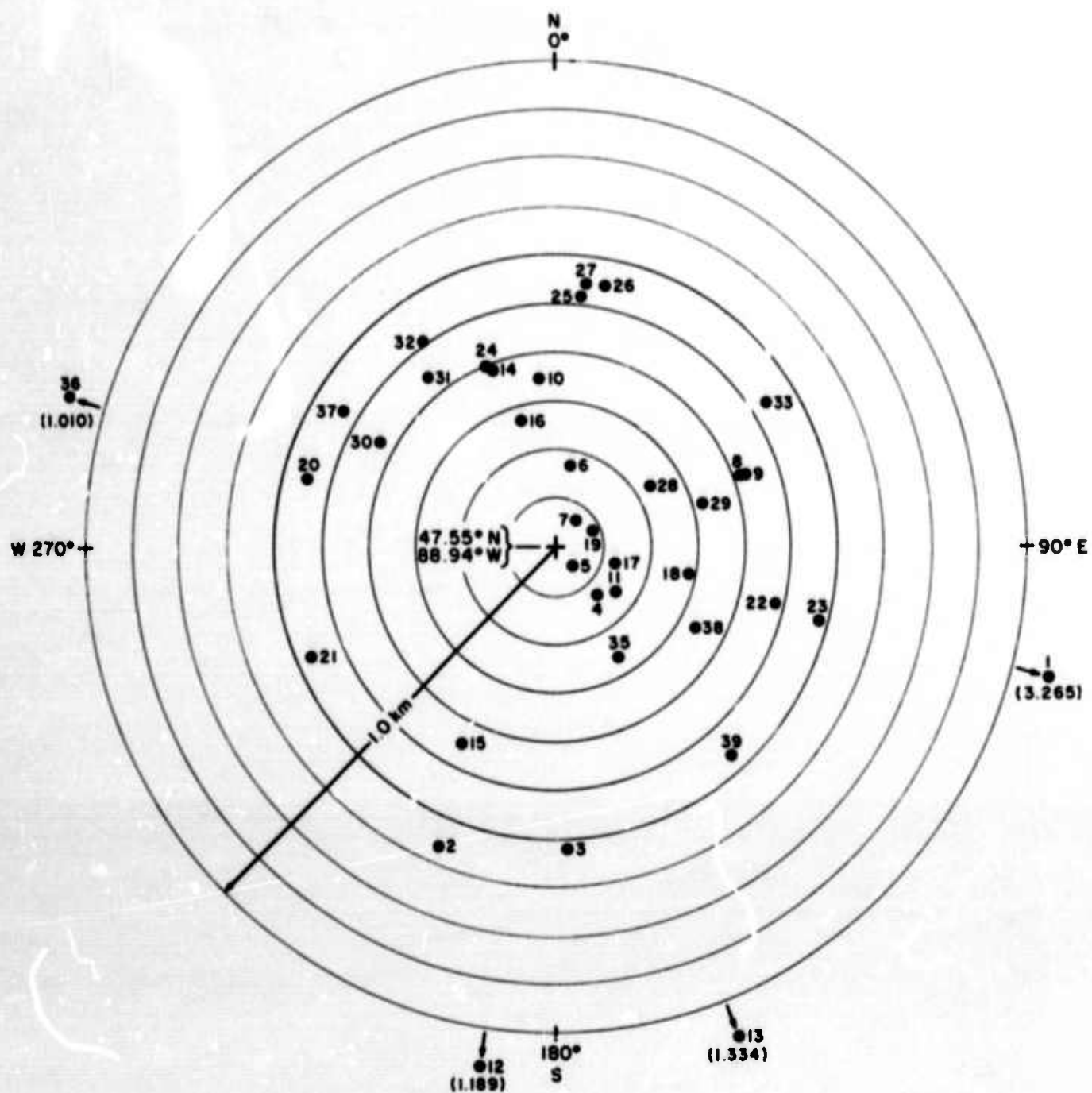


Figure 24. Locations of the 38 shots detonated during Project Early Rise. Arrows indicate directions to the shot points beyond 1 km; values in parentheses indicate the distance.

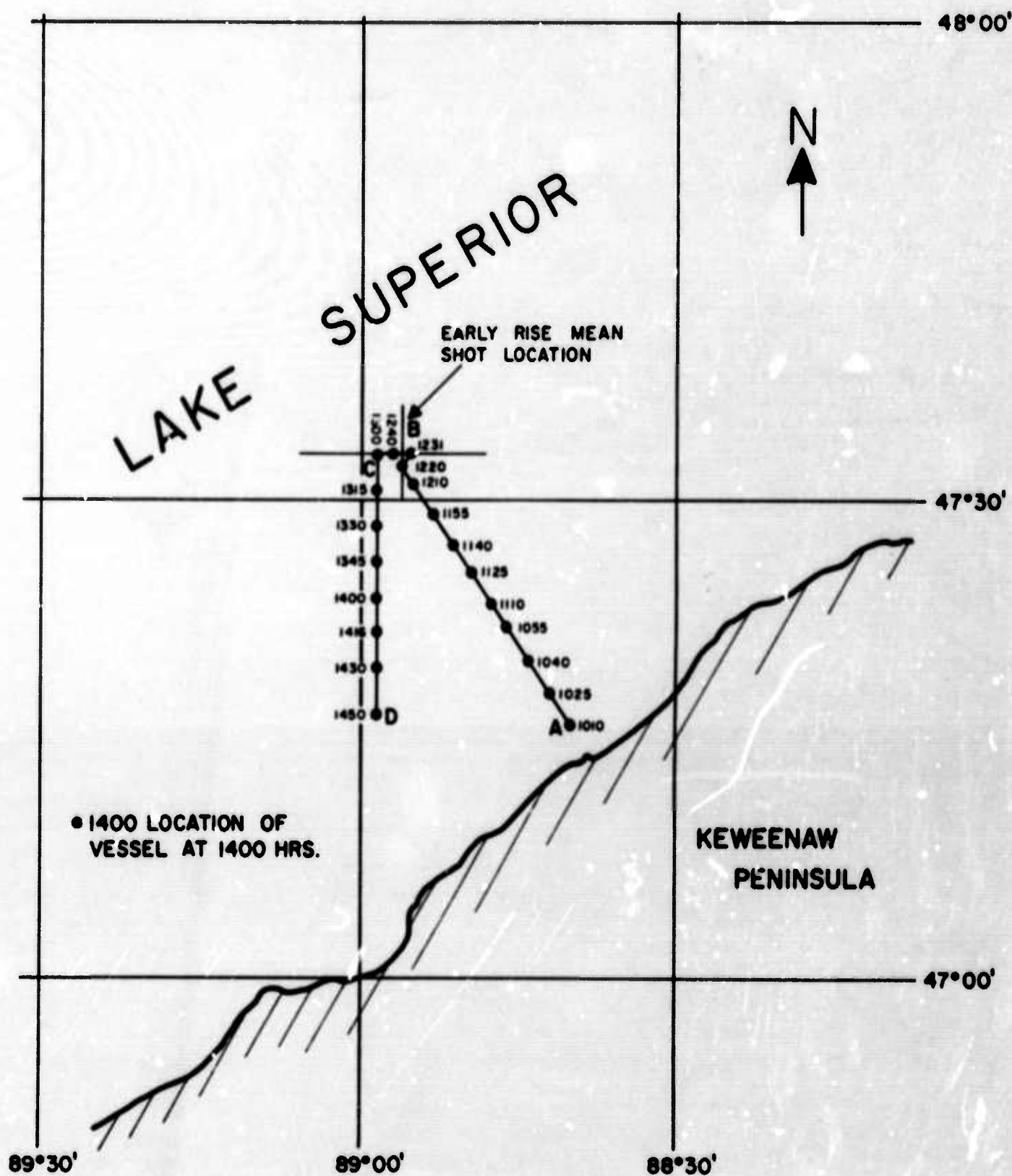


Figure 25. Location of the continuous sub-bottom profiling survey through Early Rise shot point conducted by the University of Wisconsin in 1966. Times of particular locations are indicated along each line. (Courtesy of R.J. Wold, University of Wis.)

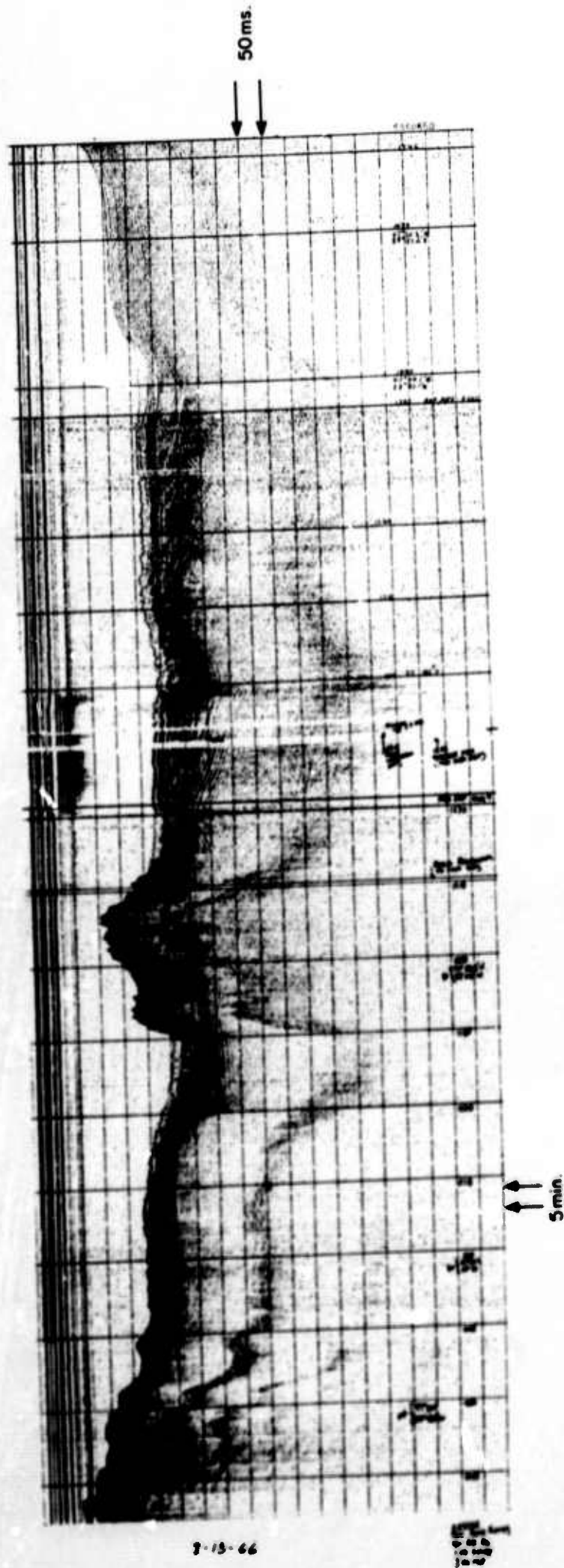


Figure 26. Continuous sub-bottom profile through Early Rise shot point recorded along track shown in Figure 25. (Courtesy of R.J. Wold, University of Wis.)

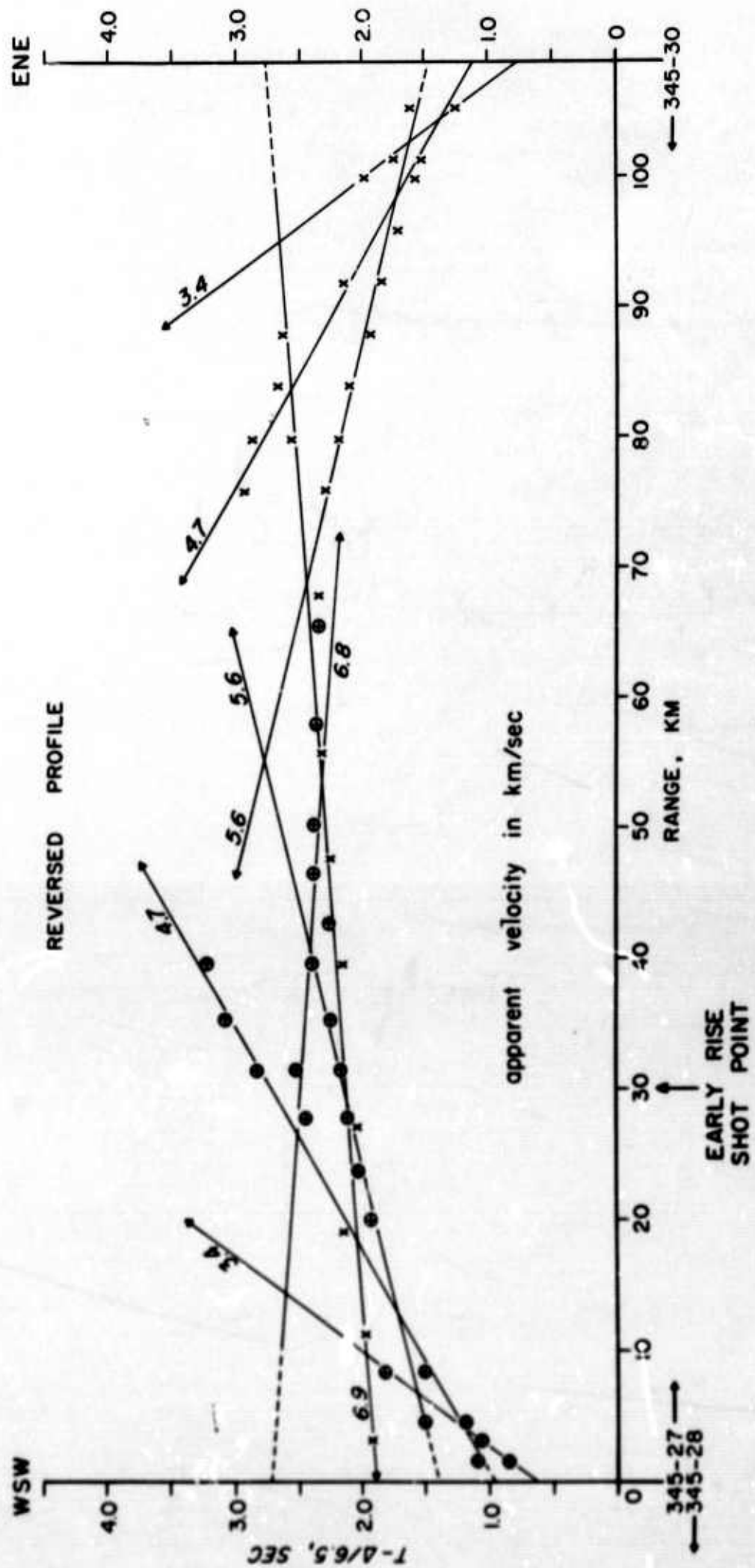


Figure 27. First arrival data from reversed seismic refraction profiles through the Early Rise shot point. (Anzoleaga et al., 1969.) Reciprocity of apparent velocities suggests the refractors are very nearly horizontal. (Courtesy of R.P. Meyer, University of Wisconsin Geophysical and Polar Research Center.)

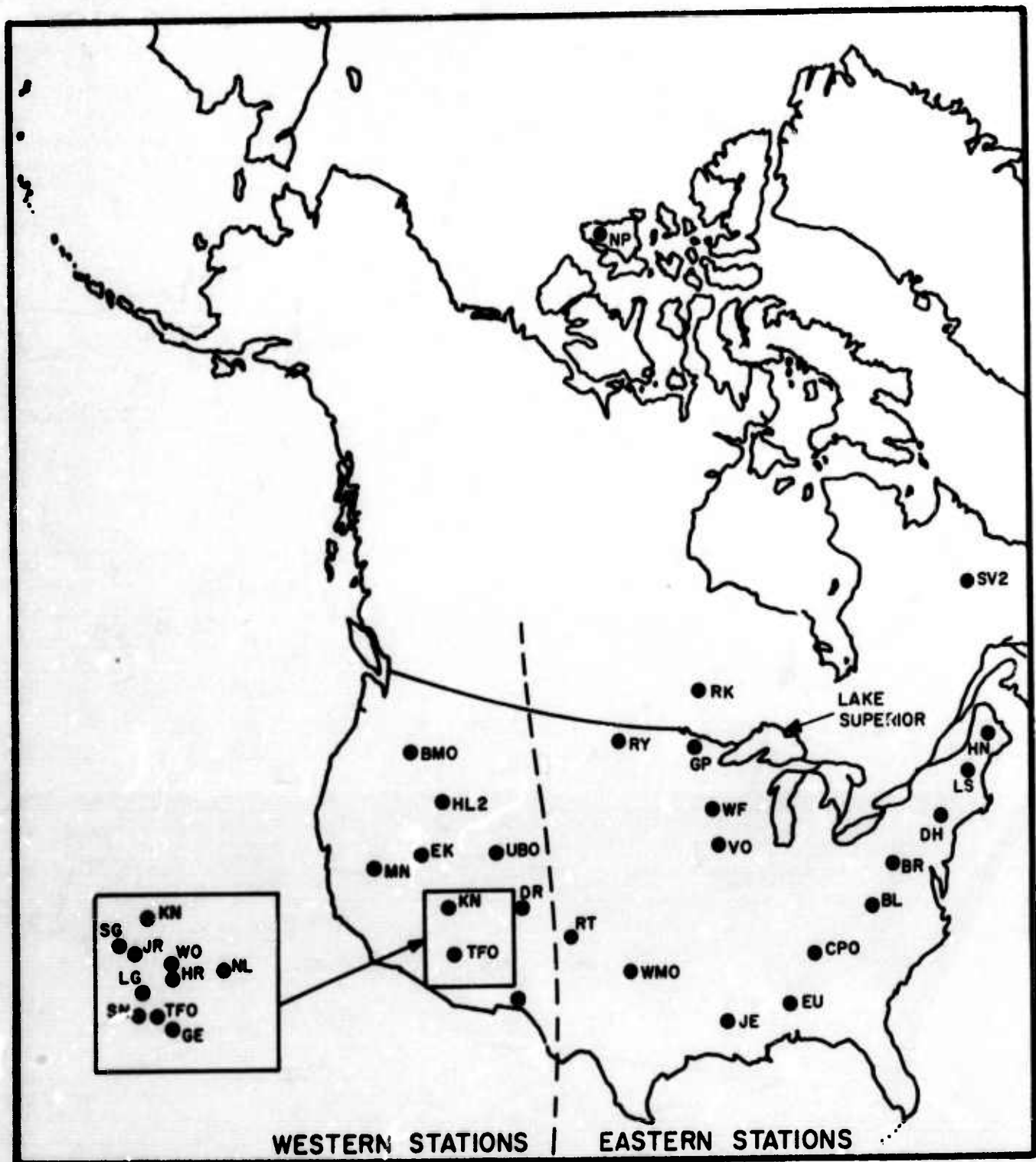


Figure 28. Locations of LRS stations and Vela Observatories which recorded some or all of the October, 1964 series of shots in Lake Superior.

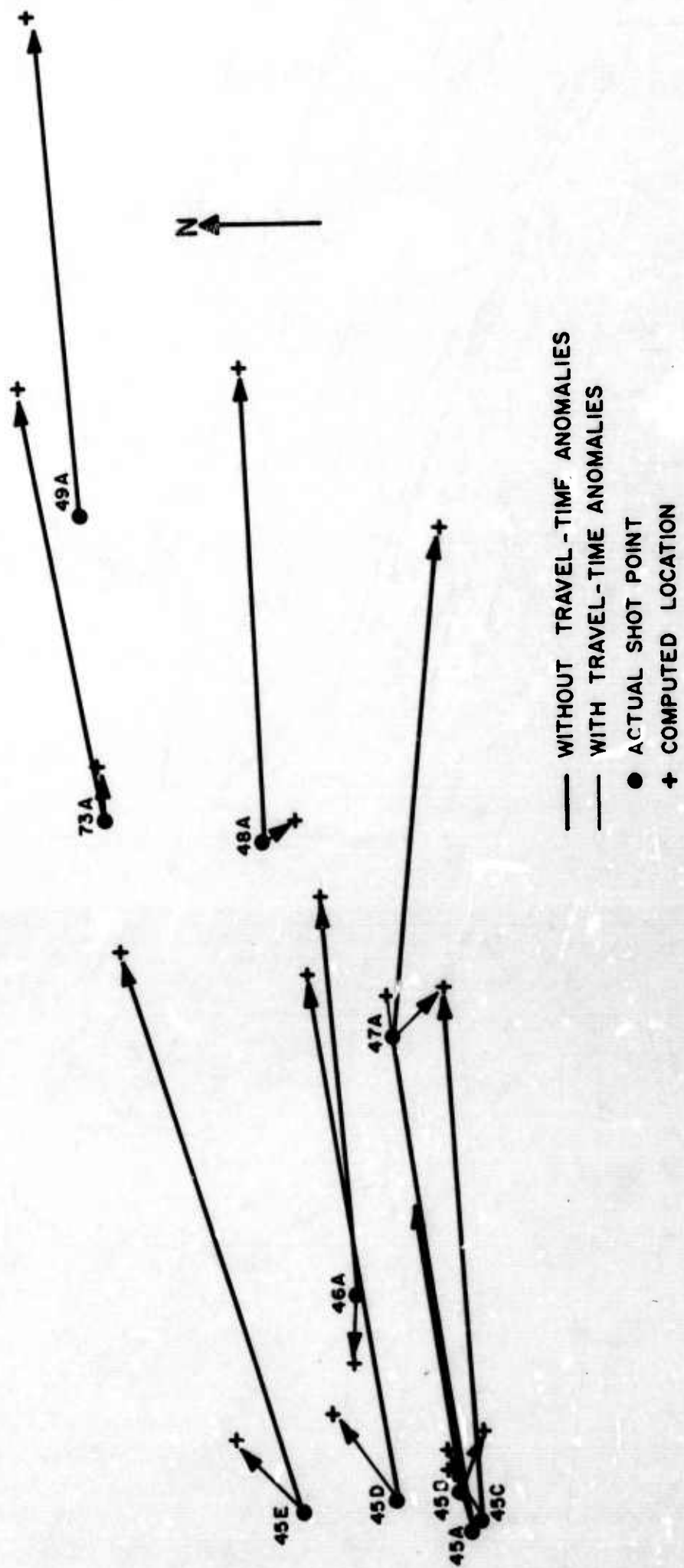


Figure 29. Actual and computed locations of the October, 1964 series of shots using the whole LRSM and observatory network.

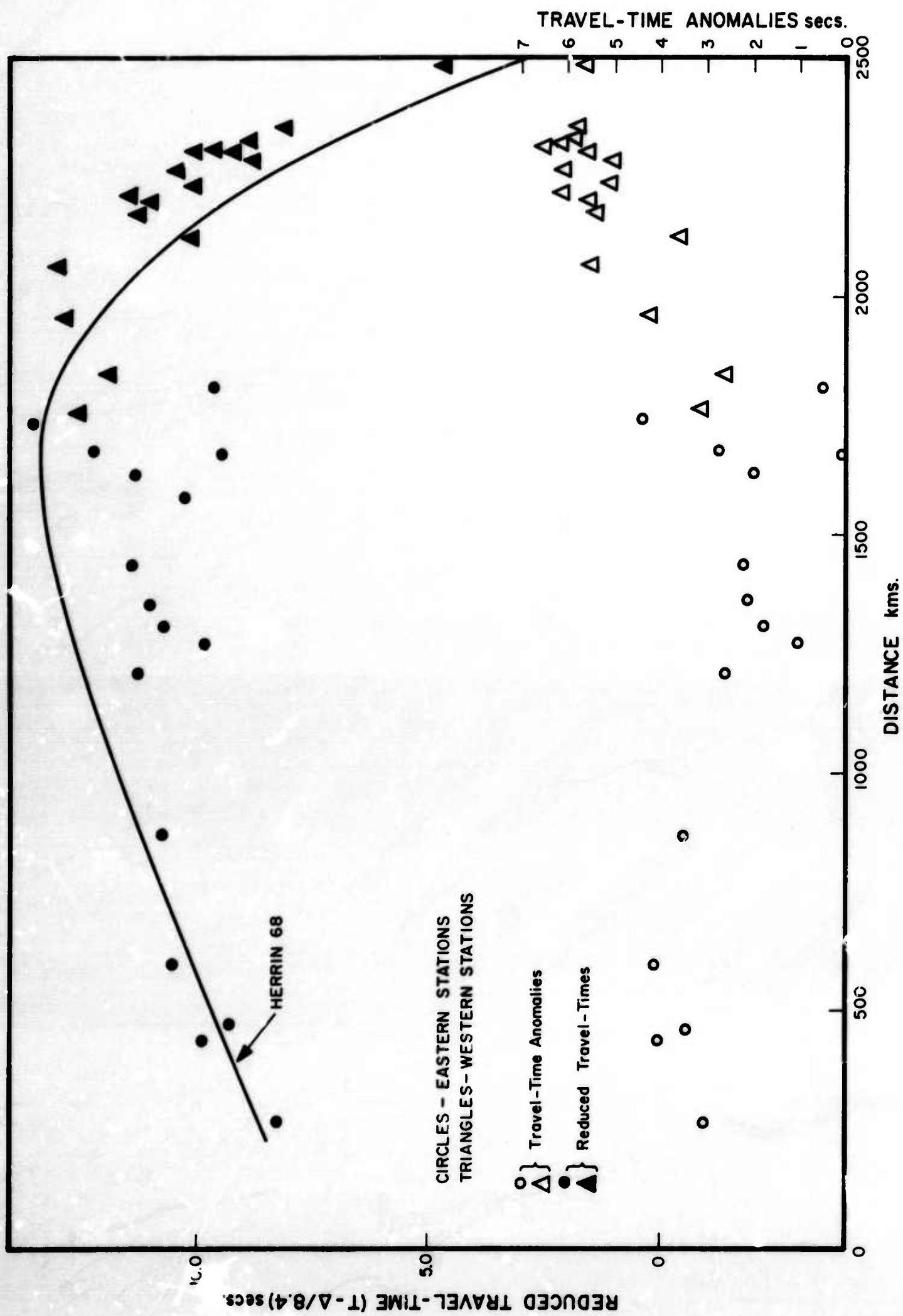


Figure 30. Reduced travel-times and travel-time anomalies relative to WMO for shot 49A.

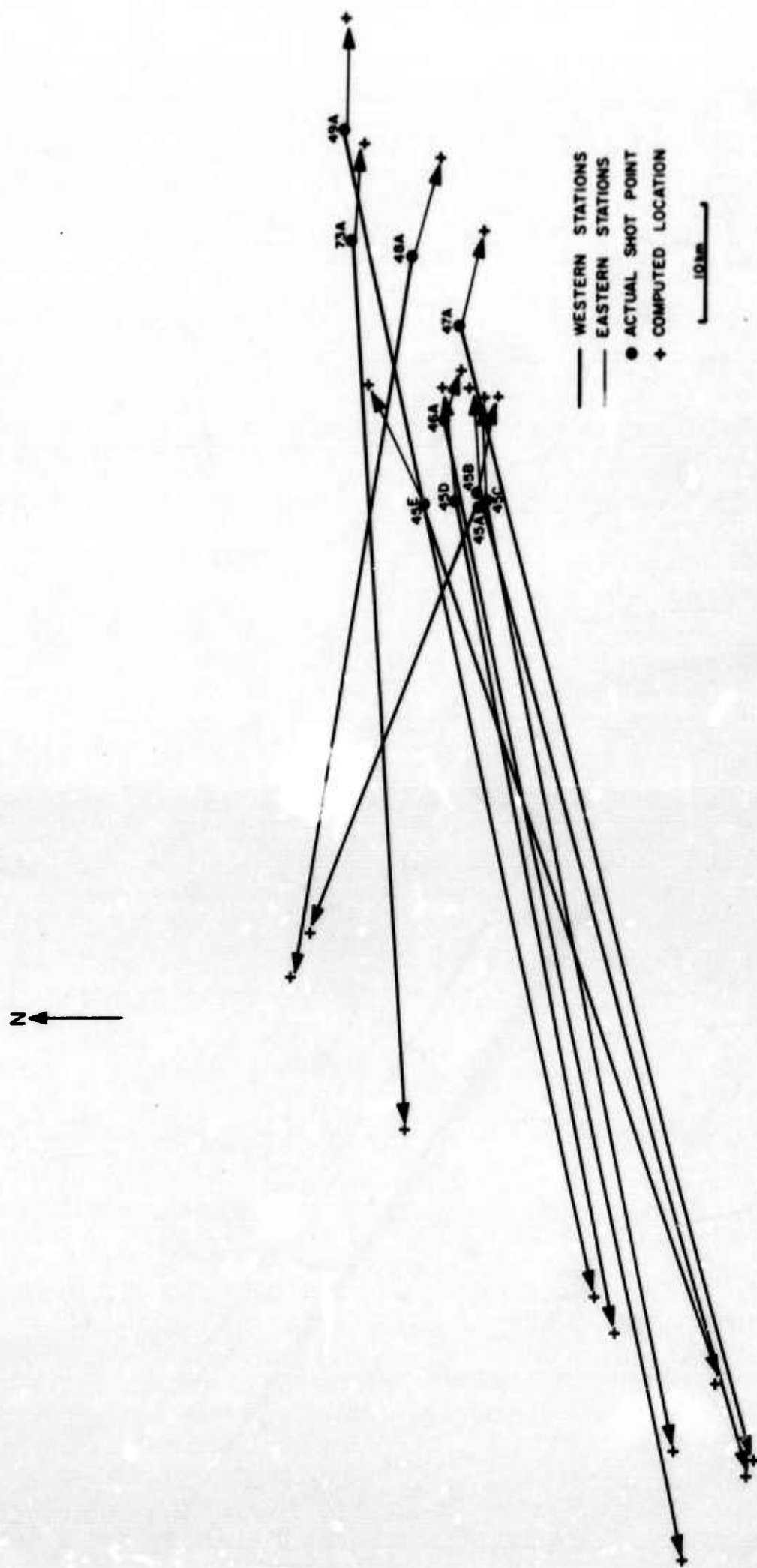


Figure 31. Actual and computed locations of October, 1964 series of shots using the eastern and western stations in the LRSM and observatory network separately.

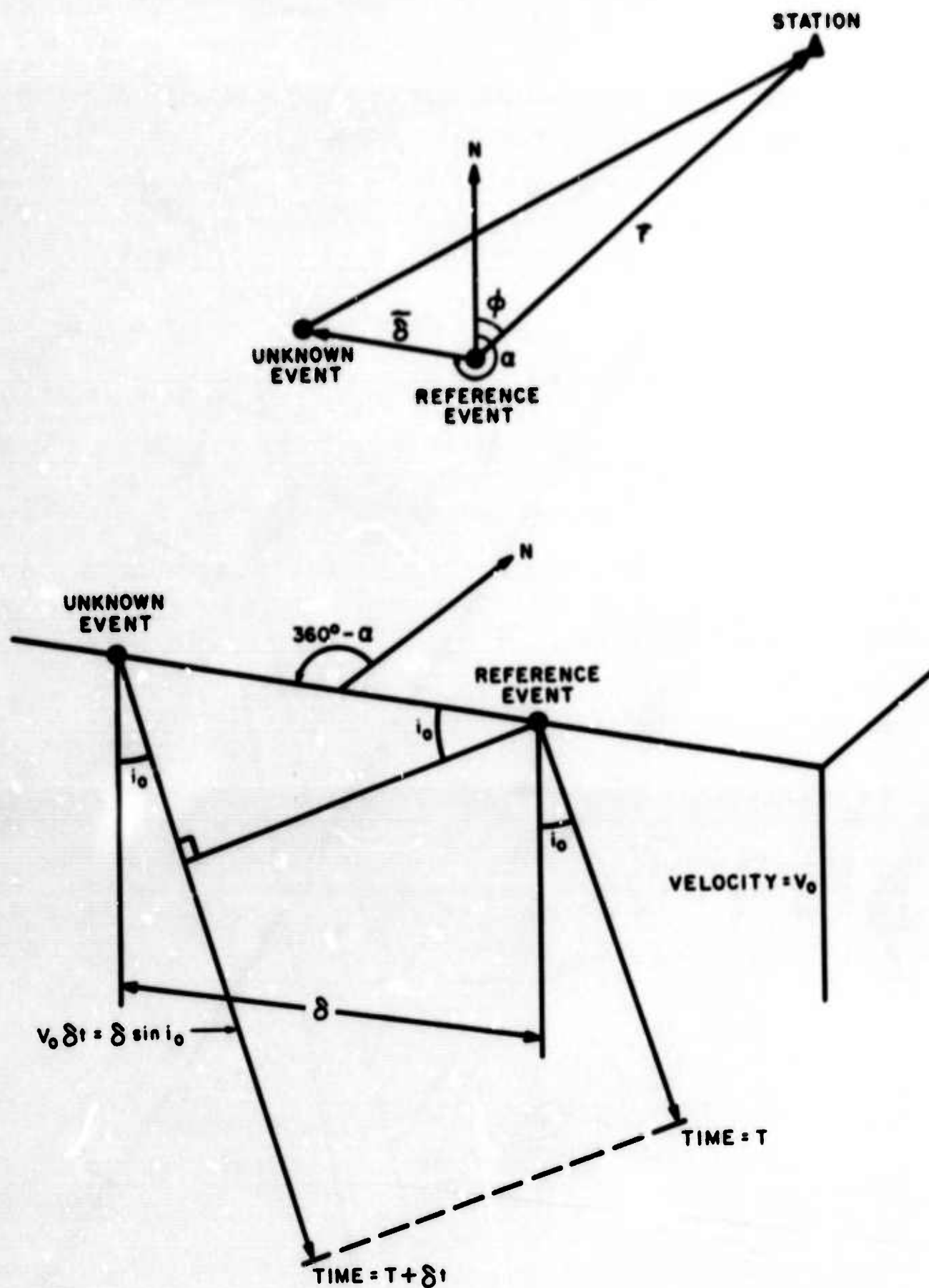


Figure 32. Assumed geometry at source in Spence and Alexander's method for relative event location.

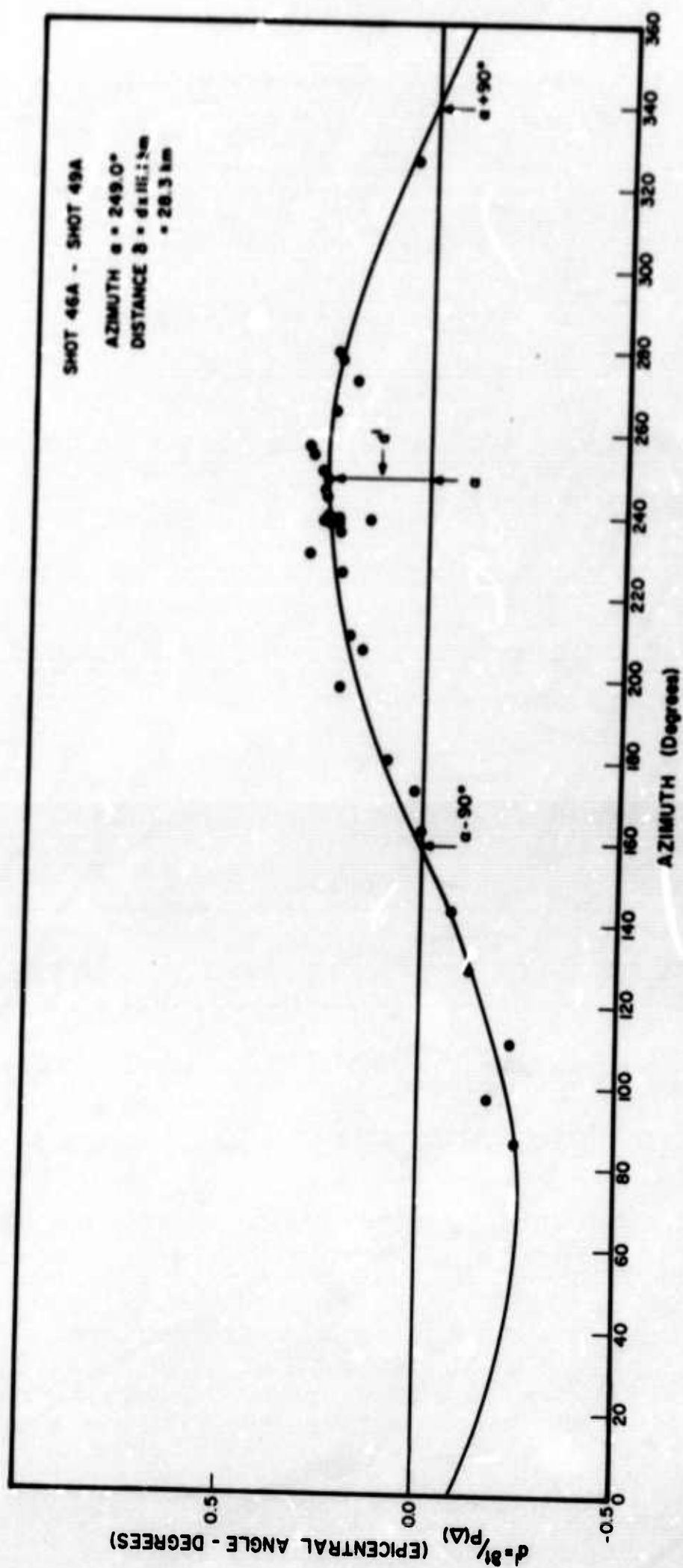


Figure 33. Plot of travel time difference between shot 46A and 49A as a function of azimuth to LRSM stations and Vela Observatories illustrating method of determining relative location of shot 46A.

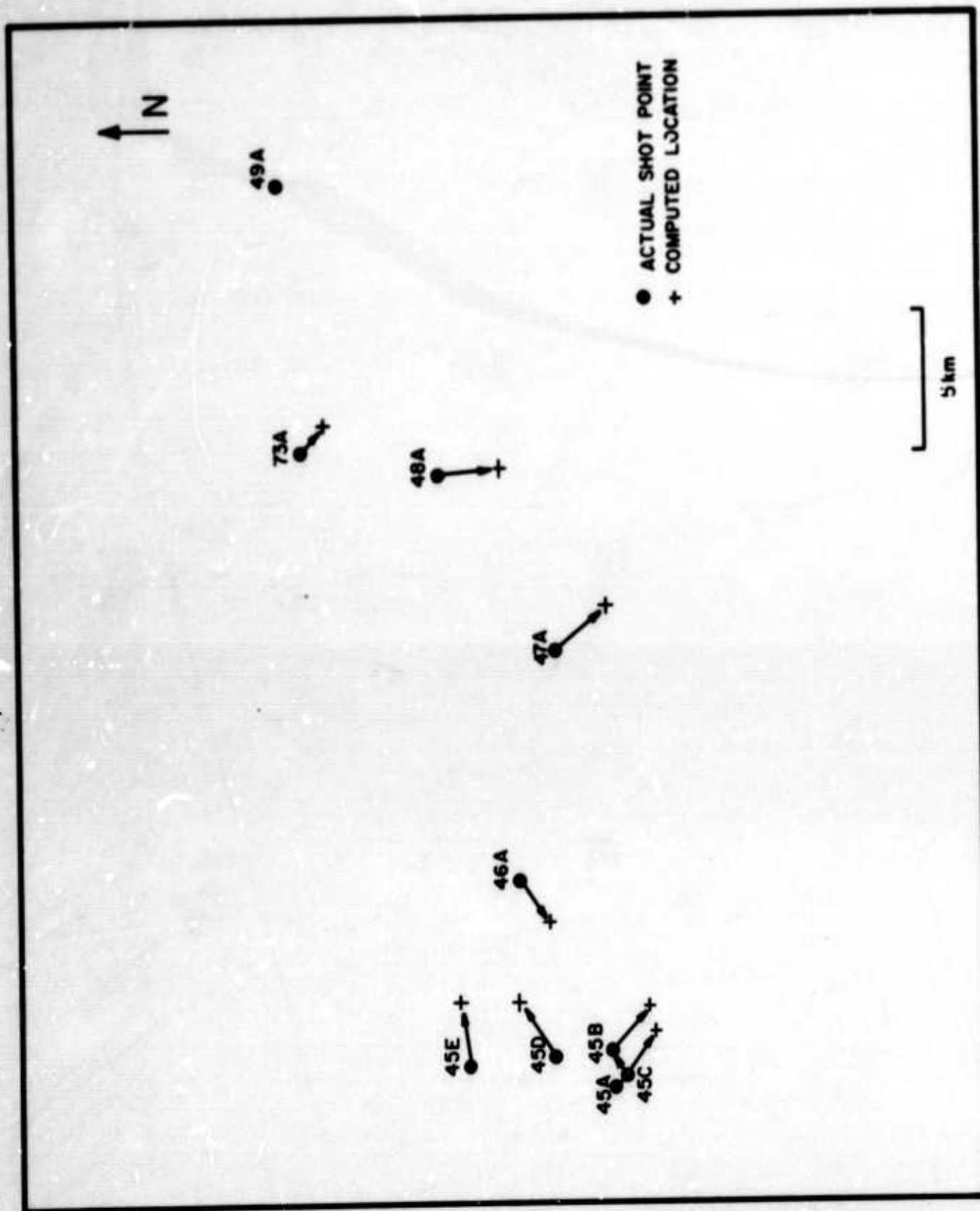


Figure 34. Locations of October, 1964 series of shots computed using Spence and Alexander's method.

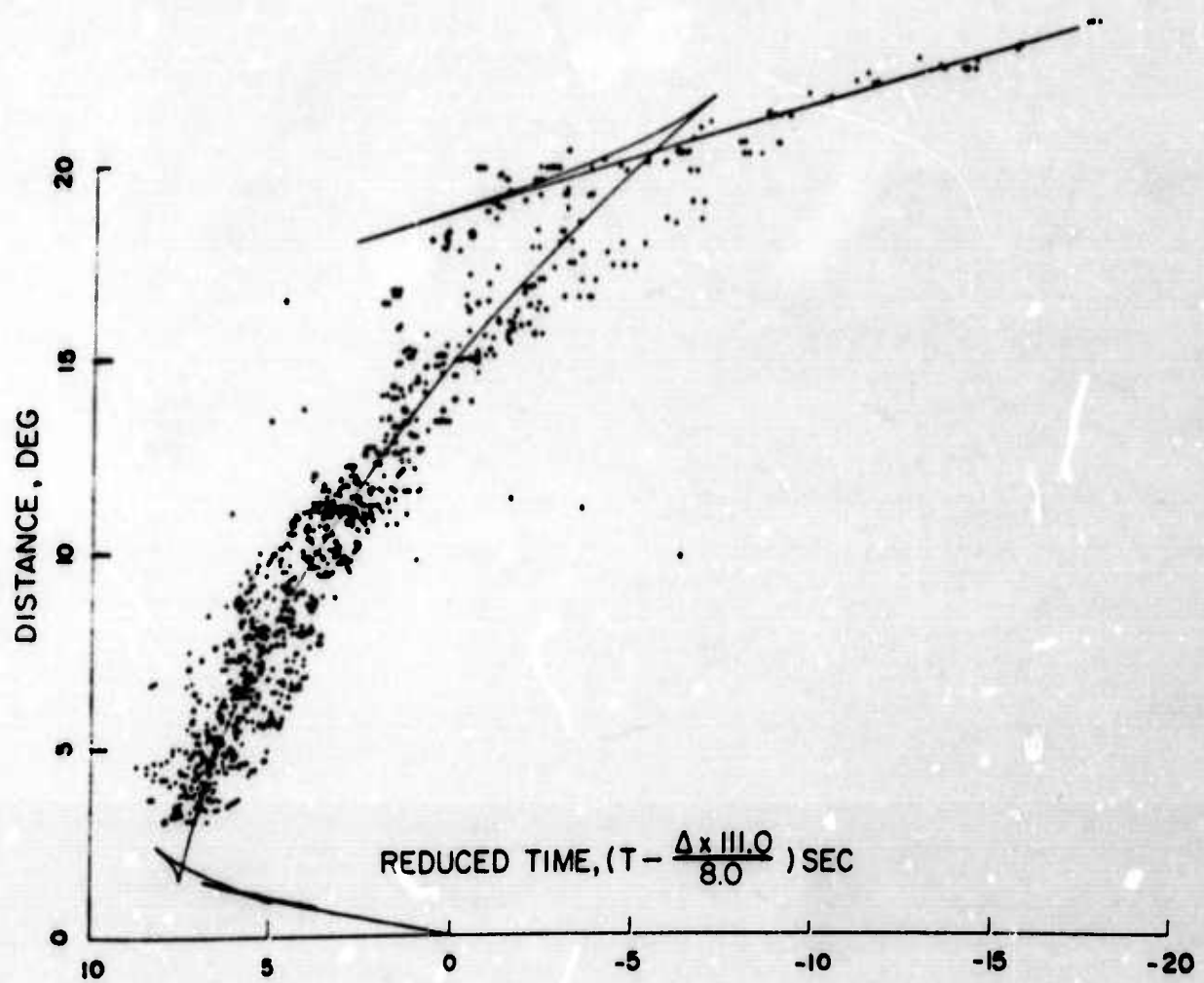


Figure 35. Reduced travel-times obtained during Project Early Rise. Solid curve represents theoretical travel-times calculated from model NCER 1. (After Iyer et al., 1969.)

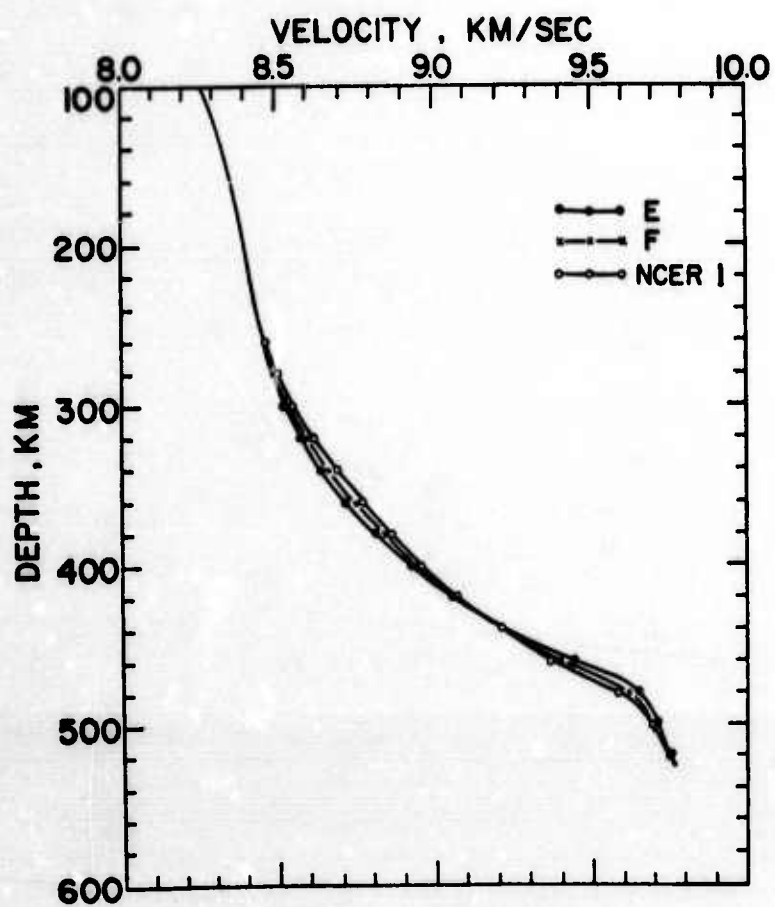


Figure 36. Model NCER 1 derived by Iyer et al., (1969) from the smoothed travel-time data collected during Project Early Rise. (After Iyer et al., 1969.)

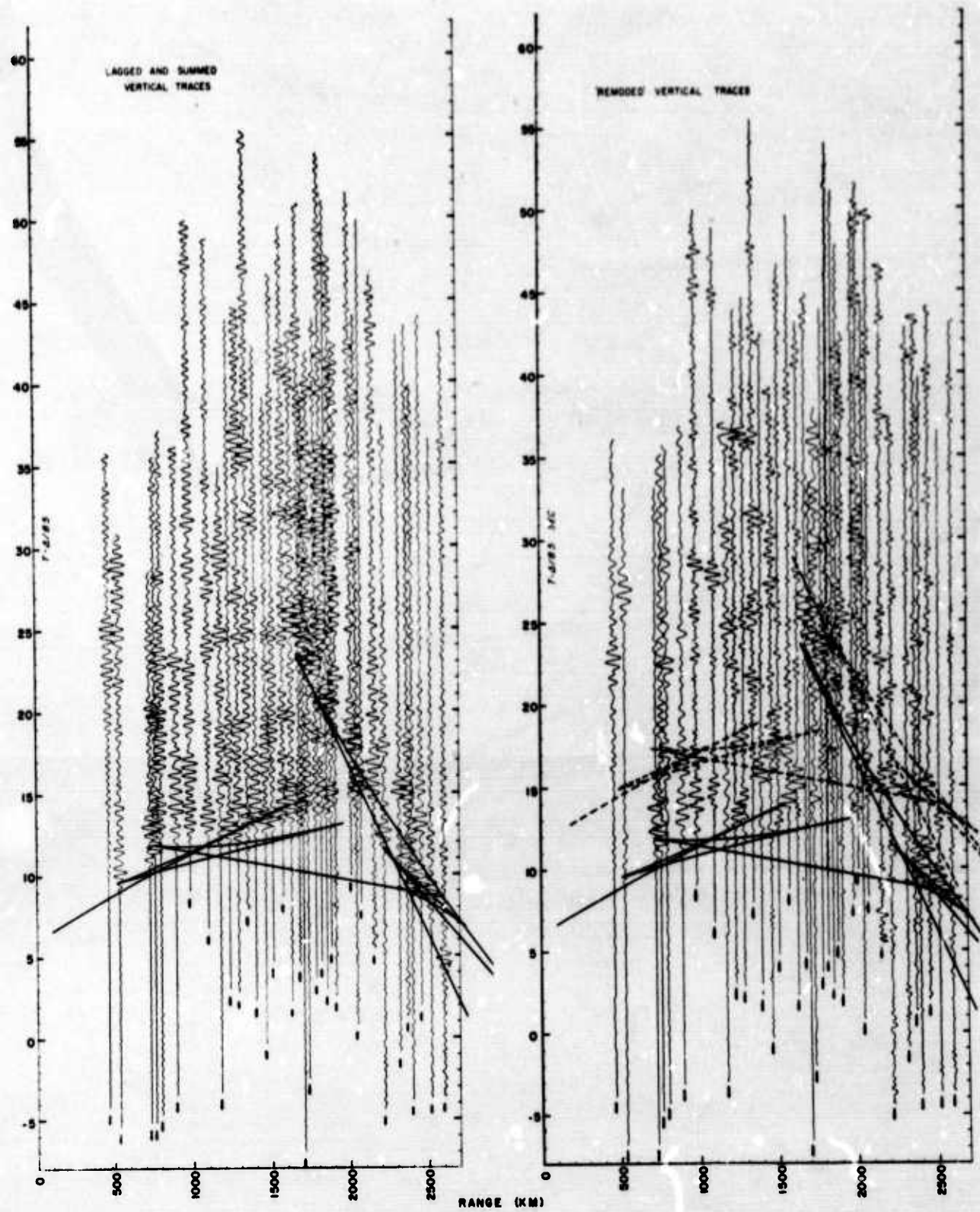


Figure 37. Calculated travel-time curves for the P-wave model of Lewis and Meyer shown in Figure 39 (solid curve) superimposed on record section from the Early Rise profile 1. Dotted curve represents theoretical travel times for P-SV conversions at base of crust. (After Lewis and Meyer, 1968.)

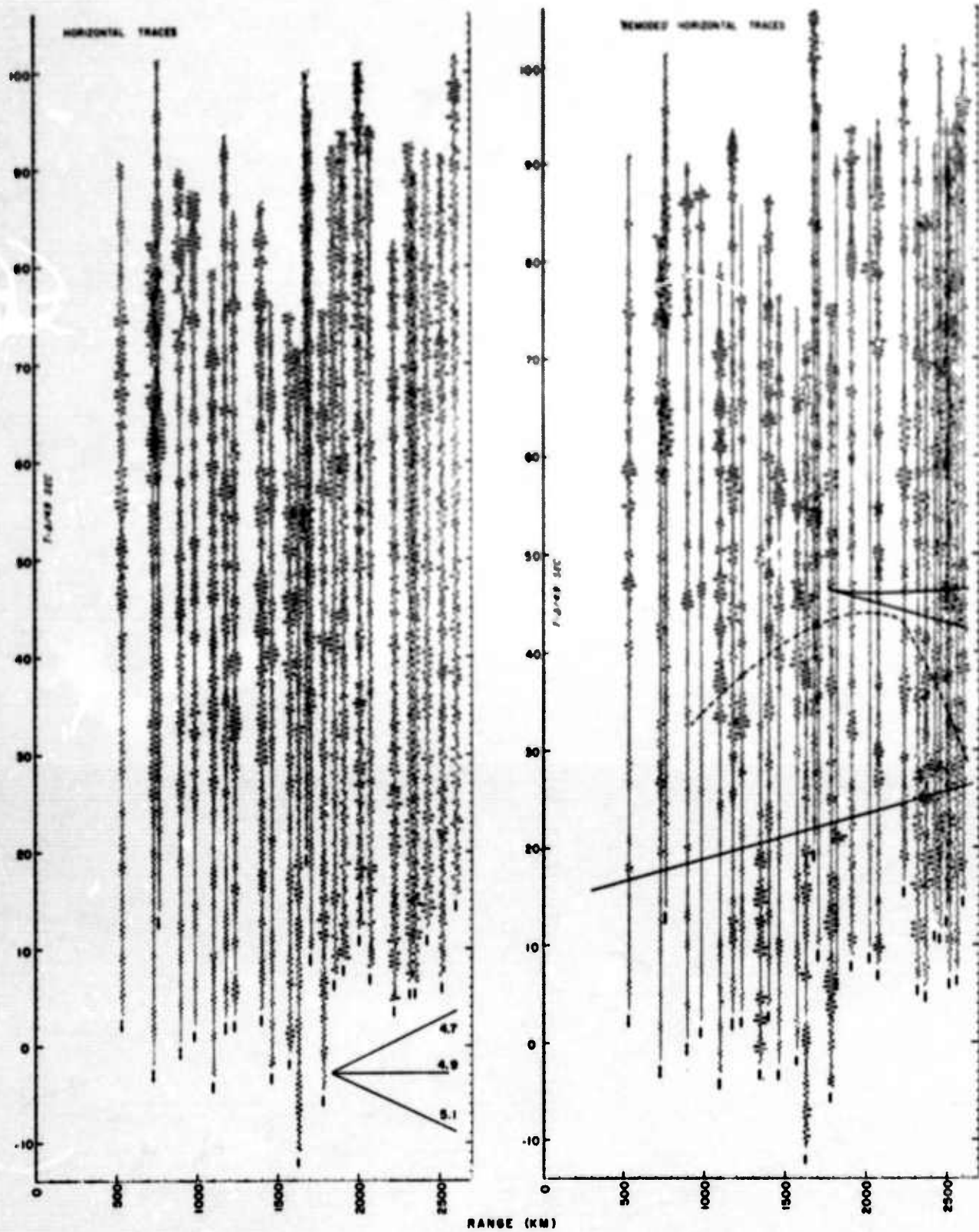


Figure 38. Record sections showing shear wave portion of filtered horizontal and vertical traces, with theoretical travel-times for Lewis and Meyer's model superimposed. (After Lewis and Meyer, 1968.)

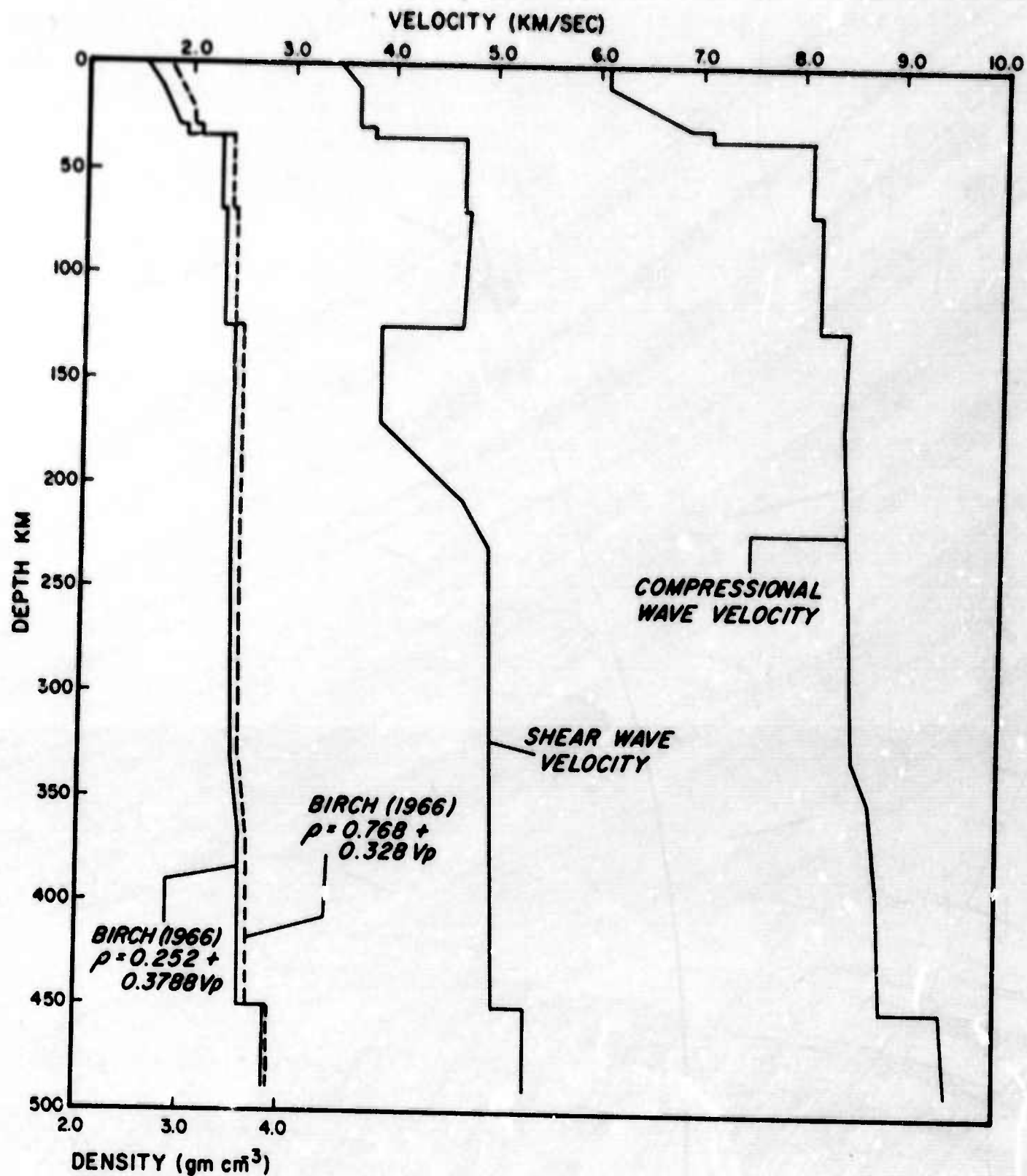


Figure 39. Model for the crust and upper mantle to the west of Lake Superior obtained by Lewis and Meyer (1968).

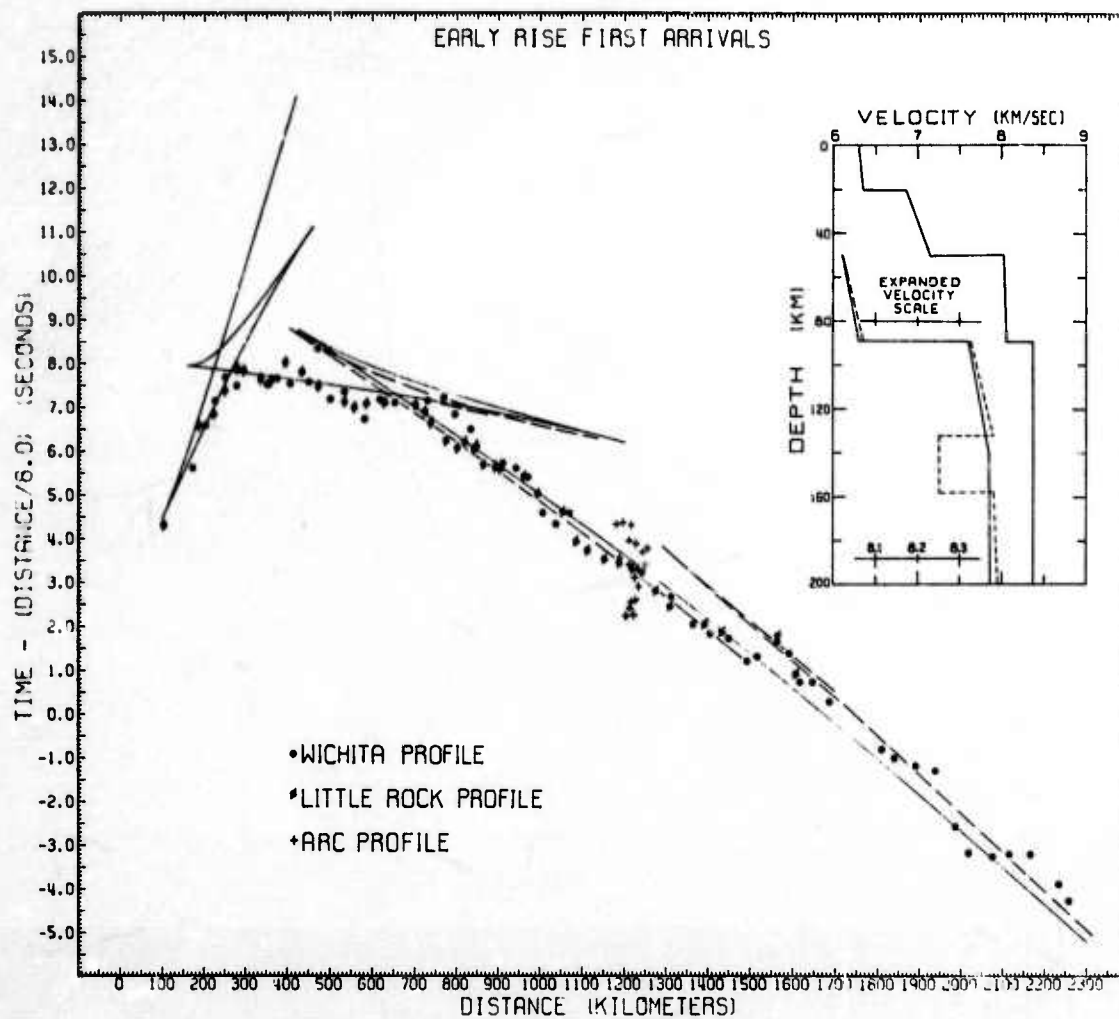


Figure 40. Reduced travel-times from Early Rise profiles 2, 3, and 4 and theoretical travel-time curves computed from Early Rise Model 1 (solid line) and Early Rise Model 2 (dashed line). Structures shown in insert. (After Green and Hales, 1968.)

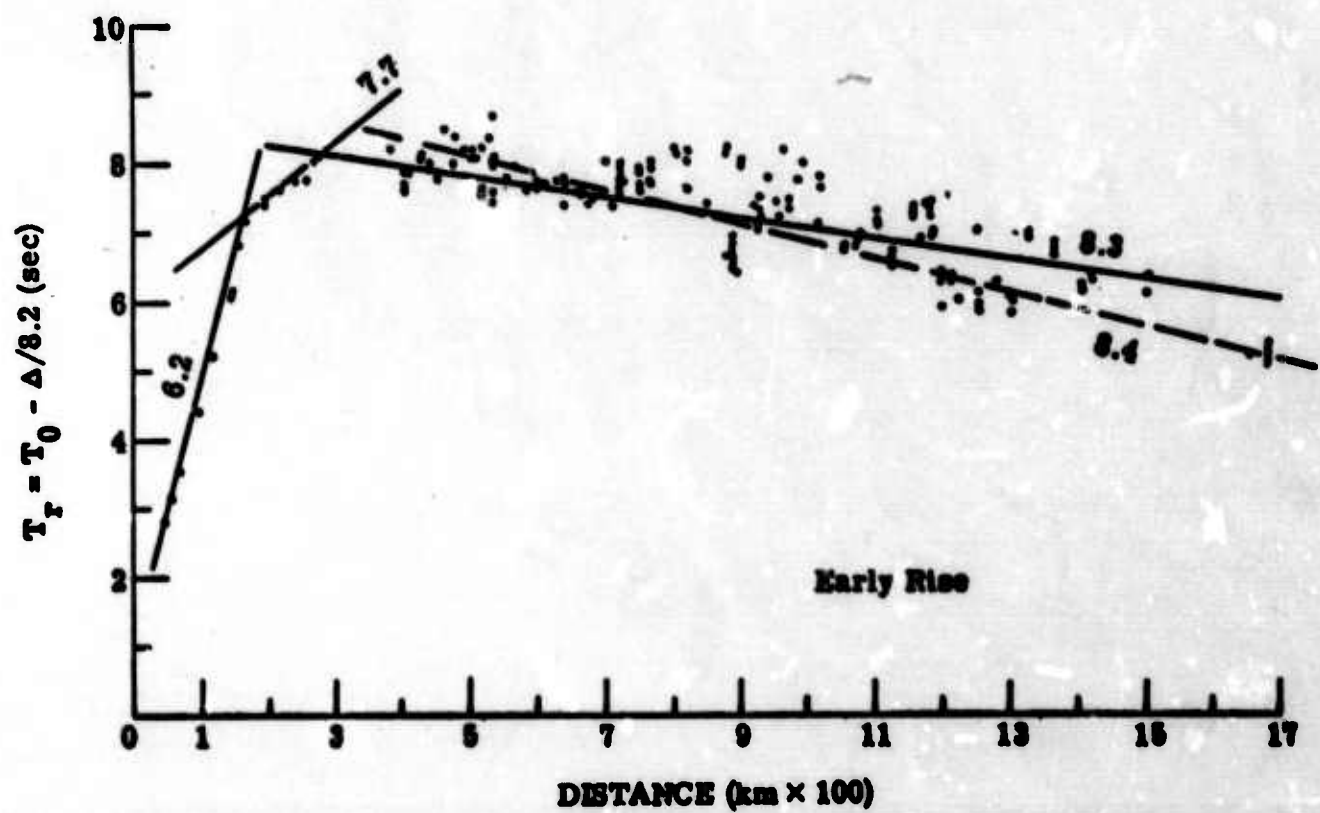


Figure 41. Reduced travel-times from Early Rise profile 5 showing four branches of travel-time curve identified by Willis (1968). Figure courtesy of D. E. Willis, University of Michigan.

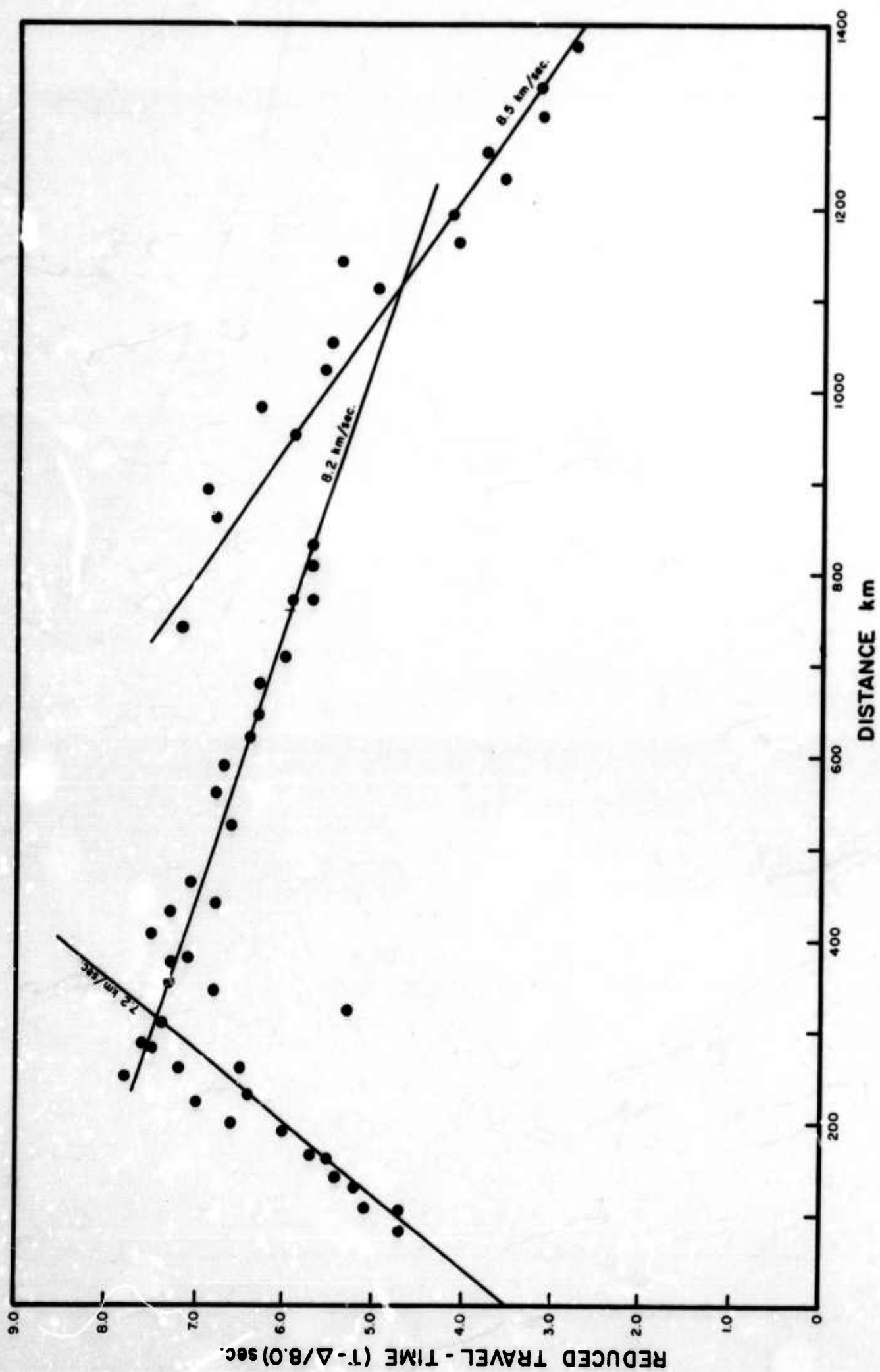


Figure 42. Reduced travel-times of first arrivals recorded along Early Rise Profile 6. (After Roller and Jackson, 1966a, b.)

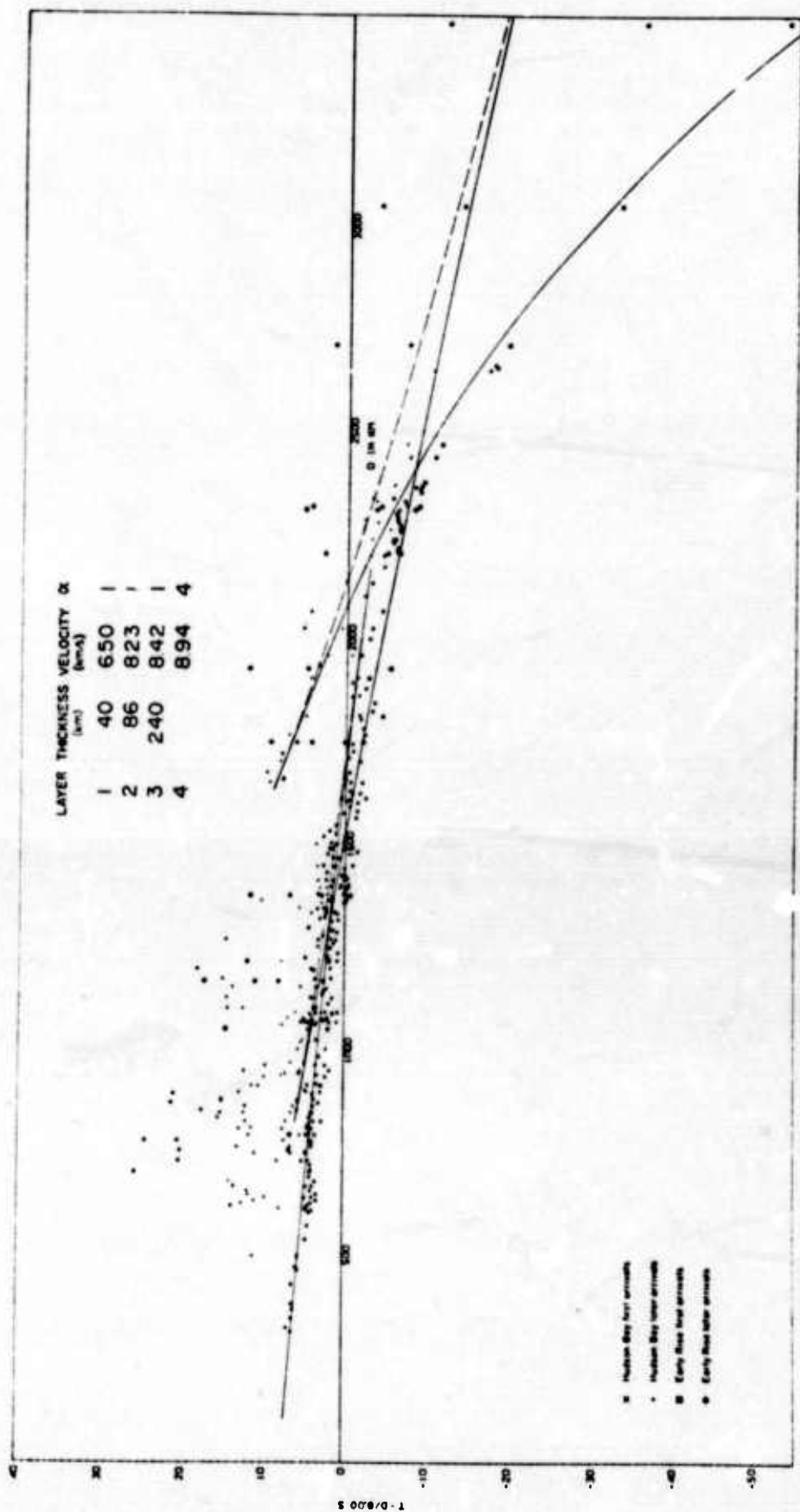


Figure 43. Reduced travel-times to Canadian stations for arrivals from Project Early Rise and the Hudson Bay seismic experiment. Solid curve represents theoretical travel-times calculated from model shown above curve. (After Barr, 1967.)

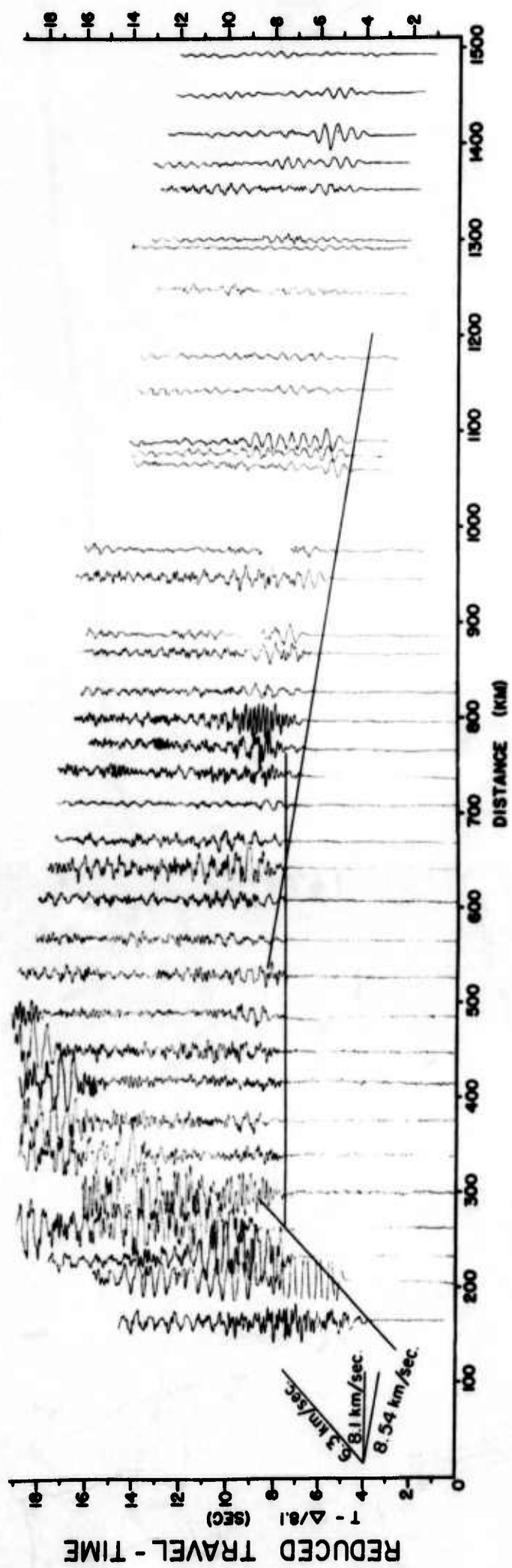


Figure 44. Record section for Early Rise profile 8 showing three distinct branches of the travel-time curve. Note small amplitudes beyond 1100 km. (After Mereu and Hunter, 1969.)

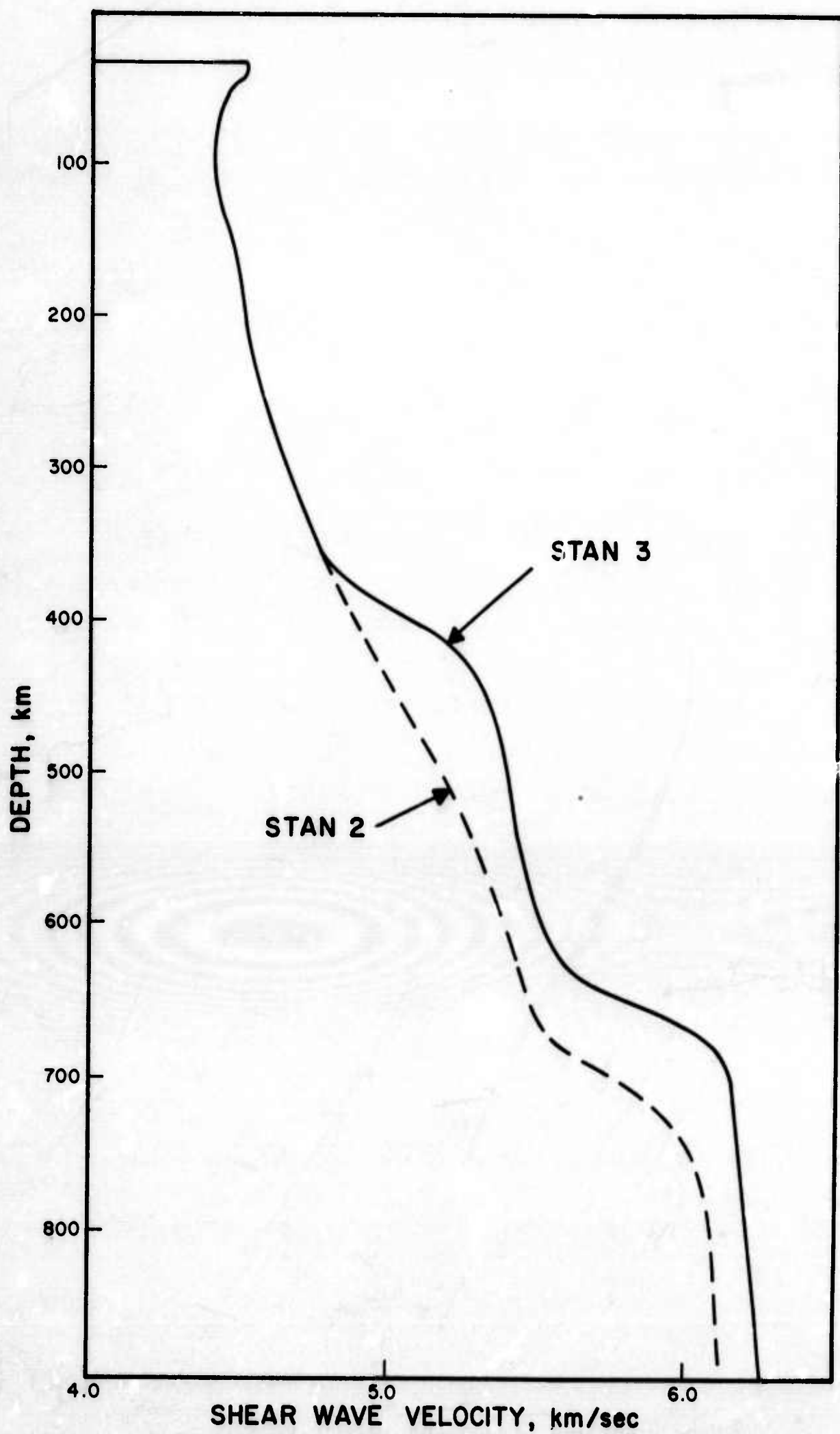


Figure 47. Shear wave velocity models for the Basin and Range mantle province derived by Kovach and Robinson (1969) from $dt/d\Delta$ measurements of long-period S-waves recorded at the extended TFO array. (Courtesy of R.L. Kovach, Stanford University).

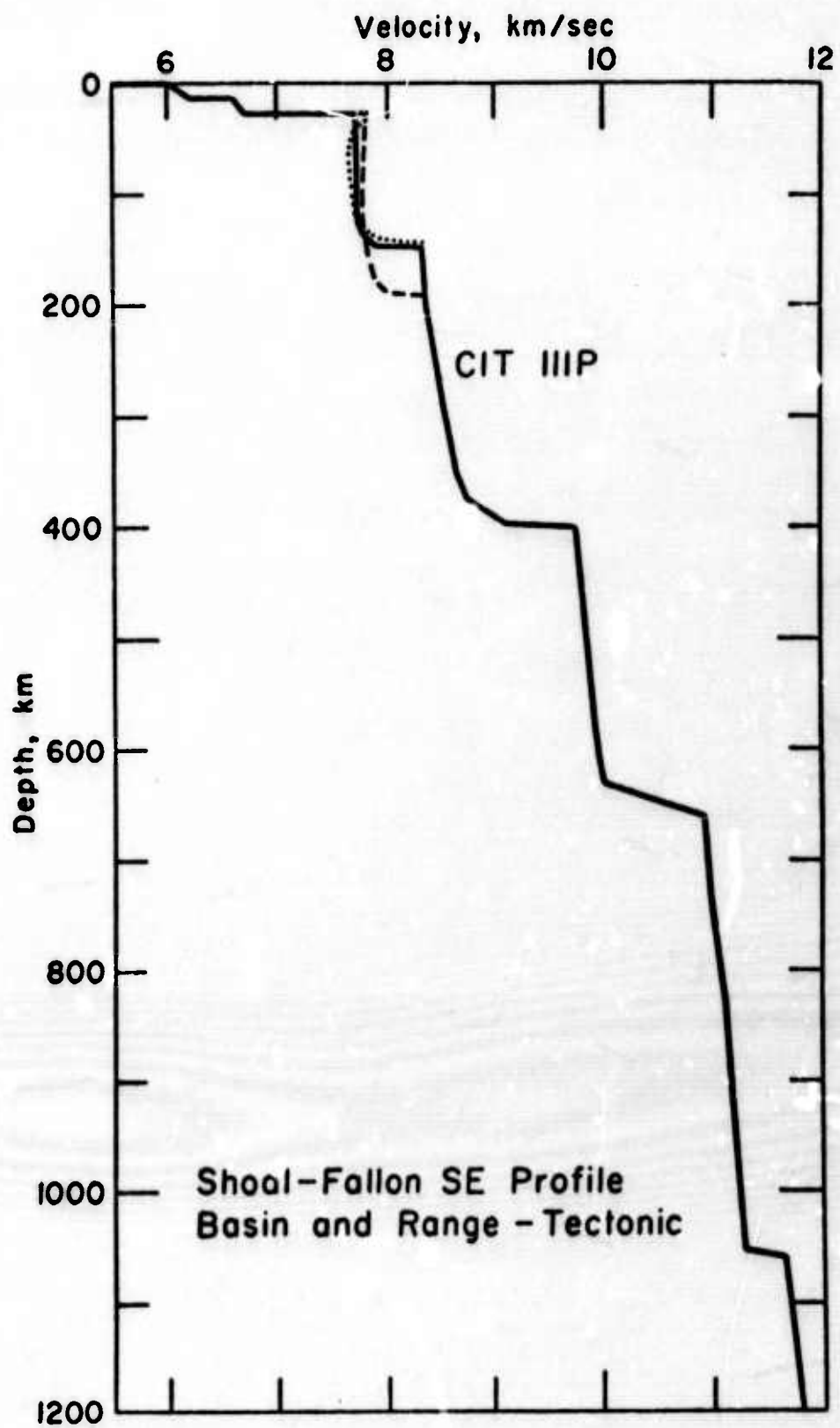


Figure 46. Model CIT 111-P for P-wave structure in the Basin and Range mantle province. (After Archambeau et al., 1969.)

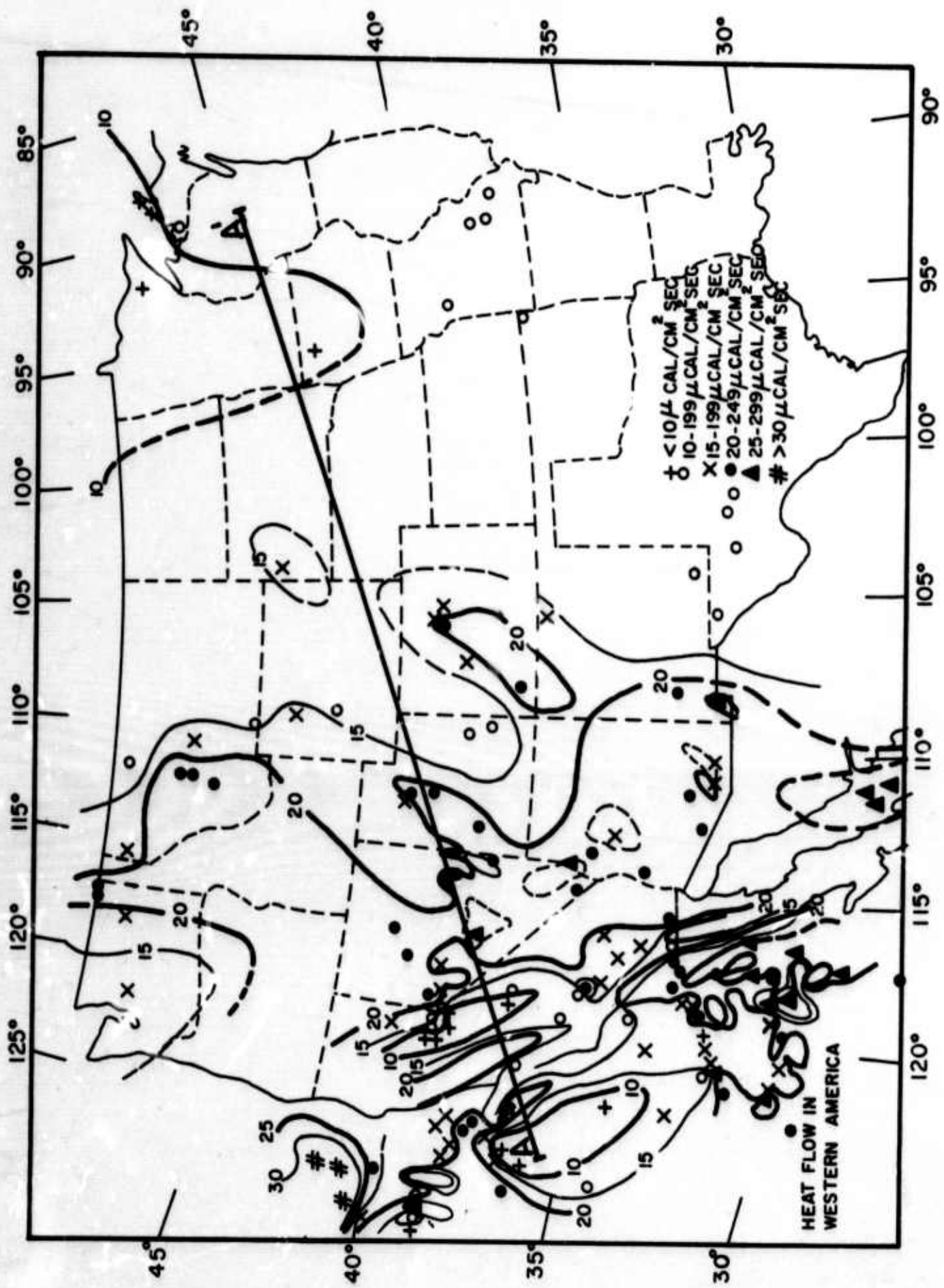


Figure 48. Heat flow in the western United States. (After Archambeau and Davies, 1969.)

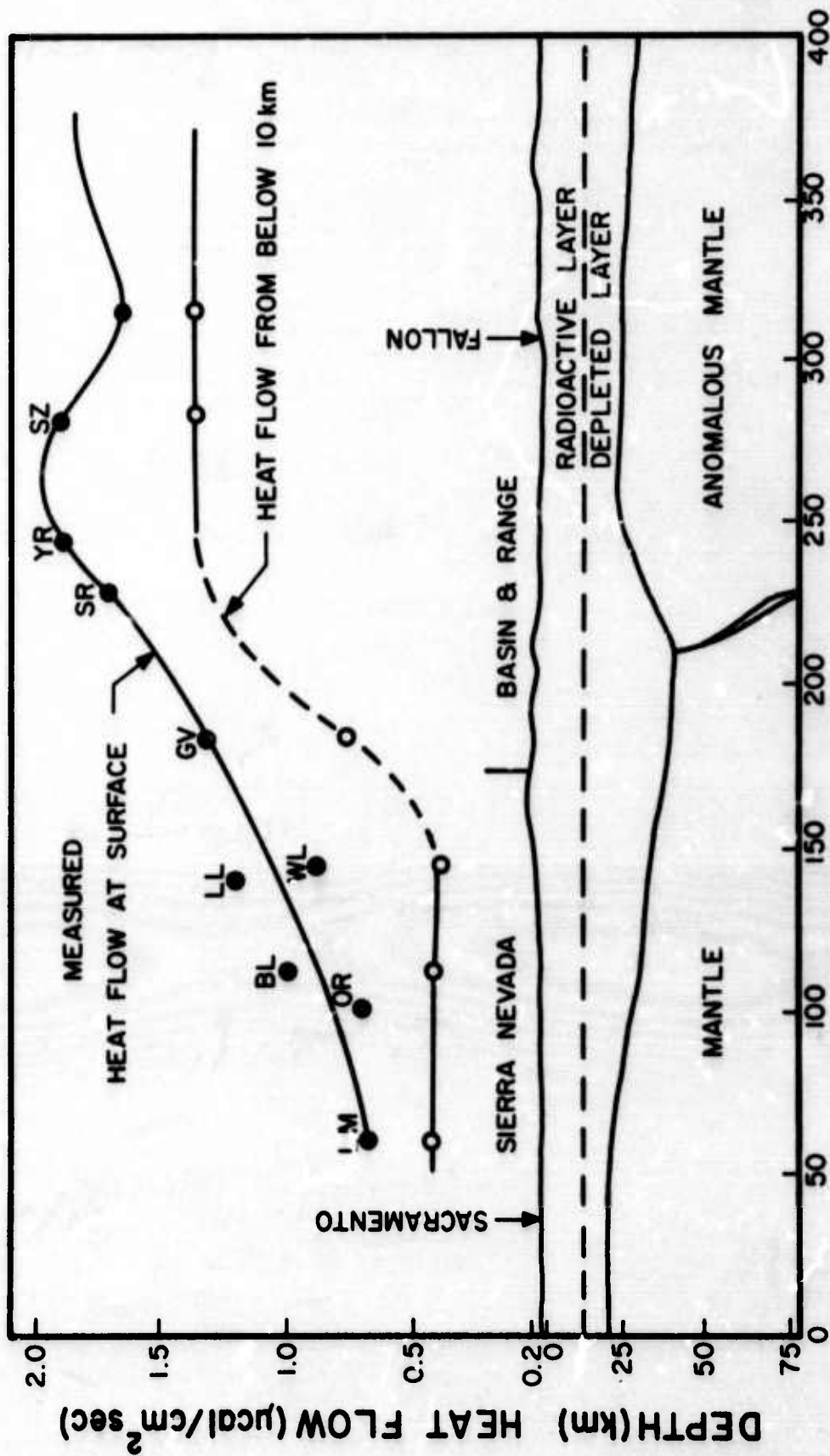


Figure 49. Profile across the Sierra Nevada and the Basin and Range showing correlation of increase in heat flow with decrease in Pn velocity across the physiographic boundary. (Courtesy of C. B. Archambeau, California Institute of Technology.)

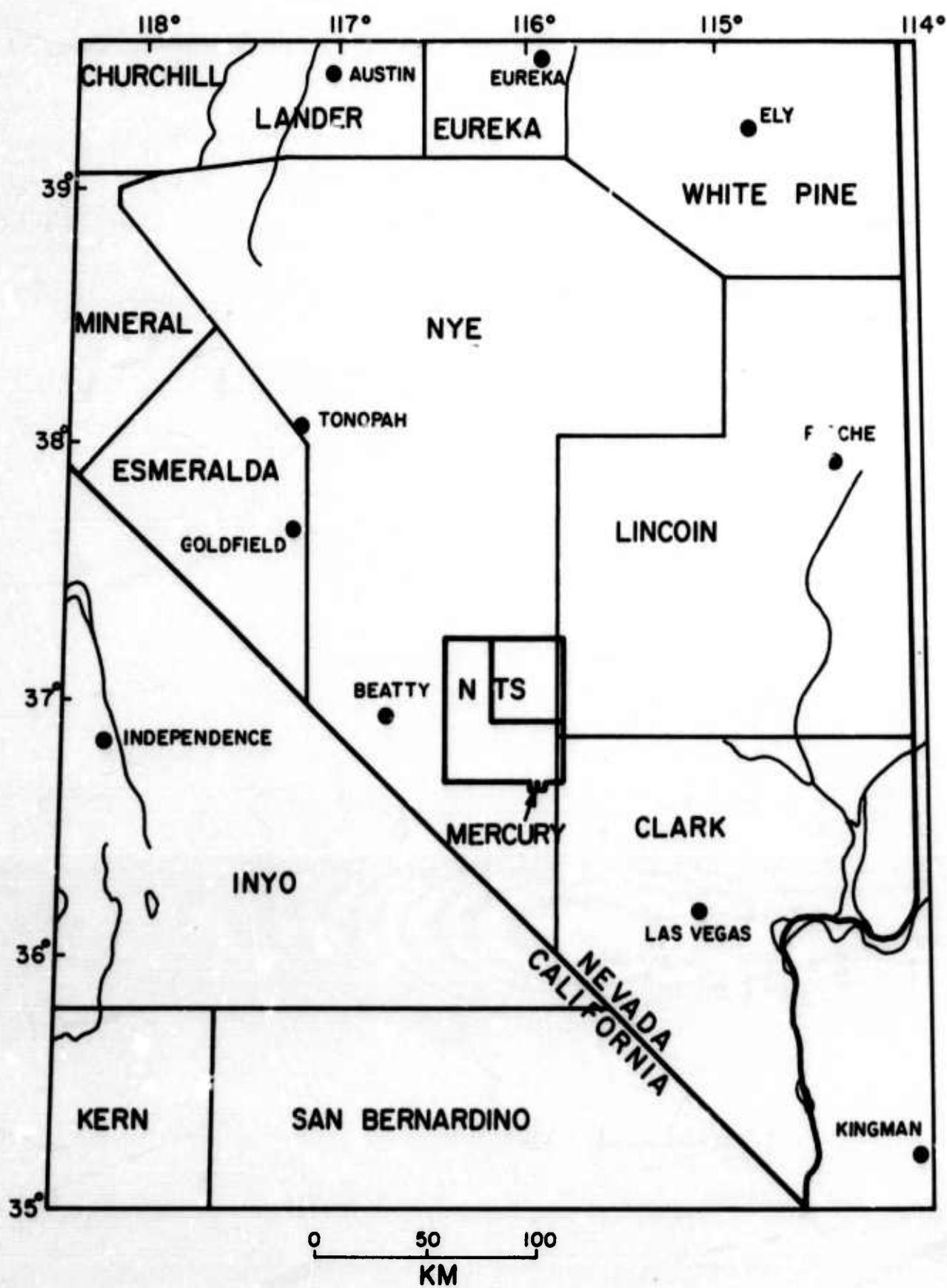


Figure 50. Location of the Nevada Test Site (NTS).

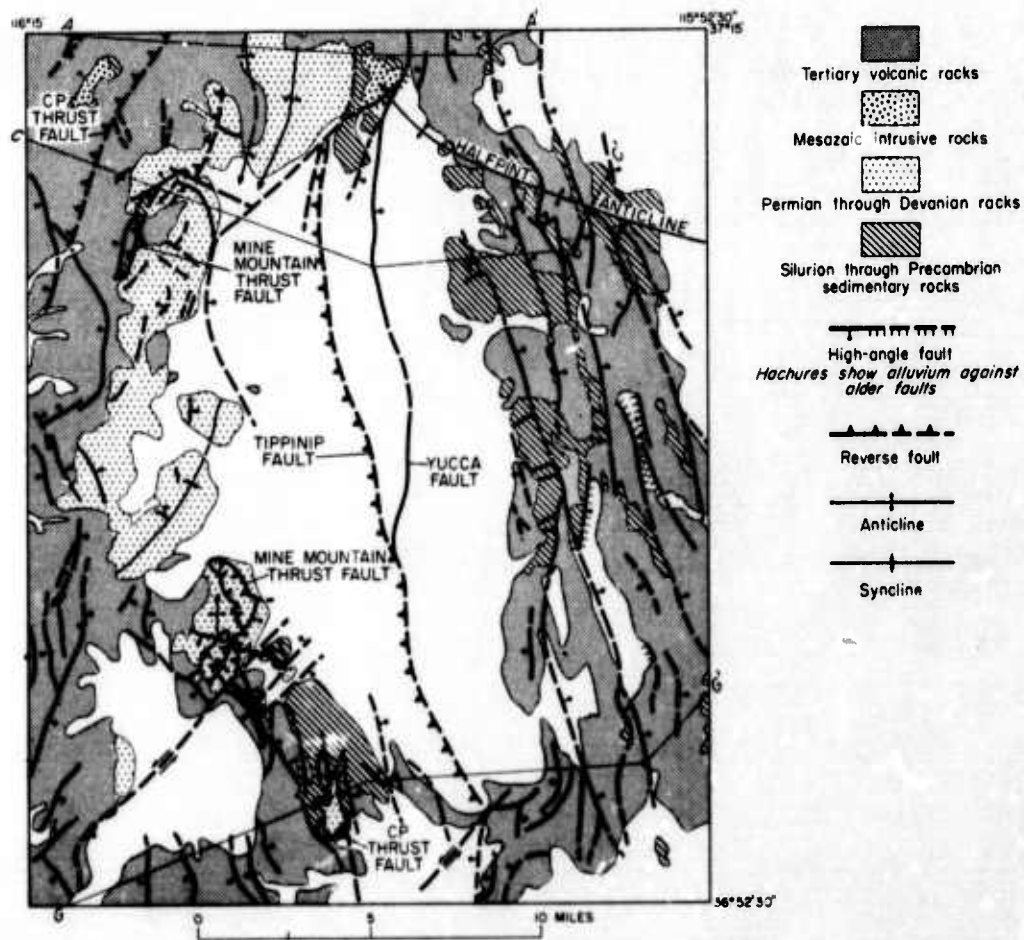


Figure 51. Generalized geologic map of the Yucca Flat area, Nevada Test Site. (After Hinrichs, 1968.)

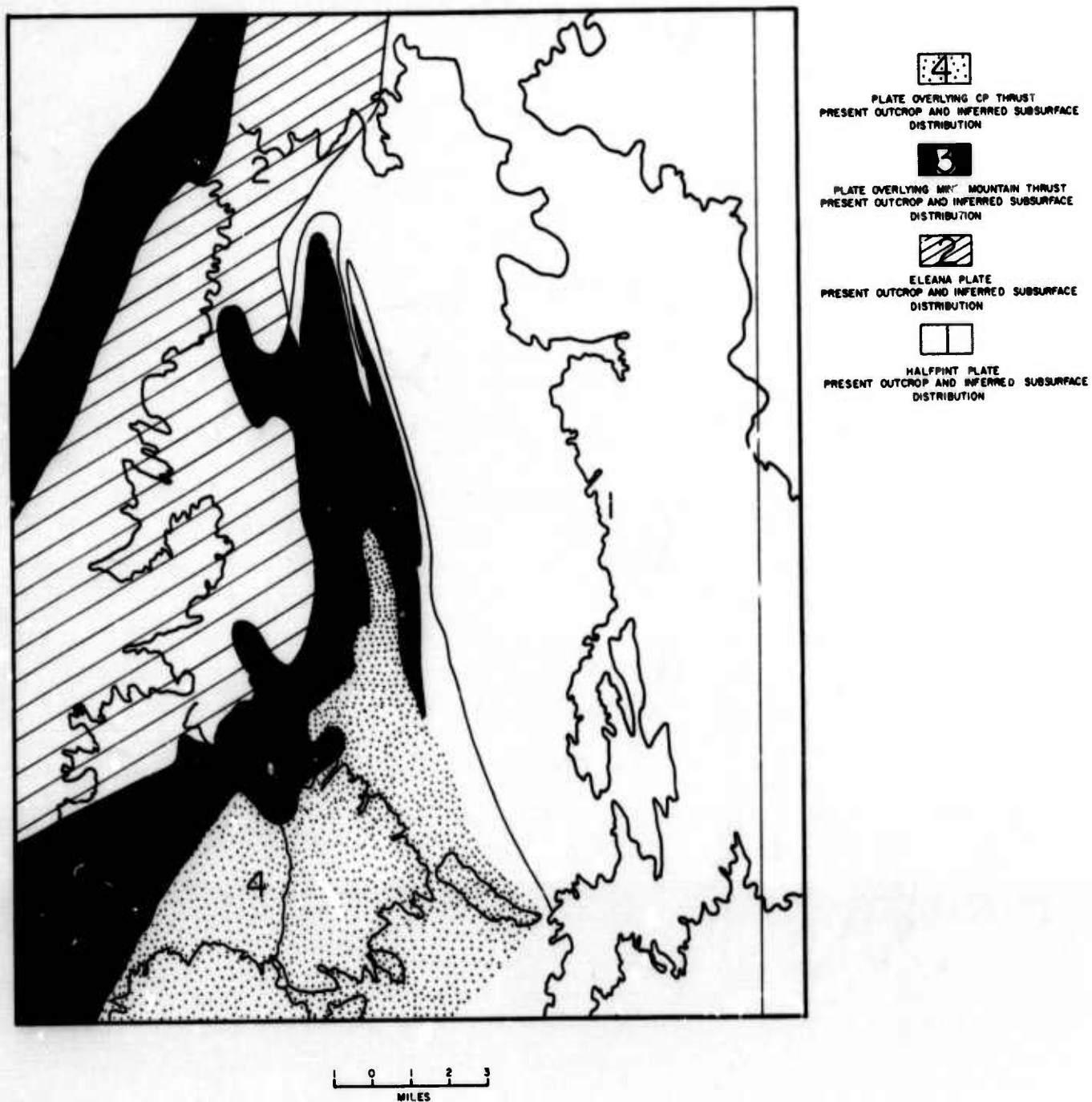


Figure 52. Structural map of the Yucca Flat area, Nevada Test Site showing major thrust plates. (Adopted from Barnes et al., 1963.)

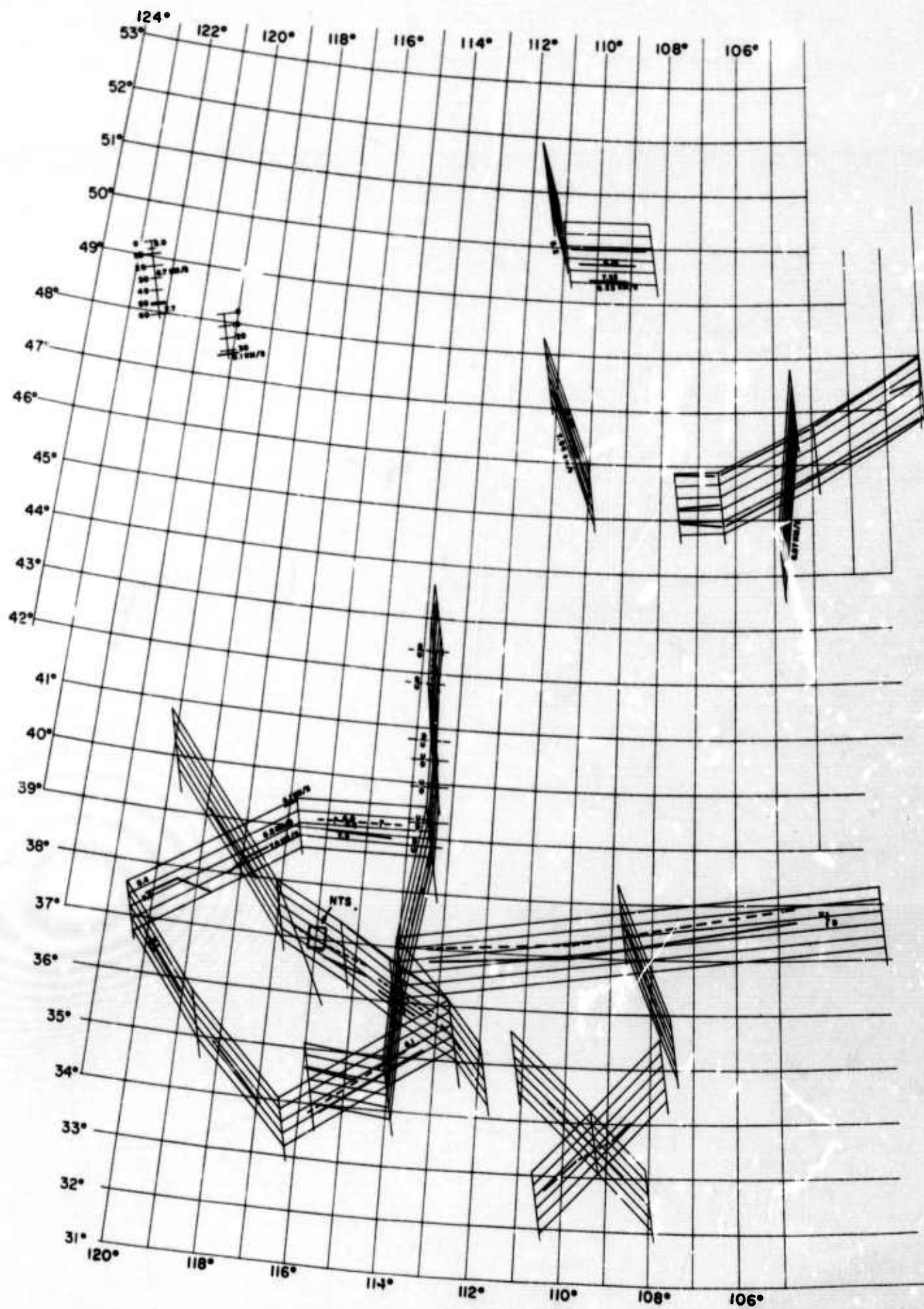


Figure 53. Compilation of results from seismic refraction surveys in the western United States plotted as a fence diagram.

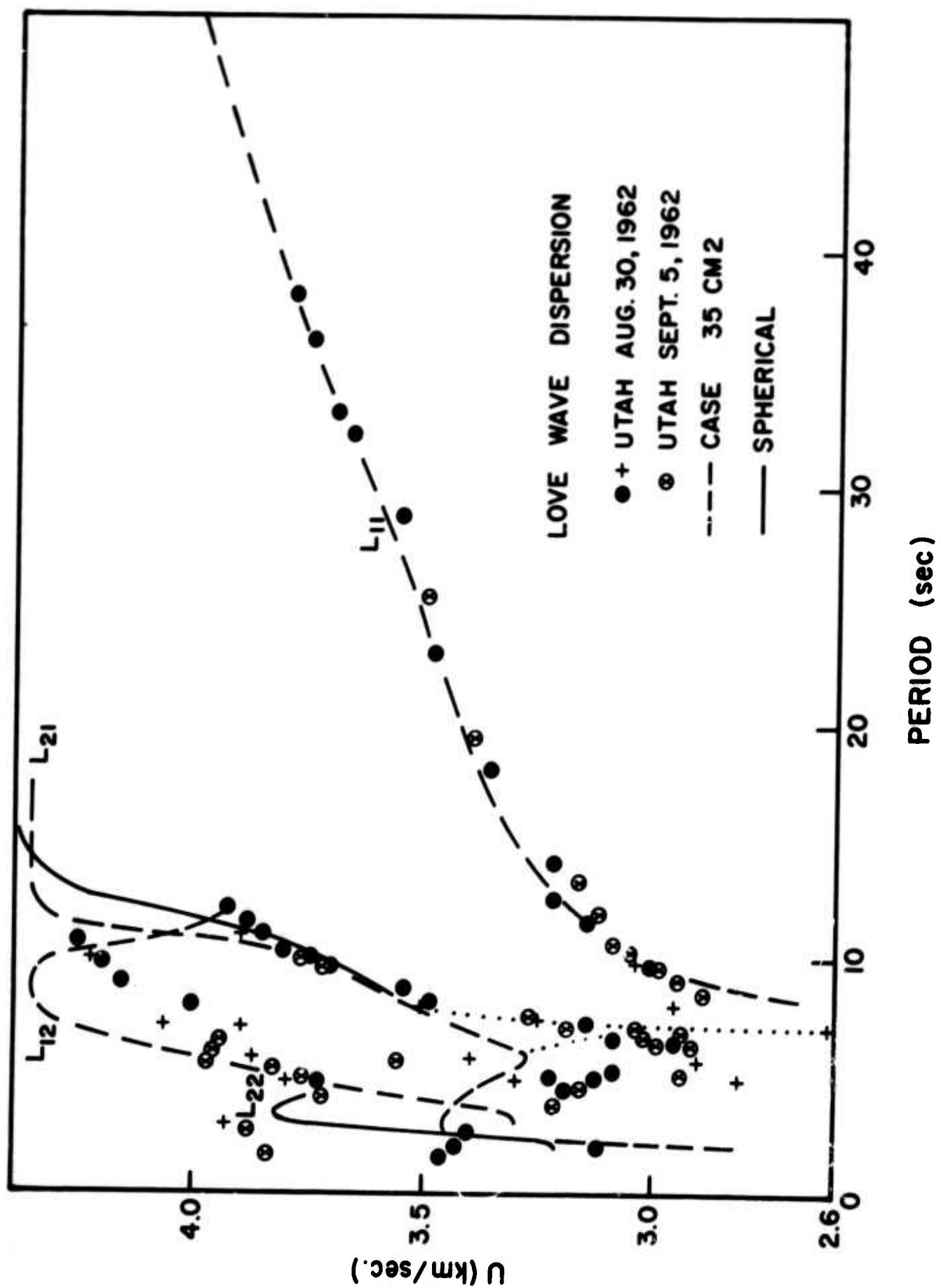


Figure 54. Fundamental and higher mode Love wave group velocity dispersion data across the Basin and Range province obtained by Alexander, 1963. Dotted lines represent theoretical, group velocity dispersion curves computed from model 35 CM 2. (After Alexander, 1963.)

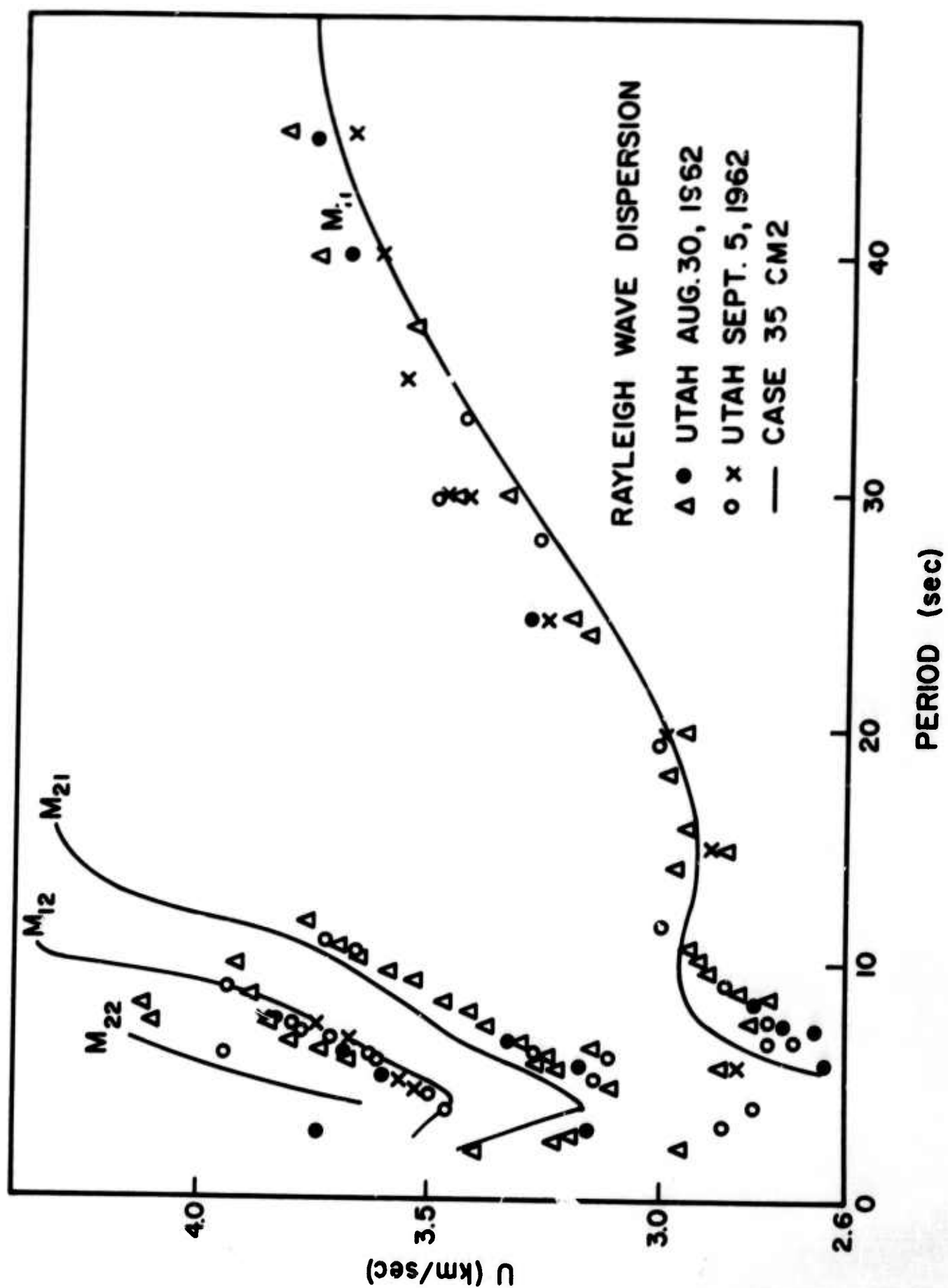


Figure 55. Fundamental and higher mode Rayleigh wave group velocity dispersion across the Basin and Range province from two events in Utah. Solid line represents theoretical group velocity curves computed from model 35 CM2. (After Alexander, 1963.)

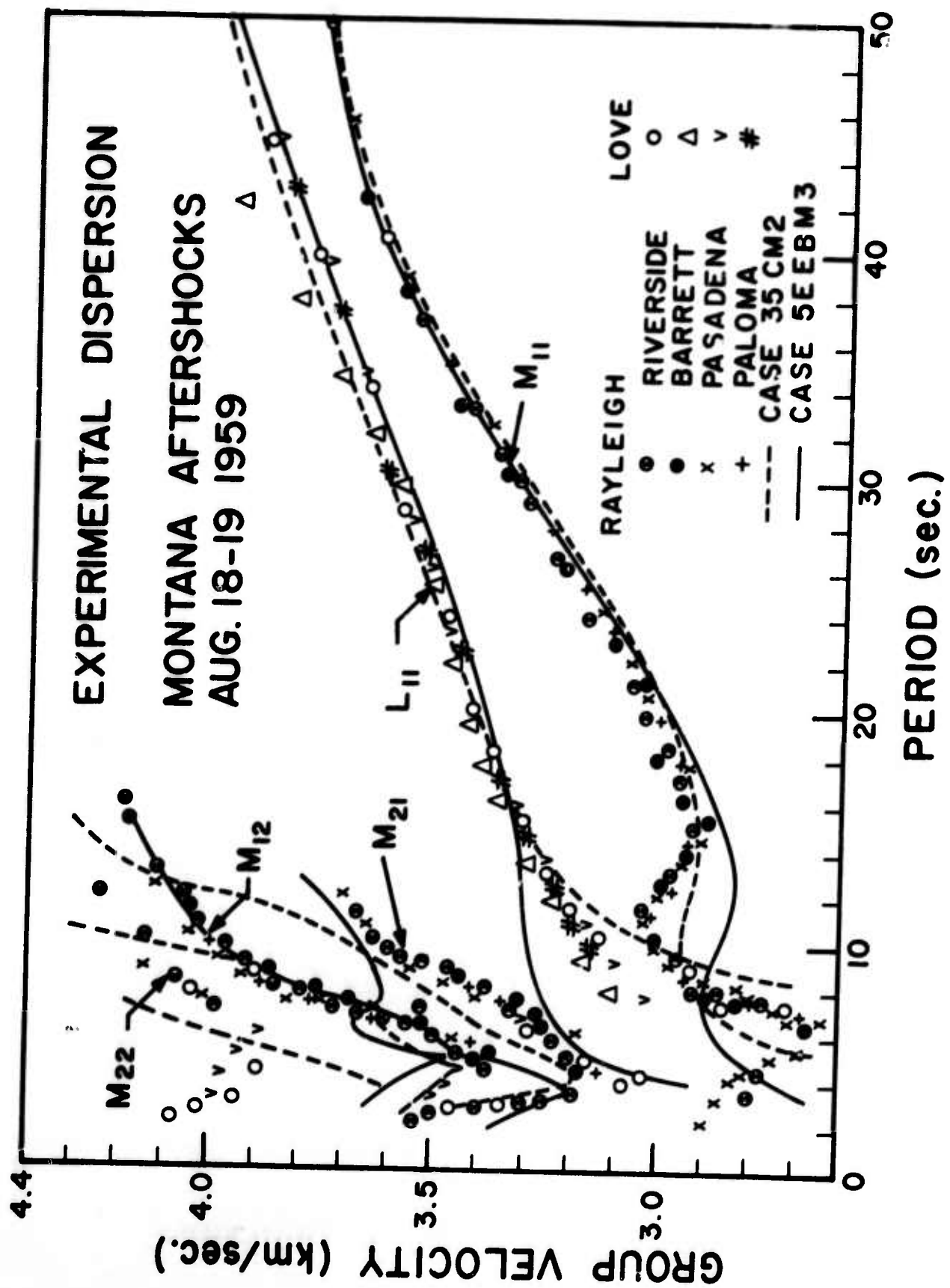


Figure 56. Fundamental and higher mode Love and Rayleigh wave group velocity dispersion across the Basin and Range province from Montana earthquake aftershock sequence. Solid line represent theoretical curves computed from model 35 CM2. (After Alexander, 1963.)

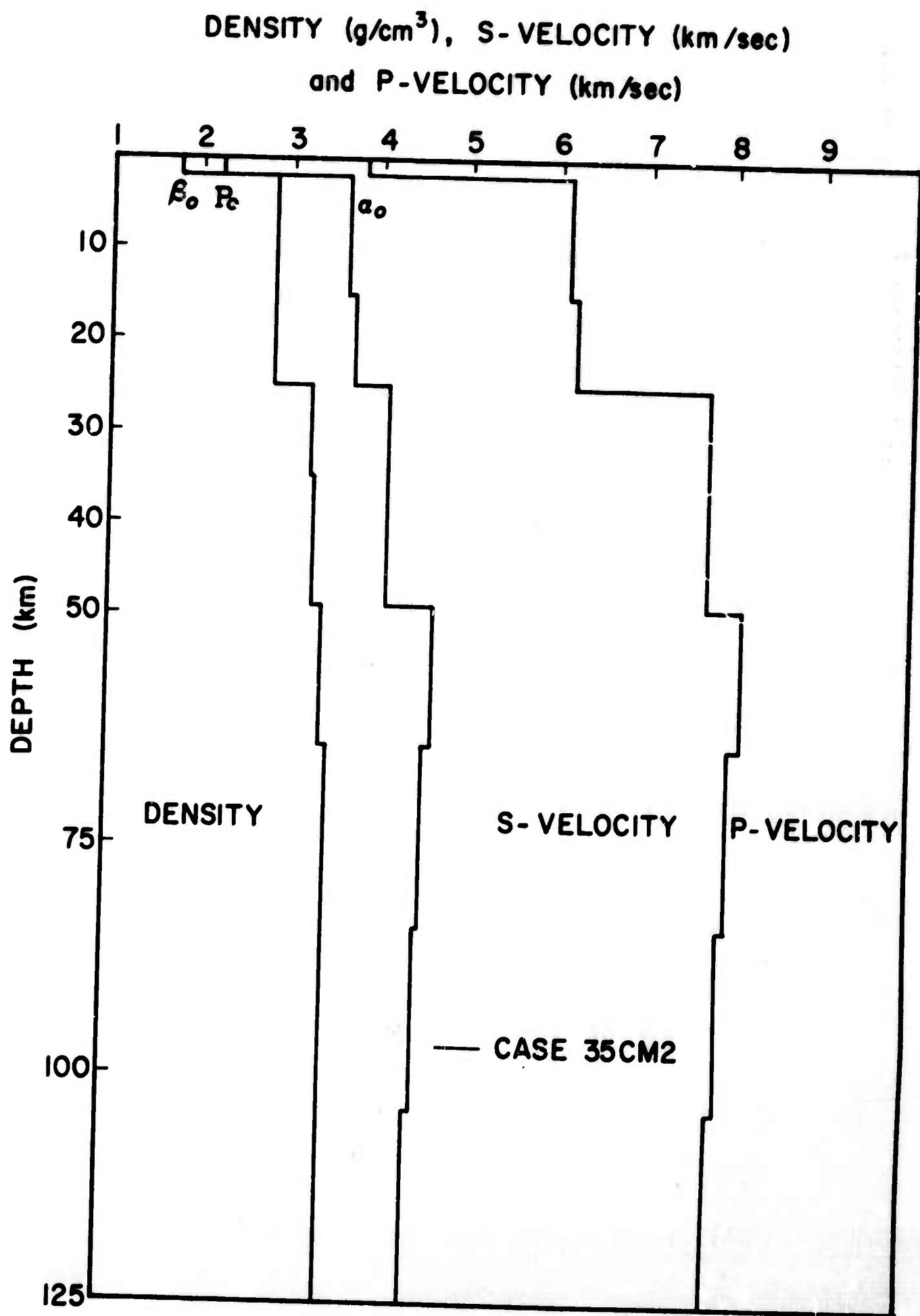


Figure 57. Model 35 CM2 for the crustal and upper mantle structure beneath the Basin and Range province. (After Alexander, 1963.)

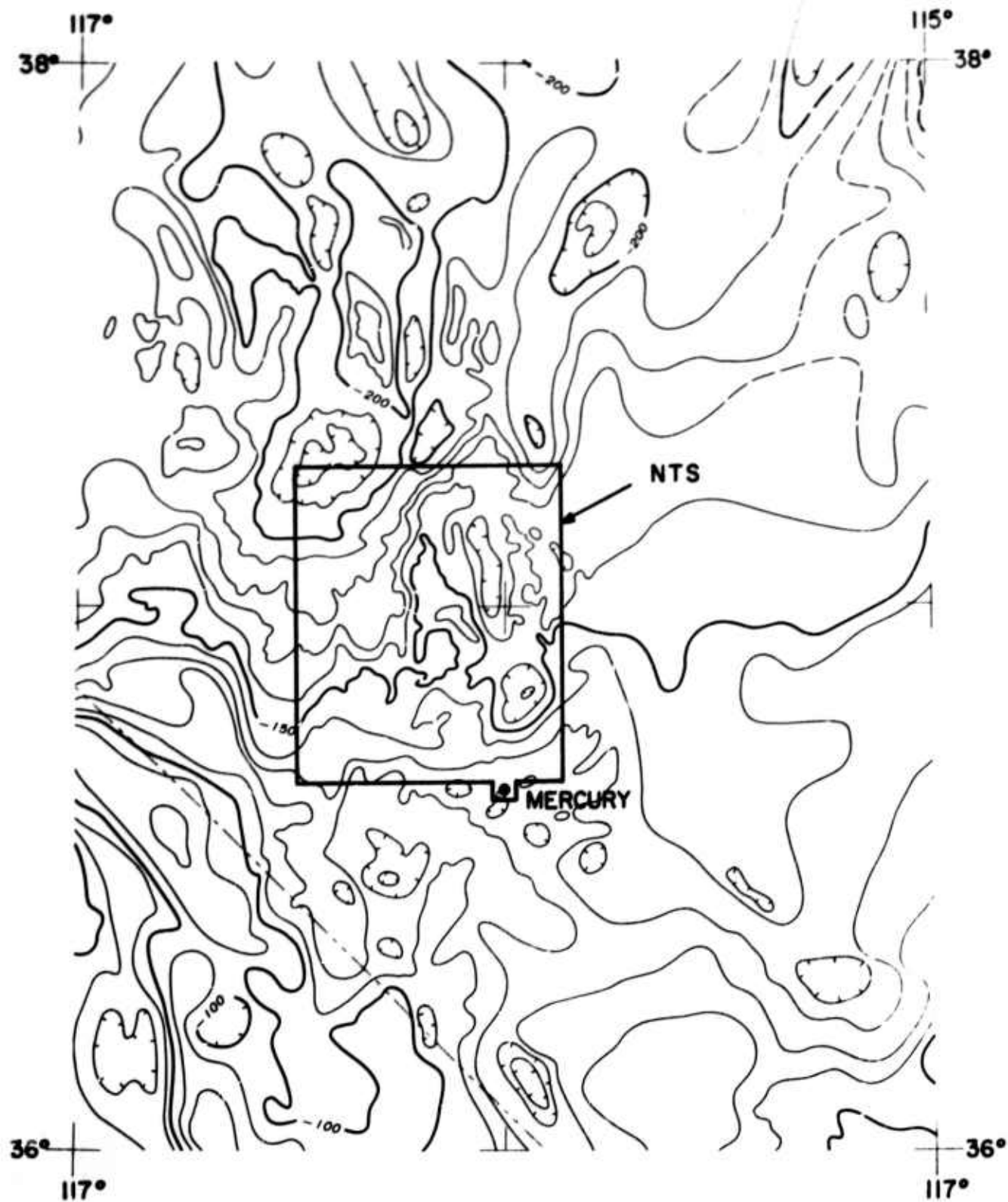


Figure 58. Regional Bouguer gravity fold in the vicinity of NTS. (Adapted from Miscellaneous Geologic Investigations Map 1-532-B, published by U.S. Geological Survey, 1968.)

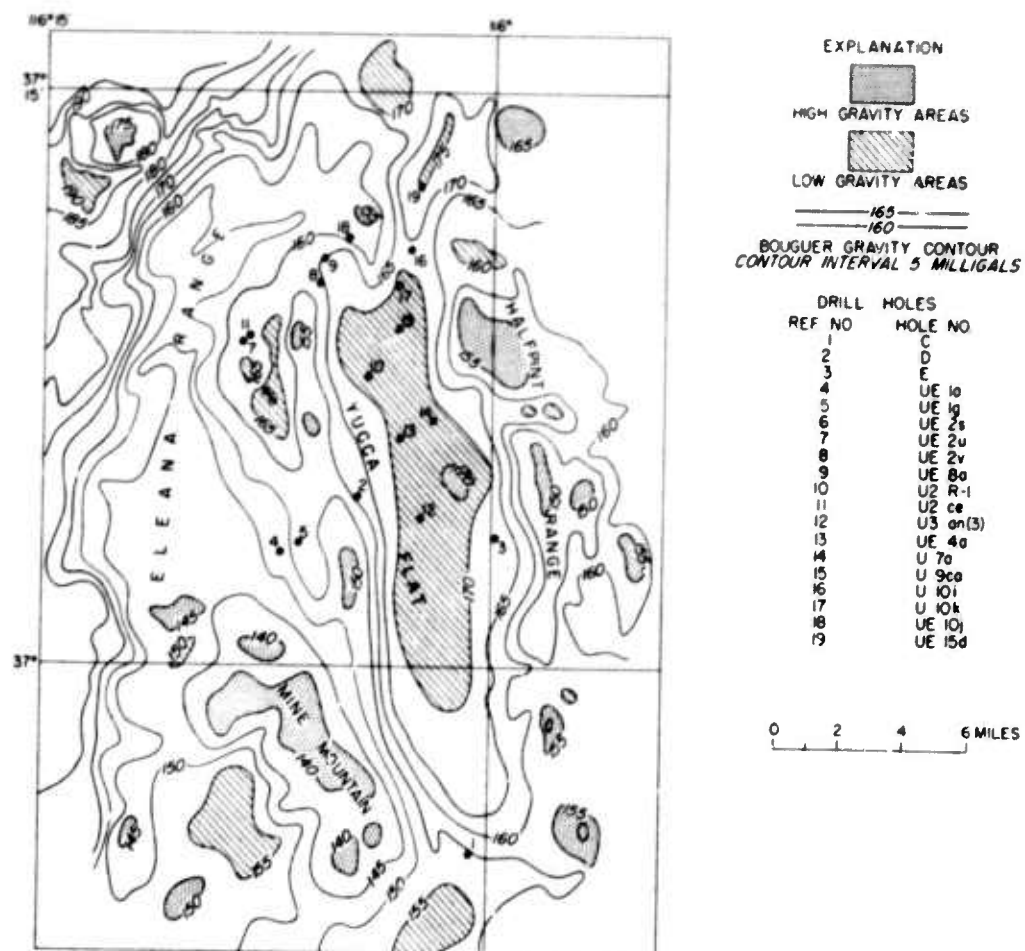


Figure 59. Detailed Bouguer gravity anomaly map of Yucca Flat, Nevada Test Site. Note that all values are negative. (After Healey, 1968.)

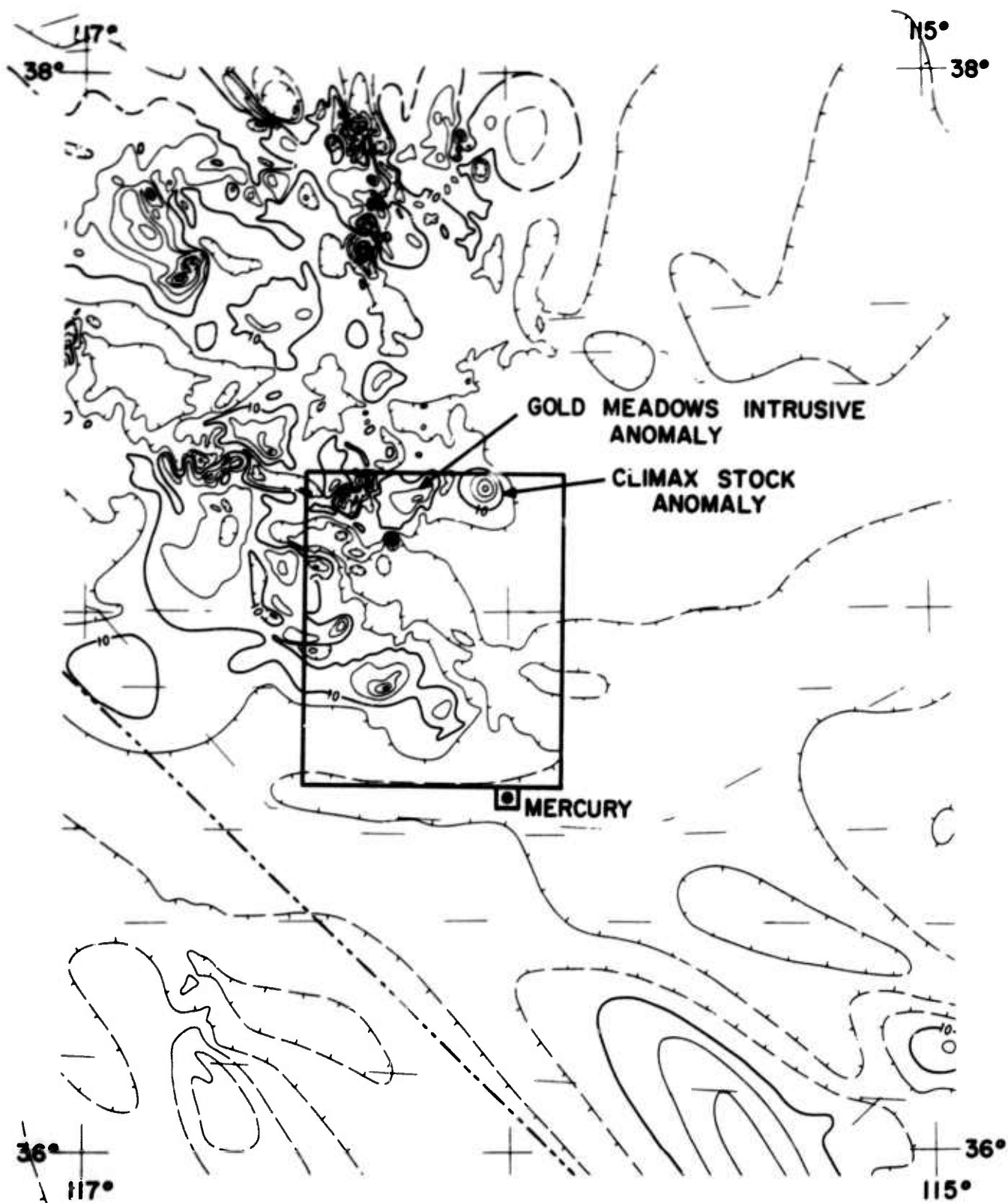


Figure 60. Total magnetic intensity in the vicinity of the Nevada Test (Adapted from Miscellaneous Geologic Investigations Map 1-532-A, published by U.S. Geological Survey, 1968.)

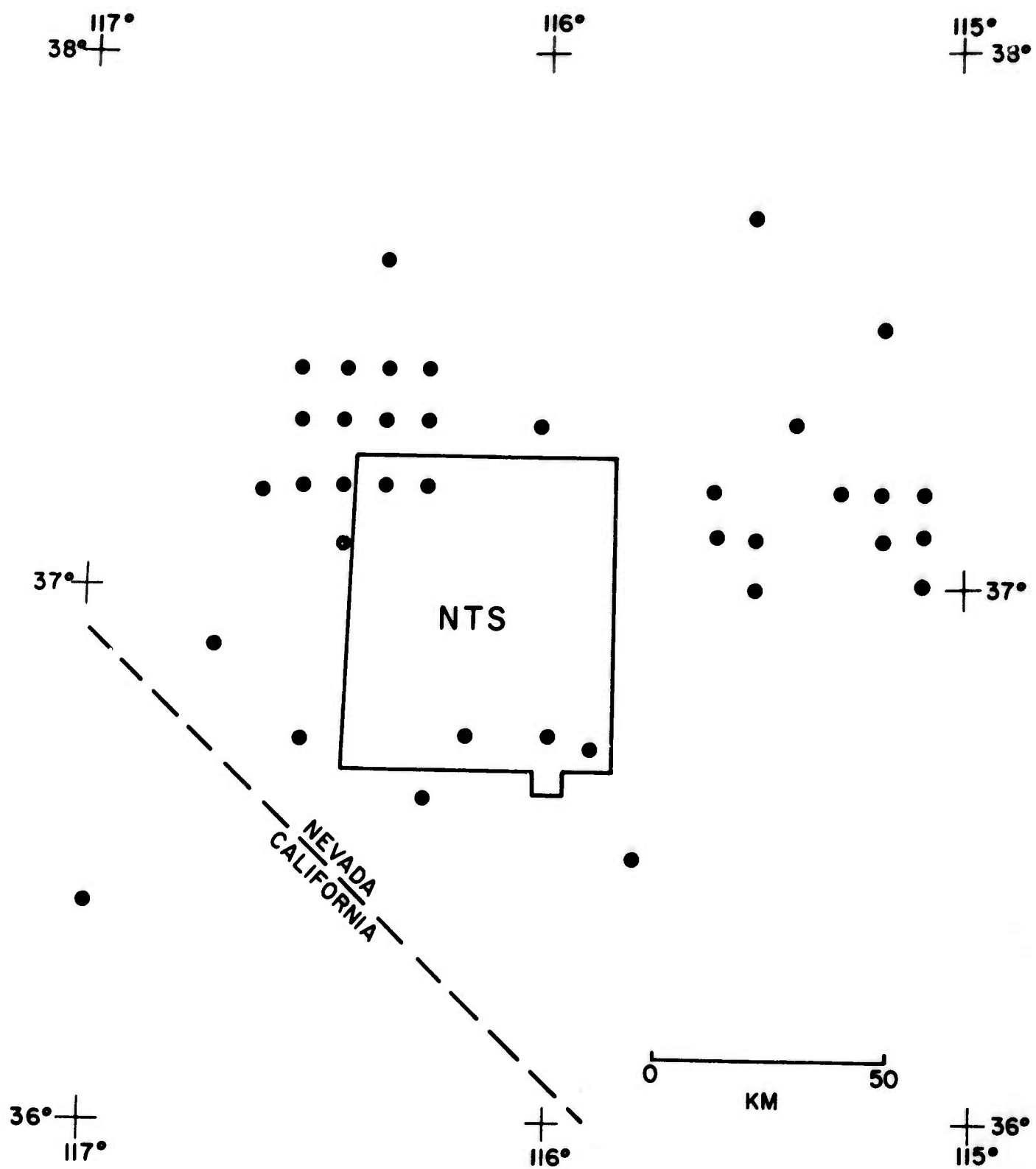


Figure 61. Epicenters of shallow events in the vicinity of the Nevada Test Site for the period January 1960 through January 1968 as determined by the U. S. Coast and Geodetic Survey. (No distinction as to number of events occurring at a given location.)

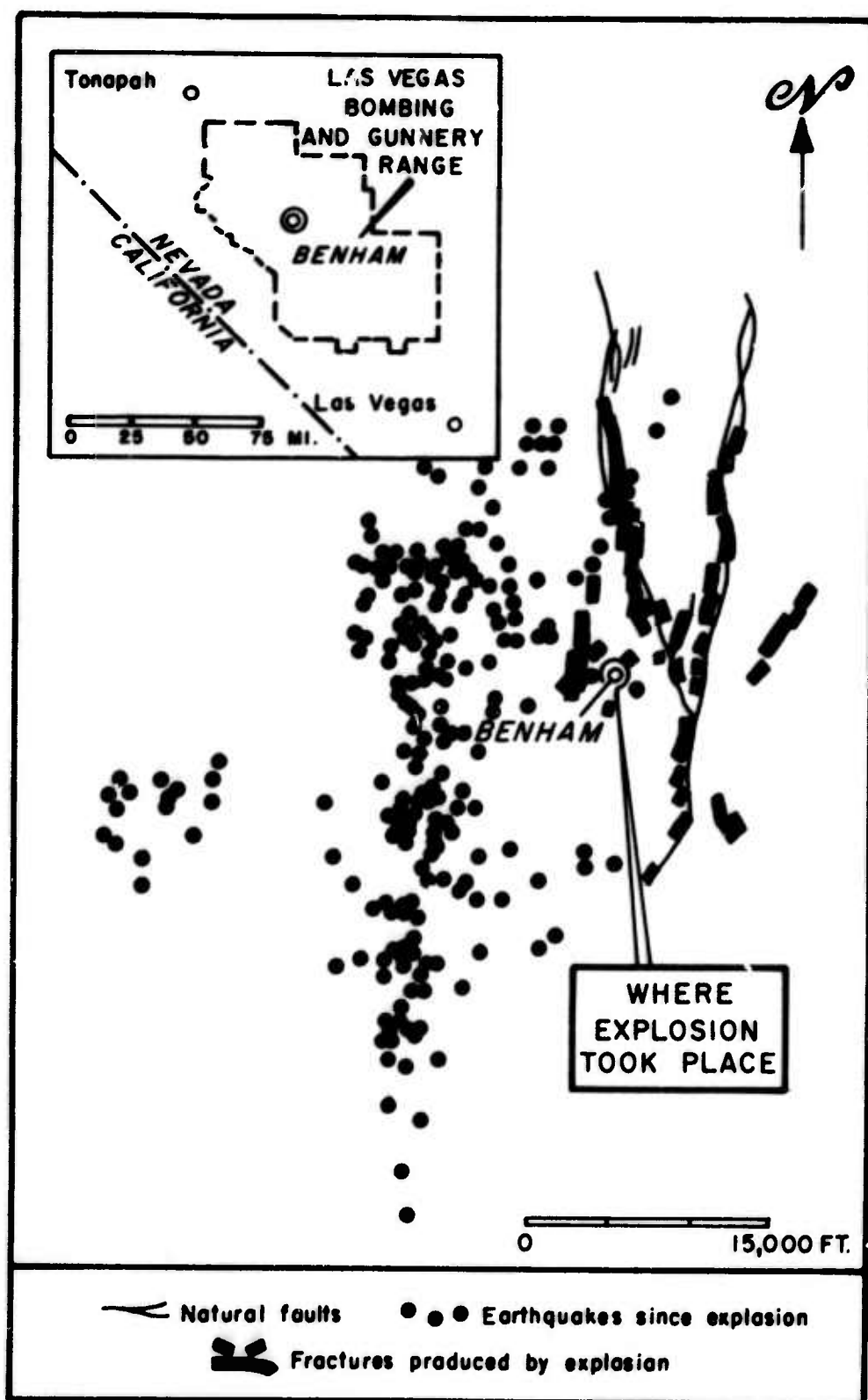


Figure 62. Locations of aftershocks following the detonation of underground nuclear explosions Benham on Dec. 19, 1968 at NTS.

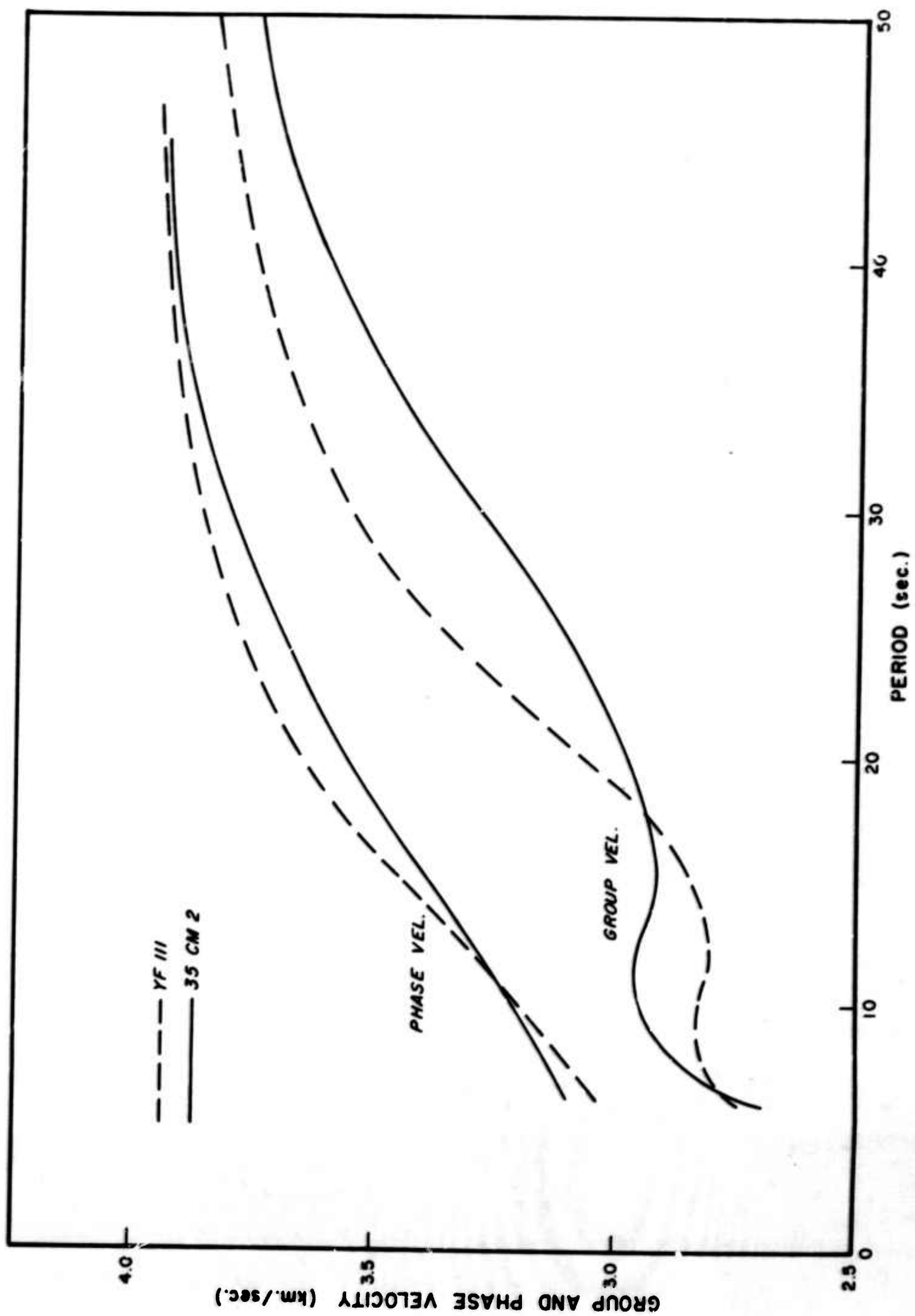


Figure 63. Theoretical fundamental mode Rayleigh wave dispersion computed from models YF11 and 35 CM2.

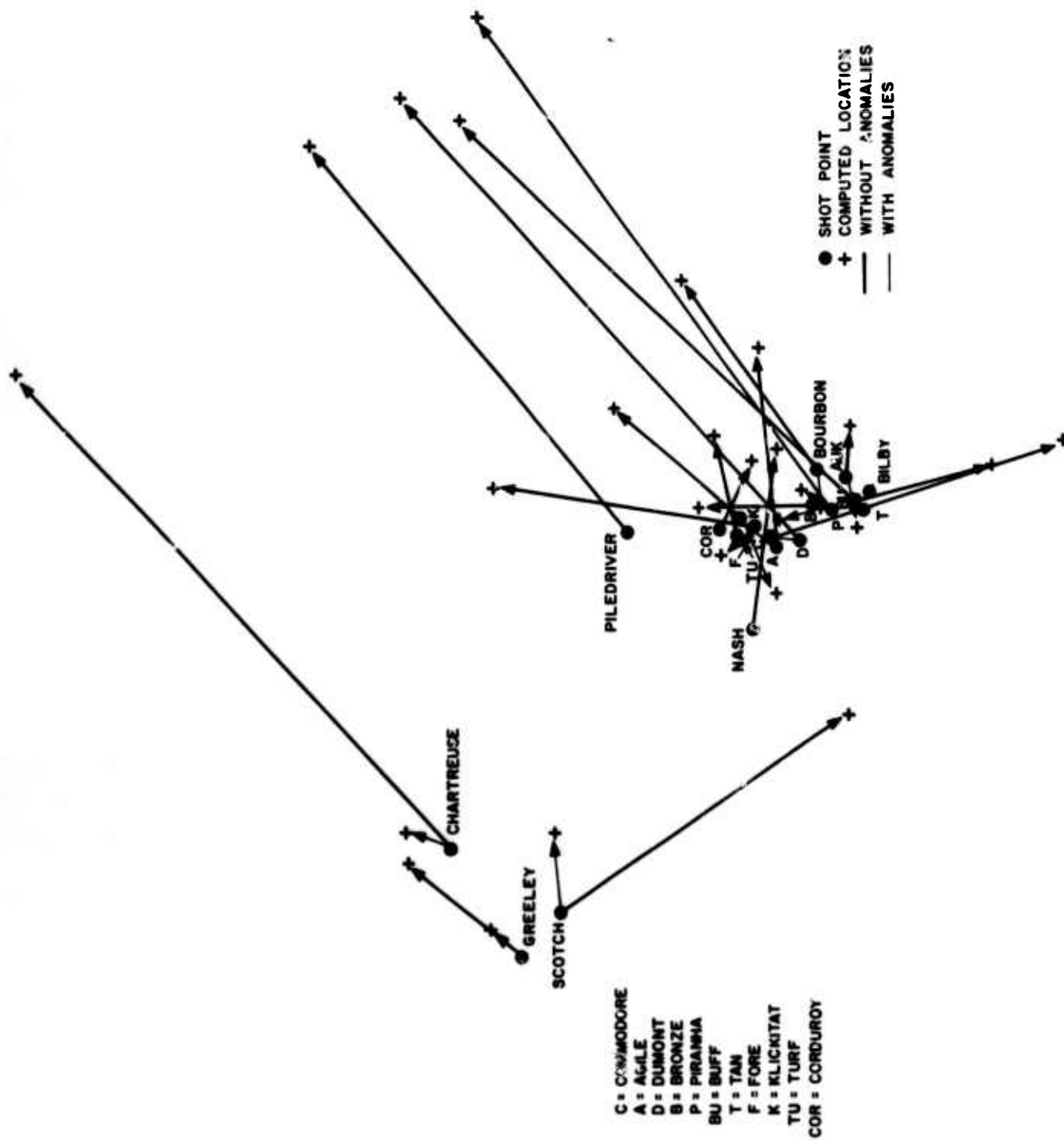


Figure 64. Locations of events at NTS computed using only stations with epicentral distances greater than seventeen degrees, with and without travel-time anomaly corrections.

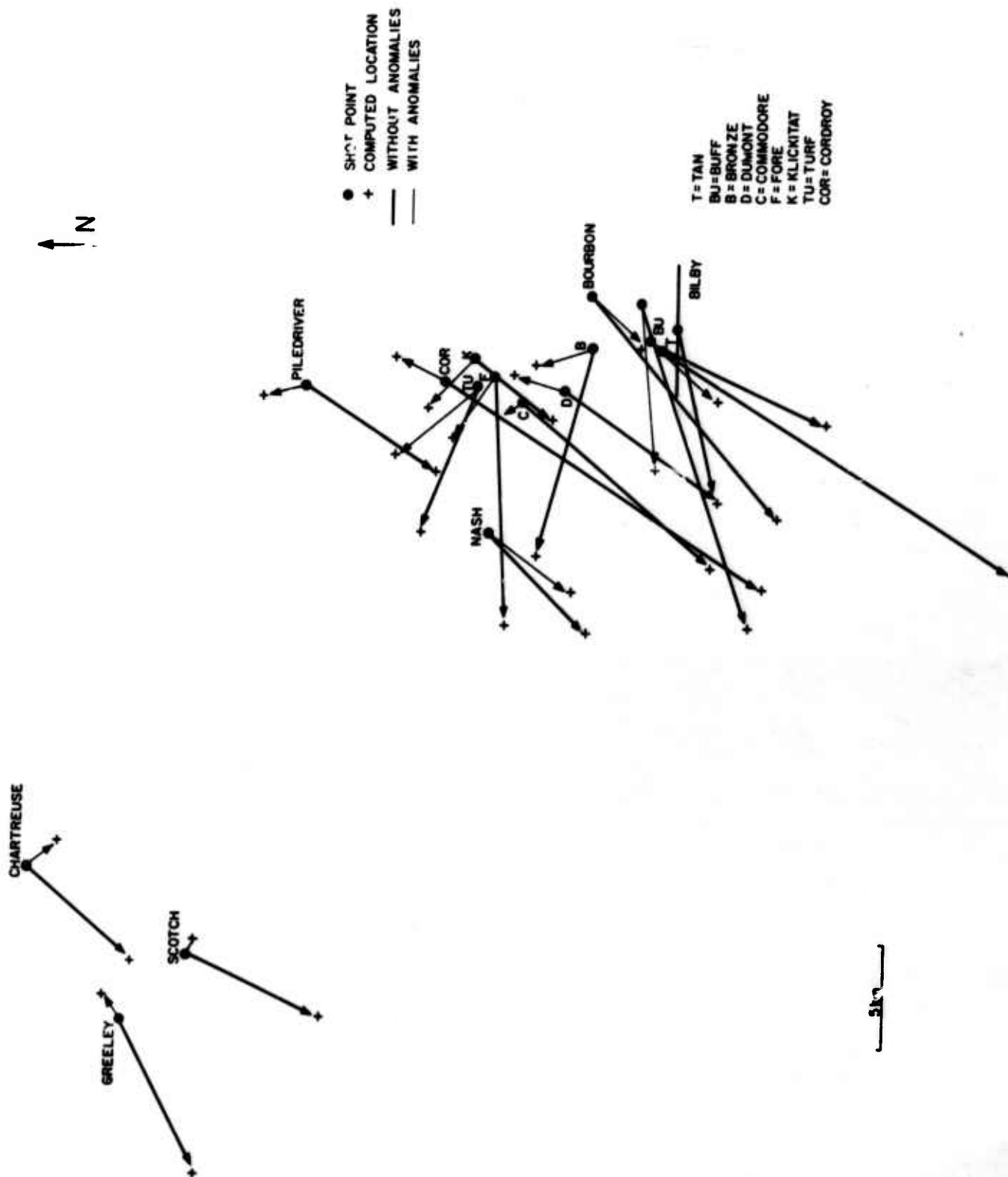


Figure 65. Locations of events at NTS computed using whole LRSM and Observatory network, with and without anomaly corrections.

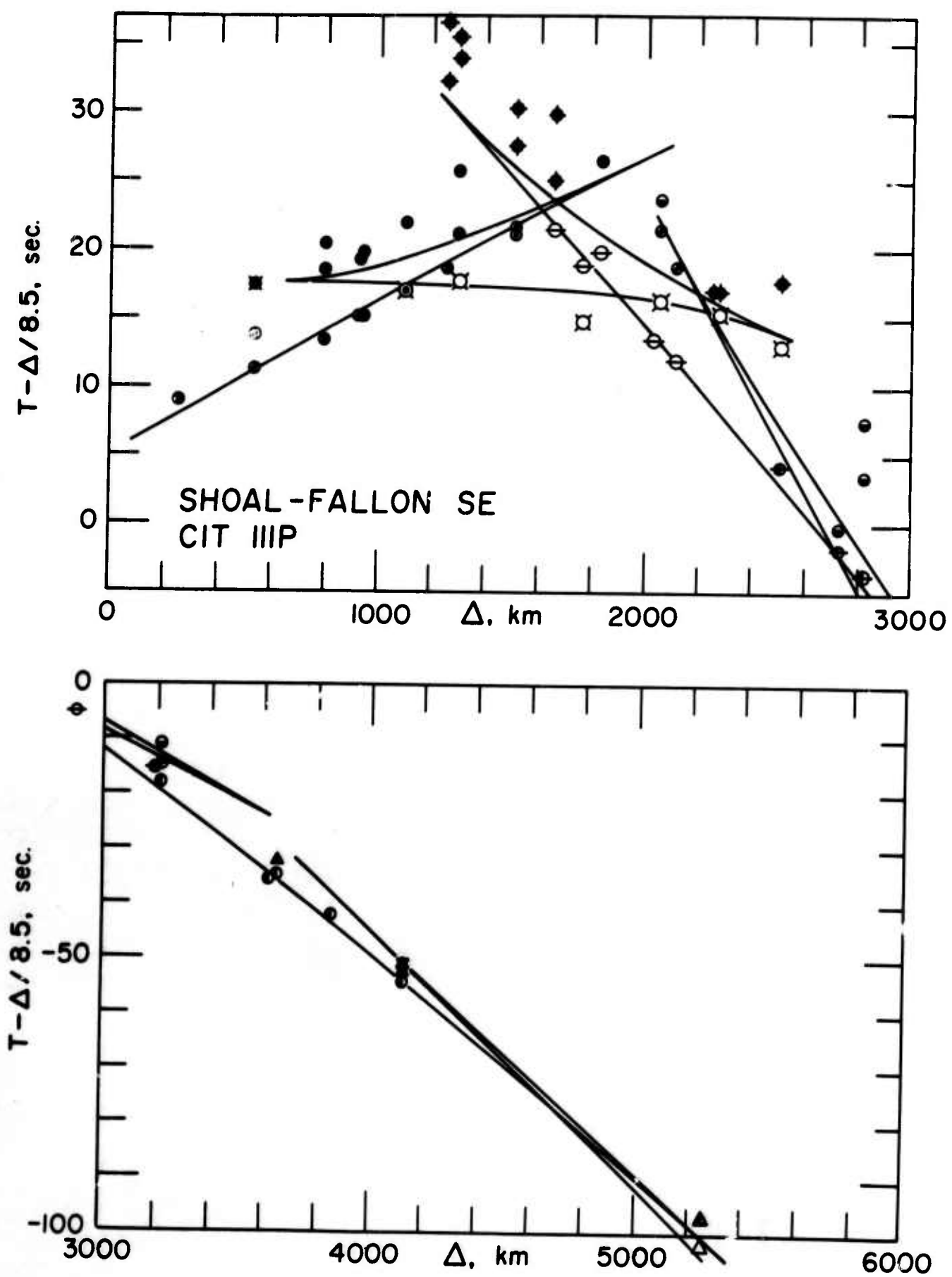


Figure 66. Observed travel-times from the Shoal-Fallon south-east profile and theoretical travel-time curve (solid line) calculated from model CIT 111P. (After Archambeau *et al.*, 1969.)

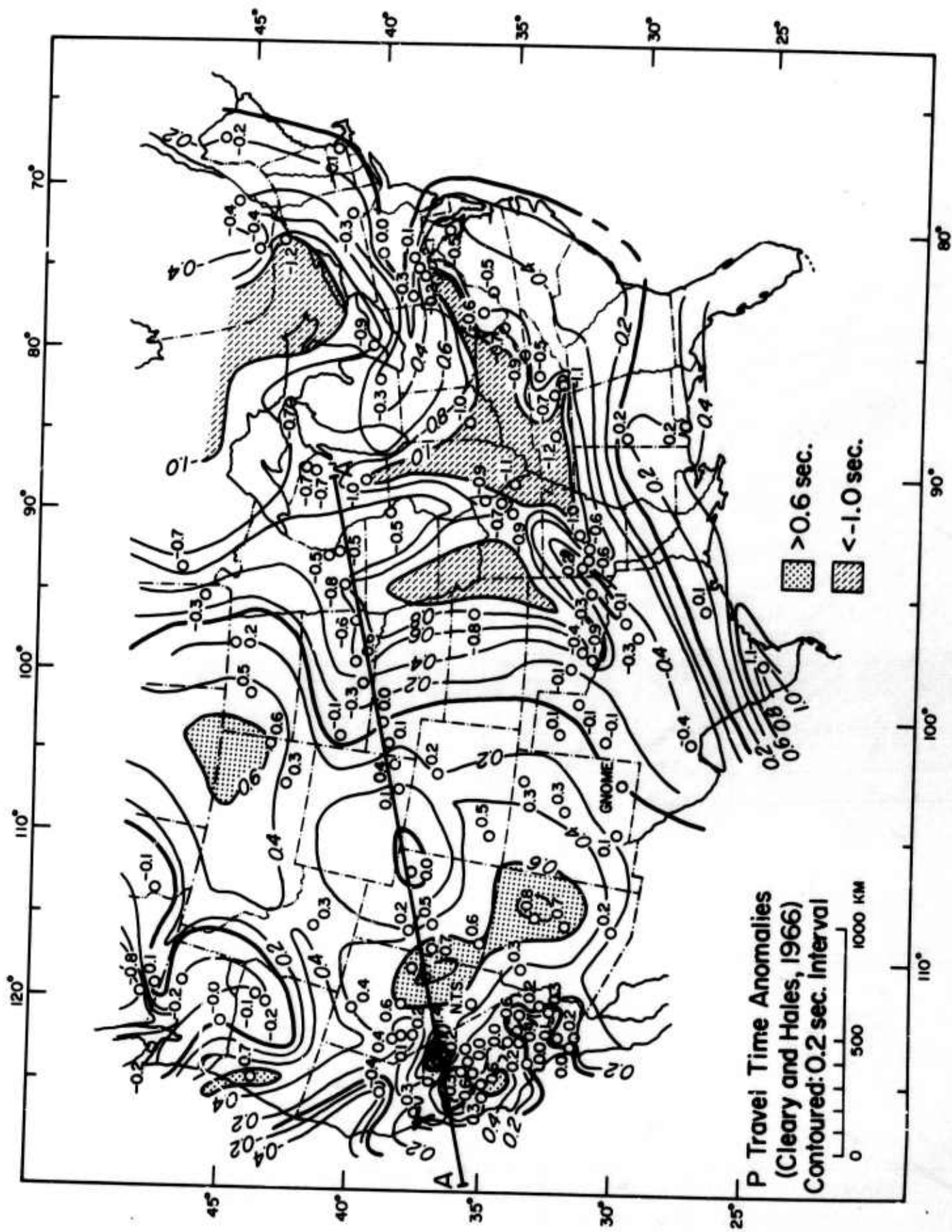


Figure 67. P-wave travel time anomalies. (After Cleary and Hales, 1966.)

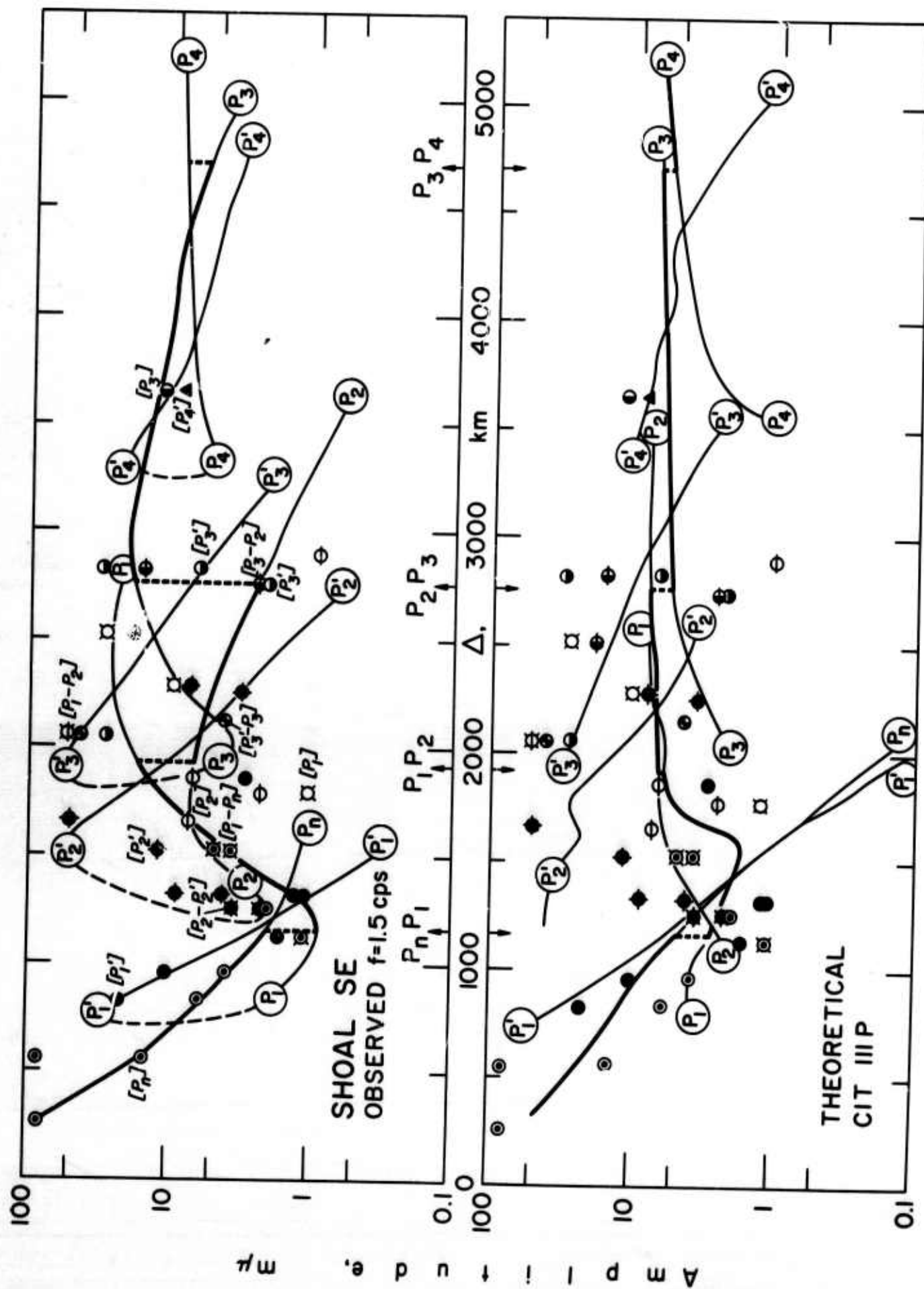


Figure 68. Observed and theoretical amplitudes from Shoal-Fallon southeast profile. (After Archambeau et al., 1969.)

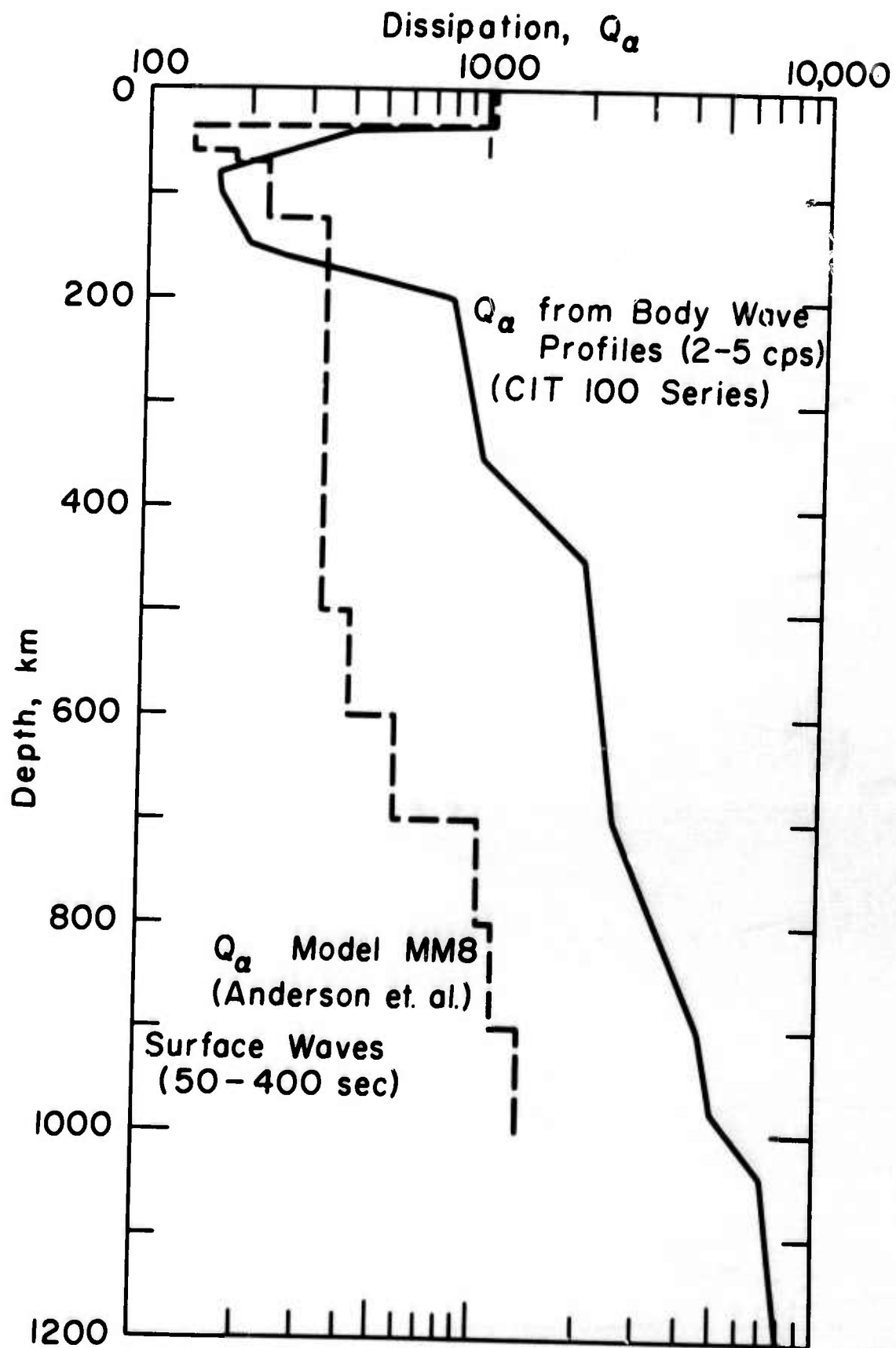


Figure 69. Q structure for CIT 100 series of models. (After Archambeau et al., 1969.)

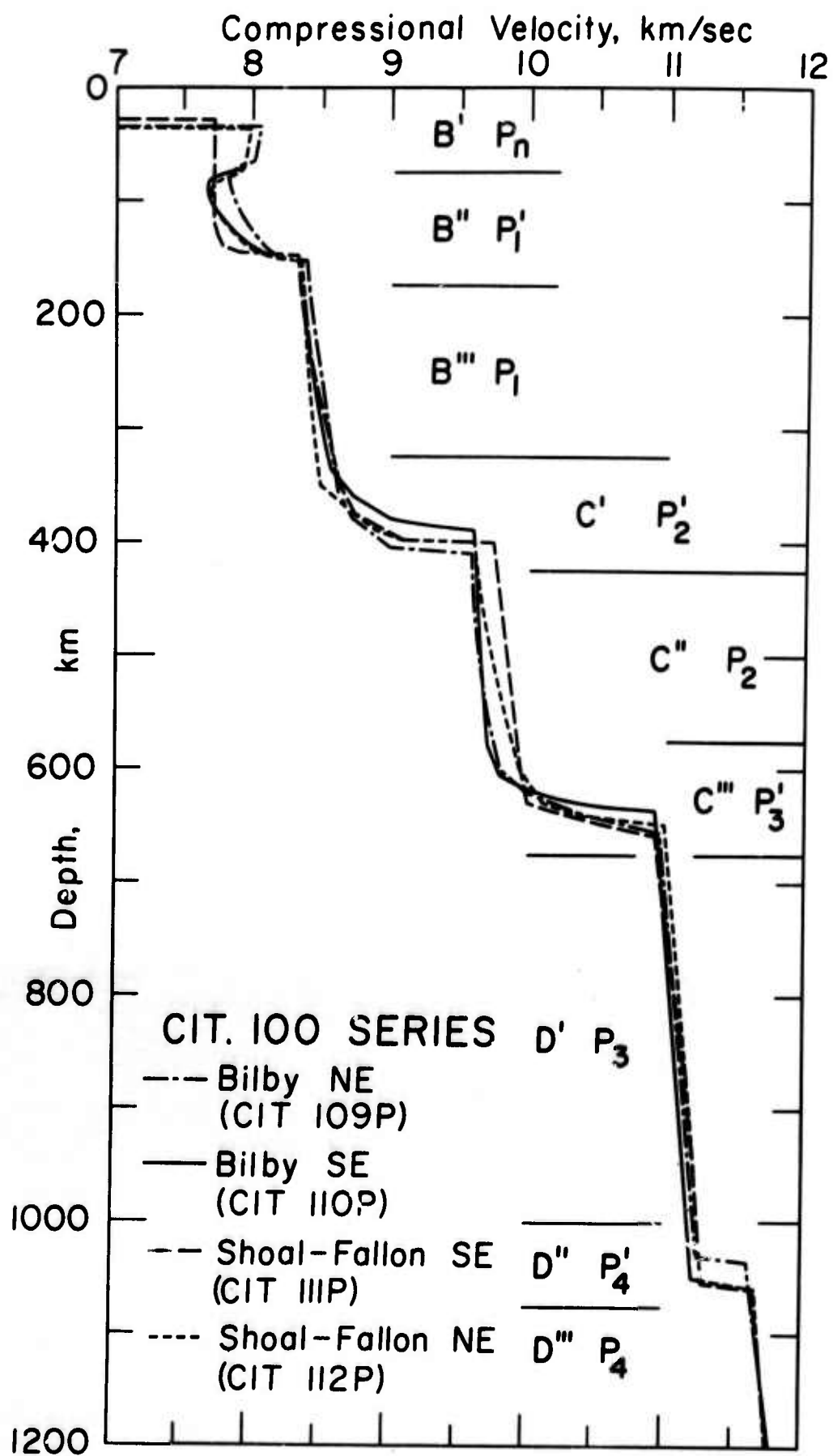


Figure 70. The CIT 100 series of models showing range of upper mantle structures in the western United States. (After Archambeau et al., 1969.)

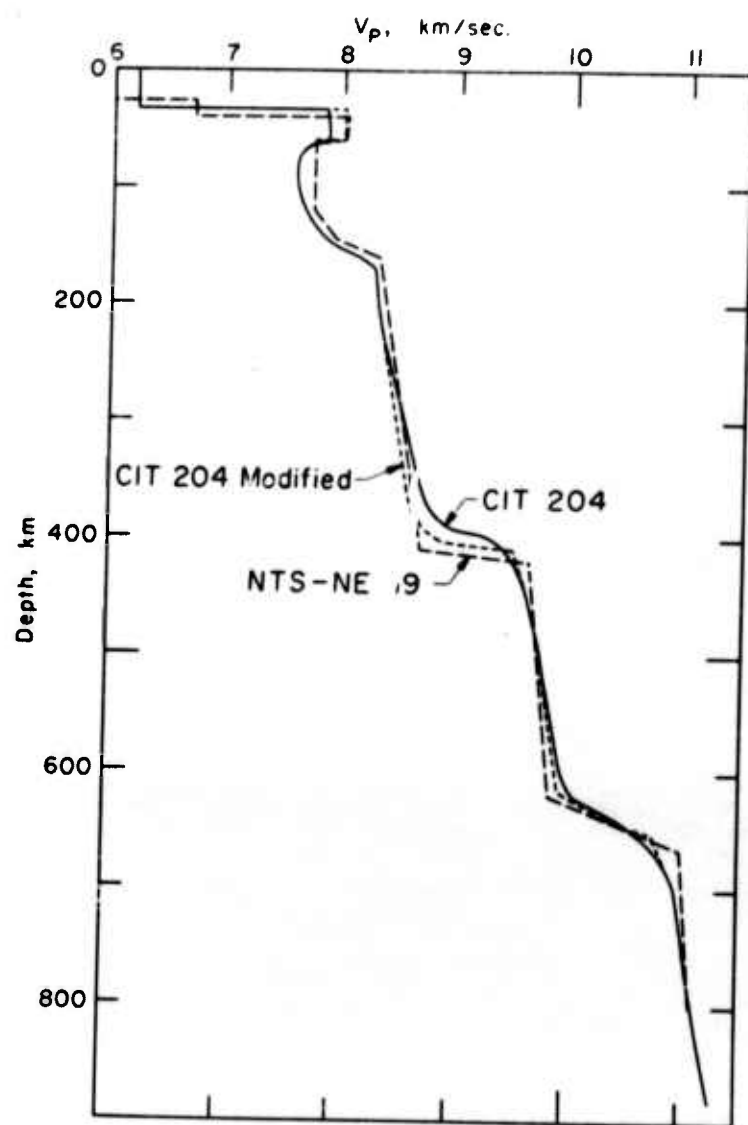


Figure 71. Upper mantle P-wave velocity distributions for model CIT 204 (Johnson 1967) and NTS-NE19. (Julian and Anderson, 1968.) Figure from Julian and Anderson, 1968.

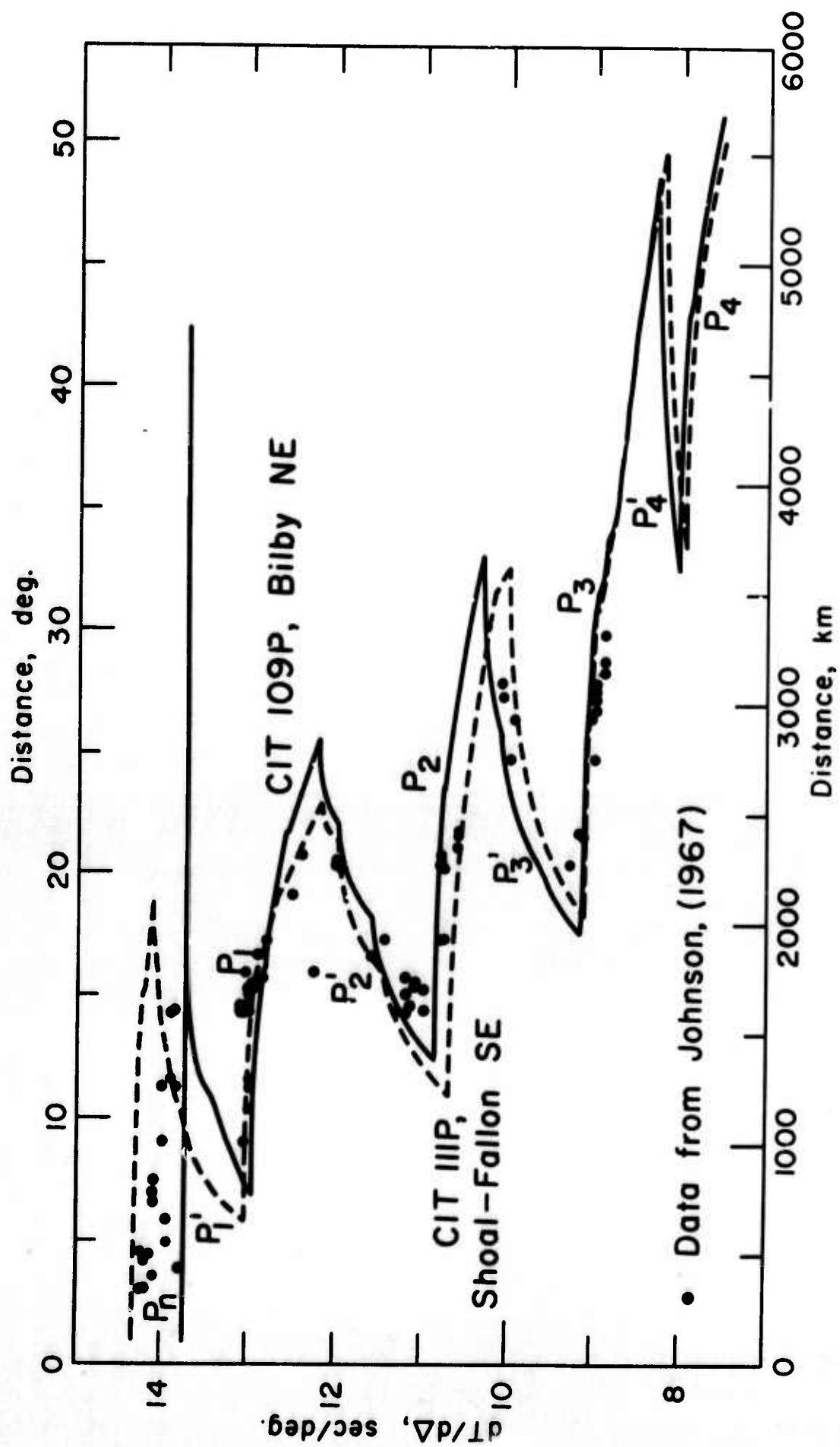


Figure 72. Fit of $dT/d\Delta$ calculated from two extreme CIT 100 series models with observed $dT/d\Delta$ at TFO. (After Archambeau *et al.*, 1969.)

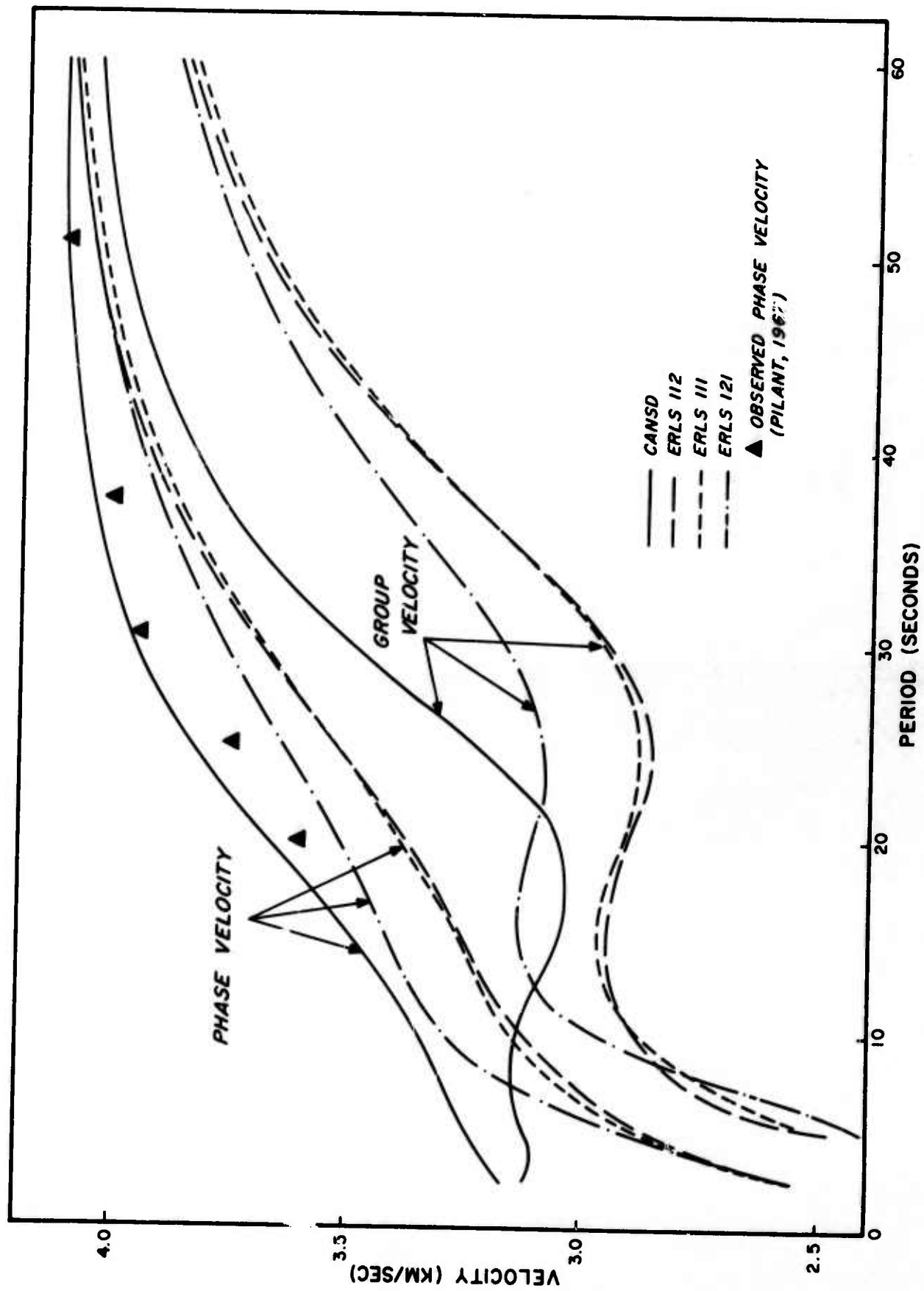


Figure 73. Comparison of a crustal column for Lake Superior based on model ERLS 112 with a similar column for NTS based on model YF111.

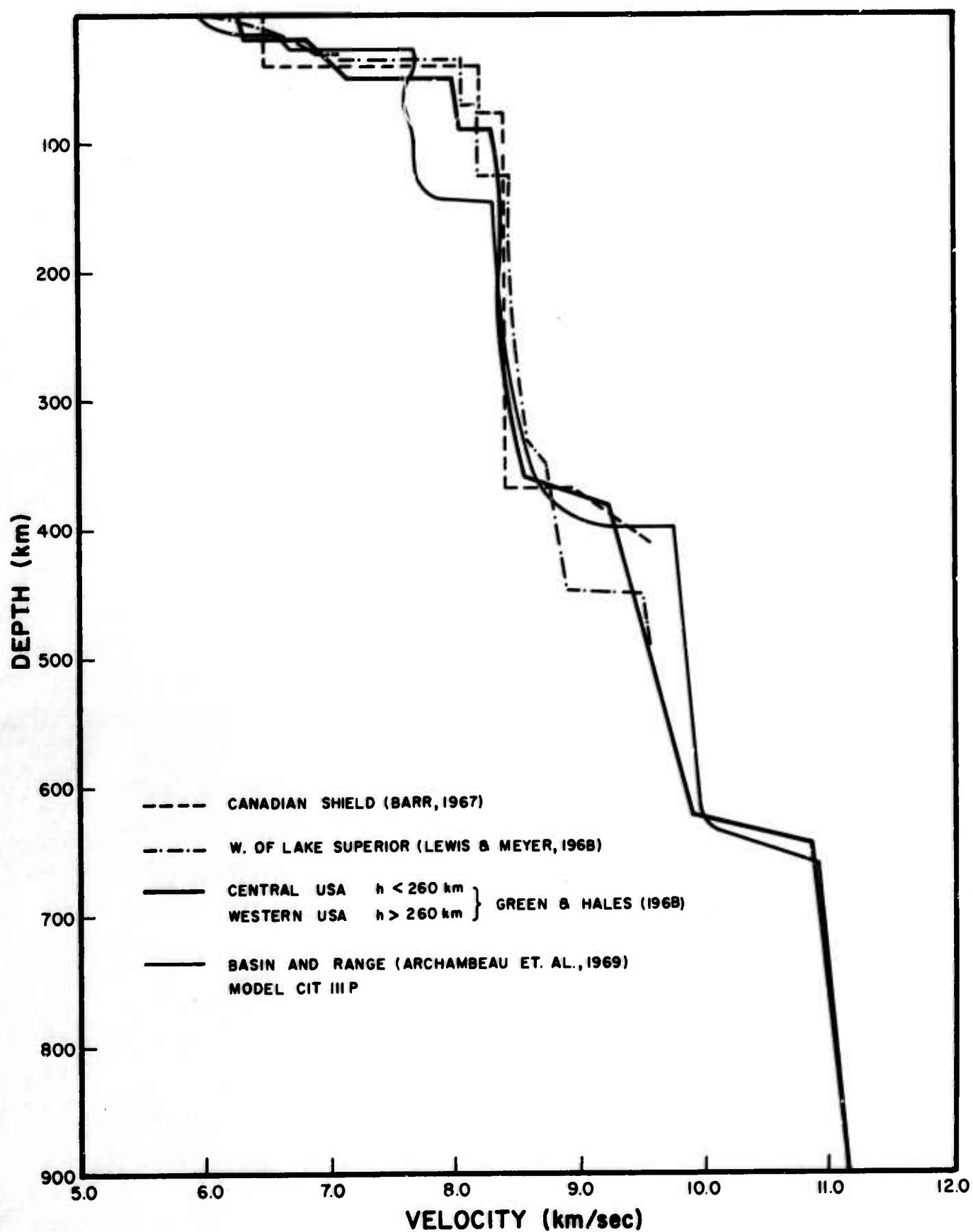


Figure 74. P-wave models from Early Rise compared with CIT111P.

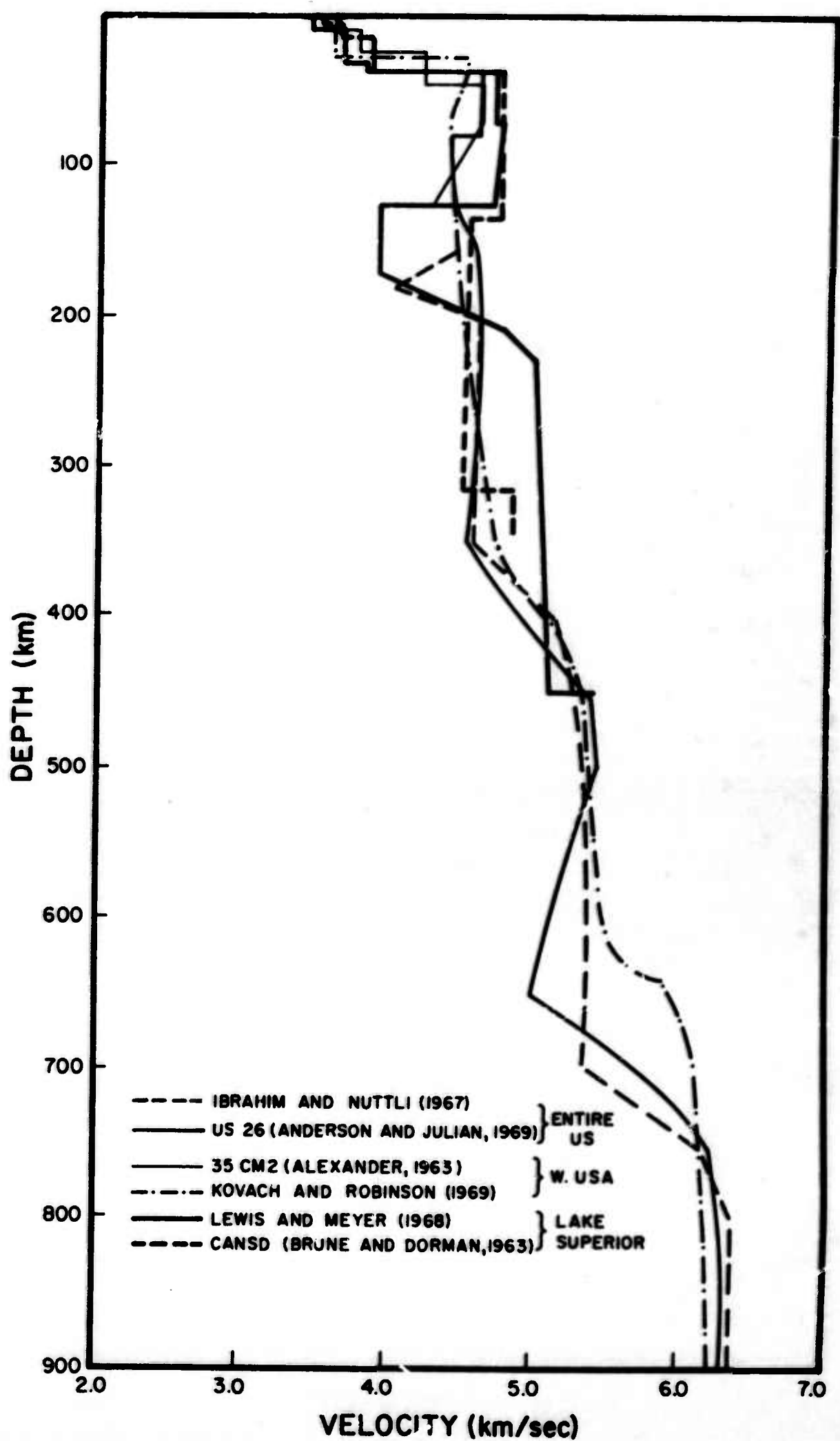


Figure 75. S-wave models for the Canadian Shield compared with models for the western United States.

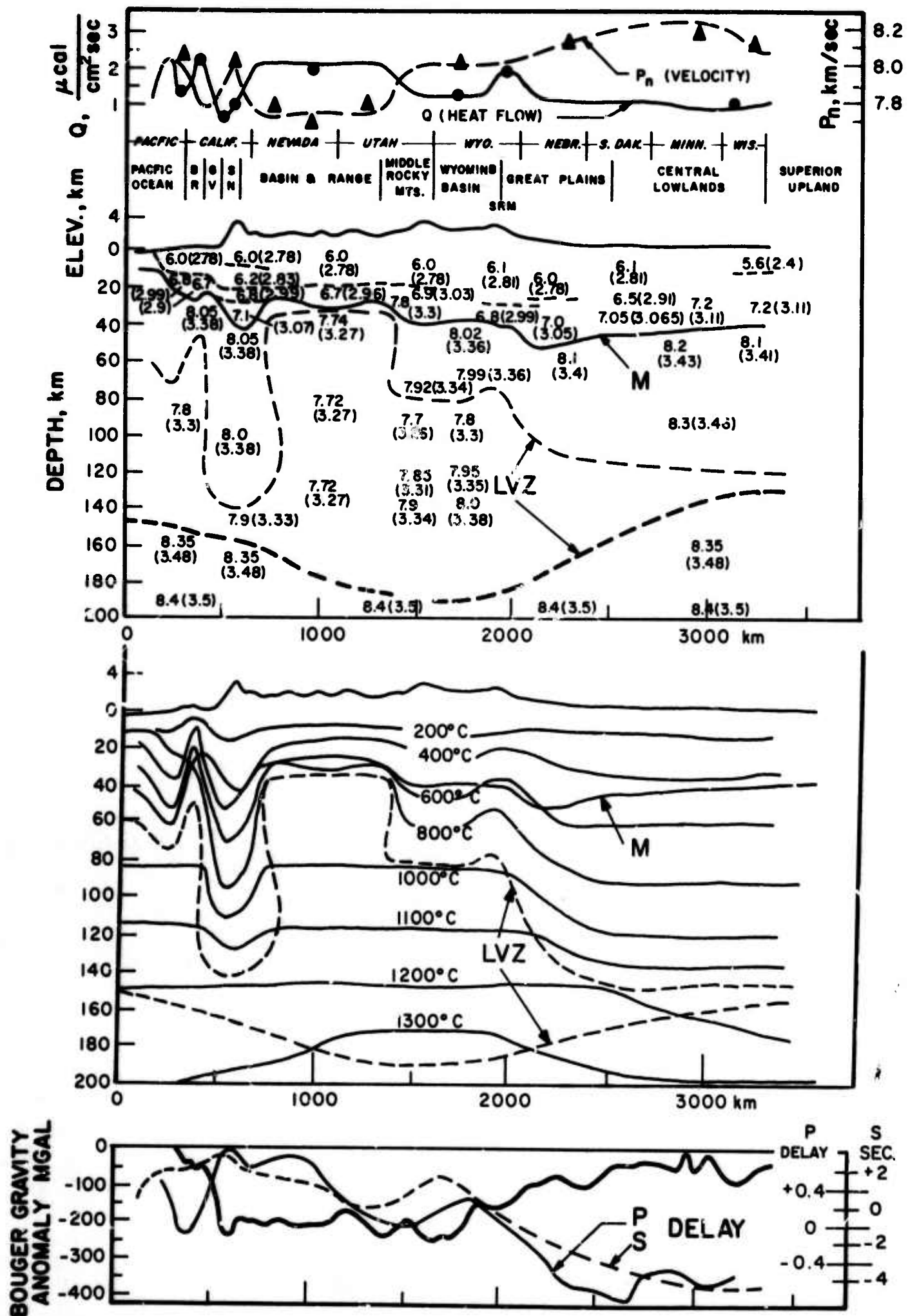


Figure 76. Summary of geophysical observations in a section from the Pacific Ocean to Lake Superior. (After Archambeau *et al.*, 1969.)

APPENDIX I - BASIC OBSERVATION DATA

The purpose of this appendix is to bring together the first-arrival data from the LRSM stations and Vela Observatories obtained during this study at SDL by standard filter analysis procedures for the October, 1964 series of shots in western Lake Superior. The travel-time data contained in these tables were used in the location calculations of Section III. Corresponding data for the NTS events (Section IV) are published elsewhere (Chiburis, 1968; and the SDL "Shot Reports" covering these events.)

Origin times, relative and absolute locations of the 38 shots fired during Project EARLY RISE are also given.

SHOT	LATITUDE			LONGITUDE			DISTANCE*	AZIMUTH*	ORIGIN TIME(Z)
1	47	32	33.6N	88	53	51.0W	3.26(5)	104.4	11:00:00.0(5)
2	47	32	40.2N	88	56	34.2W	0.66	202.3	09:30:00.0
3	47	32	40.2N	88	56	21.0W	0.61	177.7	10:30:00.0
4	47	32	57.0N	88	56	16.0W	0.13	136.5	09:30:00.0
5	47	32	58.8N	88	56	21.0W	0.05	145.9	10:30:00.0(5)
6	47	33	5.4N	88	56	21.0W	0.17	008.6	09:30:00.0
7	47	33	1.8N	88	56	20.4W	0.07	034.1	10:30:00.0
8	47	33	4.8N	88	56	3.6W	0.42	069.1	09:30:00.0
9	47	33	4.8N	88	56	3.0W	0.43	069.7	10:30:00.0
10	47	33	11.4N	88	56	24.0W	0.35	353.9	09:30:00.0
11	47	32	57.0N	88	56	16.4W	0.15	306.4	10:30:00.0
12	47	32	22.2N	88	56	32.4W	1.19	190.4	09:30:00.0
13	47	32	19.2N	88	56	25.2W	1.33	160.8	10:30:00.0
14	47	33	12.0N	88	56	28.8W	0.40	339.6	09:30:00.0
15	47	32	46.8N	88	56	31.8W	0.45	206.2	10:30:00.0
16	47	33	8.4N	88	56	25.8W	0.27	343.8	09:30:00.0
17	47	32	58.2N	88	56	16.8W	0.13	116.2	10:30:00.0
18	47	32	58.2N	88	56	9.0W	0.28	101.4	10:00:00.0
19	47	33	1.2N	88	56	18.6W	0.08	063.8	11:00:00.0
20	47	33	4.8N	88	56	48.0W	0.56	285.4	09:30:00.0
21	47	32	52.8N	88	56	47.4W	0.57	247.1	10:30:00.0
22	47	32	56.4N	88	56	0W	0.48	103.5	09:30:00.0
23	47	32	55.2N	88	55	55.8W	0.57	105.0	10:30:00.0
24	47	33	12.0N	88	56	29.4W	0.40	337.9	09:30:00.0
25	47	33	16.8N	88	56	19.8W	0.52	005.5	10:30:00.0
26	47	33	17.4N	88	56	17.4W	0.55	010.6	09:30:00.0
27	47	33	17.4N	88	56	19.2W	0.54	006.7	10:30:00.0
28	47	33	4.2N	88	56	12.6W	0.24	057.1	09:30:00.0
29	47	33	3.0N	88	56	7.8W	0.31(5)	032.9	10:30:00.0
30	47	33	7.2N	88	56	40.2W	0.44	300.6	09:30:00.0
31	47	33	11.4N	88	56	35.4W	0.45	321.9	10:30:00.0
32	47	33	13.8N	88	56	36.0W	0.51	325.9	09:30:00.0
33	47	33	9.6N	88	56	1.2W	0.53	056.0	10:30:00.0
35	47	32	53.4N	88	56	16.2W	0.26	150.0	10:30:00.0
36	47	33	13.8N	88	57	6.0W	1.01	295.0	09:30:00.0
37	47	33	9.6N	88	56	43.8W	0.54	303.3	10:30:00.0
38	47	32	54.6N	88	56	8.4W	0.33	120.0	09:30:00.0
39	47	32	46.2N	88	56	4.8W	0.56	139.5	10:30:00.0

* From mean shot point, 47.55°N, 88.94°W

TABLE A-1

Origin Times and Locations of EARLY RISE shots

SHOT NO.	CHARGE SIZE LBS.	DATE	ORIGIN TIME	LOCATION LATITUDE °N LONGITUDE °W	WATER DEPTH METERS
45A	2,000	1 Oct. 1964	11:00:00.4Z	47.236 90.309	113.4
48A	2,000	1 Oct. 1964	13:00:00.4Z	47.322 90.022	118.9
45B	4,000	2 Oct. 1964	14:00:00.3Z	47.266 90.291	117.0
73A	4,000	2 Oct. 1964	10:30:00.3Z	47.368 90.010	146.3
45C	6,000	3 Oct. 1964	10:30:00.3Z	47.260 90.306	113.4
47A	6,000	3 Oct. 1964	13:30:00.3Z	47.285 90.103	131.7
45D	12,000	4 Oct. 1964	13:00:00.2Z	47.286 90.297	113.4
46A	12,000	4 Oct. 1964	10:30:00.2Z	47.295 90.209	122.5
45E	20,000	10 Oct. 1964	10:30:00.3Z	47.312 90.299	115.2
49A	20,000	10 Oct. 1964	08:30:00.2Z	47.373 89.883	160.9

TABLE A-2

Origin Times and Locations of October 1964 Shots

TABLE A-3.
First arrival data for shot 49A

STATION	DISTANCE (KM)	AZIMUTH DEGREES	ARRIVAL TIME (Z)	TRAVEL TIME (SEC)	AMPLITUDE mu	PERIOD (SEC)	M _b
GP-MN	273.5	278.1	08:30:41.0	40.8	41.8	0.4	----
WF-MN	441.9	208.0	08:31:02.6	62.4	30.4	0.7	4.74
RK-ON	474.3	325.7	08:31:06.0	65.8	--	0.2	----
VO-IO	598.9	198.0	08:31:22.0	82.8	13.9	0.5	4.84
RY-ND	873.8	279.6	08:31:55.2	115.0	43.1	0.6	5.86
BR-PA	1213.5	129.0	08:32:35.9	155.7	3.8	0.4	5.18
BL-WV	1273.5	143.5	08:32:41.6	161.4	15.5	0.5	5.69
DH-NY	1313.1	110.2	08:32:47.2	167.0	11.8	0.5	5.47
CPO-O8	1356.2	163.1	08:32:52.7	172.5	7.7	0.5	5.79
LS-NH	1435.4	097.4	08:33:02.4	182.2	7.1	0.5	5.15
WMO-06	1582.2	210.5	08:33:17.9	197.7	6.5	0.8	3.51
EU-AL	1629.3	173.3	08:33:25.5	205.3	5.0	0.4	4.39
HN-ME	1672.5	086.5	08:33:28.7	208.5	15.2	0.8	3.58
RT-NM	1678.2	230.5	08:33:32.2	212.0	6.0	0.6	4.29
JE-LA	1740.2	186.7	08:33:41.0	220.8	13.7	0.5	4.34
UBO-10	1759.5	250.8	08:33:42.2	222.0	1.4	0.4	3.44
SV-2-QB	1807.7	054.2	08:33:45.0	224.8	2.2	0.4	3.65
DR-CO	1831.6	239.6	08:33:50.1	229.9	1.1	0.6	3.16
HL-2-ID	1956.3	266.6	08:34:05.8	266.6	2.5	0.8	3.41
NL-AZ	2066.8	239.1	08:34:19.2	259.0	3.2	0.9	3.55
BMO-03	2127.3	272.6	08:34:23.6	263.4	1.1	0.7	3.22
LC-NM	2182.9	226.4	08:34:31.3	271.1	1.1(5)	0.6	3.28
KN-UT	2204.0	246.9	08:34:33.6	273.4	2.0	0.9	3.34
WO-AZ	2214.3	238.7	08:34:35.2	275.0	5.7	0.8	3.85
HR-AZ	2240.3	238.5	08:34:36.9	276.7	6.7	0.8	3.92
EK-NV	2270.2	255.9	08:34:40.9	255.9	3.8	0.8	3.67
GE-AZ	2296.9	236.4	08:34:42.4	282.2	1.5	0.6	3.49
TFO-60	2304.6	238.6	08:34:43.7	283.5	3.0	0.8	3.68
JR-AZ	2308.0	240.9	08:34:45.1	284.9	2.5	0.6	3.72
LG-AZ	2311.4	239.3	08:34:45.0	239.3	4.3	0.8	3.83
SG-AZ	2332.2	244.5	08:34:46.8	244.5	0.6	0.4	3.26
SN-AZ	2363.9	238.5	08:34:49.6	289.4	3.0	0.7	3.73
MN-NV	2495.0	256.9	08:35:01.8	256.9	1.8	0.7	3.61
NP-NT	3484.5	346.9	08:36:22.5	382.3	2.6	0.8	4.21

Mean 4.1

First arrival data for shot 45E

Mean 4.0

TABLE A-5.
First arrival data for shot 46A

STATION	DISTANCE (KM)	AZIMUTH DEGREES	ARRIVAL TIME (Z)	TRAVEL TIME (SEC)	AMPLITUDE mu	PERIOD (SEC)	M _b
GP-MN	250.8	280.6	11:30:37.9	37.7	43.8	0.4	--
WF-MN	423.7	204.3	11:31:00.4	60.2	14.6	0.5	4.56
RK-ON	468.6	328.6	11:31:05.4	65.2	5.3	0.3	4.35
VO-IO	583.8	195.8	11:31:20.0	79.8	6.5	0.4	4.61
RY-ND	851.6	280.2	11:31:52.0	111.8	79.8	0.4	6.30
BR-PA	1228.1	127.7	11:32:37.6	157.4	10.2	0.5	5.51
BL-WV	1282.0	142.2	11:32:42.7	162.5	4.2	0.3	5.24
DH-NY	1334.2	109.3	11:32:50.4	170.2	2.6	0.4	4.92
CPO-O8	1355.8	161.8	11:32:52.7	172.5	3.0	0.3(5)	5.03
LS-NH	1459.8	096.8	11:33:04.8	184.6	3.2	0.5	4.81
WMO-06	1562.8	209.6	11:33:15.4	195.2	7.4	0.8	4.57
EU-AL	1624.3	172.2	11:33:25.3	205.1	10.3	0.4	4.71
HN-ME	1698.9	086.1	11:33:32.0	211.8	2.5	0.5	4.00
RT-NM	1654.3	229.9	11:33:28.3	208.1	2.8	0.6	3.96
JE-LA	---	---	-----	---	-	-	--
UBO-10	1734.2	250.5	11:33:38.7	218.5	1.0	.4	3.29
SV-2-QB	---	---	-----	---	-	-	--
DR-CO	1806.8	239.2	11:33:47.0	226.8	0.3	0.4	2.81
HL-2-ID	1932.3	266.5	11:34:02.8	242.6	0.7	0.7	2.88
NL-AZ	2042.0	238.7	11:34:17.5	257.3	0.4	0.5	2.79
BMO-03	3104.4	272.6	11:34:21.4	261.2	0.2	0.5	2.55
LC-NM	2159.7	225.9	11:34:28.8	225.9	0.5	0.5	3.04
KN-UT	2178.8	246.6	11:34:30.6	270.4	0.8	0.8	3.01
WO-AZ	2189.5	238.3	11:34:32.3	272.1	1.6	0.6	3.44
HR-AZ	2215.6	238.1	11:34:34.3	274.1	3.3	0.8	3.62
EK-NV	2245.2	255.7	11:34:37.6	277.4	0.5	0.6	2.96
GE-AZ	2272.3	235.9	11:34:39.9	279.7	0.3	0.7	2.68
TFO-60	2279.8	238.2	11:34:41.1	280.9	2.4	0.8	3.58
JR-AZ	---	---	-----	---	-	-	--
LG-AZ	2286.5	238.9	11:34:42.5	282.3	2.0	0.6	3.63
SG-AZ	2307.1	244.2	11:34:44.0	283.8	0.5	0.6	3.00
SN-AZ	---	---	-----	---	-	-	--
..N-NV	2407.1	256.7	11:34:58.7	298.5	1.1	0.7	3.40
NP-NT	---	---	-----	---	-	-	--

Mean 3.9

TABLE A-6.
First arrival data for shot 45D

STATION	DISTANCE (KM)	AZIMUTH DEGREES	ARRIVAL TIME (Z)	TRAVEL TIME (SEC)	AMPLITUDE mu	PERIOD (SEC)	M _b
GP-MN	244.3	281.1	14:00:37.2	37.0	24.6	0.3	--
WF-MN	419.8	203.5	14:01:00.0	59.8	18.1	0.3	4.88
RK-ON	465.7	329.3	14:01:05.1	64.9	7.3	0.3	4.48
VO-IO	580.7	195.1	14:01:19.5	79.3	16.9	0.5	4.93
RY-ND	844.7	280.3	14:01:51.4	111.2	36.1	0.3	6.08
BR-PA	1232.1	127.4	14:02:38.0	157.8	8.8	0.4	5.55
BL-WV	1284.8	141.9	14:02:42.8	162.6	7.2	0.4	5.36
DII-NY	1339.3	109.1	14:02:50.4	170.2	10.8	0.4	5.53
CPO-O8	1356.5	161.5	14:02:52.8	172.6	1.8	0.4	4.75
LS-NH	1465.3	096.6	14:03:04.6	184.4	4.9	0.6	4.91
WMO-06	1558.2	209.4	14:03:15.0	194.8	7.7	0.8	4.59
EU-AL	1623.8	171.9	14:03:24.8	206.6	9.2	0.5	4.57
HN-ME	1704.4	086.0	14:03:31.6	211.4	1.6(5)	0.4	3.92
RT-NM	1648.0	229.9	14:03:28.6	208.4	0.8	0.4	3.60
UBO-10	---	---	-----	---	-	-	--
SV-2-QB	1726.8	218.5	14:03:38.7	250.4	0.7	0.5	3.02
DR-CO	---	---	-----	---	-	-	--
HL-2-ID	1799.8	239.0	14:03:46.5	226.3	0.2	0.4	2.51
NL-AZ	1924.5	266.5	14:04:02.1	241.9	0.5	0.5	2.88
BMO-03	2034.1	238.6	14:04:17.2	257.0	0.4	0.5	2.79
LC-NM	2096.5	272.6	14:04:20.7	260.5	0.2	0.5	2.55
KN-UT	2153.7	225.7	14:04:27.6	267.4	0.7	0.5	3.16
WO-AZ	2171.4	266.5	14:04:30.0	269.8	1.2	0.8	3.18
HR-AZ	---	---	-----	---	-	-	--
EK-NV	2208.7	238.0	14:04:33.7	273.5	3.7	0.8	3.67
GE-AZ	2237.5	255.7	14:04:37.2	277.0	0.6	0.6	3.04
TFO-60	2265.5	235.8	14:04:39.4	279.2	0.3	0.7	2.68
JR-AZ	2272.9	238.1	14:04:40.5	280.3	1.7(5)	0.8	3.34
LG-AZ	---	---	-----	---	-	-	--
SG-AZ	2279.6	238.8	14:04:41.7	281.5	1.4	0.7	3.40
SN-AZ	2299.8	244.1	14:04:43.8	283.6	0.7	0.8	3.06
MN-NV	---	---	-----	---	-	-	--
P-NT	2462.3	256.7	14:04:58.2	298.0	2.5	0.8	3.69

Mean 3.90

'First arrival data for shot 47A

Mean	3.7
------	-----

TABLE A-8.
First arrival data for shot 45C

STATION	DISTANCE (KM)	AZIMUTH DEGREES	ARRIVAL TIME (Z)	TRAVEL TIME (SEC)	AMPLITUDE mu	PERIOD (SEC)	M _b
GP-MN	244.2	281.8	11:30:37.4	37.1	15.9	0.4	--
WF-MN	416.9	203.5	11:30:59.7	59.4	6.1	0.3	4.41
RK-ON	467.8	329.5	11:31:05.5	65.2	5.2	0.3	4.34
VO-IO	577.8	195.1	11:31:19.2	78.9	8.3	0.4	4.72
RY-ND	---	---	-----	--	-	-	--
BR-PA	1231.0	157.8	11:32:38.1	157.8	6.2	0.4	5.39
BL-WV	1283.0	141.7	11:32:42.9	162.6	4.3	0.4	5.13
DH-NY	1339.1	109.0	11:32:50.4	170.1	8.0	0.4	5.40
CPO-O8	1354.1	161.4	11:32:53.1	172.8	1.7	0.4	4.74
LS-NH	1456.7	096.5	11:33:05.1	184.8	3.4	0.5	4.83
WMO-06	1555.4	209.4	11:33:14.6(5)	194.3(5)	3.7	0.4	4.57
EU-AL	1621.1	171.8	11:33:24.3	204.0	3.7	0.4	4.24
HN-ME	---	---	-----	--	-	-	--
RT-NM	1705.3	085.9	11:33:32.2	211.9	2.2	0.4	4.04
JE-LA	---	---	-----	--	-	-	--
UBO-10	1725.2	250.5	11:33:38.6	218.3	0.7	0.5	3.02
SV-2-QB	---	---	-----	--	-	-	--
DR-CO	1797.8	239.1	11:34:46.6	226.1	0.2	0.4	2.51
HL-2-ID	1923.6	266.5	11:34:02.1	241.8	0.2	0.5	2.58
NL-AZ	2033.0	238.6	11:34:16.6	256.3	0.4	0.5	2.49
BMO-03	2095.9	272.6	11:34:20.9	260.6	0.2	0.5	2.55
LC-NM	2151.2	225.8	11:34:28.0	267.7	1.2	0.6	3.31
KN-UT	2169.6	246.6	11:34:29.7	269.4	0.5	0.6	2.95
WO-AZ	2180.5	238.3	11:34:31.7	271.4	0.8	0.4	3.29
HR-AZ	2206.6	238.1	11:34:33.4	273.1	3.7	0.8	3.67
EK-NV	2236.1	255.7	11:34:37.4	277.1	0.8	0.6	3.12
GE-AZ	2263.4	235.9	11:34:39.3	279.0	0.8	0.8	3.03
TFO-60	2270.8	238.1	11:34:40.5	280.2	1.5	0.8	3.27
JR-AZ	---	---	-----	--	-	-	--
LG-AZ	2277.5	238.9	11:34:41.8	281.5	2.0	0.7	3.45
SG-AZ	2298.0	244.2	11:34:43.3	283.0	1.5	0.7	2.42
SN-AZ	2330.1	238.0	11:34:46.6	286.3	1.6	0.7	3.46
LN-NV	2461.0	256.7	11:34:58.1	297.8	1.6	0.8	3.51
NP-NT	---	---	-----	--	-	-	--

Mean 3.8

TABLE A-9.
First arrival data for shot 73A

STATION	DISTANCE (KM)	AZIMUTH DEGREES	ARRIVAL TIME (Z)	TRAVEL TIME (SEC)	AMPLITUDE mu	PERIOD (SEC)	M _b
GP-MN	264.1	278.4	11:30:40.0	39.7	34.9	0.5	--
WF-MN	437.2	205.8	11:31:01.9	61.6	9.2	0.5	4.37
RK-ON	469.4	326.7	11:31:05.6	65.3	2.4	0.4	3.87
VO-IO	595.6	197.1	11:31:21.2	80.9	3.4	0.4	4.33
RY-ND	864.5	279.6	11:31:54.0	113.7	71.9	0.5	6.16
BR-PA	1220.7	128.6	11:32:36.7	156.4	1.2(5)	0.5	4.70
BL-WV	1278.8	143.1	11:32:42.5	162.2	6.8	0.4	5.26
DH-NY	1322.0	110.0	11:32:48.1	167.8	13.3	0.4	5.62
CPO-O8	1358.6	162.7	11:32:53.3	173.1	3.9	0.5	5.00
LS-NH	1444.9	097.3	11:33:02.5	182.2	1.9	0.4	4.68
WMO-06	1576.9	210.1	11:33:17.1	196.8	1.3	0.5	4.02
EU-AL	---	---	-----	---	-	-	--
HN-ME	1682.1	086.4	11:33:29.8	209.5	2.9	0.6	3.98
RT-NM	1670.5	230.2	11:33:31.3	211.0	1.2	0.5	3.66
JE-LA	---	---	-----	---	-	-	--
UBO-10	1750.3	250.6	11:33:40.6	220.3	0.7	0.5	3.03
SV-2-QB	---	---	-----	---	-	-	--
DR-CO	---	---	-----	---	-	-	--
HL-2-ID	1946.7	266.5	11:34:04.6	244.3	0.3	0.7	2.58
NL-AZ	2058.4	238.9	11:34:19.2	258.9	1.0	0.5	3.31
BMO-03	2117.7	272.5	11:34:22.8	262.5	0.2	0.5	2.55
LC-NM	2175.7	226.2	11:34:30.6	270.3	1.4	0.5	3.43
KN-UT	---	---	-----	---	-	-	--
WO-AZ	---	---	-----	---	-	-	--
HR-AZ	2231.9	238.3	11:34:36.0	275.7	2.4	0.5	3.68
EK-NV	---	---	-----	---	-	-	--
GE-AZ	---	---	-----	---	-	-	--
TFO-60	2296.2	238.4	11:34:43.2	282.9	0.6	0.5	3.18
JR-AZ	---	---	-----	---	-	-	--
LG-AZ	2302.9	239.1	11:34:43.8	283.5	2.0	0.7	3.55
SG-AZ	---	---	-----	---	-	-	--
SN-AZ	---	---	-----	---	-	-	--
N-NV	---	---	-----	---	-	-	--
NP-NT	---	---	-----	---	-	-	--

Mean 4.0

TABLE A-10.
First arrival data for shot 45P

STATION	DISTANCE (KM)	AZIMUTH DEGREES	ARRIVAL TIME (Z)	TRAVEL TIME (SEC)	AMPLITUDE mu	PERIOD (SEC)	M _b
GP-MN	245.2	281.5	15:00:37.5	37.2	-	-	--
WF-MN	418.0	203.6	15:00:59.6	59.3	10.8	0.5	4.43
RK-ON	467.8	329.4	15:01:05.5	65.2	3.7	0.3	4.19
VO-IO	578.7	195.2	15:01:19.5	79.2	8.6	0.4	4.73
RY-ND	845.5	280.4	15:01:52.4	112.1	25.1	0.4	5.80
BR-PA	1230.4	127.4	15:02:37.8	157.5	3.8	0.4	5.17
BL-WV	1282.7	141.8	15:02:42.5	162.2	5.0	0.5	5.10
DH-NY	1338.2	109.0	15:02:50.3	170.0	5.3	0.4	5.22
CPO-Q8	1354.3	161.5	15:02:53.0	172.7	1.2	0.3	4.70
LS-NH	1464.6	096.5	15:03:05.5	185.2	2.2	0.5	4.65
WMO-06	1556.5	209.4	15:03:14.8	194.5	1.9	0.4	4.28
EU-AL	---	---	-----	---	-	-	--
HN-ME	1704.1	085.9	15:03:52.2	211.9	2.2	0.4	4.04
RT-NM	1646.9	229.8	15:03:28.4	208.1	0.8	0.5	3.49
JE-LA	---	---	-----	---	-	-	--
UBO-10	1726.5	250.5	15:03:38.8	218.5	0.9	0.5	3.15
SV-2-QB	---	---	-----	---	-	-	--
DR-CO	---	---	-----	---	-	-	--
HL-2-ID	---	---	-----	---	-	-	--
NL-AZ	2034.3	238.6	15:04:16.8	256.5	2.3	0.6	3.49
BMO-03	2097.0	272.6	15:04:20.6	260.3	0.2	0.5	2.55
LC-NM	2152.5	225.8	15:04:28.0	267.7	1.3	0.5	3.26
KN-UT	---	---	-----	---	-	-	--
WO-AZ	---	---	-----	---	-	-	--
HR-AZ	2207.9	238.1	15:04:33.6	273.3	2.1	0.4	3.72
EK-NV	---	---	-----	---	-	-	--
GE-AZ	---	---	-----	---	-	-	--
TFO-60	2272.1	238.1	15:04:40.5	280.2	0.5	0.6	2.94
JR-AZ	---	---	-----	---	-	-	--
LG-AZ	2278.8	238.9	15:04:41.7	281.4	1.6	0.6	3.43
SG-AZ	---	---	-----	---	-	-	--
SN-AZ	---	---	-----	---	-	-	--
...N-NV	---	---	-----	---	-	-	--
NP-NT	---	---	-----	---	-	-	--

Mean 4.1

TABLE A-11.

First arrival data for shot 48A

STATION	DISTANCE (KM)	AZIMUTH DEGREES	ARRIVAL TIME (Z)	TRAVEL TIME (SEC)	AMPLITUDE mu	PERIOD (SEC)	M _b
GP-MN	264.0	279.6	14:00:39.9	39.5	11.8	0.4	--
WF-MN	432.2	206.0	14:01:01.4	61.0	5.4	0.5	4.14
RK-ON	473.2	327.1	14:01:06.6	66.2	2.2	0.3	3.97
VC-IO	590.4	197.1	14:01:21.0	80.6	5.9	0.4	4.57
RY-ND	864.5	279.9	14:01:54.1	113.7	33.3	0.4	5.92
BR-PA	1218.2	128.4	14:02:36.5	155.1	1.9	0.4	4.87
BL-WV	1275.3	142.9	14:02:41.4	161.0	3.3	0.5	5.02
DH-NY	1321.1	109.7	14:02:48.5	168.1	11.8	0.4	5.57
CPO-OS	1353.9	162.5	14:02:52.6	172.2	1.2	0.4	4.57
LS-NH	1445.1	097.1	14:03:03.0	182.6	2.2	0.5	4.65
WMO-06	1572.0	210.2	14:03:16.6	196.2	1.2	0.4	4.10
EU-AL	---	---	-----	---	-	-	--
HN-ME	1683.4	086.3	14:03:29.9	209.5	2.2	0.4	4.04
RT-NM	1666.5	230.3	14:03:30.8	210.4	0.3	0.5	3.09
UBO-10	1747.7	250.7	14:03:40.9	720.5	0.2	0.4	2.60
SV-2-QB	---	---	-----	---	-	-	--
DR-CO	---	---	-----	---	-	-	--
HL-2-ID	1945.5	266.6	14:04:04.5	244.1	0.1	0.6	2.26
NL-AZ	2054.9	239.0	14:04:19.6	258.6	0.4(5)	0.6	2.78
BMO-03	2117.1	272.6	14:04:22.5	262.1	0.2	0.5	2.55
LC-NM	---	---	-----	---	-	-	--
KN-UT	2192.1	246.9	14:04:32.4	272.0	0.2	0.4	2.71
WO-AZ	---	---	-----	---	-	-	--
HR-AZ	2228.5	238.4	14:04:35.8	275.4	0.6	0.4	3.19
EK-NV	2258.6	255.9	14:04:39.5	279.1	0.2	0.5	2.65
GE-AZ	---	---	-----	---	-	-	--
TFO-60	2292.7	238.5	14:04:42.7	282.3	0.6	0.5	3.17
JR-AZ	---	---	-----	---	-	-	--
LG-AZ	2299.5	239.2	14:04:43.6	283.2	0.3	0.4	2.99
SG-AZ	2320.3	244.4	14:04:45.5	285.1	0.2	0.6	2.70
SN-AZ	2352.0	238.4	14:04:48.2	287.8	0.4	0.6	2.92
MN-NV	2483.5	256.9	14:05:00.3	299.9	0.4(5)	0.7	3.01
NP-NT	---	---	-----	---	-	-	--
						Mean	3.7

TABLE A-12.
First arrival data for shot 45A

STATION	DISTANCE (KM)	AZIMUTH DEGREES	ARRIVAL TIME (Z)	TRAVEL TIME (SEC)	AMPLITUDE mu	PERIOD (SEC)	M _b
GP-MN	243.9	281.7	12:00:37.4	37.0	3.5	0.4	--
WF-MN	417.1	203.5	12:00:59.7	59.3	6.2	0.5	4.19
RK-ON	467.4	329.5	12:01:05.4	65.0	2.8	0.3	4.06
VO-IO	578.1	195.1	12:01:19.4	79.0	5.0	0.4	4.50
RY-ND	844.2	280.4	12:01:52.3	111.9	12.9	0.4	5.51
BR-PA	1231.4	127.3	12:02:37.9	157.5	3.8	0.4	5.17
BL-WV	1283.4	141.7	12:02:42.7	162.3	3.3	0.5	4.92
DH-NY	1339.4	109.0	12:02:50.5	170.1	6.0	0.5	5.18
QPO-O8	1354.4	161.4	12:02:55.1	172.7	1.8	0.4	4.75
LS-NH	1465.9	096.5	12:03:05.7	185.3	2.2	0.5	4.65
WMO-06	1555.5	009.4	12:03:14.7	194.3	0.8	0.5	4.22
EU-AL	---	---	-----	---	-	-	--
HN-ME	1705.5	085.9	12:02:31.5	211.2	2.2	0.6	3.86
RT-NM	1645.7	229.8	12:03:28.8	208.4	0.5	0.4	3.42
UBO-10	1725.1	250.5	12:03:38.5	218.2	0.4	0.4	7.90
SV-2-QB	---	---	-----	---	-	-	--
DR-CO	1797.7	239.1	12:03:46.4	726.0	0.2	0.4	2.52
HL-2-ID	---	---	-----	---	-	-	--
NL-AZ	2032.9	238.6	12:04:16.5	256.1	0.2	0.4	2.54
BMO-03	2095.7	272.6	12:04:21.4	261.0	0.2	0.5	2.55
JC-NM	2151.3	225.8	12:04:27.8	267.4	0.7	0.5	3.16
KN-UT	2169.5	246.6	12:04:30.1	269.7	0.3	0.6	2.65
WO-AZ	---	---	-----	---	-	-	--
HR-AZ	2206.5	238.1	12:04:33.5	273.1	1.6	0.6	3.43
EK-NV	2235.9	255.7	12:04:37.0	276.6	0.2(5)	0.6	2.63
GE-AZ	2263.3	235.9	12:04:39.2	278.8	0.1	0.6	2.39
TFO-60	2270.8	238.1	12:04:40.5	280.1	0.6	0.6	3.03
JR-AZ	---	---	-----	---	-	-	--
LG-AZ	2277.5	238.9	12:04:41.2	280.8	0.6	0.4	3.19
SG-AZ	2297.9	244.4	12:04:43.4	283.0	0.4	0.5	3.02
SN-AZ	2330.;	238.0	12:04:46.6	286.2	0.7	0.5	3.24
MN-NV	2460.8	256.7	12:04:58.3	297.9	0.4	0.6	2.99
IP-NT	---	---	-----	---	-	-	--
						Mean	3.6

Unclassified

Security Classification

DOCUMENT CONTROL DATA - R&D

(Security classification of title, body of abstract and indexing annotation must be entered when the overall report is classified)

1. ORIGINATING ACTIVITY (Corporate author)

TELEDYNE INDUSTRIES, INC.
ALEXANDRIA, VIRGINIA

2a. REPORT SECURITY CLASSIFICATION

Unclassified

2b. GROUP

3. REPORT TITLE

A COMPARISON OF THE LAKE SUPERIOR AND NEVADA
TEST SITE SOURCE REGIONS

4. DESCRIPTIVE NOTES (Type of report and inclusive dates)

Scientific

5. AUTHOR(S) (Last name, first name, initial)

Glover, P.; Alexander, S.S. (Consultant to Seismic Data Laboratory)

6. REPORT DATE

15 January 1970

7a. TOTAL NO. OF PAGES

223

7b. NO. OF REFS

158

8a. CONTRACT OR GRANT NO.

F33657-69-C-0913-PZ01

8b. PROJECT NO.

VELA T/9706

ARPA Order No. 624

ARPA Program Code No. 9F10

9a. ORIGINATOR'S REPORT NUMBER(S)

243

9b. OTHER REPORT NO(S) (Any other numbers that may be assigned this report)

10. AVAILABILITY/LIMITATION NOTICES

This document is subject to special export controls and each transmittal to foreign governments or foreign nationals may be made only with prior approval of Chief, AFTAC.

11. SUPPLEMENTARY NOTES

12. SPONSORING MILITARY ACTIVITY

ADVANCED RESEARCH PROJECTS AGENCY
NUCLEAR MONITORING RESEARCH OFFICE
WASHINGTON, D. C.

13. ABSTRACT

Two particular source regions, Lake Superior and the Nevada Test Site are documented in detail using available geological and geophysical observations. Each is discussed individually in relation to its setting in the prevailing regional crust and upper mantle structure of the mid-continent and the Basin and Range respectively. Comparison of the two source areas indicates that they are markedly different from one another not only at shallow depths but throughout the upper mantle as well. Location accuracies for events at both sites are quite comparable, however, a large bibliography documents the extensive literature relevant to Lake Superior and the Nevada Test Sites.

14. KEY WORDS

Nevada Test Site
Crustal Structure
Epicenter Locations

Geophysical Measurements
Basin and Range

Unclassified

Security Classification